

**Investigating the Role of IGF-1R Signalling in Development  
and Maintenance of Chemoresistance in Ovarian Carcinoma**

*By*

**Ajit Chandrakant Dhadve**

**LIFE09201404011**

**Tata Memorial Centre**

**Mumbai**

*A thesis submitted to the  
Board of Studies in Life Sciences  
In partial fulfilment of requirements  
for the Degree of*

**DOCTOR OF PHILOSOPHY**

*of*

**HOMI BHABHA NATIONAL INSTITUTE**



January, 2021

# Homi Bhabha National Institute

## Recommendations of the Viva Voce Committee

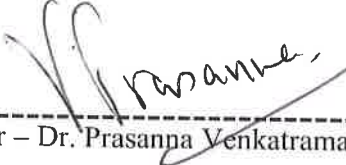
As members of the Viva Voce Committee, we certify that we have read the dissertation prepared by Mr. Ajit Chandrakant Dhadve entitled "Investigating the Role of IGF-1R Signalling in Development and Maintenance of Chemoresistance in Ovarian Carcinoma" and recommend that it may be accepted as fulfilling the thesis requirement for the award of Degree of Doctor of Philosophy.

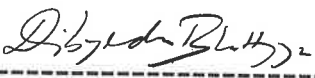
  
Chairperson - Dr. Rajiv Sarin Date: 27.01.2021

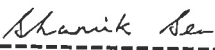
  
Guide/Convener - Dr. Pritha Ray Date: 14/1/2021

  
External Examiner - Dr. Sagar Sengupta Date: 05.01.2021

External Examiner - Dr. Sagar Sengupta Date:

  
Member - Dr. Prasanna Venkatraman Date: 15/01/2021

  
Member - Dr. Dibyendu Bhattacharyya Date: 4/1/2021

  
Technology Adviser - Dr. Shamik Sen Date: 4/1/21

Final approval and acceptance of this thesis is contingent upon the candidate's submission of the final copies of the thesis to HBNI.

I hereby certify that I have read this thesis prepared under my direction and recommend that it may be accepted as fulfilling the thesis requirement.

Date: 27/01/2021  
Place: Navi Mumbai

  
Dr. Pritha Ray  
Guide

## STATEMENT BY AUTHOR

This dissertation has been submitted in partial fulfilment of requirements for an advanced degree at Homi Bhabha National Institute (HBNI) and is deposited in the Library to be made available to borrowers under rules of the HBNI.

Brief quotations from this dissertation are allowable without special permission, provided that accurate acknowledgement of source is made. Requests for permission for extended quotation from or reproduction of this manuscript in whole or in part may be granted by the Competent Authority of HBNI when in his or her judgment the proposed use of the material is in the interests of scholarship. In all other instances, however, permission must be obtained from the author.



Ajit Chandrakant Dhadve

## DECLARATION

I, hereby declare that the investigation presented in the thesis has been carried out by me.

The work is original and has not been submitted earlier as a whole or in part for a degree

/ diploma at this or any other Institution / University.

A handwritten signature in black ink, appearing to read 'Ajit Dhadve', written over a horizontal line.

Ajit Chandrakant Dhadve

## List of Publications arising from the thesis

### Journal

- **Dhadve, A. C.,** K. Hari, B. Rekhi, M. K. Jolly, A. De and P. Ray (2020). "Decoding molecular interplay between RUNX1 and FOXO3a underlying the pulsatile IGF1R expression during acquirement of chemoresistance." Biochimica et Biophysica Acta (BBA) - Molecular Basis of Disease **1866**(6): 165754.
- Singh, R. K., **A. Dhadve,** A. Sakpal, A. De and P. Ray (2016). "An active IGF-1R-AKT signaling imparts functional heterogeneity in ovarian CSC population." Scientific Reports **6**: 36612.

**Chapters in books and lectures notes:** None

### Conferences

- **A. Dhadve** and P. Ray (2018). "RUNX1 and FOXO3a dictates IGF1R expression driving the early stages of chemoresistance development in Ovarian Cancer Cells" EACR-AACR-ISCR Conference: The Cutting Edge of Contemporary Cancer Research-Jerusalem, Israel.
- **A. Dhadve** and P. Ray (2018). "Interplay of RUNX1 and FOXO3a, a key to differential regulation of IGF-1R during acquirement of chemoresistance in Ovarian Carcinoma" International Congress of Cell Biology, CCMB, India.
- **A. Dhadve,** R. K. Singh and P. Ray (2017). "FOXO3a, a key to differential regulation of IGF-1R during acquirement of chemoresistance in Ovarian Carcinoma" All India Cell Biology Conference & International Symposium on Functional Genomics and Epigenomics, Gwalior, India.

## Others

### a. Review Article:

- **Dhadve, A.,** A. Deo, A. Bishnu, S. Mukherjee and P. Ray (2017). "MOLECULAR IMAGING IN CANCER: HOW THE HALLMARKS AID IN HUNTING." International Journal of Drug Research and Technology 7(1).

### b. Book/Book Chapters:

- **Dhadve, A.,** B. Thakur and P. Ray (2018). "Dual Modality Imaging of Promoter Activity as a Surrogate for Gene Expression and Function." Methods Mol Biol 1790: 1-12.
- **Dhadve, A.,** B. Thakur and P. Ray (2018). "Construction of Dual Modality Optical Reporter Gene Constructs for Bioluminescent and Fluorescent Imaging." Methods Mol Biol 1790: 13-27.
- A. Bishnu, A. Deo, **A. Dhadve,** B. Thakur, S. Mukherjee and P. Ray (2018). "Non Invasive Imaging in Clinical Oncology: A Testimony of Current Modalities and a Glimpse into the Future." Molecular Medicines for Cancer, CRC Press, pp. 217–262.



Ajit Chandrakant Dhadve

## DEDICATIONS

*Dedicated to Mother, Father, and brother.....*

## ACKNOWLEDGEMENTS

I would like to express my sincere gratitude to my supervisor and mentor, Dr. Pritha Ray, for her guidance, support, encouragement, and patience throughout my PhD tenure. It is her belief, patience and foresight that has helped me through crests and troughs of PhD and brought out the hidden potentials within me. I am very grateful to be part of her research group at ACTREC, TMC.

I would like to extend my gratitude to Dr. Sudeep Gupta (Director, ACTREC), Dr. Shubhada Chiplunkar (Ex-Director, ACTREC) and Dr. Prasanna Venkatraman (Dy. Director, ACTREC) for providing with an excellent academic and clinical research atmosphere. I am thankful to my doctoral committee members Dr. Rajiv Sarin, Dr. Prasanna Venkatraman, Dr. Dibyendu Bhattacharyya, and Dr. Shamik Sen for their timely and valuable suggestions for improving my doctoral research. I am grateful to Dr. Abhijit De for his valuable suggestions, critical analysis of my work during lab meetings and for Molecular imaging facility at ACTREC. I would also like to extend my gratitude to the staff at the Common Instrument Facility, Animal House Facility, ACTREC Digital Imaging Facility, Flow Cytometry Facility, Real-time for their constant support. I am very thankful to the ACTREC-TMC for providing me with PhD fellowship and Homi Bhabha National institute for supporting international travel.

This journey has been one of its kind and would have never been complete without the all the previous and current lab members of Imaging Cell Signaling and Therapeutics Lab, Lata di who has been backbone for all cell culture, my seniors Snehal, Ram, Suboshree, Bhushan and then juniors Abhilash, Aniketh, Souvik, Pratham, Megha, Priti and trainees not all I can pen down but they always made lab jovial. Thank you all for making this journey possible. Ram, Aniketh, Abhilash and Souvik have been very supportive throughout tough times and looked that I sailed through it. I am also thankful

to my batchmates. Harish, very dear friend of me, who took care of many things during tough times, thank you would be far less for his support. Before this list ends, I am lucky to have friends (Vipul, Subramoni, Ritesh, Sanket, Niranjana, Shilpa, Seema, Khushboo, Swapnita, Gauri and Shruti) who has always been crazy and supportive. Finally, I am blessed with family which has given me unconditional love and support.

<b>Table of Contents</b>	
Synopsis Report .....	13
<b>Chapter 1: Introduction and review of literature .....</b>	<b>39</b>
<b>1.1 Therapy resistance: A conundrum for cancer disease management .....</b>	<b>39</b>
<b>1.2 Chemoresistance: Many routes to one escape.....</b>	<b>42</b>
<b>1.2.1 Modulation of drug transport and metabolism .....</b>	<b>43</b>
<b>1.2.2 Altered cell cycle regulation.....</b>	<b>47</b>
<b>1.2.3 Enhanced DNA damage repair (DDR) mechanisms .....</b>	<b>49</b>
<b>1.2.4 Cellular plasticity.....</b>	<b>52</b>
<b>1.2.5 Tumour microenvironment (TME).....</b>	<b>55</b>
<b>1.2.6 Evading cell death and promoting cell survival.....</b>	<b>57</b>
<b>1.3 Insulin-like growth factor signalling.....</b>	<b>61</b>
<b>1.3.1 Insulin-like growth factor family.....</b>	<b>61</b>
<b>1.3.2 IGF1R structure and signalling.....</b>	<b>62</b>
<b>1.3.3 Role of IGF1R signalling in therapy resistance .....</b>	<b>64</b>
<b>1.3.4 Targeting IGF1R.....</b>	<b>69</b>
<b>1.4 Ovarian Cancer.....</b>	<b>70</b>
<b>1.4.1 Epidemiology.....</b>	<b>70</b>
<b>1.4.2 Classification .....</b>	<b>71</b>
<b>1.4.3 Diagnosis and staging .....</b>	<b>73</b>
<b>1.4.4 Disease management and treatment .....</b>	<b>73</b>
<b>1.4.5 Chemoresistance in EOC .....</b>	<b>75</b>
<b>Chapter 2: Identification of key molecular regulators of IGF1R during development of Cisplatin-Paclitaxel resistance in Ovarian Carcinoma.....</b>	<b>80</b>
<b>2.1 Introduction.....</b>	<b>80</b>
<b>2.2 Methodology .....</b>	<b>84</b>
<b>2.3 Results.....</b>	<b>91</b>

2.3.1	<b>IGF1R promoter activity oscillates during acquirement of chemoresistance</b> .....	91
2.3.2	<b>Potential regulators of IGF1R promoter in chemoresistant EOC cells</b> ....	94
2.3.3	<b>RUNX1 a novel regulator of IGF1R promoter in EOC cells</b> .....	99
2.3.4	<b>FOXO3a and RUNX1 positively regulate IGF1R promoter at the onset of chemoresistance</b> .....	103
2.3.5	<b>RUNX1 dictates FOXO3a binding to IGF1R promoter</b> .....	106
2.3.6	<b>AKT-FOXO3a negative feedback loop leads to pulsatile expression of IGF1R</b>	112
2.4	<b>Discussion</b> .....	115
<b>Chapter 3: Investigating the role of IGF1R signalling in maintenance of chemoresistance, tumorigenesis and cancer stem cell properties</b> .....		124
3.1	<b>Introduction</b> .....	124
3.2	<b>Methodology</b> .....	129
3.3	<b>Results</b> .....	132
3.3.1	<b>IGF1R regulates CSC phenotype and chemoresistance in EOC cells</b> ....	132
3.3.2	<b>IGF1R promotes cell proliferation and cell survival in early resistant cells</b>	136
3.3.3	<b>Impeding AKT inhibition induced IGF1R expression sensitizes the late resistant cells to AKT inhibition</b> .....	138
3.3.4	<b>Inhibiting RUNX1/FOXO3a axis sensitizes early resistant to Cisplatin-Paclitaxel.</b> .....	140
3.3.5	<b>Ro5-3335 and Cisplatin-Paclitaxel attenuate IGF1R promoter and chemoresistance invivo</b> .....	145
3.4	<b>Discussion</b> .....	151
<b>Chapter 4: Summary and Conclusion</b> .....		159
4.1	<b>Summary</b> .....	159
4.2	<b>Conclusion</b> .....	163
<b>Chapter 5: Materials and Methods</b> .....		165

## Table of Contents

<b>5.1</b>	<b>Cell culture</b> .....	165
<b>5.2</b>	<b>Bacterial culture</b> .....	177
<b>5.3</b>	<b>Molecular cloning</b> .....	181
<b>5.4</b>	<b>Real time quantification of gene transcripts</b> .....	186
<b>5.5</b>	<b>Nuclear-Cytoplasmic fractionation</b> .....	191
<b>5.6</b>	<b>Western blot</b> .....	193
<b>5.7</b>	<b>Immunofluorescence</b> .....	198
<b>5.8</b>	<b>Promoter binding transcription factor (TF) profiling array</b> .....	200
<b>5.9</b>	<b>Luciferase reporter assay</b> .....	204
<b>5.10</b>	<b>Co-Immunoprecipitation (Co-IP)</b> .....	206
<b>5.11</b>	<b>Chromatin immunoprecipitation (ChIP) and sequential ChIP-re-ChIP</b>	208
<b>5.12</b>	<b>Immunohistochemistry</b> .....	213
<b>5.13</b>	<b>Small animal bioluminescence imaging</b> .....	216
<b>5.14</b>	<b>Statistics</b> .....	217
	<b>References</b> .....	218
	<b>Re-Prints of Publications</b> .....	235

## List of Figures

<b>Figure 1: Chemotherapy resistance mechanisms .....</b>	<b>42</b>
<b>Figure 2: Transporter proteins involved in influx-efflux of chemotherapy drugs</b>	<b>43</b>
<b>Figure 3: Drug metabolism pathways .....</b>	<b>46</b>
<b>Figure 4: Cell Cycle regulation .....</b>	<b>48</b>
<b>Figure 5: DNA damage repair pathways.....</b>	<b>50</b>
<b>Figure 6: Cellular plasticity of cancer cells.....</b>	<b>53</b>
<b>Figure 7: Tumor microenvironment .....</b>	<b>55</b>
<b>Figure 8: Deregulation of apoptotic pathways in cancer .....</b>	<b>58</b>
<b>Figure 9: Insulin like growth factor signaling.....</b>	<b>61</b>
<b>Figure 10: Schematics representation of IGF1R structure and activation .....</b>	<b>63</b>
<b>Figure 11: Schematics of targeted therapies directed against IGF pathway .....</b>	<b>69</b>
<b>Figure 12: Top 10 prevalent cancer types among women across world and India</b>	<b>71</b>
<b>Figure 13: Classification of OC based on site of origin .....</b>	<b>72</b>
<b>Figure 14: Classification of OC based on clinical and molecular markers.....</b>	<b>72</b>
<b>Figure 15: Primary treatment modalities for EOC .....</b>	<b>74</b>
<b>Figure 16: Transcriptional regulation of IGF1R promoter .....</b>	<b>82</b>
<b>Figure 17: Development of chemoresistance models.....</b>	<b>85</b>
<b>Figure 18: NCBI Nucleotide blast alignment of IGF1R promoter .....</b>	<b>86</b>
<b>Figure 19: Cloning of IGF1R promoter from IGF1R-Gluc to IGF1R-hRL-eGFP</b>	<b>87</b>
<b>Figure 20: Schematics for promoter-binding transcription factor plate array .....</b>	<b>88</b>
<b>Figure 21: Schematic representation of ChIP and ChIP-re-ChIP protocol.....</b>	<b>90</b>
<b>Figure 22: Standardization of chromatin sonication and PCR for site specific ChIP of IGF1R promoter .....</b>	<b>91</b>
<b>Figure 23: IGF1R promoter demonstrates dynamic modulation during acquisition of chemoresistance.....</b>	<b>92</b>
<b>Figure 24: IGF1R promoter activity resides in -460 to +205 bp region of promoter in EOC cells.....</b>	<b>93</b>
<b>Figure 25: IGF1R-Promoter-binding TF plate array in A2780-dual<sup>ER</sup> cells.....</b>	<b>95</b>
<b>Figure 26: Prediction of TF binding motifs using JASPAR-TF database .....</b>	<b>96</b>

<b>Figure 27: Validation of IGF1R promoter binding TFs identified through Promoter-binding TF plate array.....</b>	<b>98</b>
<b>Figure 28: RUNX1 inhibition downregulates IGF1R transcript levels in EOC cells .....</b>	<b>99</b>
<b>Figure 29: RUNX1 shows enhanced expression in resistant EOC cells .....</b>	<b>101</b>
<b>Figure 30: RUNX1 ChIP across A2780 and OAW42 Cis-Pac resistant models ..</b>	<b>102</b>
<b>Figure 31: FOXO3a positively regulates IGF1R promoter activity in EOC cells</b>	<b>103</b>
<b>Figure 32: Increased expression and activation of FOXO3a at early stage of chemoresistance development.....</b>	<b>104</b>
<b>Figure 33: FOXO3a ChIP across A2780 and OAW42 Cis-Pac resistant models</b>	<b>105</b>
<b>Figure 34: RUNX1 and FOXO3a synergistically regulate IGF1R promoter activity in EOC cells during chemoresistant development.....</b>	<b>106</b>
<b>Figure 35: RUNX1 and FOXO3a show enhanced interaction at early stage of chemoresistance development.....</b>	<b>107</b>
<b>Figure 36: RUNX1-FOXO3a (ChIP-re-ChIP) show enhanced co-occupancy on IGF1R promoter at early stage of chemoresistance development.....</b>	<b>108</b>
<b>Figure 37: FOXO3a-RUNX1 (ChIP-re-ChIP) show enhanced co-occupancy on IGF1R promoter at early stage of chemoresistance development.....</b>	<b>109</b>
<b>Figure 38: RUNX1 inhibition attenuates FOXO3a binding to IGF1R promoter..</b>	<b>111</b>
<b>Figure 39: RUNX1 dictates FOXO3a binding to IGF1R promoter.....</b>	<b>112</b>
<b>Figure 40: AKT-FOXO3a feedback loop negatively regulates IGF1R expression at late-resistant stages.....</b>	<b>114</b>
<b>Figure 41: Proposed model of dynamic model of IGF1R promoter modulation by RUNX1/FOXO3a/AKT during acquisition of chemoresistance development ..</b>	<b>122</b>
<b>Figure 42: IGF1R inhibition chemosensitizes EOC cells to Cisplatin &amp; Paclitaxel .....</b>	<b>133</b>
<b>Figure 43: IGF1R silencing abrogates CSC phenotype in sensitive and early resistant cells .....</b>	<b>134</b>
<b>Figure 44: IGF1R regulates chemoresistance of CSC-like SP cells in early resistant cells.....</b>	<b>135</b>
<b>Figure 45: IGF1R silencing abrogates MAPK/ERK pathway, but not PIK3CA/AKT pathway in A2780-Cis-Pac resistant model.....</b>	<b>136</b>

<b>Figure 46: IGF1R silencing inhibits proliferation and induces apoptosis in early resistant cells of A2780-Cis-Pac resistant model.....</b>	<b>138</b>
<b>Figure 47: Impeding AKT inhibition induced IGF1R expression sensitizes the late resistant cells to AKT inhibition .....</b>	<b>139</b>
<b>Figure 48: Blocking RUNX1 activity by CBF<math>\beta</math> knockdown sensitizes resistant cells to Cisplatin-Paclitaxel.....</b>	<b>141</b>
<b>Figure 49: CBF<math>\beta</math>-KD and Platinum-Taxol attenuate IGF1R promoter activity and chemoresistance invivo .....</b>	<b>143</b>
<b>Figure 50: CBF<math>\beta</math>-KD and Platinum-Taxol downregulates IGF1R, abrogates tumor proliferation and decreases chemoresistance invivo.....</b>	<b>144</b>
<b>Figure 51: Cytotoxicity of Ro5-3335 in A2780 and OAW42 cells across different concentration.....</b>	<b>145</b>
<b>Figure 52: Ro5-3335 in combination with Cisplatin-Paclitaxel attenuates chemoresistance in early resistant cells .....</b>	<b>146</b>
<b>Figure 53: Ro5-3335 mediated RUNX1 inhibition and Platinum-Taxol attenuate IGF1R promoter activity and chemoresistance invivo.....</b>	<b>148</b>
<b>Figure 54: IGF1R downregulation post Ro5-3335/Cisplatin-Paclitaxel/ combination treatment positively correlates with reduced tumor proliferation and increased necrosis .....</b>	<b>150</b>
<b>Figure 55: Ro5-3335 and Platinum-Taxol downregulates IGF1R, abrogates tumor proliferation and decreases chemoresistance invivo.....</b>	<b>150</b>
<b>Figure 56: Proposed model of IGF1R/MAPK/ERK signalling mediated chemoresistance through maintenance of CSC phenotype and suppression of apoptosis at and for indirect targeting of the augmented expression of IGF1R at onset of chemoresistance development by blocking transcriptional regulators of IGF1R promoter in EOC cells .....</b>	<b>158</b>
<b>Figure 57: Schematic representation of data analysis for DCV side population assay.....</b>	<b>173</b>
<b>Figure 58: Schematic representation of plasmid isolation protocol using NucleoSpin® Plasmid kit.....</b>	<b>180</b>
<b>Figure 59: Schematic representation of PCR clean up protocol using NucleoSpin® PCR clean up kit .....</b>	<b>182</b>
<b>Figure 60: Schematic representation of PCR steps for site directed mutagenesis.....</b>	<b>185</b>

**Figure 61: Schematic representation of RNA isolation using Qiagen RNA isolation**  
..... 187

**Figure 62: Schematic representation of PCR steps for cDNA Synthesis** ..... 188

List of Tables

**Table 1: Examples of Clinical trials comparing efficacy of drug combinations....40**

**Table 2: List of EOC chemoresistance models.....85**

**Table 3: Number of the predicted binding sites of the TFs on IGF1R promoter as predicted by JASPAR-TF database (threshold>75%).....97**

**Table 4: List of SDM primers.....185**

**Table 5: List of real time primers.....189**

**Table 6: List of antibody dilutions for western blot.....197**

**Table 7: List of antibody dilutions for immunofluorescence.....199**

**Table 8: List of ChIP real time primers.....212**

**Table 9: List of antigen retrieval conditions and antibody dilution for IHC.....215**

## Chapter 4: Summary and Conclusion

### 4.1 Summary

The race to develop anti-IGF1R targeted therapies for cancer has been hindered due to failure of clinical trials to yield clinical benefits. However, the mounting evidence suggest that not only IGF1R overexpression is ubiquitous across different cancer types but it is also a key signalling molecule underlying the resistance mechanisms against wide range of chemotherapeutic agents and targeted therapies [440]. The first anti-IGF1R targeted therapy (Teprotumumab) has been recently (January, 2020) approved, although not for cancer treatment, but for treatment of Graves' orbitopathy [441]. Several pre-clinical studies have started reevaluation of anti-IGF1R agents, not as a standalone treatment, but in combination with chemotherapeutic agents and other targeted therapies along with identification of predictive biomarkers to unlock the full potential of anti-IGF1R targeted therapies in cancer [440]. Using indigenously developed isogenic EOC chemoresistance models against Cisplatin/Paclitaxel/Cisplatin-Paclitaxel combination, we reported a pulsatile nature of IGF1R expression during acquirement of chemoresistance development. The augmented levels of IGF1R were shown to impart chemoresistance against Cisplatin-Paclitaxel at early stages of chemoresistance development; moreover, we observed similar therapy induced upregulation of IGF1R expression in tumors of a small cohort of high grade serous EOC patients [252]. The underlying mechanisms behind this undulating IGF1R expression during progression of chemoresistance has led to this investigation which deciphers two important questions pertaining the role of IGF1R signalling in chemoresistance development of EOC, A) unraveling the complex circuitry of modulators governing IGF1R expression and B) decoding the molecular mechanisms behind IGF1R mediated chemoresistance and identifying potential approach to indirectly target IGF1R through its regulators in IGF1R addicted or therapy resistant cancers.

IGF1R overexpression in many cancer types is significantly attributed to the transcriptional modulation rather than to rare instances of gene amplification, hence we used an IGF1R promoter driven bi-fusion (bioluminescence-fluorescence) reporter sensor to uncover the mechanisms behind this oscillating IGF1R expression during progression of resistance. The IGF1R-promoter-reporter sensor showed similar pulsatile nature as previously observed for endogenous IGF1R transcript and protein levels, significantly upregulated at early stages of chemoresistance and declined in late resistance stages. Next, using a transcription factor binding IGF1R promoter competition assay we identified eight new transcription factors (RXR, SOX9, VDR, GFI1, ROR, RUNX1, NKX2.5 and SOX18) along with SP1 (a known IGF1R regulator) as potential regulators of IGF1R promoter in chemoresistant EOC cell. Sarfstein. et. al. (2009), using biotinylated IGF1R promoter reported identification of several transcription factors binding to IGF1R promoter in breast cancer cells [363]. However, this is first report where we identify potential regulators of IGF1R promoter in chemoresistant cancer cells, apart from pVHL and FOXO1 regulating IGF1R in 5-Fluorouracil and etoposide resistant renal cell carcinoma and PI3K- $\delta$  inhibitor resistant chronic lymphocytic leukaemia respectively [300, 442]. Though transcription factor-promoter array analysis in this study identified several unique transcriptional regulators, perturbation of only RUNX1 activity (RUNX1-CBF $\beta$  inhibitor, Ro5-3335) significantly attenuated IGF1R transcriptional and promoter activity in chemoresistance models. RUNX1, a significantly altered gene in acute myeloid leukaemia and functions as a pioneering transcription factor in haematopoiesis [341], showed increased expression and nuclear localization of RUNX1 along with enhanced binding of RUNX1 to IGF1R promoter at both early and late stages of chemoresistance. Despite increased RUNX1 expression and functional activities (nuclear localization and enhanced binding on IGF1R promoter) across both stages of chemoresistance, specific inhibition of IGF1R by Ro5-3335 was observed

only in early-resistant cells, which signifies for contributory role of other regulator/s for optimal activation. Using JASPAR, a TF binding prediction software we found that consensus binding sites of transcription factors identified from transcription factor array and previously reported IGF1R binding transcription factor are scattered throughout IGF1R promoter. Intriguingly, RUNX1 and FOXO3a (a known IGF1R regulator) [328] binding elements showed proximity to each other on IGF1R promoter. As opposed to RUNX1, FOXO3a exhibited a similar pulsatile pattern like IGF1R across resistant stages with increased nuclear localization of both total and transcriptionally active FOXO3a (p-S413) and higher IGF1R promoter occupancy in early resistant cells. Mutating FOXO3a binding elements on IGF1R promoter in combination with Ro5-3335 treatment showed significant synergism in attenuating IGF1R promoter activity in early resistant cells as compared to FOXO3a binding element mutant IGF1R promoter or Ro5-3335 treatment alone. Indeed, the co-immunoprecipitation results demonstrated a stage specific interaction pattern between RUNX1 and FOXO3a which was highest in early resistant cells but minimal in sensitive and late resistant cells. This stage specific interaction pattern seems to influence their IGF1R promoter binding capacity as maximal RUNX1-FOXO3a co-occupancy was evident during onset of resistance which subsequently decreased at late-resistant stages as revealed by Chip-re-Chip assay, thus signifying cooperativity between RUNX1 and FOXO3a in regulation of IGF1R promoter activity. This cooperativity became evident from genetic (CBF $\beta$  knockdown) and pharmacological inhibition (Ro5-3335 treatment) of RUNX1 activity, which abolished FOXO3a binding in early-resistant cells indicating that RUNX1 binding is an obligatory step for FOXO3a occupancy specifically at the onset of resistance. This cooperative interaction of RUNX1-FOXO3a, however falls apart as cells reach late resistant cells due to simultaneous presence of hyperactivated AKT, which downregulates FOXO3a by nuclear exclusion. Indeed, AKT inactivation either through

serum starvation or by an inhibitor restores FOXO3a levels in late resistant cells upregulating IGF1R expression.

Once, upstream molecular players regulating IGF1R expression were identified, we next checked the biological consequences of augmented IGF1R expression in maintaining chemoresistance properties of EOC cells. IGF1R silencing significantly chemosensitized the early resistant cells to chemotherapeutic agents Cisplatin-Paclitaxel alone. More importantly IGF1R was shown to maintain CSC phenotype in early resistant cells through upregulation of pluripotency transcription factors Sox2, Oct4 and Nanog. The CSC-like SP cells were highly resistant to Cisplatin-Paclitaxel compared to the respective NSP and MP cells, more importantly IGF1R knockdown showed enhanced chemosensitization of SP cells. Among the two major signalling arms, AKT showed gradual activation with increasing resistance, whereas, ERK1/2 showed highest activation in only early resistant cells. Silencing IGF1R revealed that the MAPK/ERK signalling arm is activated downstream of IGF1R, whereas PIK3CA/AKT signalling largely remains unaffected across the chemoresistant model. The increased levels of IGF1R in early resistant cells induced the levels of anti-apoptotic proteins BCL-2 and BCL-XL, whereas it antagonized the induction of pro-apoptotic protein BAD post Cisplatin-Paclitaxel treatment in early resistant cells, thus suppressing the Cisplatin-Paclitaxel induced apoptosis in early resistant cells. Interestingly, AKT inhibition in late resistant cells induced IGF1R, which was shown to impart resistance against AKT inhibition, as dual inhibition of AKT and IGF1R significantly reduced cell survival of late resistant cells. The augmented levels of IGF1R imparting resistance against Cisplatin-Paclitaxel in early resistant cells and AKT inhibition induced IGF1R limiting efficacy of AKT inhibitor, both were regulated by transcriptional modulation of IGF1R promoter by RUNX1/FOXO3a.

In present study we have shown that RUNX1/FOXO3a maintain augmented IGF1R promoter activity at onset of chemoresistance development in EOC cells leading to increased expression of IGF1R. Thus, we investigated the potential of blocking RUNX1/FOXO3a/IGF1R axis to assess the biological implication of this axis in targeting early onset of chemoresistance. Pharmacological (Ro5-3335 treatment) or genetic ablation (CBF $\beta$  knockdown) of RUNX1 activity attenuated IGF1R promoter activity, reduced IGF1R expression, impaired tumor proliferation and showed enhanced chemosensitization to Cisplatin-Paclitaxel both *invitro* and *invivo* in early resistant cells. RUNX1 is indispensable for establishment of definitive haematopoiesis in vertebrates. However, no obvious illness was observed in long term use of 300mg/kg/day of Ro5-3335 in mice [337] and a single dose of 5mg/kg of Ro5-3555 protects LPS induced death in mice by reducing inflammation [439]. We applied similar low dose in fractionated manner (2mg/kg/day/5days) and observed that low dose RUNX1 inhibitor with platinum-taxol could effectively delay resistance development. However, a detail dose dependent study is warranted to assess potential of RUNX1 inhibition combating the platinum-taxol resistance in cancers with augmented IGF1R expression.

## **4.2 Conclusion**

Here, for the first time we report RUNX1 as a unique regulator of IGF1R promoter which exerts a cooperative interaction with FOXO3a and dynamically modulate IGF1R expression during acquirement of chemoresistance in EOC cells. Genetic and pharmacological inhibition followed ChIP and ChIP-re-ChIP assay revealed that RUNX1 strengthened FOXO3a occupancy on IGF1R promoter, leading to a transcriptional surge during initiation of resistance which is lost at the late stages. Further an active AKT-FOXO3a negative feedback loop was shown to maintain the pulsatile behaviour of IGF1R and FOXO3a. We also showed that upregulated IGF1R at onset of resistance confers resistance to Cisplatin-

Paclitaxel through modulation of CSC phenotype and inhibition apoptosis by downstream IGF1R signalling. Perturbation of RUNX1 activity severely compromised IGF1R promoter activity and sensitized the tumors of early resistant cells to platinum-taxol treatment, as monitored by non-invasive imaging. Altogether our findings delineate a dynamic interplay between several molecular regulators (RUNX1/FOXO3a/AKT) driving pulsatile IGF1R expression and identifies a new avenue for targeting EOC through RUNX1-IGF1R axis during acquirement of chemoresistance.

## Chapter 4: Summary and Conclusion

### 4.1 Summary

The race to develop anti-IGF1R targeted therapies for cancer has been hindered due to failure of clinical trials to yield clinical benefits. However, the mounting evidence suggest that not only IGF1R overexpression is ubiquitous across different cancer types but it is also a key signalling molecule underlying the resistance mechanisms against wide range of chemotherapeutic agents and targeted therapies [440]. The first anti-IGF1R targeted therapy (Teprotumumab) has been recently (January, 2020) approved, although not for cancer treatment, but for treatment of Graves' orbitopathy [441]. Several pre-clinical studies have started reevaluation of anti-IGF1R agents, not as a standalone treatment, but in combination with chemotherapeutic agents and other targeted therapies along with identification of predictive biomarkers to unlock the full potential of anti-IGF1R targeted therapies in cancer [440]. Using indigenously developed isogenic EOC chemoresistance models against Cisplatin/Paclitaxel/Cisplatin-Paclitaxel combination, we reported a pulsatile nature of IGF1R expression during acquirement of chemoresistance development. The augmented levels of IGF1R were shown to impart chemoresistance against Cisplatin-Paclitaxel at early stages of chemoresistance development; moreover, we observed similar therapy induced upregulation of IGF1R expression in tumors of a small cohort of high grade serous EOC patients [252]. The underlying mechanisms behind this undulating IGF1R expression during progression of chemoresistance has led to this investigation which deciphers two important questions pertaining the role of IGF1R signalling in chemoresistance development of EOC, A) unraveling the complex circuitry of modulators governing IGF1R expression and B) decoding the molecular mechanisms behind IGF1R mediated chemoresistance and identifying potential approach to indirectly target IGF1R through its regulators in IGF1R addicted or therapy resistant cancers.

IGF1R overexpression in many cancer types is significantly attributed to the transcriptional modulation rather than to rare instances of gene amplification, hence we used an IGF1R promoter driven bi-fusion (bioluminescence-fluorescence) reporter sensor to uncover the mechanisms behind this oscillating IGF1R expression during progression of resistance. The IGF1R-promoter-reporter sensor showed similar pulsatile nature as previously observed for endogenous IGF1R transcript and protein levels, significantly upregulated at early stages of chemoresistance and declined in late resistance stages. Next, using a transcription factor binding IGF1R promoter competition assay we identified eight new transcription factors (RXR, SOX9, VDR, GFI1, ROR, RUNX1, NKX2.5 and SOX18) along with SP1 (a known IGF1R regulator) as potential regulators of IGF1R promoter in chemoresistant EOC cell. Sarfstein. et. al. (2009), using biotinylated IGF1R promoter reported identification of several transcription factors binding to IGF1R promoter in breast cancer cells [363]. However, this is first report where we identify potential regulators of IGF1R promoter in chemoresistant cancer cells, apart from pVHL and FOXO1 regulating IGF1R in 5-Fluorouracil and etoposide resistant renal cell carcinoma and PI3K- $\delta$  inhibitor resistant chronic lymphocytic leukaemia respectively [300, 442]. Though transcription factor-promoter array analysis in this study identified several unique transcriptional regulators, perturbation of only RUNX1 activity (RUNX1-CBF $\beta$  inhibitor, Ro5-3335) significantly attenuated IGF1R transcriptional and promoter activity in chemoresistance models.

RUNX1, a significantly altered gene in acute myeloid leukaemia and functions as a pioneering transcription factor in haematopoiesis [341], showed increased expression and nuclear localization of RUNX1 along with enhanced binding of RUNX1 to IGF1R promoter at both early and late stages of chemoresistance. Despite increased RUNX1 expression and functional activities (nuclear localization and enhanced binding on IGF1R promoter) across both stages of chemoresistance, specific inhibition of IGF1R by Ro5-3335 was observed

only in early-resistant cells, which signifies for contributory role of other regulator/s for optimal activation. Using JASPAR, a TF binding prediction software we found that consensus binding sites of transcription factors identified from transcription factor array and previously reported IGF1R binding transcription factor are scattered throughout IGF1R promoter. Intriguingly, RUNX1 and FOXO3a (a known IGF1R regulator) [328] binding elements showed proximity to each other on IGF1R promoter. As opposed to RUNX1, FOXO3a exhibited a similar pulsatile pattern like IGF1R across resistant stages with increased nuclear localization of both total and transcriptionally active FOXO3a (p-S413) and higher IGF1R promoter occupancy in early resistant cells. Mutating FOXO3a binding elements on IGF1R promoter in combination with Ro5-3335 treatment showed significant synergism in attenuating IGF1R promoter activity in early resistant cells as compared to FOXO3a binding element mutant IGF1R promoter or Ro5-3335 treatment alone. Indeed, the co-immunoprecipitation results demonstrated a stage specific interaction pattern between RUNX1 and FOXO3a which was highest in early resistant cells but minimal in sensitive and late resistant cells. This stage specific interaction pattern seems to influence their IGF1R promoter binding capacity as maximal RUNX1-FOXO3a co-occupancy was evident during onset of resistance which subsequently decreased at late-resistant stages as revealed by Chip-re-Chip assay, thus signifying cooperativity between RUNX1 and FOXO3a in regulation of IGF1R promoter activity. This cooperativity became evident from genetic (CBF $\beta$  knockdown) and pharmacological inhibition (Ro5-3335 treatment) of RUNX1 activity, which abolished FOXO3a binding in early-resistant cells indicating that RUNX1 binding is an obligatory step for FOXO3a occupancy specifically at the onset of resistance. This cooperative interaction of RUNX1-FOXO3a, however falls apart as cells reach late resistant cells due to simultaneous presence of hyperactivated AKT, which downregulates FOXO3a by nuclear exclusion. Indeed, AKT inactivation either through

serum starvation or by an inhibitor restores FOXO3a levels in late resistant cells upregulating IGF1R expression.

Once, upstream molecular players regulating IGF1R expression were identified, we next checked the biological consequences of augmented IGF1R expression in maintaining chemoresistance properties of EOC cells. IGF1R silencing significantly chemosensitized the early resistant cells to chemotherapeutic agents Cisplatin-Paclitaxel alone. More importantly IGF1R was shown to maintain CSC phenotype in early resistant cells through upregulation of pluripotency transcription factors Sox2, Oct4 and Nanog. The CSC-like SP cells were highly resistant to Cisplatin-Paclitaxel compared to the respective NSP and MP cells, more importantly IGF1R knockdown showed enhanced chemosensitization of SP cells. Among the two major signalling arms, AKT showed gradual activation with increasing resistance, whereas, ERK1/2 showed highest activation in only early resistant cells. Silencing IGF1R revealed that the MAPK/ERK signalling arm is activated downstream of IGF1R, whereas PIK3CA/AKT signalling largely remains unaffected across the chemoresistant model. The increased levels of IGF1R in early resistant cells induced the levels of anti-apoptotic proteins BCL-2 and BCL-XL, whereas it antagonized the induction of pro-apoptotic protein BAD post Cisplatin-Paclitaxel treatment in early resistant cells, thus suppressing the Cisplatin-Paclitaxel induced apoptosis in early resistant cells. Interestingly, AKT inhibition in late resistant cells induced IGF1R, which was shown to impart resistance against AKT inhibition, as dual inhibition of AKT and IGF1R significantly reduced cell survival of late resistant cells. The augmented levels of IGF1R imparting resistance against Cisplatin-Paclitaxel in early resistant cells and AKT inhibition induced IGF1R limiting efficacy of AKT inhibitor, both were regulated by transcriptional modulation of IGF1R promoter by RUNX1/FOXO3a.

In present study we have shown that RUNX1/FOXO3a maintain augmented IGF1R promoter activity at onset of chemoresistance development in EOC cells leading to increased expression of IGF1R. Thus, we investigated the potential of blocking RUNX1/FOXO3a/IGF1R axis to assess the biological implication of this axis in targeting early onset of chemoresistance. Pharmacological (Ro5-3335 treatment) or genetic ablation (CBF $\beta$  knockdown) of RUNX1 activity attenuated IGF1R promoter activity, reduced IGF1R expression, impaired tumor proliferation and showed enhanced chemosensitization to Cisplatin-Paclitaxel both *invitro* and *invivo* in early resistant cells. RUNX1 is indispensable for establishment of definitive haematopoiesis in vertebrates. However, no obvious illness was observed in long term use of 300mg/kg/day of Ro5-3335 in mice [337] and a single dose of 5mg/kg of Ro5-3555 protects LPS induced death in mice by reducing inflammation [439]. We applied similar low dose in fractionated manner (2mg/kg/day/5days) and observed that low dose RUNX1 inhibitor with platinum-taxol could effectively delay resistance development. However, a detail dose dependent study is warranted to assess potential of RUNX1 inhibition combating the platinum-taxol resistance in cancers with augmented IGF1R expression.

## **4.2 Conclusion**

Here, for the first time we report RUNX1 as a unique regulator of IGF1R promoter which exerts a cooperative interaction with FOXO3a and dynamically modulate IGF1R expression during acquirement of chemoresistance in EOC cells. Genetic and pharmacological inhibition followed ChIP and ChIP-re-ChIP assay revealed that RUNX1 strengthened FOXO3a occupancy on IGF1R promoter, leading to a transcriptional surge during initiation of resistance which is lost at the late stages. Further an active AKT-FOXO3a negative feedback loop was shown to maintain the pulsatile behaviour of IGF1R and FOXO3a. We also showed that upregulated IGF1R at onset of resistance confers resistance to Cisplatin-

Paclitaxel through modulation of CSC phenotype and inhibition apoptosis by downstream IGF1R signalling. Perturbation of RUNX1 activity severely compromised IGF1R promoter activity and sensitized the tumors of early resistant cells to platinum-taxol treatment, as monitored by non-invasive imaging. Altogether our findings delineate a dynamic interplay between several molecular regulators (RUNX1/FOXO3a/AKT) driving pulsatile IGF1R expression and identifies a new avenue for targeting EOC through RUNX1-IGF1R axis during acquirement of chemoresistance.

## Chapter 1: Introduction and review of literature

### **1.1 Therapy resistance: A conundrum for cancer disease management**

The three frontiers that collectively contribute to the cancer management are prevention, diagnosis, and treatment. The current long-term population-based studies are still in early stage to provide conclusive evidence on impact of preventive healthcare practices and screening programs on cancer incidence [1-6]. The improved 5-year overall survival rates across different cancer types observed in population-based survival trends of last four decades are attributed to advancements in diagnostic methods and treatment modalities. Deeper understanding of these long-term survival trend for individual cancers reveals three broad clusters of cancers based on absolute change in 5-year overall survival, first for which there was significant improvement in overall survival, followed by others who were benefited to a moderate extent and third for which there was less or no change was observed in overall survival [7-9]. These observed differences in progress of overall survival among different cancers are majorly due to variances in treatment response of both primary and relapsed tumors and disease-free periods as well the stage of diagnosis. If Detected early, for majority of cancers, complete cytoreduction followed by chemo/radio therapy significantly improves disease free and overall survival compared to advanced stage disseminated disease. Chemotherapy alone or in combination with other treatment strategies continues to be a prime treatment modality, as it is effective against multiple tumor types for both primary and metastatic disease. It is also used prior to surgery to reduce tumor burden and as palliative care for recurrent disease [10-14]. Combination of chemotherapeutic agents or combination with other therapies such as hormone therapy, immuno therapy and targeted therapy (antibodies/small molecular inhibitors) have been proven to improve overall survival and disease-free survival compared to single agent treatment in various cancer types (Table 1). Even though

chemotherapy has been successful as first line therapy in many cancer types if not all, it suffers a major roadblock of resistance development. Response to these various treatment modalities vary in different cancer types and even among patients within the same cancer type. Though majority of the patients respond well to first line therapy (Chemotherapy alone or combination therapy), very often relapsed disease either shows poor response or no response to first line therapy. Thus, a secondary line of therapy is inducted for disease management which also eventually succumb to therapy resistance. Both intrinsic and acquired chemoresistance continues to be an inevitable fate of all chemotherapeutic agents limiting efficacy of the chemotherapy. Amid several challenges in cancer treatment, chemoresistance remains persistent hurdle significantly contributing to the mortality primarily due to recurrent therapy resistant tumors [15, 16]. The phenomenon of chemoresistance is a perilous aspect of tumor biology and is governed by aberrantly regulated signaling networks that fine tune multiple mechanisms of chemoresistance to help cancer cells endure the chemotherapeutic challenge.

**Table 1: Examples of Clinical trials comparing efficacy of drug combinations**

Patient inclusion criteria	Drug combination	Clinical response rate	Overall survival (Months)	Ref.
<b>Breast Cancer</b>				
Anthracycline-pre-treated metastatic disease	Paclitaxel Vs (Gemcitabine + Paclitaxel)	26% Vs 41%	15.8 Vs 18.6	[17]
Progressive Her2 overexpressing disease	Lapatinib Vs (Lapatinib + Trastuzumab)	29% Vs 51%	9.5 Vs 14	[18]
<b>Ovarian Cancer</b>				
Advanced stage sub-optimally operated disease	(Cisplatin + Cyclophosphamide) Vs (Cisplatin + Paclitaxel)	31% Vs 51%	24 Vs 38	[19]

Patient inclusion criteria	Drug combination	Clinical response rate	Overall survival (Months)	Ref.
Platinum-Refractory and -Resistant disease	Paclitaxel Vs (Paclitaxel + Doxorubicin)	17% Vs 34%	12 Vs 14	[20]
Platinum sensitive recurrent disease	(Carboplatin + Paclitaxel) Vs (Carboplatin + Paclitaxel + Bevacizumab)	55% Vs 78%	35.7 Vs 43.2	[21]
<b>Head and neck cancer</b>				
Stage III or IV locally advanced disease	(Cisplatin + 5-FU) Vs (Docetaxel + Cisplatin + 5-FU)	48% Vs 62%	30 Vs 71	[22]
<b>Cervical Cancer</b>				
Advanced recurrent or persistent disease	Cisplatin Vs (Cisplatin + Topotecan)	13% vs 27%	6.5 Vs 9.4	[23]
Metastatic, persistent, or recurrent	(Cisplatin + Paclitaxel) Vs (Cisplatin + Paclitaxel + Bevacizumab)	34% Vs 48%	13.3 Vs 17	[24]
<b>Colorectal cancer</b>				
Unresectable metastatic disease	(5-FU+ Leucovorin+Irinotecan) Vs (5-FU+Leucovorin+Oxaliplatin +Irinotecan)	41% Vs 61%	17 Vs 23	[25]
previously untreated metastatic disease	(Irinotecan + 5-FU + Leucovorin) Vs (Irinotecan + 5-FU + Leucovorin + Bevacizumab)	35% Vs 46%	15.6 Vs 20.3	[26]
<b>Gastric cancer</b>				
Locally advanced, resectable gastric or gastro-oesophageal	(5-FU + Epirubicin + Cisplatin) Vs (5-FU + Docetaxel + Oxaliplatin + Leucovorin)	40% Vs 59%	35 Vs 50	[27]
Gastric or gastro-oesophageal cancer	(Cisplatin + Capecitabine) Vs (Cisplatin + Capecitabine + Trastuzumab)	38% Vs 53%	10.9 Vs 13.8	[28]

## 1.2 Chemoresistance: Many routes to one escape

Integrated functional and genomic studies have revealed cancer as a pathological condition which is highly heterogenous, vastly dynamic and savagely adaptive in nature.

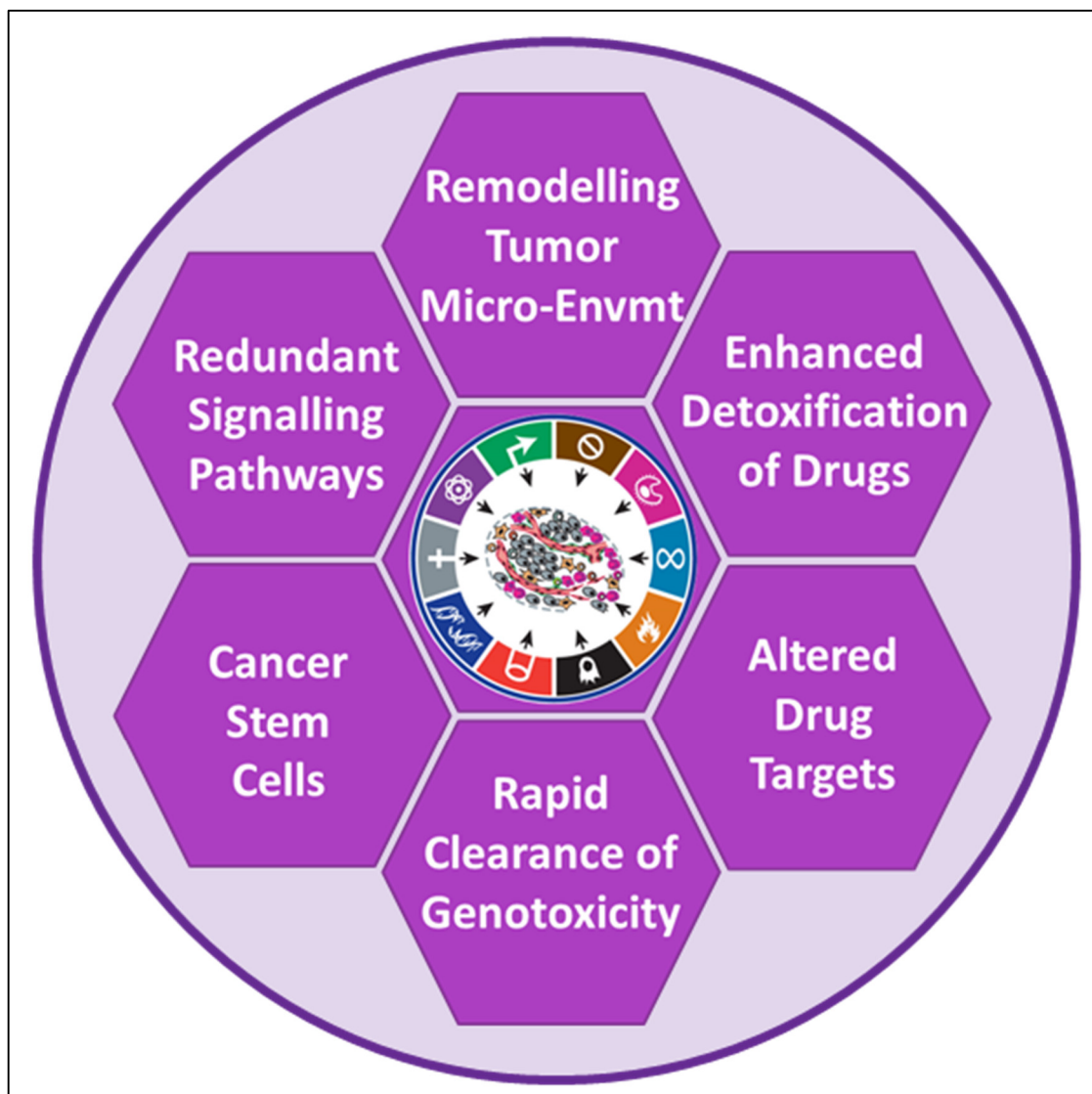


**Figure 1: Chemotherapy resistance mechanisms**

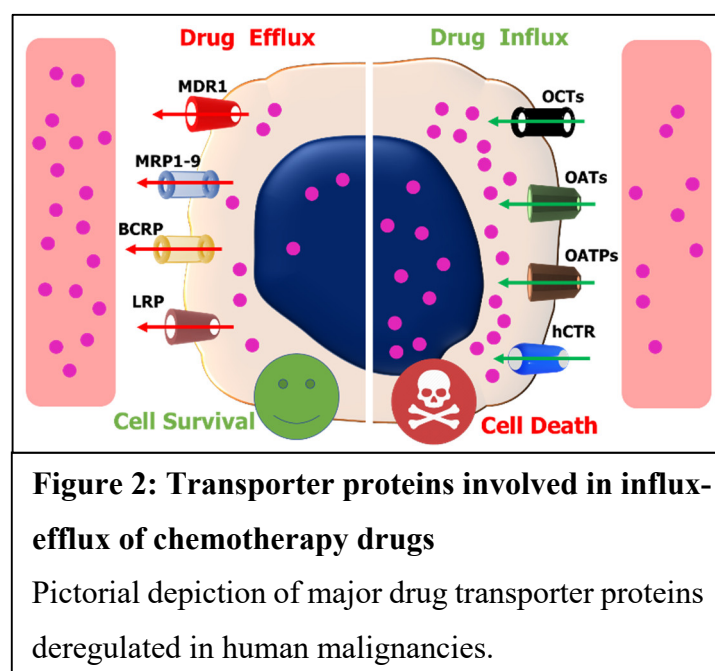
Pictorial depiction of major mechanisms involved in chemoresistance that are interwoven by cross-roads of signalling pathways.

These same characteristics contribute to the phenomenon of drug resistance (intrinsic or acquired) and the full spectrum of mechanisms involved in resistance are variable across different cancer types for a given therapeutic agent. Mechanisms behind drug resistance are multifactorial, both genetic (hereditary/somatic mutations, fusion proteins, deletions,

and amplifications) and non-genetic (epigenetics, altered protein expression and post-translational modifications) and are further influenced by tumor heterogeneity. The mechanisms underlying chemoresistance mainly involve alterations in drug transport and drug metabolism, target alterations, altered cell cycle check points, enhanced DNA repair mechanisms and hyperactivation of anti-apoptotic/cell survival pathways. Also, there is increasing evidence that tumor microenvironment and cancer stem cells (CSCs) play an integral role in therapy resistance (Fig. 1) [29].

### 1.2.1 Modulation of drug transport and metabolism

One of the common mechanisms of chemoresistance to be identified early on was associated with transport and metabolism of chemotherapeutic agents by cancer cells.



Membrane transporter proteins play important role in uptake of metabolites into and efflux of xenobiotics out of the cells under normal physiological conditions to sustain cell survival along with the metabolic detoxification pathways [30-

34]. Many of these transporter proteins and metabolic detoxification pathways have been linked chemoresistance against wide spectrum of chemotherapeutic drugs in all cancer types, affecting the therapeutic efficacy of the chemotherapy [35-37].

Transporter proteins are classified into two major families, the ATP-binding cassette (ABC) transporters, which transport substrates by ATP hydrolysis [38] and the solute carrier (SLC) transporters, which facilitate passive (concentration dependent) or active

transport (dependent on transport of another molecule) of substrates (Fig. 2) [39]. ABC transporters primarily function as efflux pumps for chemotherapy drugs and are most widely studied drug transporter proteins due to their association with multidrug resistance (MDR) and CSC phenotype. Acute myeloid leukaemia (AML) patients undergoing induction chemotherapy of Mitoxantrone, Cytosine arabinoside and etoposide or Daunorubicin and Cytosine arabinoside show increased expression levels MDR1, breast cancer resistance protein (BCRP) and MDR related protein 1 (MRP1) [40-43]. Two independent studies of adult AML patients using functional dye efflux assay show association of high level MDR1 activity with non-responders, reduced complete remission of disease, and decreased overall survival. [43, 44]. Expression of MDR1, BCRP and MRP1 were also shown to be upregulated in Ovarian cancer (OC) patients post chemotherapy [45-48] and were shown to be involved in efflux of Paclitaxel, Topotecan, Doxorubicin and Olaparib [49, 50]. Hedgehog signaling pathway transcription factor Gli1 was shown to upregulate expression of MDR1 and MRP1 in OC cell lines (A2780, OVACR3 and OVCAR8) and provide resistance against Paclitaxel, Doxorubicin and Cisplatin [51]. Activation of OC stem cell marker CD44 by hyaluronic acid was shown to induce the expression of ABC drug transporters (ABCB3, ABCC1, ABCC2, and ABCC3) in OC cells OVCAR3, SKOV3 and OV90 leading to Carboplatin resistance. Moreover, serum hyaluronic acid levels were found to be upregulated post-chemotherapy (Carboplatin alone or in combination with Paclitaxel) in OC patients and was associated with decreased overall survival [52]. The wint- $\beta$ -catenin activation post Cisplatin treatment was shown to upregulate expression of MDR1 and MRP1 in Non-small cell lung cancer (NSCLC) patients [53]. The Epithelial mesenchymal transition (EMT) transcription factors Snail, Twist1 and Zeb1 were shown to induce expression of MDR1, MRP1 and BCRP in Doxorubicin/Mitoxantone resistant MCF7 cells (Breast

cancer) [54-56], Cisplatin resistant Hella cells (Cervical cancer) [57], Mitoxantone resistant TPC-1 cells (Thyroid papillary carcinoma) [58] and 5-Flurouracil resistant HLF cells (Hepatocellular carcinoma) [59].

In contrast to ABC transporters, SLC transporters can act as both influx as well efflux pumps for chemotherapeutic drugs. Organic cation transporter proteins OCT1/2/3 are shown to increase uptake of platinum-based drugs (Cisplatin, Oxaliplatin and Picoplatin) and Imatinib in patient derived Colorectal cancer (CRC) [60-63], OC [62] and Chronic myeloid leukaemia (CML) [64] primary cell lines respectively and served as good prognostic marker. Similarly, OCT1 expression in lymphoma cells was shown to increase the susceptibility to irinotecan and paclitaxel [65]. In opposite OCT1 and OCT2 levels were shown to be downregulated through DNA methylation in Hepatocellular carcinoma (HCC) patients and was associated with progressive disease and reduced overall survival [66-68]. High expression of organic anion-transporting polypeptide 1A2 and organic cation transporter 6 which are involved in the uptake of taxanes and anthracyclines respectively, pre- neoadjuvant chemotherapy serve as predictive biomarker for pathological complete response in triple negative breast cancer patients [69]. Higher expression of Organic anion-transporting polypeptides, OATP1B1 and OATP1B3 were shown to be good prognostic marker in OC and CRC patients, and were shown to increase intracellular uptake of Paclitaxel and Irinotecan respectively [70, 71]. Human copper transporter proteins, hCTR1 and hCTR2 which increase intracellular uptake of platinum-based drugs (Cisplatin and Oxaliplatin), have been extensively shown to be down regulated in OC, NSCLC, Endometroid cancer (EC), CRC and Gastric cancer (GC) patients which are resistant to platinum-based chemotherapy [72-79].

Apart from drug transporter proteins, cancer cells are also known to take advantage of cellular detoxification machinery to inactivate the chemotherapeutic drugs contributing to the drug resistance (Fig. 3) [37]. Aldehyde dehydrogenase (ALDH) primarily known

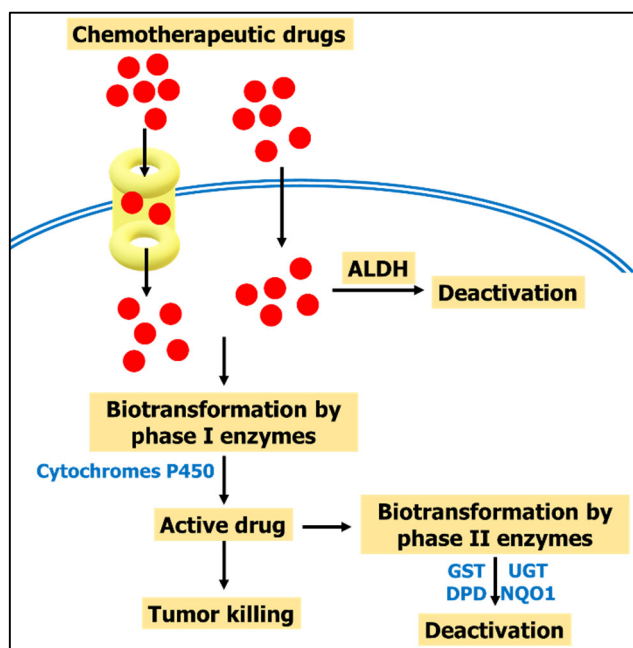


**Figure 3: Drug metabolism pathways**

Pictorial depiction of major drug metabolizing enzymes deregulated in human

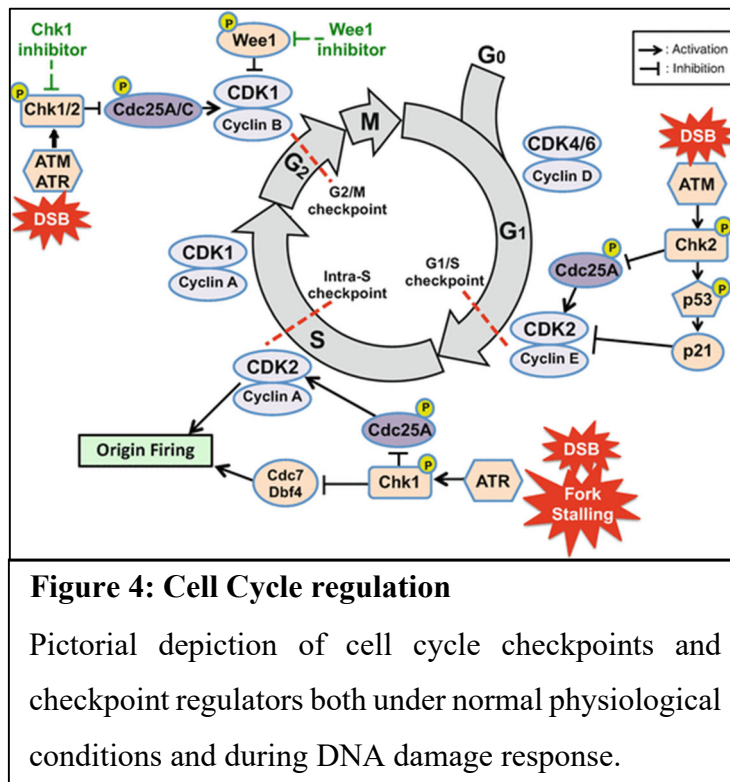
as CSC marker across different cancer types functions as detoxifying enzyme for nitrogen mustard class of antineoplastic drugs such as Cyclophosphamide, Mafosfamide and Ifosfamide [80]. ALDH1A1 and ALDH3A1 were shown to be over expressed in both primary and metastatic Breast cancer (BC), Medulloblastoma, AML and OC patients and served as predictive biomarker by failure of

Cyclophosphamide chemotherapy [81-84]. Biotransformation of the chemotherapeutic drugs mainly involves the oxidation, reduction, and hydrolysis called the phase-I reactions carried by Cytochromes P450, followed by conjugations with hydrophilic compounds such as glutathione and glucuronic acid in phase-II reactions for elimination. [85, 86]. CYP2D6, the P450 catalysing formation of active Tamoxifen metabolites, and UGT2B15, a Phase II enzyme responsible for elimination of these active metabolite were found to be upregulated in BC patients treated with Tamoxifen and showed high risk of disease recurrence and poor survival [87]. Similarly, drug metabolizing enzymes (CYP2C8, UGT2B4 and UGT2B17) and drug transporter (ABCB4) were shown to impart Adriamycin resistance in BC cell lines (MCF-7, MDA-MB-231, and MDA-MB-

468) and predicted poorer survival in BC patients undergone neoadjuvant Adriamycin chemotherapy [88]. Pregnane-X-receptor induced expression of UGT1A1, UGT1A9 and UGT1A10 were shown to impart Irinotecan resistance in CRC cells (LS174T, SW480 and SW620) and overexpression of Pregnane-X-receptor and UGT1A in human CRC negatively correlated with chemotherapy response [89]. Elevated expression of GST- $\pi$  in Osteosarcoma patients was associated with higher relapse rate and a poor clinical outcome and shown to be associated with Cisplatin, Doxorubicin and Methotrexate resistance in U-2OS and Saos-2 Osteosarcoma cell lines [90]. Similarly, in GC patient derived primary cells GST- $\pi$  activity was shown to impart resistance against Cisplatin, 5-Fluorouracil and mitomycin [91]. In prospective study of OC patients who had not undergone chemotherapy, high expression of GST- $\pi$  shown to be bad prognostic marker and was significantly associated with Cisplatin resistance and poor overall survival [92, 93].

### **1.2.2 Altered cell cycle regulation**

Chemotherapeutic agents primarily target actively proliferating cancer cells; hence they majorly rely upon unresolved genotoxic stress and cell-cycle arrest to induce cell death. The fundamental process of cell cycle is tightly regulated by complex interaction between an array of proteins that are also intimately linked to programmed cell death, thus making dysregulation of cell cycle an important mechanism for chemoresistance. Cell cycle progression is regulated by cyclin dependent kinases (CDK), Cyclins (A, B, D and E) and CDK inhibitors along with tumor suppressors (Fig. 4) [94].



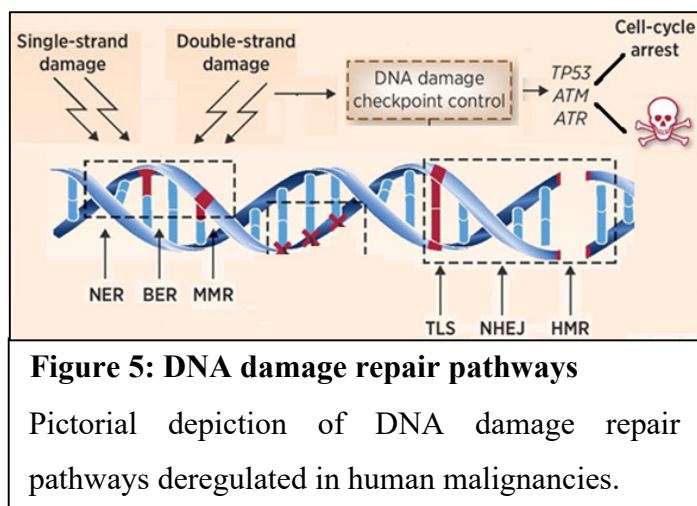
Overexpression of cyclins such as cyclinD1/E1 along with loss of tumor suppressors Rb, TP53, p27<sup>Kip1</sup>, p21<sup>Cip1</sup>, p16<sup>Ink4a</sup> and p14<sup>ARF</sup> that link cell-cycle checkpoints to DNA-damage response pathways and apoptotic pathways leads to aberrant cell cycle progression in cancer cells.

Microarray profiling of epithelial OC cell lines (HeyA8 and SKOV3) and patients resistant to paclitaxel identified upregulation of both expression and activity of CDK1, a central regulator that drives cells through G2 phase and mitosis. Increased expression of CDK1 correlated with Paclitaxel resistance in HeyA8-MDR cells, OVCAR3 and SKO3 Paclitaxel resistant cells [95]. Cell division cycle 25 A (CDC25A), an important molecule for progression from G1 to the S phase of the cell cycle, was shown to be critical for B7-H3 mediated chemoresistance against Oxaliplatin and 5-Fluorouracil in CRC patients [96]. CDC25A was also shown to be important to maintain CSC-like spheroid phenotype in OC patient derived cells. CDC25A impeded cell cycle progression with high level of p21 expression and imparted resistance against Cisplatin and Paclitaxel [97]. Treatment of different chemotherapeutic agents (5-Fluorouracil, Paclitaxel, Doxorubicin, Colchicine and Vincristine) in BC cells (MCF-7, MDA MB231 and T47D) and patient derived primary cultures showed increased expression of p21 and selection of residual cells with senescent phenotype, elevated levels of NRF2 and CSC markers CD133 and Oct4.

Concurrently BC patients undergoing neoadjuvant chemotherapy showed high expression of NRF2, CSC markers Oct4 and CD133 [98]. In Cisplatin-resistant Triple negative BC [99] and Head and neck cancer (HNC) [100], Temozolomide-resistant Glioma [101] and PIK3-inhibitor resistant Glioblastoma [102] increased Wee-1 expression leads to G2-M cell cycle arrest through inhibition of CDK1, which halt DNA replication thus reducing therapy-induced lethality along with activation of CHK1, ATM and ATR responsible for enhanced clearance of DNA damage [99, 103]. The spindle assembly checkpoint antagonist p31<sup>comet</sup> is shown to induce premature securin destruction in Mad2-dependant manner leading to mitotic slippage in cancer cells (HeLa, MCF7, A549, DLD-1, H1299, HCT116, HepG2, HT-29, PC3, SK-N-SH, and U2OS) treated with anti-mitotic drugs, such as taxol, Nocodazole and Monastrol. Moreover, overexpression of p31<sup>comet</sup> rendered cells resistant to apoptosis and this resistance was correlated with p31<sup>comet</sup>/Mad2 protein expression level ratio [104, 105]. Another important kinase involved in spindle assembly checkpoint is Arora-A, commonly overexpressed in many cancers. Arora-A kinase was shown to impart Cisplatin resistance in BC (MCF-7 and MDA-MB-231), Pancreatic ductal adenocarcinoma (PDAC) (PANC-1 and BXPC3) and OC (OVCA420 and OVCA429) cells [106, 107].

### **1.2.3 Enhanced DNA damage repair (DDR) mechanisms**

A complex set of cellular responses are elicited following DNA damage leading to activation of DDR pathways depending on type of DNA damage which mainly includes, base excision repair (BER), nucleotide excision repair (NER), mismatch repair (MMR), trans-lesion DNA synthesis (TLS), homologous recombination repair (HMR) and nonhomologous end joining repair (NHEJ) pathways (Fig. 5) [108]. Cancer cells show dichotomy when it comes to DDR pathways, while defects in DDR pathways enable



tumor cells to accrue genomic alterations (loss of tumor suppressors and gain of oncogenes or oncogenic mutations) contributing to disease progression, cancer cells also heavily rely on DDR pathways to endure therapy

induced genotoxic stress for cell survival.

Heterodimeric endonuclease complex, excision repair 1 endonuclease non-catalytic subunit (ERCC1) and excision repair 4 endonuclease catalytic subunit (ERCC4) play important in NER, TLS and HMR DNA repair pathways. Overexpression of ERCC1 and ERCC4 were found to be associated with poor response to platinum-based chemotherapy and expression of both were found to be elevated in patients undergoing platinum-based chemotherapy in many cancer types including, OC [109], Melanoma [110], NSCLC [111], BC [112], GC [113], HNC [114] and Bladder cancer (BLAC) [115]. Like Cisplatin, CCR1 was also shown to be overexpressed in Anthracycline and taxen resistant early stage or locally advanced BC patients [116]. In Cisplatin resistant OC cells (A27820 and PEO14) and Melanoma cells (A375) Cisplatin treatment was shown to upregulate ERCC1 expression in MAPK/ERK dependent manner [117, 118], whereas, ERCC1 expression was induced post Cisplatin treatment by Snail transcription factor in HNC [114]. CCR1-CCR4 induction post drug treatment showed increased NER as well as TLS activity leading to enhanced clearance of DNA lesions and adducts. The TLS DNA damage tolerance pathway enables cells bypass the single stranded DNA lesions during DNA replication, wherein replicative DNA polymerase is momentarily substituted by a

TLS specific polymerase (pol  $\zeta$  or  $\eta$ ) [119]. Increased expression of REV3L (catalytic subunit of pol  $\zeta$ ) was associated with poor clinical response to chemotherapy and disease progression in NSCLC, Glioma, Oesophageal squamous cell carcinoma (OESCC) and Cervical cancer (CC) [120-123]. REV1 (TLS scaffold protein) and REV7 (TLS adaptor protein) were also shown to impart resistance against Adriamycin and Cisplatin in p53-mutated BC cells (MDA-MB-231 and T-47D) [124] and Ovarian clear cell carcinoma cells (ES-2 and KOC-7C) [125] respectively and were associated with reduced progression free survival.

Cancer cells are also shown to heavily rely of NHEJ DNA repair pathway to rapidly resolve the chemotherapy induced genotoxic stress. In HCC, OC and CRC patients resistant to Cisplatin and 5-Fluorouracil respectively, augmented expression of X-ray repair cross-complementing-like factor (XLF), which interacts with ligase-IV/XRCC4 and enhances end-joining process, was shown to be associated with poor progression free survival [126-128]. Both HCC (HCT116 and LS174T) and CRC (PLC/PRF/5, Huh7 and MHCC97H) cell lines post drug treatment (5-Fluorouracil, Oxaliplatin and Doxorubicin) showed increased expression of XLF and enhanced NHEJ activity [126, 127]. Similarly, HCC cells resistant to 5-Fluorouracil or Oxaliplatin (HCT116 and LS174T) and Glioblastoma cells resistant to Temozolomide (LN18 and U87) showed increased expression of XLF and enhanced NHEJ activity [127, 129]. Another important molecule in NHEJ DNA repair pathway, catalytic subunit of DNA-dependent protein kinase (DNA-PKcs) which regulates the Artemis endonuclease activity responsible for holding the two broken ends of DNA molecules together, was shown to be overexpressed in Mitoxantrone or Chlorambucil resistant B-cell- Chronic lymphocytic leukaemia (CLL), Carboplatin resistant OC and Anthracycline resistant BC patients. Increased expression of DNA-PKcs was associated with poor therapy response, progression of disease and

poor overall survival [130-135]. Mechanistically the heightened NHEJ activity in patient derived Chlorambucil resistant B-cell-CLL primary cultures was due to both increased expression of DNA-PKcs and increased DNA binding of Ku70/80 which recruits DNA-PKcs at double stranded DNA breaks [130].

Several of the HR pathway genes like ARID1A, BRCA1 BRCA2, ATM, CHECK2 and ATRX are either mutated or epigenetically silenced in many cancer types [136, 137] and has been associated with genetic instability that drives cancer progression and sensitivity of cancers to chemo/radio therapy. Though HR pathway is impaired cancers cells are shown to override these impairments either by circumventing the classical mechanisms or re-expression of inactivated HR genes [138]. RAD51 and RAD52 were shown to be responsible for active HR activity in BRCA deficient B-cell ALL, CLL, PDAC, OC, and BC patients [139-144]. RAD51 and RAD52 recruitment at DNA double strand breaks was shown to be independent of BRCA1/2 in PARP inhibitor resistant Breast cancer and Ovarian cancer cells [139, 141, 142]. Further it was shown that RAD51 recruitment at DNA double strand breaks was ATR dependent and blocking ATR disrupted RAD51 recruitment and stalled forks in PARP inhibitor resistant OC cells [142].

### **1.2.4 Cellular plasticity**

Tumors are heterogenic in nature and exhibit a high degree of aberrations in transcriptional and epigenetic pathways that drive the phenomenon of cellular plasticity enabling tumor cells to toggle between different cellular phenotypes. EMT and de-differentiation of tumor cells into stem cell like cells are the two cellular plasticity process that can rewire the cellular programs leading to transient or enduring chemoresistant tumor cells [145-147]. EMT and CSC, though identified as two distinctive phenomena, the growing body evidence suggest cross-talk between the underlying regulatory

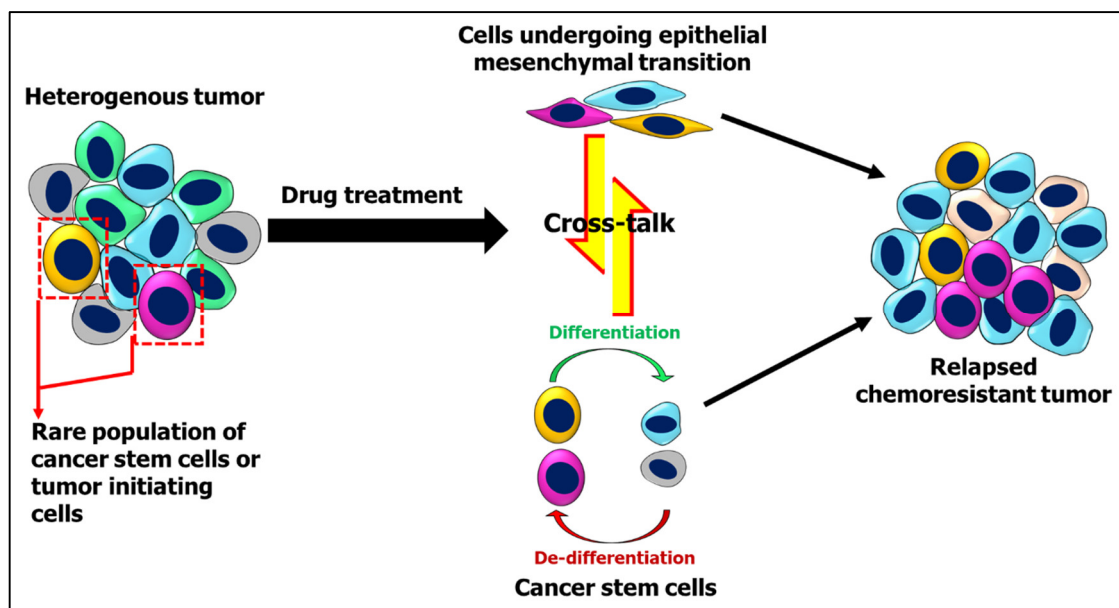


**Figure 6: Cellular plasticity of cancer cells**

Pictorial depiction of dynamic cellular plasticity driving EMT and CSC phenotype in heterogenous tumor populations and their crosstalk.

mechanisms leading to tumor maintenance, metastasis, and therapy resistance (Fig. 6) [148].

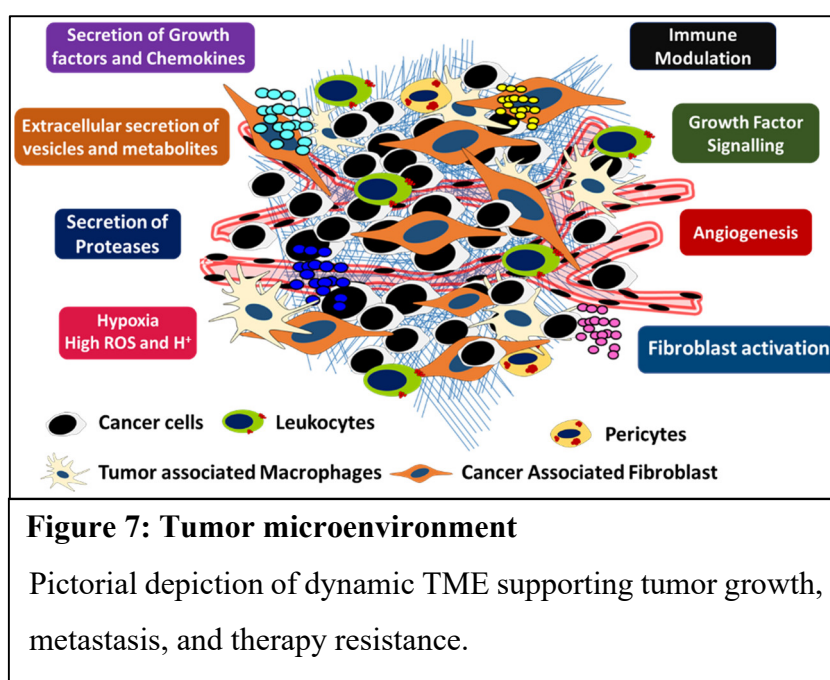
CRC patients undergoing adjuvant Oxaliplatin and 5-Fluorouracil chemotherapy overexpression of Twist1 or Hes1 overexpression was associated with higher recurrence rate and poor overall survival. Twist1 and Hes1 promoted EMT and chemoresistance against Oxaliplatin and 5-Fluorouracil *in vitro* in CRC cell lines (SW480, HCT116, RKO and HCT8) through upregulation of drug transporters ABCC1, ABCC2 and MDR1 [149, 150]. Quiescent/slow cycling cells with stem cell features derived from chemo naïve CRC patients showed increased expression of EMT transcription factor (Zeb2, Snail1 and Slug) and stem cell markers (Bmi1, CD133 and Nanog). Patients undergoing 5-Fluorouracil chemotherapy and Colorectal cancer cell lines post 5-Fluorouracil treatment showed increased expression of Zeb2, activated apoptosis signal-regulating kinase 1 and c-RAF signalling leading to enrichment of cells with stemness/EMT phenotype and was associated with poor chemotherapy response [151]. Similar crosstalk between EMT and

CSC phenotype was reported in two other studies of CRC patients. E3-ubiquitin ligase FBXW7 loss led to increased levels of Zeb2 mediating enrichment of CSCs, metastasis and 5-Fluorouracil chemoresistance [152], whereas increased expression of integrin-linked kinase was shown to be associated with tumor progression, EMT, CSC markers and therapy resistance against 5-Fluorouracil and Oxaliplatin [153]. Pre-chemotherapy high level of CSC<sup>+ve</sup>/EMT<sup>+ve</sup> circulating tumor cells (CTCs) were correlated with increased risk of lung metastasis and decreased progression free survival in BC patients and chemotherapy (taxen or anthracycline) resulted in significant increase in incidence of CSC<sup>+ve</sup>/EMT<sup>+ve</sup> CTCs [154]. Primary cultures derived from recurrent BC tumors, pro-apoptotic protein-4 was epigenetically silenced by EMT transcription factor Twist1 and pharmacological inhibition of EZH2 and HDAC1/2 relieved repression of pro-apoptotic protein-4 making primary cultures sensitive to Docetaxel and Vincristine [155]. CSC marker Nestin and EMT transcription factors Zeb1 and Slug were shown to impart resistance against Doxorubicin, 5-Fluorouracil, Adriamycin and Oxaliplatin in HCC cells through activation of Wnt/ $\beta$ -catenin and protein kinase C alpha activation respectively and was associated with shorter progression free survival and overall survival [156, 157]. Similarly, Zeb1 expression was shown to be predictive biomarker for poor Temozolomide response and poor overall survival in Glioblastoma patients [158]. Chemotherapy-induced lncRNA-1 and SOX8 were independently associated with as poor prognosis in Tongue squamous cell carcinoma (TSCC) and were found to be overexpressed in Cisplatin resistant TSCC patients. Both Chemotherapy-induced lncRNA-1 and SOX8 activated Wnt/ $\beta$ -catenin pathway by inducing expression of Frizzled-7 and Wnt5A respectively, promoted both EMT and CSC phenotype and maintained Cisplatin resistance in TSCC cells [159, 160]. Overexpression of miR-128-3p in NSCLC was associated with poor response to Cisplatin chemotherapy, shorter

progression free period and poor overall survival. Moreover, miR-128-3p was overexpression was negatively correlated with negative regulators of  $\beta$ -catenin Axin1, SFRP2 and WIF1 in NSCLC patients [161]. In patient derived CSCs from PDAC and OC patients enhanced activation of CHEK1 and increased NF $\kappa$ B activity were shown to promote EMT and mediate resistance against Gemcitabine and Cisplatin respectively [162-166]. OC tumor derived CSCs also show increased expression of DNA polymerase  $\eta$  (Pol  $\eta$ ) which drives enhanced DNA repair through trans-lesion DNA synthesis and mediate Cisplatin resistance[167].

### 1.2.5 Tumour microenvironment (TME)

Cancer cells lose cell-cell and cell-basement membrane contacts (tight junctions and cadherin junctions) that maintain tissue architecture and secrete extracellular proteases,



metastasis and therapy resistance (Fig. 7) [168].

Fibroblasts are quiescent stromal cells which are activated during wound healing and extensively modulated in TME. Stimuli from cancer cells and immune cells in TME leads to activation of fibroblast that are known as cancer associated fibroblasts (CAFs) [169].

growth factors, chemokines that leads to aberrant vasculature, activation of fibroblasts and modulation of tumor infiltrating immune cells that support tumor growth,

Interleukin 6 secretion by CAFs has been shown to promote EMT in cancer cells, maintain CSC phenotype and promote chemoresistance in Oesophageal adenocarcinoma (OEAC), GC, OC and NSCLC [170-173]. High serum IL6 levels in OEAC and increased IL6 in tumor stroma of NSCLC patients was correlated with EMT and predicted unfavourable responses to neoadjuvant chemotherapy. OEAC and NSCLC patient derived CAFs were shown to induce IL6 mediated EMT in OEAC primary cultures and induce TGF $\beta$  expression in NSCLC cancer cells (A549 and NCI-H358) respectively, promoting resistance against Carboplatin and Paclitaxel [170, 171]. Stromal secretion IL6 was positively correlated with increased expression of ALDH1A post neoadjuvant chemotherapy in OC patients. The OC omental derived CAFs promoted enrichment of ALDH1A positive CSCs in OC cell lines (A2780, OVCAR4 and Kuramochi) post Cisplatin treatment through IL6 mediated STAT3 signaling [173, 174]. Secretion of TGF $\beta$  and TIAM1 by CAFs was associated with poor therapy response and poor prognosis of CRC patients. Under hypoxic conditions TGF $\beta$  mediated activation of HIF1 $\alpha$  and GLI2 or TIAM1 induced expression of Nanog, Oct-4, and ALDH in CRC cell lines (HCT116 and SW480) induced CSC enrichment and chemoresistance against 5-fluorouracil Oxaliplatin and Irinotecan [175, 176].

Tissue resident or myeloid derived tumor infiltrating macrophages are known as tumor associated macrophages (TAMs) and are known to secrete pro-inflammatory cytokines like IL6, IL13, IL10, I $\beta$  and TGF $\beta$  which are involved in both tumor development and modulation of other immune cells in TME [177]. IL34 secretion by Doxorubicin-resistant A549 and Cisplatin-resistant H1299 LC cells, induced monocyte differentiation into immunosuppressive M2-macrophages. Doxorubicin or Cisplatin treatment in primary lung adenocarcinoma cells induced IL34 secretion and increased expression of IL34 significantly correlated with poor prognosis of LC patients [178]. CRC patients

undergoing 5-Fluorouracil, Oxaliplatin and Leucovorin treatment, increased expression of IL6 was associated with poor chemotherapy response and was positively correlated with increased expression of drug transporter MDR1 and anti-apoptotic protein BCL2. CRC cell lines (DLD1, HCT-8, HT-29, and LoVo) suppressed miR-155-5p levels, a negative regulator of IL6, in macrophages, promoted IL6 secretion and in turn IL6 induced MDR1 and BCL2 in CRC cells [179]. In PDAC increased infiltration of M2-TAMs was associated with increased peritoneal metastasis. Patient derived M2-TAMs promoted EMT of PDAC cell lines and increased resistance to Gemcitabine [180].

Altered metabolic pathways foster the never-ending demand of energy and essential building blocks in tumor cells leading to high ROS generation in TME [181]. FOXO3a is negatively regulated by PIK3CA/AKT pathway, while under ROS stress conditions it induces p27 dependent growth arrest in G1 phase and transcriptionally activates stress related genes such as MnSOD and GAD45A. In Cisplatin resistance OC cells (A2780-CisR, SKOV3 and CAOV-3) SIRT5 induces MnSOD and SOD2 through activation of FOXO3a and NRF2 [182]. ROS induced HIF-1 $\alpha$  stabilization promotes EZH2 dependent proliferation and cisplatin-resistance in CRC cell lines SW480 and HT29 [183]. The drug (Docetaxel or Doxorubicin or 5-FU) induced multinucleated giant cells were shown to dependent on elevated levels of ROS-induced HIF-1 $\alpha$  in regulation of chemoresistance in TNBC cell lines MDA-MB-231 and MDA-MB-468. These MNGCs secreted vascular endothelial growth factor and macrophage migration inhibition factor, activating RAS/RAF/MAPK pathway to induce anti-apoptotic proteins BCL2 and BCL-XL and downregulation of pro-apoptotic proteins BAK and BAX [184].

### **1.2.6 Evading cell death and promoting cell survival**

Defying cell death and fostering cell survival underpin both tumorigenesis and chemoresistance. B-Cell Lymphoma family member anti-apoptotic proteins (BCL2,

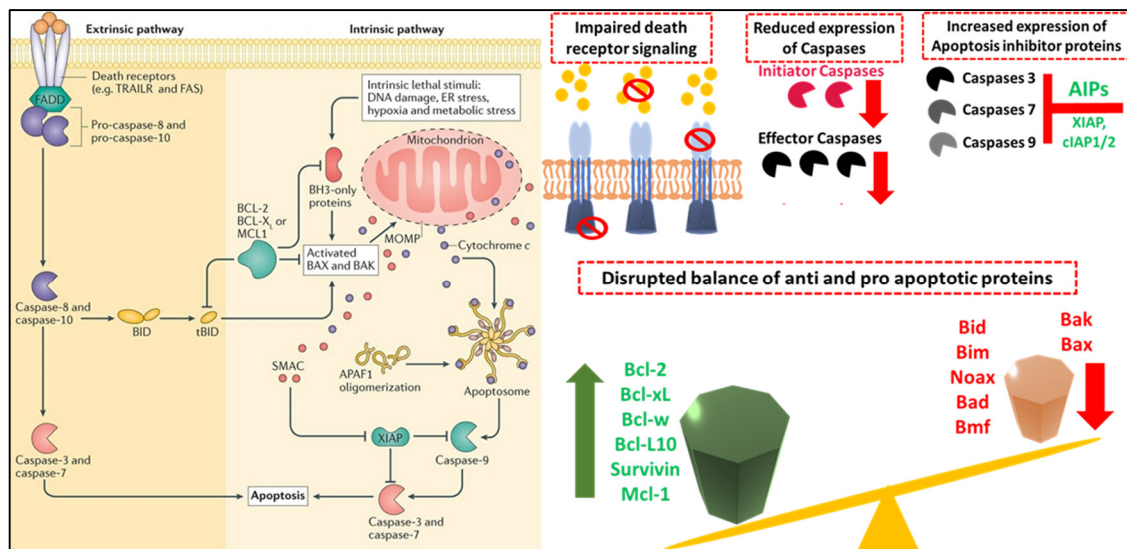


**Figure 8: Deregulation of apoptotic pathways in cancer**

Extrinsic and intrinsic apoptotic pathways and their deregulation in cancer by impaired death receptor signaling, reduced expression of caspase, increased expression of negative regulators of apoptosis (IAPs) and disrupted balance of anti and pro-apoptotic proteins.

BCL-xL, BCL-W, Mcl-1 and BCL2a1) promote cell survival by primarily direct binding and confiscation of executioner proteins, BAX and BAK. On the other hand, BH3-only pro- apoptotic proteins promote apoptosis either by direct activation (Bim and tBid) of BAX and BAK or by hindering binding of anti-apoptotic proteins (Noax, Bik, Bad, Bmf, Hrk and Puma) to BAX and BAK. Another important class of proteins involved in regulation of apoptosis are inhibitor of apoptosis proteins, which prevent activation of caspases [185, 186]. Defects in cell death pathways in combination with deregulated cell signaling pathways help cancer cells to endure genotoxic stress induced by chemotherapy (Fig.8).

Increased expression of anti-apoptotic protein BCL-2 and downregulation of pro-apoptotic protein Bax, have been linked to poor chemotherapy response and promote chemoresistance in many cancer types including, BC (Paclitaxel and Anthracycline), B-cell CLL (Chlorambucil), GC (5-Flurouracil), OC (Cisplatin and Paclitaxel) and LC (Cisplatin) [187-191]. Overexpression of miR-650 in LC patients was shown to be

associated with poor response to Docetaxel-based adjuvant chemotherapy, shorter disease-free survival and served as poor prognosis marker. Docetaxel treatment in LC cell lines (SPC-A1 and H1299) was shown to induce miR-650, which downregulates tumor suppressor inhibitor of growth-4 responsible to maintain levels of BCL2 and BAX. Downregulation of ING4 increased Bcl-2 expression and decreased BAX levels promoting cell survival, moreover inhibitor of growth-4 down regulation was negatively correlated with miR-650 and BCL-2 expression in LC patients [192]. Similarly, in GC patients decreased expression of inhibitor of growth-4 was associated with 5-Fluorouracil resistance though upregulation of BCL-2 and down regulation of BAX and negatively correlated with miR-4516 expression [193]. BCL-xL and Mcl-1 are another two important anti-apoptotic proteins that sequester BAK/BAX and inhibit apoptosis. Increased expression of both BCL-xL and Mcl-1 have been found to be associated with poor chemotherapy response and recurrent chemoresistant tumors in OC and promote resistance against Cisplatin, Paclitaxel, Topotecan and Gemcitabine in OC tumor xenografts overexpressing BCL-xL [194]. Mitochondrial phosphoglycerate mutase/protein phosphatase-5 was shown to stabilize the Bcl-xL and prevent Bax mediated apoptosis and increased expression of phosphoglycerate mutase/protein phosphatase-5 was shown to be associated with 5-Fluorouracil resistance in HCC patients [195]. Oral squamous cell carcinoma (OSCC) patient derived primary cultures and cell lines resistant to Docetaxel, Cisplatin and 5-Fluorouracil showed mRNA upregulation and protein stabilization of Mcl-1 by STAT3 and AKT/GSK3 $\beta$  signaling pathways respectively [196]. Increased expression of the IAPs, X-linked-IAP, Cellular-IAPs (cIAP1 and cIAP2) and baculoviral inhibitors of apoptosis proteins repeat-containing-6 were shown to be associated with poor chemotherapy response and shorter disease-free intervals in OC, NSCLC, BC, HCC, HNC and Lymphoma [197-203]. USP9X, a mitotic

deubiquitinase was shown to stabilize the X-linked-IAP in B-cell lymphoma primary cells leading to increased resistance to mitotic inhibitors such Paclitaxel, Nocodazole and Doxorubicin [202], whereas Pellino-1 is an E3 ubiquitin ligase, was shown to stabilize the cIAP1 and cIAP2 by polyubiquitination post Cisplatin/Paclitaxel treatment in LC cells (A549 and H1299) and conferred resistance to Cisplatin/Paclitaxel induced apoptosis [200].

Altogether, these mechanisms converge on evading apoptosis and promoting cell survival thus helping cancer cells to withstand chemotherapeutic challenge. Underlying these mechanisms are aberrant gene regulatory networks and intricate network of signaling pathways that are activated by membrane receptors (growth factor receptors, G-protein-linked receptors, chemokine receptors and integrins) which are often deregulated in cancer and serve as interface between cancer cells and tumor microenvironment [204-208]. While majority of these receptors are overexpressed in different cancer types with high degree of genetic alterations (amplification, oncogenic fusions and activating mutations), Insulin like growth factor 1 receptor (IGF1R) was found to be more commonly overexpressed across different cancer types with low level of amplification (3-6% in Sarcoma, Breast cancer, Ovarian cancer, Esophageal and Stomach adenocarcinoma) and lack of activating oncogenic mutations [209, 210]. In a comprehensive study of 152 human carcinoma samples and 63 normal tissue (samples from 15 different anatomical sites), membrane IGF1R expression was found to be between 50-100% in 10 out of 15 different cancer types, which includes ovarian cancer, endometrial cancer, bladder cancer, colon cancer, breast cancer, lung cancer, gastric cancer, pancreatic cancer, prostatic cancer and liver cancer [211]. Also, overexpression of IGF1R has been strongly correlated with loss of tumor suppressor genes (TP53,

BRCA1/2, WT1 and VHL) [212], a hallmark of cancer and thus shedding light on pragmatic role of IGF1R in tumorigenesis across different cancer types.

### 1.3 Insulin-like growth factor signalling

Identification of a hormonally controlled serum factor promoting cellular proliferation lead to subsequent discovery of growth hormones and receptors that share homology with insulin receptor (IR) and collectively known as Insulin-like growth factor family.

#### 1.3.1 Insulin-like growth factor family

Insulin like growth factor family consist of Insulin receptor, Insulin like growth factor 1 receptor and Insulin like growth factor 2 receptor (a decoy receptor that lacks intracellular kinase domain) along with ligand Insulin, IGF1 and IGF2 respectively and IGF-binding proteins (IGFBP) (Fig. 9) [213]. Although IR signalling plays important role in glucose

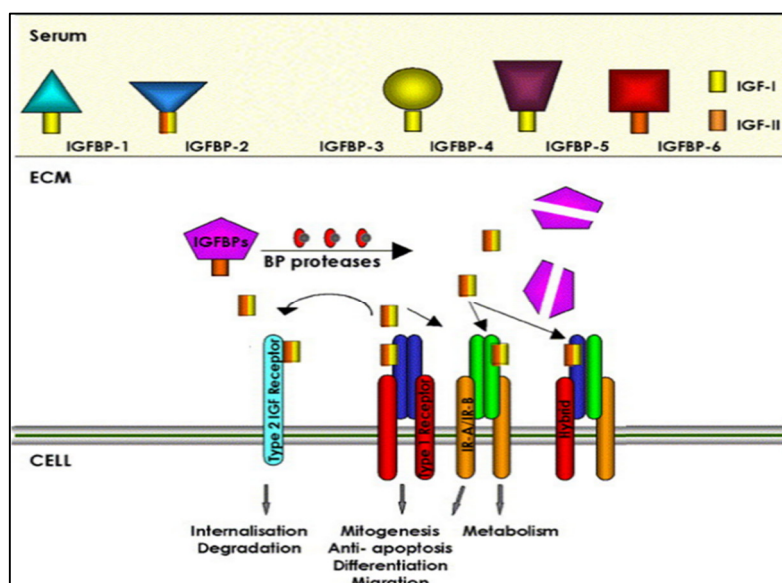


**Figure 9: Insulin like growth factor signaling**

The IGF1R and IR receptors bind to IGF1/2 and Insulin respectively. The IGF2R acts as a decoy receptor competing with IGF1R for ligand binding. The serum-IGFBPs modulate bioavailability of ligands.

metabolism and IGF1R plays critical role in cellular proliferation, metabolism, protein synthesis and cell survival [214], IGF1R and IR share 58% sequence homology and relay downstream signal through largely conserved molecular mechanisms [215]. The

ligands are synthesized primarily in liver and by extra-hepatic cells such as stromal

fibroblast and act in endocrine and paracrine secretions under normal physiological conditions, while cancer cells also secrete the ligands that act in autocrine manner [216]. The IGFBPs control the bio-availability and serum half-life of the ligands is leading to regulation of IGF1R signalling [217]. Cation-independent mannose-6-phosphate receptor or IGF2R primarily transports the lysosomal acid hydrolase precursors but is also involved in negative regulation of IGF1R signalling by acting as a decoy receptor [218].

### **1.3.2 IGF1R structure and signalling**

IGF1R is a homo-dimeric receptor, each subunit is formed from single polypeptide known as pro-IGF1R. The pro-IGF1R polypeptide undergoes a furin-like cleavage into  $\alpha$  and  $\beta$  chains that are linked through disulphide bonds. The mature IGF1R subunit consists of six extracellular domains (L1, CR, L2, Fn1, Fn2, and Fn3), a transmembrane region, a juxta-membrane region, a tyrosine kinase domain and a C-terminal tail [219] (Fig. 10). Unlike other RTKS IGF1R is a pre-formed homodimer and do not require the ligand binding to initiate dimerization. Among the ligands IGF1 has highest binding affinity for IGF1R followed by IGF2. The ligand binding to IGF1R disrupts the autoinhibited IGF1R dimer ( $\Lambda$ -shaped) and triggers conformational reorganization that primes formation of a symmetric active dimer ( $\Gamma$ -shaped), this dimer is then stabilized by extensive interaction of ligand with multiple extracellular domains of IGF1R. These structural reorganizations diminish the distance between the two intracellular domains promoting trans-autophosphorylation of IGF1R (Fig. 10) [220, 221]. Autophosphorylation of three tyrosine residues (Tyr-1135, Tyr-1131, and Tyr-1136) forms an active receptor which leads to subsequent binding of adaptor proteins IRS1/2 and SHC which relay the activation signal through two different arms PIK3CA/AKT and MAPK/ERK respectively [222, 223]. While IGF1R activation mainly happens after

ligand binding, it has also been reported to form ternary complexes with integrins and GPCRs leading to its activation [224-226].

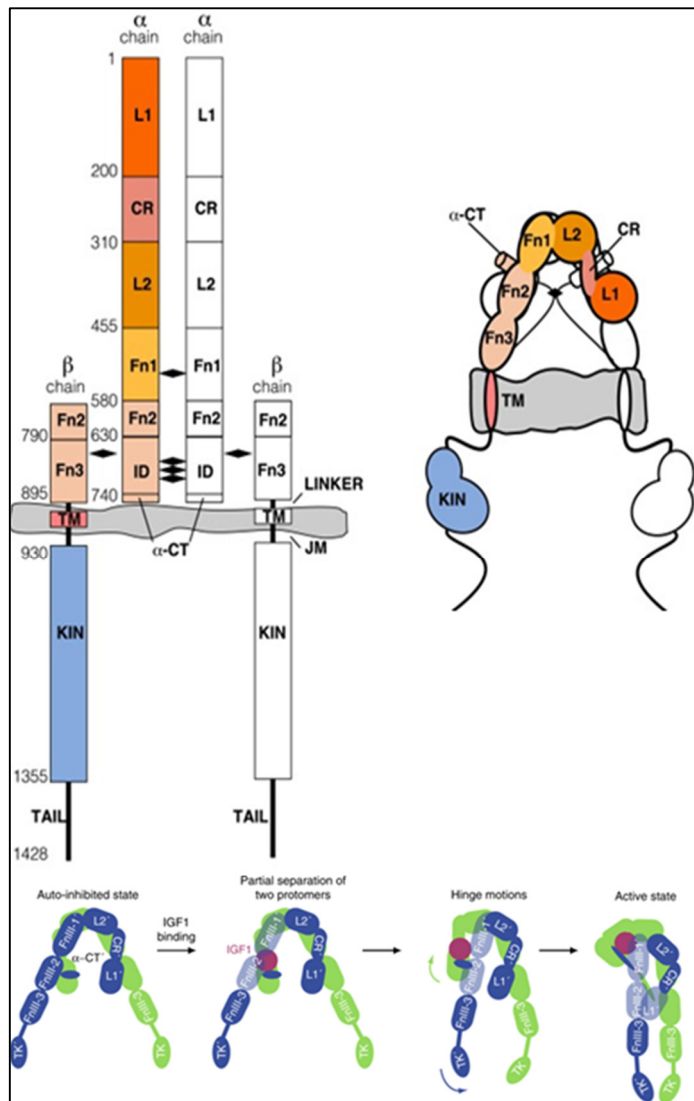


**Figure 10: Schematics representation of IGF1R structure and activation**

IGF1R homo-dimeric receptor with monomers bound bisulfide linkages, upon ligand binding undergoes conformational change leading to trans-autophosphorylation of receptor.

Germline deletion of the both IGF1R alleles results in severe growth retardation and fibroblast established from IGF1R knockout mice show impaired cell cycle and resist neoplastic transformation by viral and cellular oncogenes [227]. The knockout studies involving either IGF1R or IGF1/2 established IGF1R as an important growth hormone during embryo development and neonatal growth. Activation of PIK3CA/AKT survival pathway downstream of IGF1R antagonizes apoptosis by inhibiting activity of pro-apoptotic proteins BAD [228], BAX [229] and

Caspase9 [230]. It also induces phosphorylation of Mdm2 at S166/188 residues which is necessary for translocation of Mdm2 into nucleus to diminish cellular levels of p53 [231].

Activated AKT also phosphorylates mTOR, p70S6 kinase and elongation factor 4E-BP

inducing protein synthesis machinery [232, 233] as well as induces expression of matrix-metallo proteinase-2 necessary for cell motility [234]. The major effect of MAPK/ERK pathway downstream of IGF1R is induction of proliferation. ERK activation induced CyclinD1 expression thus leading to inactivation of Rb protein and release of E2F1 transcription factor enabling transition of cells from G1 to S [235]. Another direct target of ERK is MAP kinase-interacting serine/threonine-protein kinase-1 which induces phosphorylation of translation initiation factor 4E leading to increase translation of proteins [236]. Furthermore ERK negatively regulates TCS2, an inhibitor of mTOR, either by directly phosphorylating it at S664 residue [237] or through RSK1 at S1798 residue [238], thus contributing to elevated mRNA translation. Receptor internalization and signal attenuation of IGF1R takes place through both clathrin and caveolin routes, in a ligand-dependent manner. After ubiquitination of IGF1R by either Mdm2 [239] or Nedd4 [240] E3 ubiquitin ligases it enters endocytic vesicles. After internalization IGF1R degradation is mediated by both proteasome and lysosomal pathways or again recycled to membrane [241].

### **1.3.3 Role of IGF1R signalling in therapy resistance**

Extensive studies in recent past have unravelled IGF1R signaling as a crucial molecule for cancer cells to proliferate and endure during the multistep process of tumorigenesis and chemoresistance development. The receptor, ligand and IGF1R are found to be deregulated with serious implication in both tumour development and therapy resistance in many cancer types. While many oncogenic signalling pathways show high degree of genetic alterations (amplification, activating mutations and oncogenic fusions), components of IGF1R signaling show low level of amplification while activating mutations are rare, rather IGF1R signalling is heavily deregulated at transcriptional and posttranslational levels in human malignancies.

### 1.3.3.1 Resistance to chemotherapy

The first evidence pointing towards involvement of IGF1R in resistance to chemotherapy came from its ability to inhibit apoptosis in fibroblast cells exposed to various stress stimuli including the chemotherapeutic agents. The 5-FU or Oxaliplatin resistant CRC cells show increased expression of IGF1R and treatment with an anti-IGF1R antibody demonstrated growth inhibition of the resistant tumours [242]. In cohort of 41 CRC patients expression of MicroRNA-143 negatively correlated with IGF1R expression. Overexpression of MicroRNA-143 in SW1116 cells inhibited cell proliferation, migration, tumour growth and increased chemosensitivity to Oxaliplatin [243]. Interestingly in a non-canonical way IGF1R was shown to locate to the nucleus of cells upon ligand activation through sumoylation. Nuclear IGF1R promoted proliferation and migration of human fibroblast, human non-malignant breast epithelial cell line MCF10A, BC cell line MCF7, human normal pancreatic cell line M12 and transformed pancreatic cancer cell line P69 [244]. IGF1R-ChIP-seq identified several regions of chromatin bound by IGF1R in prostate cancer cell line DU145. Among the identified targets IGF1R showed ligand dependent recruitment to promoters of JUN and FAM21 in freshly isolated prostate cancer cells which was inhibited by ligand-neutralizing antibodies [245]. In a cohort of 470 metastatic CRC patients nuclear accumulation of IGF1R has been correlated with poor overall survival [246]. In study involving stromal-cancer interaction, macrophage secreted IGF1 and IGF2 activated IGF1R in SUIT-2 and MIA-PaCa-2 pancreatic cancer cells and conferred resistance to Gemcitabine. In a small cohort of 53 PDAC patient 72% of patients showed activation of IGF1R and positively correlated with infiltration of tumor associated macrophages [247]. In another study radiotherapy was shown to induce IGF1 secretion from cancer associated fibroblasts which activates IGF1R in CRC cell lines HCT8, HT29, and COLO320DM leading to metabolic

reprogramming through mTOR activation, which corroborated with higher mTOR activation in matched paired samples from CRC patients after neoadjuvant chemoradiotherapy [248]. IGF1R signalling is also found to be predominantly active in OC. In a cohort of 109 epithelial OC (EOC) patients IGF2 mRNA level were strongly associated with the grade of disease and poor overall survival [249]. IGF1R or IGF2 overexpression conferred resistance to Cisplatin and Paclitaxel in OC lines HEY, OVCAR-8, SKOV-3, BG-1, and A2780 [250, 251]. We recently reported a pulsatile nature of IGF1R during acquirement of platinum-taxol resistance in EOC cells [252]. The increased IGF1R expression at the onset of resistance plays an integral role in maintenance of drug resistance, cancer stem cells and tumorigenicity, while cells that achieved complete and irreversible resistance possess low level of IGF1R indicating active IGF1R signalling might be dispensable at late stages of resistance [252, 253]. Drug induced enhancement of IGF1R expression was also observed in a small cohort of advanced stage high grade serous EOC patients after 3-4 cycles of platinum-taxol treatment [252]. Along with the receptor and ligands of IGF family the IGFbps were also found to be involved in therapy resistance mechanisms in many cancer types. Temozolamide treatment was shown to induce expression of IGF1R and IGF2 were as decrease the expression of IGFBP6 in Glioma cell lines and patient-derived xenograft cell lines. Also elevated levels of IGF1R and IGF2 were associated with the poor overall survival. Interestingly IGFBP6 secreted by Temozolamide sensitive cells abrogated IGF1R activation in resistant cells leading to decrease proliferation and increased sensitivity to Temozolamide [254]. Similarly, Treatment with IGFBP7 was shown to induce cell death in AML cell lines (HEL, NB4, HL60, K562, KG-1 and Kasumi-1) by inducing cell cycle arrest in G2 phase and decreased tumour growth. Pre-treatment with IGFBP7 sensitized acute myeloid leukaemia cell lines to doxorubicin, etoposide and

cytarabine. Moreover, in a cohort of 102 AML patients, high IGFBP7 expressing patients showed better disease free and overall survival compared to those with low IGFBP7 [255]. In another study IGFBP3 overexpression blocked IGF1 induced cellular proliferation, induced DNA damage and promoted apoptosis in tumours of NSCLC cell lines [256]. IGF1R signalling emerged as one of many signalling molecules that help cancer stem cells endure chemotherapy induced cells death. Picropodophyllin, an IGF1R inhibitor blocked proliferation of leukaemia stem cells and induced apoptosis which was rescued by overexpression of pluripotency transcription factor Nanog. It was found Nanog was overexpressed in CD34+ve populations isolated from acute myeloid leukaemia cells [257]. Chemoresistance model developed against Oxaliplatin of HCC cell line (MHCC97H) both *invitro* and *invivo* identified IGF1/IGF1R signalling pathway that maintains cancer stem cell phenotype and Oxaliplatin resistance in these cells [258]. Radiation induced secretion of IGF1 and upregulation of IGF1R maintains Glioma stem cells and protect against radiation induced cell death. Continuous IGF1 stimulation downregulates AKT and ERK signalling in Glioma stem cells leading to enhanced stabilization of FOXO3a which results in self-renewal, while after radiotherapy increased IGF1R expression protects cells by activation of AKT [259].

### **1.3.3.2 Resistance to targeted therapy**

Advancement in identifying the oncogenic pathways to which cancer cells remain dependent for survival lead to use of plethora of small molecule inhibitors and antibodies that target these pathways. As there were few success stories in targeted therapies many of those eventually showed development of resistance, IGF1R is among the many molecules involved in resistance against targeted therapies.

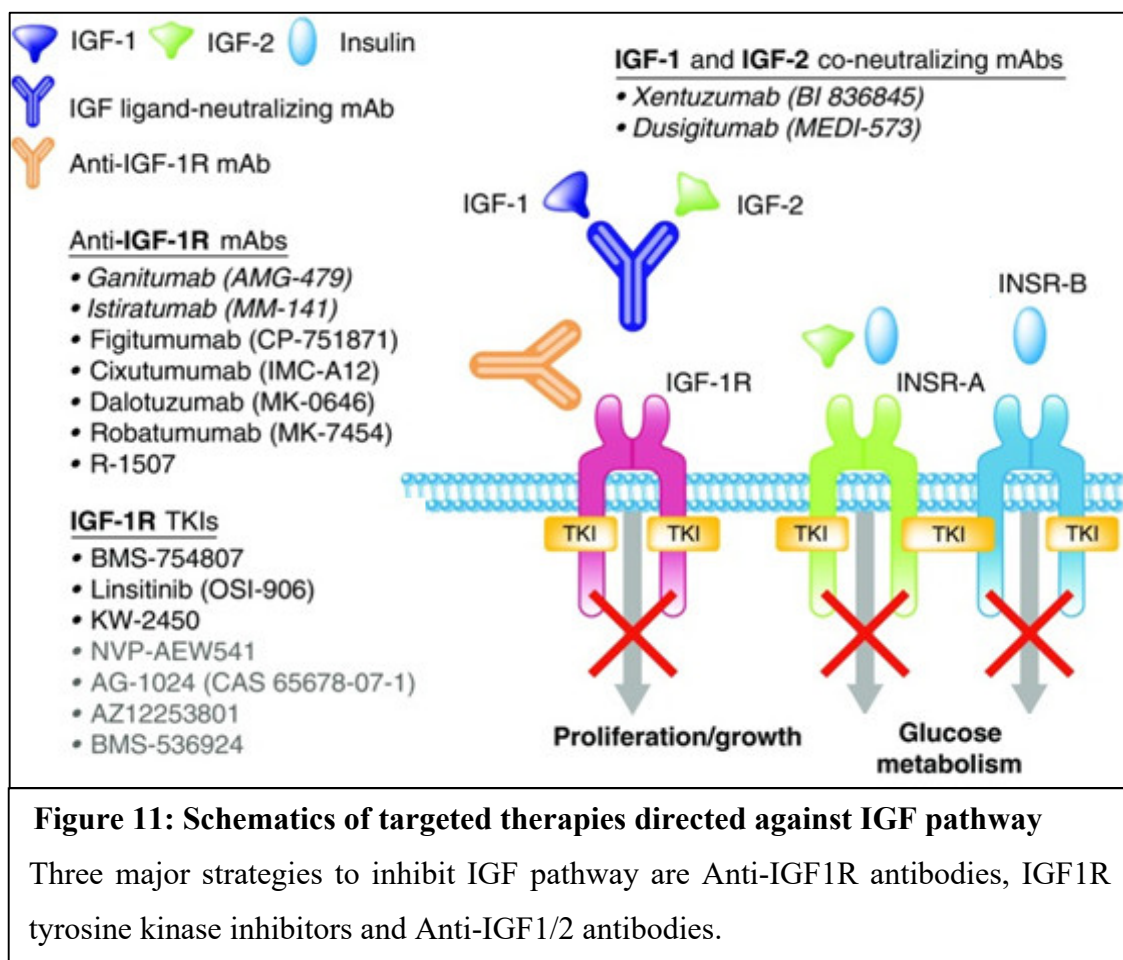
Trastuzumab (Herceptin) a monoclonal antibody against HER2 has improved progression free survival in HER2 overexpressing breast cancer patients, however the

median duration of response was less than one year suggesting gradual development of resistance to Trastuzumab. Augmented IGF-IR membrane staining in 40 operable, stage II/III BC patients was linked with lower response to preoperative trastuzumab plus vinorelbine, with a 50% median response rate in the high IGF1R group versus 97% in the low IGF1R group [260]. Similarly IGF1R overexpression or phosphorylation (inactivation) of pro-apoptotic protein BAD (IGF1R/PIK3CA/AKT target) showed positive correlation with shorter progression free survival in 67 HER2 over expressing BC patients with early stage disease treated with Trastuzumab [261]. Several preclinical studies have shown upregulation of IGF1R in Trastuzumab resistant BC cell lines supporting clinical observations suggesting involvement of IGF1R in mediating Trastuzumab resistance [262-264]. Similarly, IGF1R and HER3 upregulation was associated with Trastuzumab resistant OC cells SKOV3/T [265].

IGF1R is also found to be involved in mediating resistance to small molecule inhibitors. In a 62-patient cohort of NSCLC, High IGF1R expression was poor prognostic factor for response to EGFR tyrosine kinase inhibitors. Patients with higher IGF1R expression had lower progression free survival compared to those with lower IGF1R expression (9.1 vs. 20.1 months) [266]. In another study involving 70 Gefitinib-treated NSCLC patients high IGF1R expression was associated with shorter overall survival (14.7 vs 29.1 months) and progression free survival (4.6 vs 12.0 months) as compared to those with lower IGF1R [267]. Preclinical studies involving EGFR small molecular inhibitors such as Gefitinib, erlotinib, WZ4002 and PF299804 show upregulation or activation of IGF1R signalling mediating resistance to EGFR inhibitors [268-273]. Similarly upregulation of IGF1R expression has been found to confer resistance PIK3 inhibitors such as BYL719, Taselisib and Idelalisib in OC, BC and AML [274-276].

### 1.3.4 Targeting IGF1R

A large body of preclinical experimental evidence showed IGF1R is more commonly overexpressed in many cancer types and plays important role in neoplastic transformation, tumour progression and metastasis. These observations lead to development of targeted therapies against IGF1R which were clinically evaluated but failed to deliver the output due to complexity of pathway involving the IGF1R, shared homology with insulin receptor and majorly due to lack of predictive biomarker and Phase 2/3 trials in unselected patients, ultimately leading to cessation of several clinical trials involving IGF1R. However, in recent development IGF1R has emerged as one of the key signalling molecules underlying the resistance mechanisms against wide range of chemotherapeutic agents and targeted therapies, thus has started re-evaluation of strategies to target IGF1R in cancer. Three major strategies namely, Anti-IGF1R



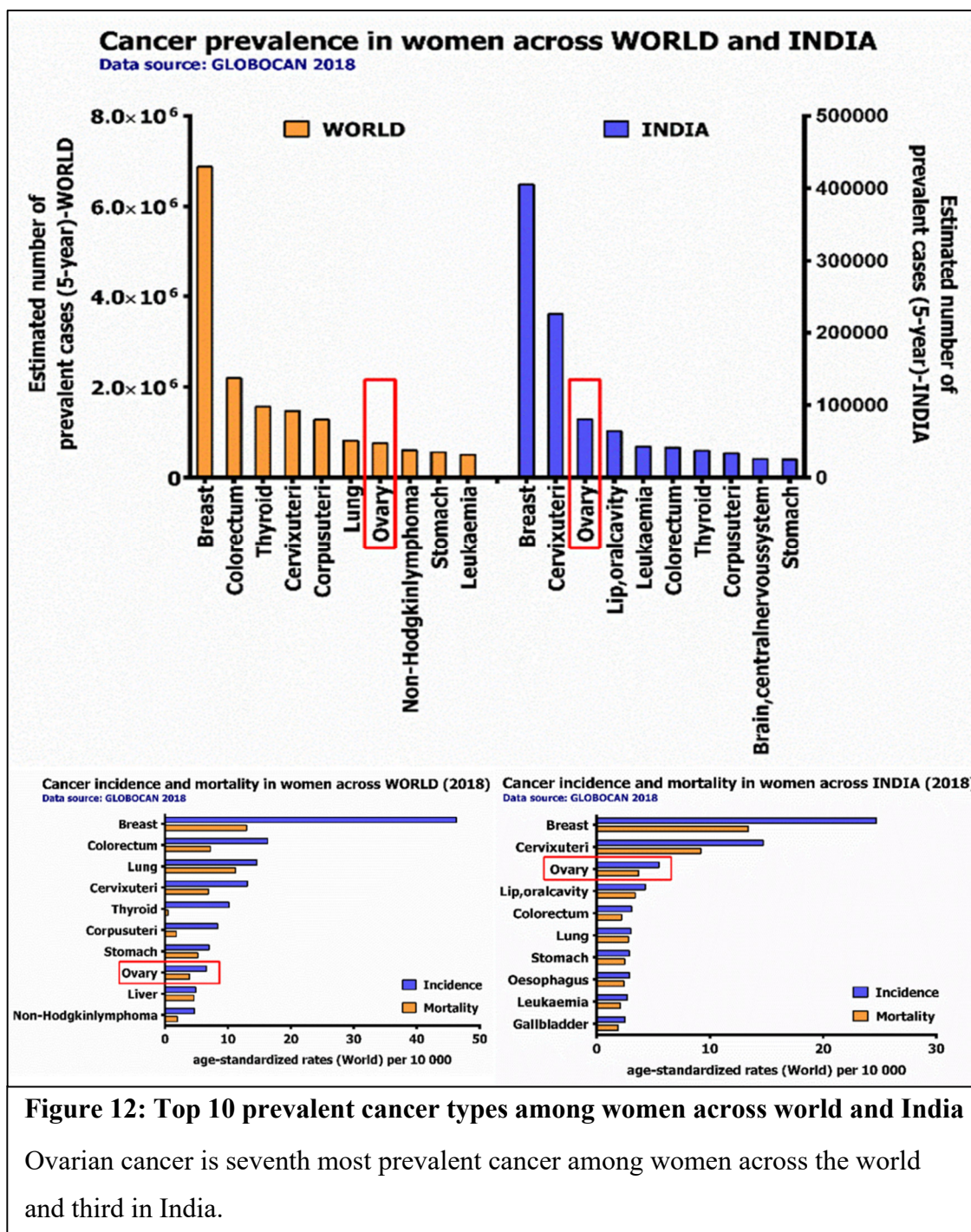
antibodies, IGF1R tyrosine kinase inhibitors and Anti-IGF1/2 antibodies have been utilised to inhibit the IGF system (Fig. 11).

Lessons from failures and mounting evidence showing importance of IGF1R in both tumorigenesis and chemoresistance suggest anti-IGF1R targeted therapies hold therapeutic potential [277-279] and possibly indirect approaches by targeting IGF1R transcription or translation rather than targeting the protein may result in more successful strategy. Hyperactivation of IGF1R signaling pathway in chemoresistance and ubiquitous overexpression of IGF1R and its ligands in many human malignancies has put anti-IGF1R targeted therapies as line of treatment which can be extended to those cancers which solely depended on chemotherapy, have no or limited targeted therapy options and face severe challenges from chemoresistance such as Ovarian cancer.

## **1.4 Ovarian Cancer**

### **1.4.1 Epidemiology**

Ovarian cancer is seventh most prevalent cancer among women across the world and third in India (Fig. 12) [280-282]. The cause behind ovarian cancer are poorly understood, however low parity, lactation, use of contraception, age at menopause and familial history of breast and ovarian cancer are known risk factors associated with the disease. Among the gynaecological malignancies the mortality rate remains high for ovarian cancer and is seventh leading cause of the death due to malignancies in women across world and third in India (Figure 12) [280-282]. Ovarian cancer though highly heterogeneous disease with distinct clinicopathological features and prognosis, has been treated as single disease. However extensive studies on genetic landscape of Ovarian cancer has revealed distinct molecular features associated with heterogeneity of the disease [283].



### 1.4.2 Classification

Ovarian cancer is broadly classified into three categories epithelial, germ cell and sex cord-stromal cell carcinoma depending upon the site of origin (Fig. 13). More than 90% of ovarian cancers are of epithelial origin and are believed to originate from surface epithelium of ovaries, however the site of origin is debatable, and some evidence suggest

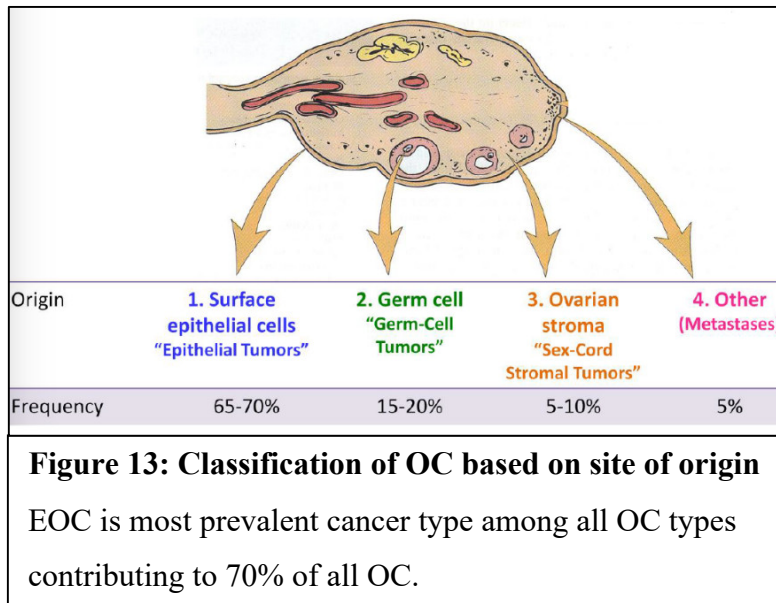


**Figure 13: Classification of OC based on site of origin**

EOC is most prevalent cancer type among all OC types contributing to 70% of all OC.

some of these could be of fallopian origin. The EOC are further subdivided into four subtypes, serous (70%), endometrioid (15%), mucinous (5%), clear cell (5%) and mixed or carcinosarcomatous

müllerian tumours (less than 5%) based on histology (Fig. 13) [284]. More recently, depending on molecular and clinical features EOCs are being reclassified as type I and type II tumors. The type I tumors include low grade serous, clear cell, endometrioid and mucinous tumors, which predominantly characterized by lack of both Tp53 and BRCA

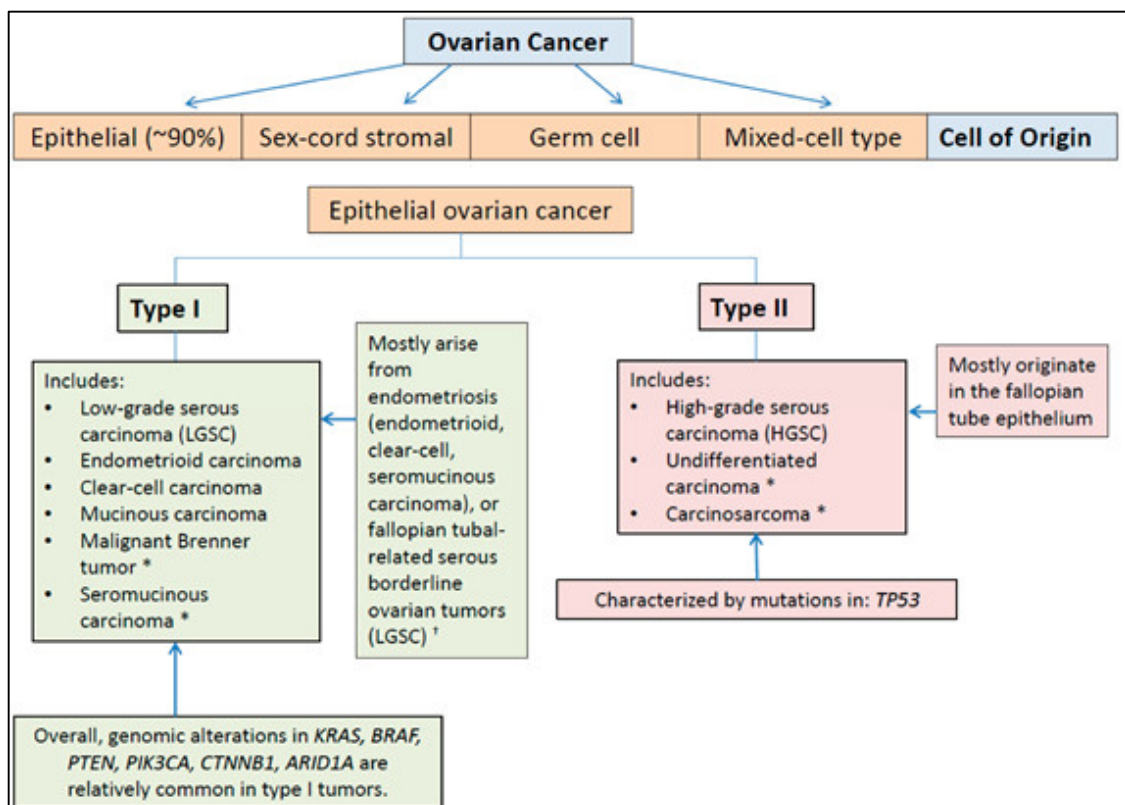


**Figure 14: Classification of OC based on clinical and molecular markers**

mutations and harbour activating mutations in BRAF, KRAS and  $\beta$ -catenin, high microsatellite instability. On the other hand, type II tumors include high grade serous and mixed type tumors, which show frequent Tp53 mutations (>80%), PIK3CA and AKT amplification (Fig. 14) [284].

### 1.4.3 Diagnosis and staging

Unlike other malignancies diagnosis of ovarian cancer is difficult and remains a challenge for early detection. Majority of the EOC symptoms overlap with other gynaecological and gastrointestinal diseases and thus remains under diagnosed. While abdominal swelling along with increased in peritoneal fluid (which contains malignant ascites) is an observable symptom, diagnosis of EOC mainly performed using transvaginal ultrasound and measuring the serum CA125 levels. While serum CA125 remains gold standard in EOC diagnosis, a combination of other serum markers has been identified such as human epididymis protein 4, carbohydrate antigen 19-9, and carcinoembryonic antigen [285]. The positron emission tomography, computed tomography and magnetic resonance imaging are often utilized for staging of disease, treatment planning and follow up [286]. Ovarian cancer is briefly classified into four main stages of disease progression (Stage I to IV) which are further subclassified according to the International Federation of Gynaecology and Obstetrics of classification [287].

### 1.4.4 Disease management and treatment

Since majority of the times EOC is detected at late stage of the disease the primary therapy plan mainly involves a combination of either upfront debulking surgery followed by six cycles of adjuvant chemotherapy when disease is operable at diagnosis, if not debulking surgery is done after 3 cycles of neo-adjuvant chemotherapy followed by another 3 cycles of adjuvant chemotherapy (Fig. 15) [288]. The debulking surgery is

performed with intent of complete macroscopic resection of tumor, while adjuvant chemotherapy is given for residual microscopic disease.

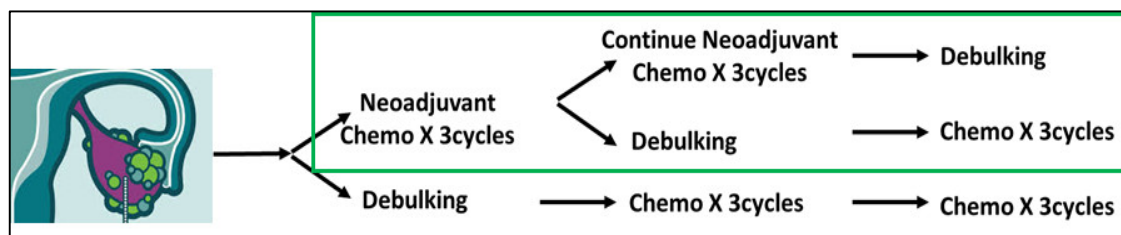


**Figure 15: Primary treatment modalities for EOC**

The two different treatment strategy for EOC. Option 1 where surgery is followed by six cycles of adjuvant chemotherapy and option 2 where surgery is done after neoadjuvant chemotherapy.

Primary chemotherapy for EOC is a combination of platinum-based compound (Cisplatin or Carboplatin), inducing DNA adducts and Paclitaxel which stabilizes microtubule polymerization. Nearly 80% of patients show clinical response to platinum-taxol treatment, whereas remaining 20% of the patients either don't respond or progress during platinum-taxane based therapy, these patients are termed as platinum-refractory. The patients which initially responded to first line platinum-taxol chemotherapy relapsing within 6 months of drug free interval are termed as platinum-resistant, while those relapse after 6 months are termed as platinum-sensitive. Platinum sensitive patients are continued on platinum based second line chemotherapy, the platinum refractory and resistant patients are given second line of therapy such as liposomal Doxorubicin and Paclitaxel, Etoposide or Topotecan (topoisomerase inhibitors) Gemcitabine (nucleoside analogue) and Tamoxifen (oestrogen antagonist) [289]. PARP inhibitors in combination with chemotherapy remains the only approved first line targeted therapy for patients with BRCA gene mutations [290], whereas PARP inhibitors and anti-angiogenic therapy (Bevacizumab) are approved as maintenance therapy for platinum-sensitive relapsed disease [291].

**1.4.5 Chemoresistance in EOC**

The current treatment modalities have improved the life quality and expectancy of the EOC patients in last three decades, however as compared to majority of the cancers the five-year overall survival for EOC patients remains less than 40% [292]. Both the intrinsically and acquired chemoresistance remain major obstacle in improving five-year over-all survival in EOC patient. Understanding the cellular and molecular mechanisms behind chemoresistance hold the key to development of new therapeutic strategies for management of chemoresistant patients.

The drug transporter proteins MDR1, BCRP and MRP have been found to be induced post chemotherapy in OC patients. Hedgehog signaling pathway transcription factor Gli1 was shown to upregulate expression of MDR1 and MRP1 in OC cell lines (A2780, OVACR3 and OVCAR8) and provide resistance against Paclitaxel, Doxorubicin and Cisplatin [51]. Activation of OC stem cell marker CD44 by hyaluronic acid (HA) was shown to induce the expression of ABC drug transporters (ABCB3, ABCC1, ABCC2, and ABCC3) in OC cells OVCAR3, SKOV3 and OV90 leading to Carboplatin resistance. Moreover, serum HA levels were found to be upregulated post-chemotherapy (Carboplatin alone or in combination with Paclitaxel) in OC patients and was associated with decreased overall survival [52]. Human copper transporter proteins, hCTR1 and hCTR2 which increase intracellular uptake of platinum-based drugs (Cisplatin and Oxaliplatin), have been extensively shown to be down regulated in OC which are resistant to platinum-based chemotherapy [72-74]. Also, increased expression of drug metabolizing enzymes ALDH1 and GST- $\pi$  shown to be bad prognostic marker and was significantly associated with Cisplatin resistance and poor overall survival of OC patients who had not undergone chemotherapy [92, 93]. Cisplatin resistant and refractory EOC patients undergoing platinum-based primary chemotherapy have been shown to

upregulate expression of anti-apoptotic proteins BCL-2, Mcl-1, BCL-xL and XIAP and downregulate pro-apoptotic proteins Fas, Bim, BAK and BAX [194, 293-295]. High grade serous EOC is characterized by high frequency of Tp53 mutations leading to loss function and is known to negatively regulate the PI3KCA. Our group using isogenic models of Cisplatin resistant OC cells (A2780, OAW42) and intrinsically Cisplatin resistant OC cells (SKOV3), shown that sustained PI3K/AKT pathway mediates Cisplatin resistance which is repressed in Cisplatin sensitive cells by wild type Tp53. The active PI3KCA/AKT and NFκB pathway promoted cell survival, slow proliferation, enrichment of CSC population and resistance to cell death [296, 297]. Chemoresistant EOC cells are also shown to possess heightened DNA repair pathways. Overexpression of ERCC1 and ERCC4 were found to be associated with poor response to platinum-based chemotherapy and expression of both were found to be elevated in patients undergoing platinum-based chemotherapy [109]. In Cisplatin resistant OC cells (A27820 and PEO14) and Melanoma cells (A375) Cisplatin treatment was shown to upregulate ERCC1 expression in MAPK/ERK dependent manner [117, 118]. In EOC tumors, higher CD44, c-Kit expression is shown to be associated with highly invasive and resistant CSCs and which correlates with shorter progression free survival. The tyrosine kinase receptor, c-Kit upregulated pluripotency transcription factors (Oct4, Sox2 and Nanog) through several pathways, including PI3K/AKT and MAPK/ERK. In patient derived CSCs from OC patients enhanced activation of CHEK1 and increased NFκB activity were shown to promote EMT and mediate resistance against Cisplatin [163-165]. OC tumor derived CSCs also show increased expression of DNA polymerase η (Pol η) which drives enhanced DNA repair through trans-lesion DNA synthesis and mediate Cisplatin resistance[167].

Chemoresistance continues to be a major hurdle in management of OC and yet chemotherapy continues to be major line of treatment for platinum-resistant relapsed disease. Hence there is an unmet need of more efficient treatment strategies, particularly the targeted therapies for chemoresistant EOC. IGF1R signaling has been found to be predominantly active in tumorigenesis and during acquirement of chemoresistance in EOC, thus making IGF1R an attractive molecule for targeted therapy [249, 250, 298]. We recently reported a pulsatile nature of IGF1R during acquirement of platinum-taxol resistance in isogenic chemoresistant models of EOC cells A2780 and OAW42, developed by treating cells with incremental dose of Cisplatin and Paclitaxel alone or in combination [252]. Interestingly, IGF1R expression was found to be upregulated at the onset of resistance (early resistant stage) in these chemoresistant models, which subsequently decreased as cells complete and irreversible resistance (late resistant stage). Low dose treatment of Picropodophyllin (IC20), an IGF1R inhibitor, in combination with Cisplatin-Paclitaxel (IC20) inhibited long-term survival and reversed chemoresistance specifically at early stages. Drug induced enhancement of IGF1R expression was also observed in a small cohort of advanced stage high grade serous EOC patients after 3-4 cycles of platinum-taxol treatment [252]. The underlying mechanisms behind this undulating IGF1R expression during progression of resistance that points towards a complex regulatory circuit has not been deciphered.

### Rationale

In the absence of significant amplification of IGF1R gene, overexpression of IGF1R across different cancer types is determined, to a large extent, at transcriptional level. The unique GC-rich IGF1R promoter lacks TATA or CAAT box motifs [299] and is either regulated directly by SP1, E2F1, WT1 and FOXO3a or in conjunction with SP1 to induce (ER $\alpha$ , KLF6 and HMGA1) or repress (BRCA1, TP53 and VHL) IGF1R expression in variety of cancer cells in different circumstances [212]. However, etiology underlying increased expression of IGF1R in chemoresistance development is poorly understood. Apart from VHL loss and FOXO1 activation leading to transcriptional activation and increased IGF1R expression in 5-Fluorouracil and Etoposide resistant RCC and PI3K- $\delta$  inhibitor resistant CLL respectively [275, 300], probable action of other transcriptional regulator/s in mediating cancer therapy resistance through IGF1R are unknown. Such molecular knowledge of regulation of IGF1R expression which in turn affect the downstream MAPK/ERK and PI3KCA/AKT signaling during chemoresistance development is important to identify both therapeutic and diagnostic markers for the IGF1R addicted cancers including EOC.

### Hypothesis

IGF1R expression showed modulation at both transcript and protein levels during chemoresistance development in EOC cell lines and observed increased IGF1R transcript levels in primary tumors high grade serous EOC patients after 3-4 cycles of platinum-taxol treatment, we hypothesize that IGF1R promoter which is a hotspot for transcriptional modulation may be regulated differentially during chemoresistance development. Also, combination of chemotherapeutic agents and IGF1R inhibitor effectively reversed the resistance at early stage, thus understanding molecular mechanisms both upstream and downstream of IGF1R at onset of resistance development are important for devising more successful anti-IGF1R targeted therapies.

### Aim

Investigating the role of IGF1R signalling in development and maintenance of chemoresistance in Ovarian Carcinoma.

### Key Questions

3. What are the key regulators that can differentially modulate expression of IGF1R at early and late stage of Cisplatin-Paclitaxel dual resistance?
4. How does IGF1R regulate chemoresistance, tumorigenic and cancer stem cell properties at early stages of chemoresistance?

### Objectives

**To address these key questions following objectives were designed**

**Objective 1:** Identification of key molecular regulators of IGF1R during development of Cisplatin-Paclitaxel dual resistance.

**Objective 2:** Investigating the role of IGF1R signaling in maintenance of chemoresistance, tumorigenesis and cancer stem cell properties.

## Chapter 2: Identification of key molecular regulators of IGF1R during development of Cisplatin-Paclitaxel resistance in Ovarian Carcinoma

### 2.1 Introduction

The ubiquitously expressed receptor tyrosine kinase, IGF1R, plays vital role in embryonic and postnatal growth, hematopoietic stem and progenitor cells maintenance and differentiation, adult neural proliferation and differentiation, bone development, carbohydrate metabolism and skeletal muscle growth [301]. Importance of IGF1R in tumorigenicity came in light with the resistance of R-cells (murine fibroblasts IGF1R<sup>-/-</sup>) to undergo oncogenic transformation by variety of cellular and viral oncogenes (SV40 large T antigen, human papillomavirus E7 protein, h-Ras, c-Src and Ewing's sarcoma fusion protein) [302]. The loss of tumor suppressor genes is a typical hallmark of cancer. Loss of tumor suppressor genes, such as Tp53, BRCA1, WT1 and pVHL which are known to negatively regulate IGF1R promoter, have been shown to strongly correlate with overexpression of IGF1R [303]. Involvement of IGF1R signaling as a strong inducer of mitogenicity and potent inhibitor of apoptosis against various apoptotic inducers (TNF $\alpha$ , chemotherapeutic drugs and ionizing/non-ionizing radiation), overexpression of oncogenes (c-myc) and abnormal growth conditions (growth factor withdrawal, osmotic shock and high ROS) specifically in anchorage independent growth (anoikis), further strengthened the crucial role of IGF1R in enduring the multistep process of tumorigenesis and chemoresistance development [304, 305]. Recent clinical and preclinical data suggest that IGF1R overexpression is not only associated with different cancer types, but also emerged as a key signalling molecule underlying the resistance mechanisms against wide range of chemotherapeutic agents and targeted therapies [277, 306]. While majority of the growth

factor receptors are overexpressed in different cancer types with high degree of genetic alterations (amplification, oncogenic fusions and activating mutations), overexpression of IGF1R is found to be associated with low level of amplification (3-6% in Sarcoma, Breast cancer, Ovarian cancer, Oesophageal and Stomach adenocarcinoma) and lack of activating oncogenic mutations [209, 210] indicating a robust control at transcriptional level.

Although IGF1R is relatively unperturbed by genetic alterations, IGF1R gene is known to be a hotspot for transcriptional modulation. The highly GC-rich IGF1R promoter (Fig. 16A) which lacks both TATA and CAAT box elements is an atypical initiator type promoter (initiator motif-core promoter driven transcription) [299, 307, 308]. Though epigenetic silencing of IGF1R promoter by hypermethylation is reported in db/db mouse model of type 2 diabetes mellitus [309] and mouse model of prenatal smoke exposure [310], such epigenetic modulation is seldom reported in cancer. In prostate cancer loss of methylation in Androgen receptor promoter but not IGF1R was associated with disease progression from benign to metastatic. However, in spite no change in promoter methylation, IGF1R expression was also increased with loss of AR promoter methylation. Treatment with 5-Azacytidine (DNA methyltransferases inhibitor in Prostate cancer cell lines was shown to demethylate the AR promoter but not IGF1R promoter, rather increased levels of AR post treatment induced upregulation of IGF1R [311]. Rather conspicuous absence of methylation by S-Adenosyl methionine, a methyl donor agent, in Glioblastoma cells and in benign and metastatic Prostate cancer cells suggest that transcription factor/s mediated regulation of IGF1R promoter is dominant over epigenetic regulation [212, 311, 312]. Zinc finger transcription factor, specificity protein 1 (SP1), binds to GC-box motifs and drives the basal IGF1R promoter activity (Fig. 16B). This regulation by SP1 is modulated by several tumor suppressors such as BRCA1, VHL and TP53 which repress the IGF1R by preventing SP1 binding (Fig. 16B) [212]. Elevated expression of IGF1R in primary Breast cancer, Ovarian

cancer, Prostate cancer, and Uterine serous carcinoma was associated with loss of BRCA1 by mutations or suppression of BRCA1 by hypermethylation of BRCA1 promoter [313-318]. Similarly, loss of VHL in Renal clear cell carcinoma and WT1 in Wilms' tumor was associated with increased expression of IGF1R [300, 319, 320]. TP53 is mutated in more than 50% of human malignancies and is shown that wtTP53 is a potent suppressor of IGF1R promoter, whereas mutant TP53 (V143A, R248W and R273H) has been shown to induce expression of IGF1R as opposed to wtTP53 (Fig. 16B) [321]. Moreover, mutant TP53 (R248W) not only induced IGF1R expression but also was shown to antagonize the BRCA1

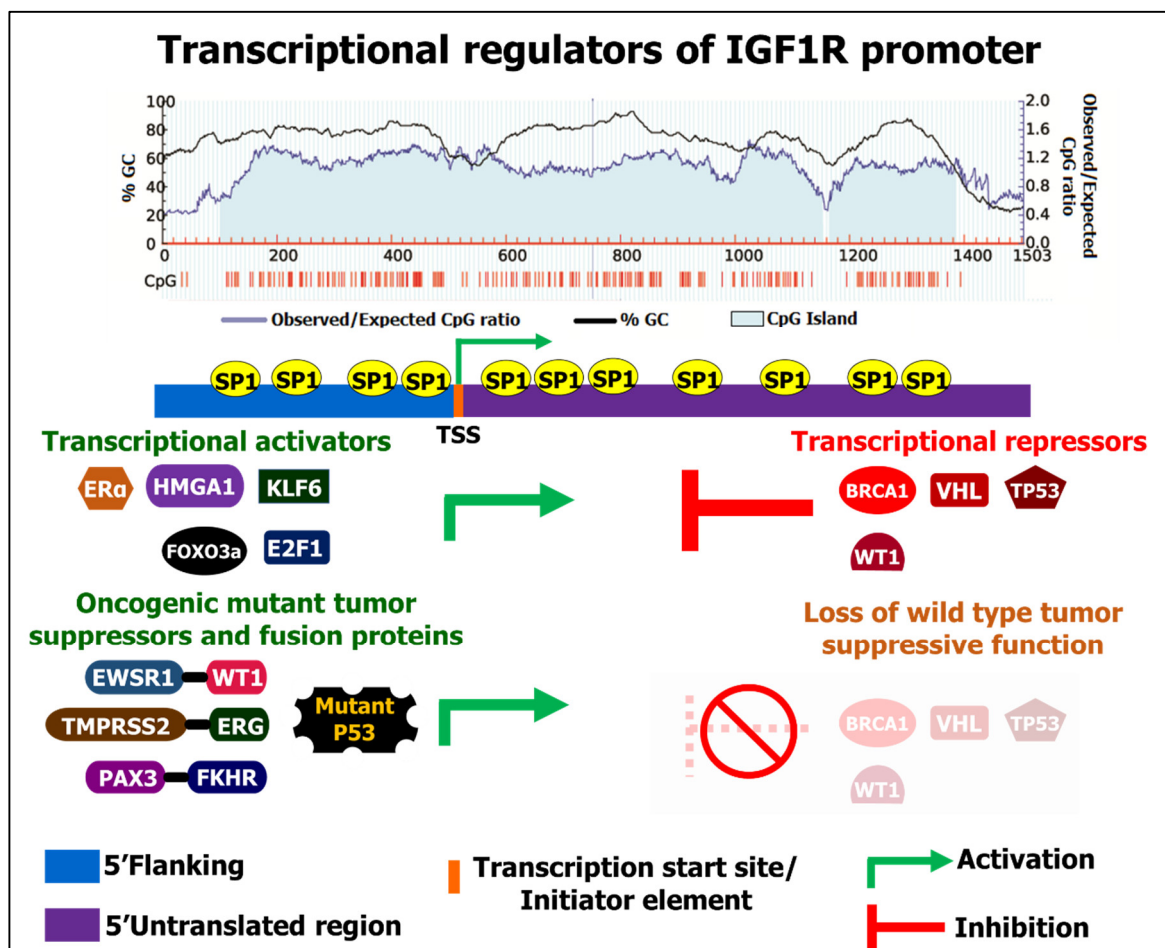


**Figure 16: Transcriptional regulation of IGF1R promoter**

**A.** Predicted CpG island distribution on IGF1R promoter using MethPrimer 2.0 (<http://www.urogene.org/cgi-bin/methprimer2/MethPrimer.cgi>). **B.** Pictorial depiction of repertoire of transcription factors either inducers or repressors governing the activity of IGF1R promoter.

and WT1 mediated suppression of IGF1R promoter in Breast cancer, Colorectal cancer, Osteosarcoma and Rhabdomyosarcoma cell lines [322, 323]. While tumor suppressors repress the IGF1R promoter, a repertoire of transcription factors trans-activate IGF1R promoter either directly (E2F1 and FOXO3a) or in conjunction with SP1 (ER, KLF6 and HMGA1) (Fig. 16B) [324-328]. The non-histone chromatin protein HMGA1 was not only shown to positively regulate IGF1R promoter activity in Hepatocellular carcinoma cells (HepG2), Papillary thyroid cancer cells (TPC-1), Anaplastic thyroid cancer cells (SW1736) and Osteosarcoma cell (Saos2), but also antagonized inhibitory effect of wtTP53 on IGF1R promoter [325]. In serum starved Hepatocellular carcinoma cells (HepG2 and SMMC-7721) active GSK3 $\beta$  was shown to induce the transcriptional activity of FOXO3 leading to increased expression of IGF1R by enhanced binding to IGF1R promoter [328]. Also, oncogenic fusion proteins such as, EWSR1-WT1 fusion in Desmoplastic small round cell tumor [329-331], TMPRSS2-ERG fusion in Prostate cancer [332, 333] and PAX3-FKHR fusion in Alveolar rhabdomyosarcoma [334] were shown to induce IGF1R promoter activity (Fig. 16B). The aberrant overexpression of IGF1R across different cancer types is majorly driven by deregulated transcription factors, however their role in upregulation of IGF1R in therapy resistant tumors is relatively poorly understood. Apart from VHL loss in 5-Fluorouracil and etoposide resistant renal cell carcinoma [319], FOXO1 activation in phosphatidylinositol-3-kinase catalytic subunit delta (PI3K- $\delta$ ) inhibitor resistant murine model [275] and SP1 activation post Neocarzinostatin (radiomimetic agent) treatment in immortalized human fibroblasts [335], probable action of other transcriptional regulator/s in mediating cancer therapy resistance through IGF1R are unknown. Such molecular knowledge is important to identify both therapeutic and diagnostic markers for the IGF1R addicted cancers.

We recently reported a pulsatile nature of IGF1R expression during acquirement of platinum-taxol resistance in isogenic chemoresistant models of EOC cells (A2780 and OAW42), developed by treating cells with incremental doses of Cisplatin and Paclitaxel alone or in combination [252]. Interestingly, IGF1R expression was found to be upregulated at the onset of resistance (early resistant stage) in these chemoresistant models, which subsequently decreased as cells reached complete and irreversible resistance (late resistant stage). Low dose treatment of Picropodophyllin (IC20), an IGF1R inhibitor, in combination with Cisplatin-Paclitaxel (IC20) inhibited long-term survival and reversed chemoresistance specifically at early stages. Drug induced enhancement of IGF1R expression was also observed in a small cohort of advanced stage high grade serous EOC patients after 3-4 cycles of platinum-taxol treatment [252]. Since acquirement of chemoresistance remains a clinical obstacle for EOC treatment, comprehending the principal molecular networks underlying IGF1R signalling in therapy resistant cancer cells might lead to better therapeutic targets. In this chapter we aim to decipher the underlying molecular mechanisms behind this undulating IGF1R expression during progression of chemoresistance that points towards a complex regulatory circuit.

## **2.2 Methodology**

### **2.2.1 Development of Cisplatin-Paclitaxel resistance models of EOC cells**

A2780 and OAW42 isogenic Cisplatin-Paclitaxel resistance models were established using pulse method previously in the laboratory (Table 2). Briefly cells were treated with the Cisplatin-Paclitaxel for 2-hours, post two-hour treatment cells were grown in drug free medium. The surviving fraction of cells after first treatment were subcultured into two parts, one for cryopreservation and second for next round of treatment. The surviving cells were again treated with same concentration of Cisplatin-Paclitaxel for 2-hours for two more successive cycles as described above. The dose of Cisplatin-Paclitaxel was increased after

every three cycles of treatment as described above and after each cycle cells were cryopreserved. Percent cell viability of cells at different stages of resistant model development was assessed by MTT assay using IC50 concentration of parental cell lines (Fig. 17).

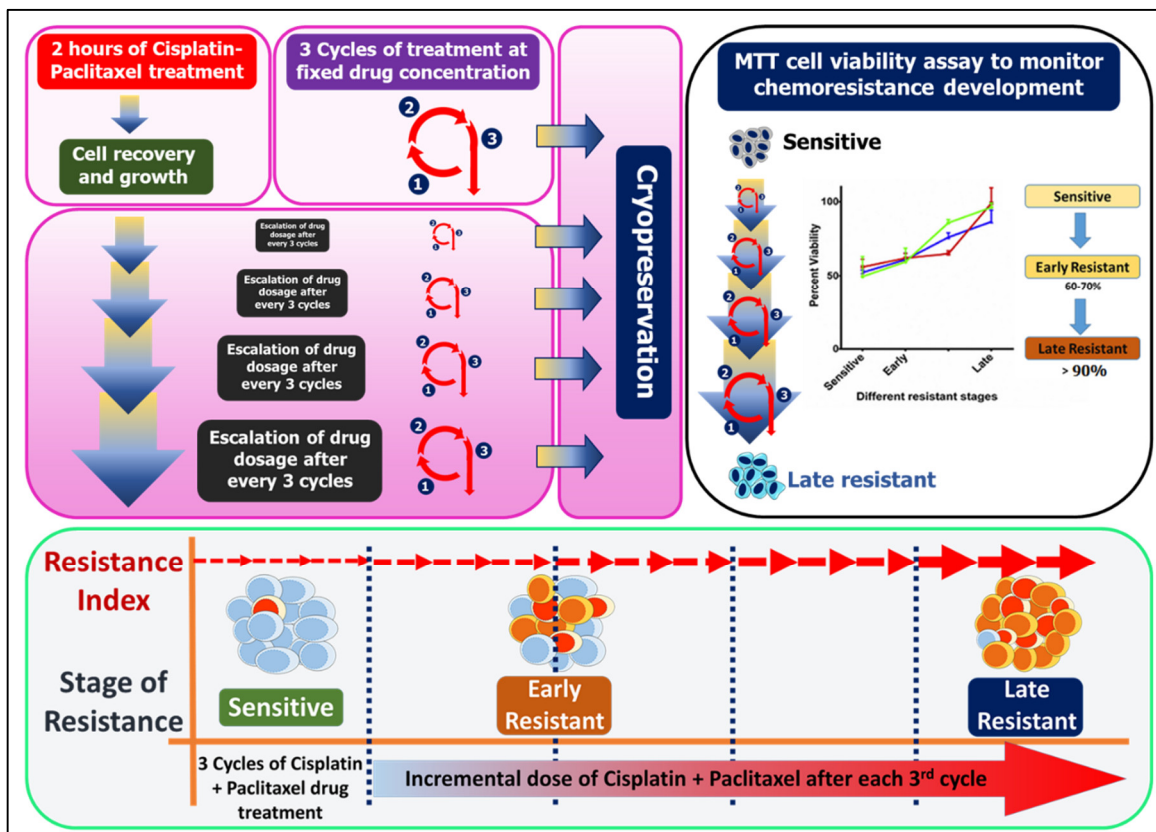


**Figure 17: Development of chemoresistance models**

**A.** Pictorial depiction of Cisplatin-Paclitaxel chemoresistance model development in EOC cells A2780 and OAW42 using pulse method. **B.** MTT cell viability assay to monitor chemoresistance development in EOC cells. **C.** Pictorial depiction of stages of chemoresistance with increasing resistance index obtained from MTT assay.

**Table 2: List of EOC chemoresistance models**

Stages	A2780 Cis-Pac resistant model	OAW42 Cis-Pac resistant model
Sensitive	A2780	OAW42
Early resistant	A2780-dual <sup>ER</sup>	OAW42-dual <sup>ER</sup>
Late resistant	A2780-dual <sup>LR</sup>	OAW42-dual <sup>LR</sup>

### 2.2.2 GF1R promoter driven luciferase-fluorescence bi-fusion reporter construction

IGF1R-promoter-Gausia luciferase-reporter construct (Cat. No. HPRM18398-PG02), consisting of 1503bp of IGF1R promoter was procured from Genecopoeia (MD, USA). The selected 1503bp IGF1R promoter consists of -460bp of 5'flanking region, an initiator element and +1043bp of 5'untranslated region, which has been previously shown to exhibit high level of promoter activity in functional assays [299, 307]. The procured IGF1R promoter fragment was sanger sequenced and aligned with Homo sapiens chromosome 15,

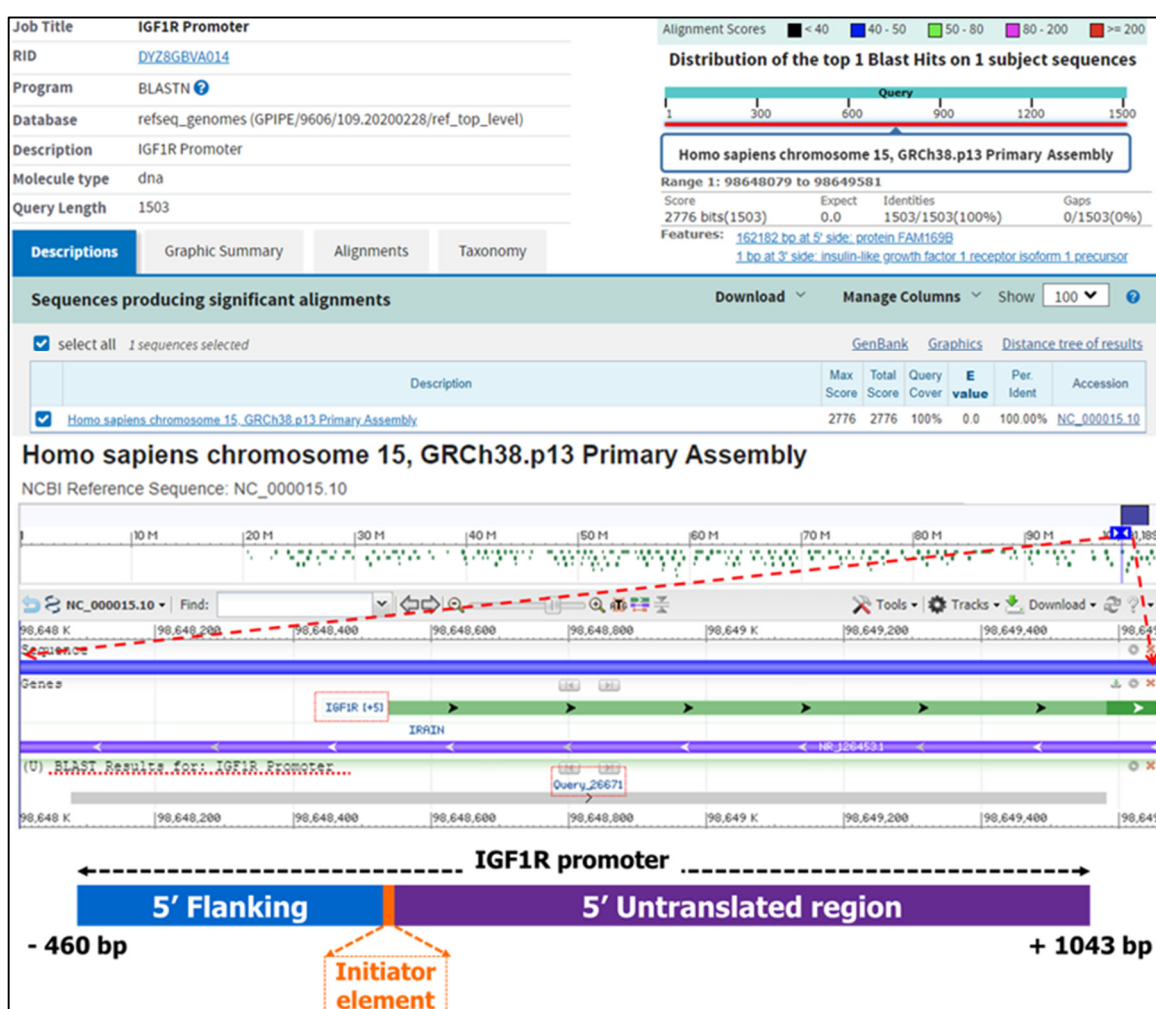


**Figure 18: NCBI Nucleotide blast alignment of IGF1R promoter**

Pictorial depiction of NCBI Nucleotide blast alignment of the selected IGF1R promoter (-460bp of 5'flanking region, an initiator element and +1043bp of 5'untranslated region) showing 100% sequence identity to IGF1R promoter region on Homo sapiens chromosome 15, GRCh38.p13 primary assembly.

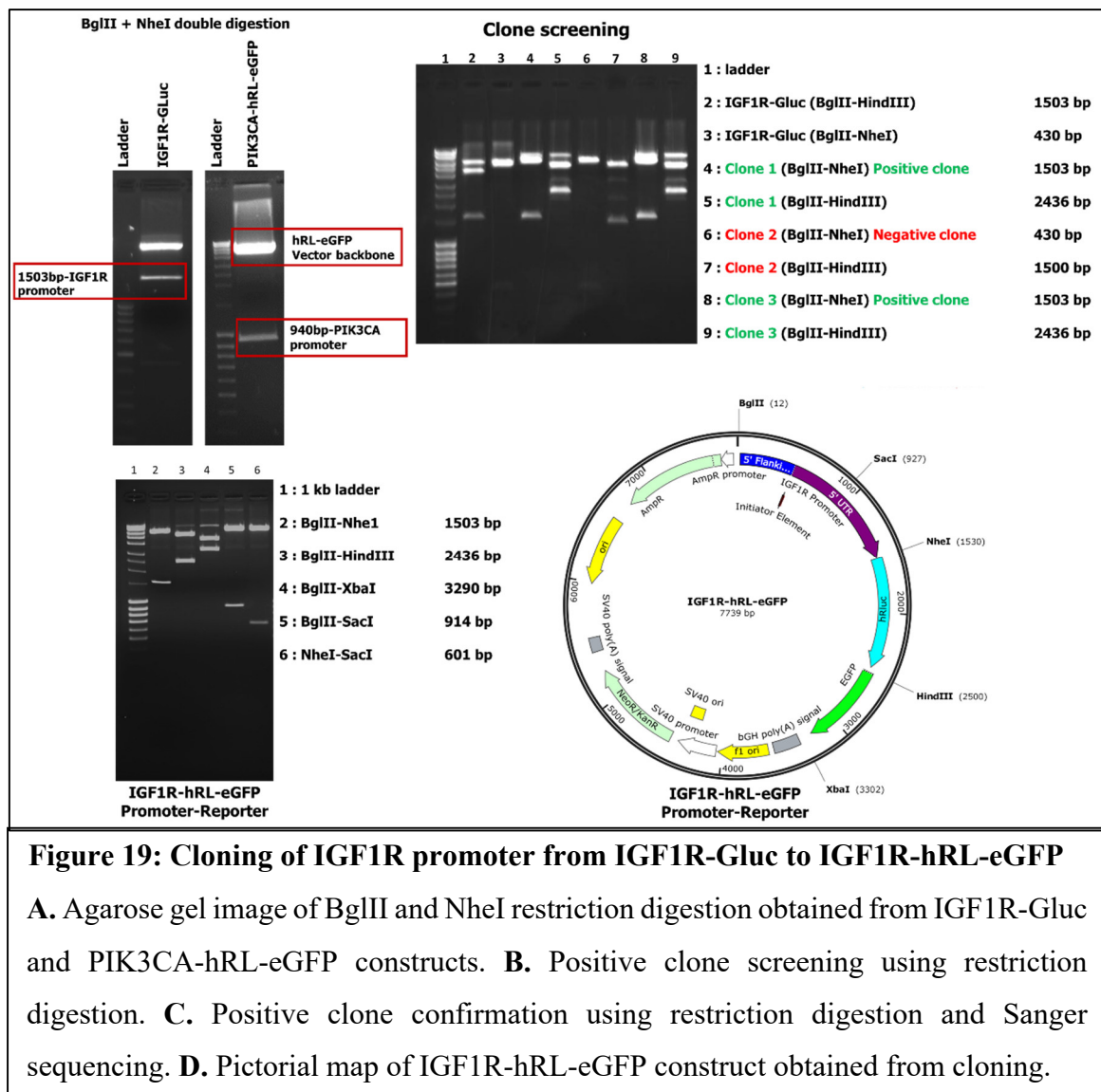


**Figure 19: Cloning of IGF1R promoter from IGF1R-Gluc to IGF1R-hRL-eGFP**

**A.** Agarose gel image of BglII and NheI restriction digestion obtained from IGF1R-Gluc and PIK3CA-hRL-eGFP constructs. **B.** Positive clone screening using restriction digestion. **C.** Positive clone confirmation using restriction digestion and Sanger sequencing. **D.** Pictorial map of IGF1R-hRL-eGFP construct obtained from cloning.

GRCh38.p13 primary assembly using NCBI nucleotide basic local alignment search tool ([https://blast.ncbi.nlm.nih.gov/Blast.cgi?LINK\\_LOC=blasthome&PAGE\\_TYPE=BlastSearch&PROGRAM=blastn](https://blast.ncbi.nlm.nih.gov/Blast.cgi?LINK_LOC=blasthome&PAGE_TYPE=BlastSearch&PROGRAM=blastn)) to confirm the 100% sequence identity to IGF1R promoter region (Fig. 18). The 1503bp IGF1R promoter was further cloned upstream of Firefly Luciferase 2- Tandem Dimeric Tomato (FL2-TDT) or humanised Renilla Luciferase-enhanced Green Fluorescent Protein (hRL-eGFP) bi-fusion reporter proteins separately in pCDNA 3.1 vector using standard cloning methods as described in section 5.3 and all constructs were verified by restriction digestion and Sanger sequencing (Fig. 19).

### 2.2.3 Site directed mutagenesis of FOXO3a binding motifs on IGF1R promoter

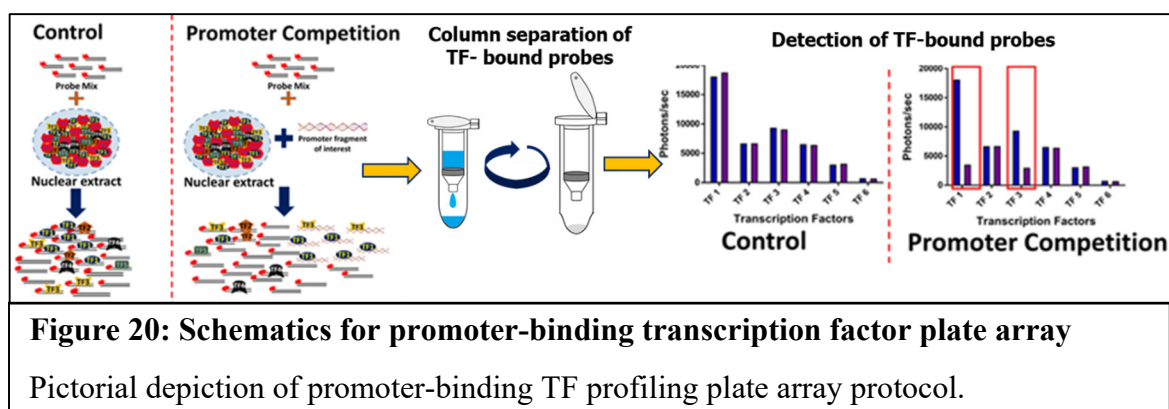
FOXO3a response element (binding motif) mutants were made in IGF1R-hRL-eGFP background by standard site directed mutagenesis (SDM) protocols and using SDM primers as described in section 5.3. The mutant IGF1R promoters were labelled as  $\Delta$ -S1 (FOXO3a-Site1),  $\Delta$ -S2 (FOXO3a-Site2) and  $\Delta$ -S1-S2 (FOXO3aSite1-2) and all constructs were verified by restriction digestion and sequencing.

### 2.2.4 Promoter-reporter luciferase assay

All the transient and stable transfections with wild type/mutant IGF1R-promoter-reporter, human sodium iodide symporter (h-NIS)-promoter-reporter and cytomegalovirus (CMV) or beta-galactosidase ( $\beta$ gal) -FL2 (normalization vectors) were performed following protocols described in section 5.9.

### 2.2.5 Promoter-binding transcription factor (TF) plate array

Promoter-binding TF profiling plate array-II, commercially available from Signosis (USA) was used to identify probable transcription factor binders of IGF1R promoter in nuclear lysate of A2780-dual<sup>ER</sup> cells using detailed protocol described in section 5.8 (Fig. 20).



### 2.2.6 Immunofluorescence

Immunofluorescence was performed for RUNX1, FOXO3a, p-S413-FOXO3a and p-S253-FOXO3 and images were acquired using Carl Zeiss, LSM 780 microscope following protocols described in section 5.7. Mean fluorescence intensity value from entire nucleus of

an individual cell and a minimum of 30 cells were quantified for each group using ImageJ software.

### **2.2.7 Co-Immunoprecipitation (Co-IP)**

Nuclear cell pellets were prepared using nuclear-cytoplasmic fractionation procedure as described in section 5.6 and nuclear cell lysates were prepared in IP lysis buffer. IP was carried out following protocol described in section 5.10 and presence of RUNX1 and FOXO3a in the Co-IP complexes was detected by western blotting using VeriBlot detection reagent (HRP) from Abcam (UK), which only recognize native (nonreduced) antibodies thereby minimizing detection of heavy and light chains if Co-IP complex is fully reduced.

### **2.2.8 Western blotting**

Whole cell, nuclear and cytosolic lysates were prepared and western blot was performed for IGF1R- $\beta$ , RUNX1, total FOXO3a, p-S253-FOXO3, total AKT, p-S473-AKT, Lamin-A and  $\alpha$ -tubulin following protocols described in section 5.6.

### **2.2.9 Quantitative real-time PCR**

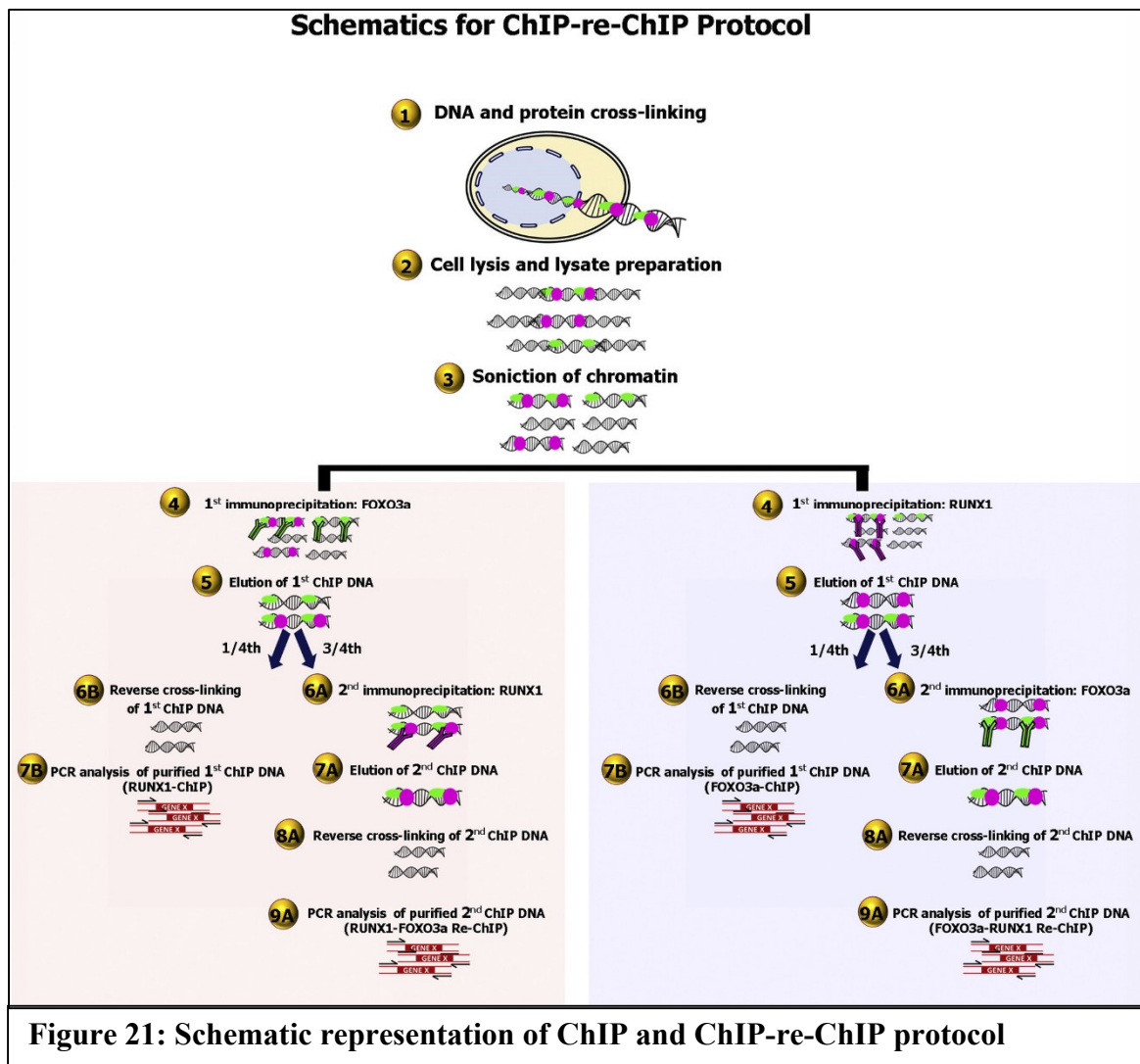
Quantitative real-time PCR was performed following protocols described in section 5.4 using SYBR Green (Invitrogen) and appropriate gene specific primers. Relative expression of target genes was estimated by  $\Delta$ -Ct method using Glyceraldehyde 3-phosphate dehydrogenase (GAPDH) as normalisation control.

### **2.2.10 CBF $\beta$ silencing by lentiviral mediated sh-RNA construct**

CBF $\beta$ - knock down lentiviral cassette was developed using a target sequence against CBF $\beta$  (5'-CCGCGAGTGTGAGATTAAGTA-3') using standard cloning methods as described in section 5.3 and all constructs were verified by restriction digestion and sequencing. Lentivirus particles were produced in HEK293FT and A2780, A2780-dual<sup>ER</sup> and A2780-dual<sup>LR</sup> cells were transduced with lentiviruses and stable cells were FACS sorted using eGFP as a marker using protocol described in section. 5.3.10

### 2.2.11 Chromatin immunoprecipitation (ChIP)

ChIP and ChIP-re-ChIP were performed with either RUNX1 or FOXO3a specific antibody following detailed protocol described in section 5.11 (Fig. 21-22). RUNX1 and FOXO3a binding on IGF1R promoter was analysed by RT-PCR to calculate the percent bound fraction compared to input using calculations described in section 5.11.



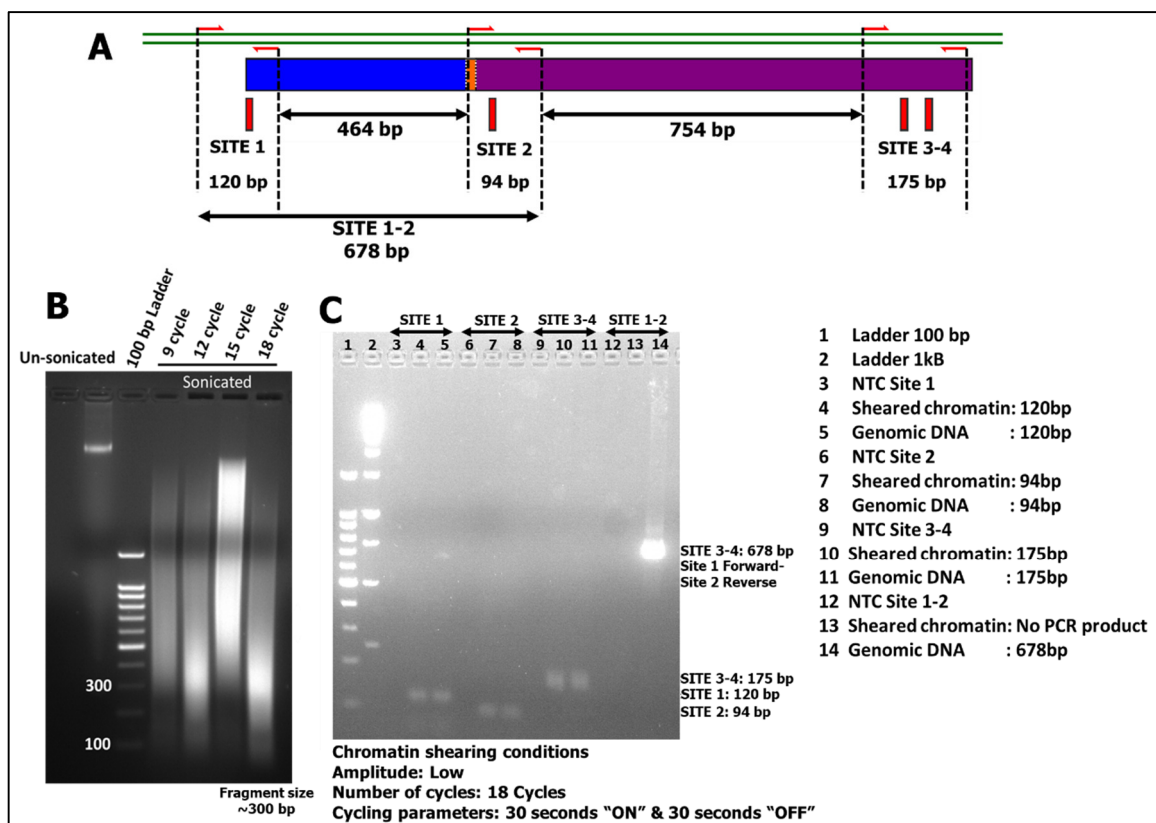


**Figure 22: Standardization of chromatin sonication and PCR for site specific ChIP of IGF1R promoter**

**A.** Schematic representation of primers sets and expected PCR product size used in site specific ChIP of IGF1R promoter. **B.** Agarose gel picture showing sonication cycle standardization, where 18 sonication cycles (30 seconds ON and 30 seconds OFF) with low amplitude showed approximately 200-400 bp chromatin shearing desired for site specific ChIP of IGF1R promoter. **C.** Agarose gel picture showing specificity of primer sets used for site specific ChIP of IGF1R promoter. No PCR product in sheared chromatin with site 1-2 primer set (site 1 forward and site 2 reverse) ensured proper chromatin shearing resulting in mutual exclusivity of site 1, site 2 and site 3 necessary for site specific ChIP of IGF1R promoter.

## 2.3 Results

### 2.3.1 IGF1R promoter activity oscillates during acquirement of chemoresistance

Our previous results showed an association of dynamic modulation in IGF1R gene expression with acquirement of chemoresistance in cisplatin-paclitaxel resistant cellular

models developed in A2780 and OAW42 EOC cells, which were categorized into early (ER) and late (LR) resistant stages based on their resistance indices [252]. To identify the underlying molecular players, a 1503bp long IGF1R promoter driving a fusion reporter (FL2-TDT or hRL-eGFP) was transiently transfected into A2780 and OAW42 Cis-Pac resistant models which showed 3.8-fold and 2.2-fold higher promoter-reporter activity in A2780-dual<sup>ER</sup> and OAW42-dual<sup>ER</sup> cells respectively compared to their sensitive counterparts (Fig. 23A-B). Similar trend was observed in A2780 Cis-Pac resistant cellular model stably expressing the IGF1R-FL2-TDT promoter-reporter, with 3.3-fold higher promoter-reporter activity in A2780-dual<sup>ER</sup> cells than A2780 sensitive cells (Fig. 23C). The

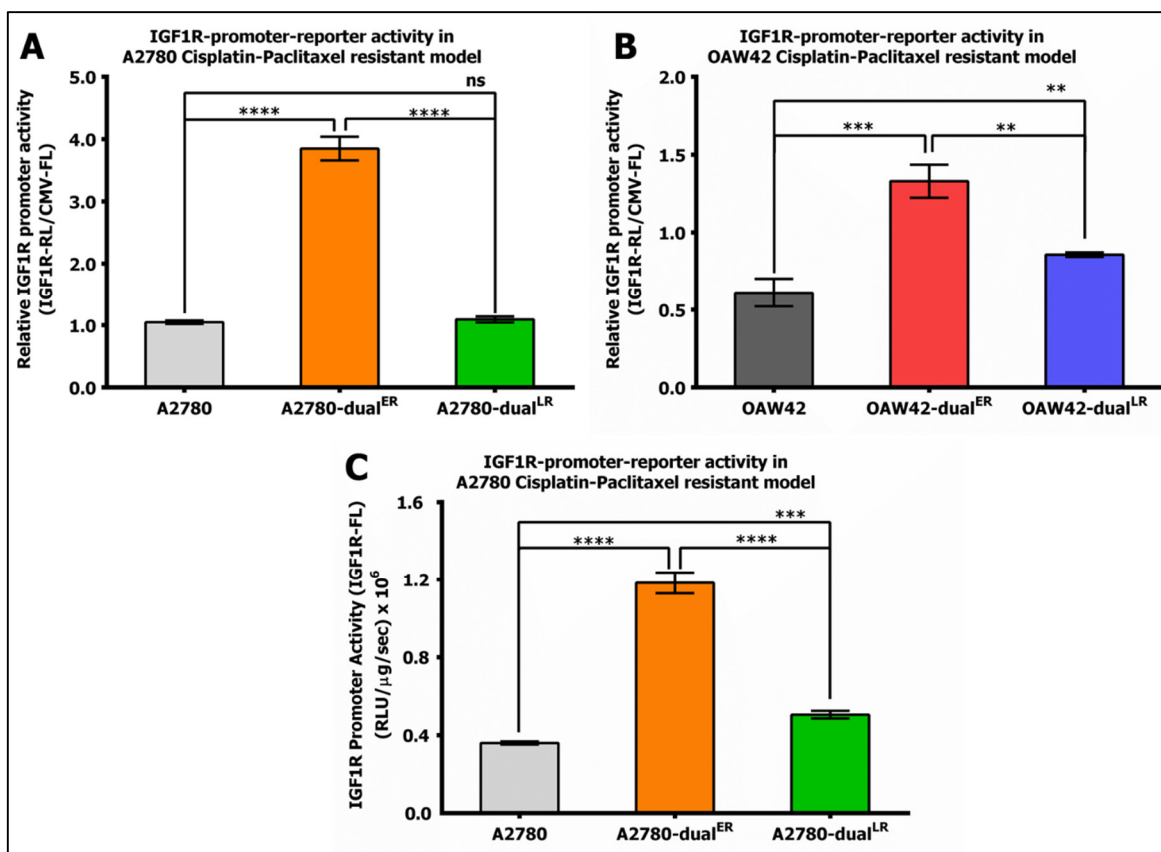


**Figure 23: IGF1R promoter demonstrates dynamic modulation during acquisition of chemoresistance**

**A-B.** Enhanced IGF1R-promoter-reporter activity was observed in ER-cells of A2780/OAW42 Cis-Pac resistant models by transient transfection. **C.** Enhanced IGF1R-promoter-reporter activity was observed in ER-cells of A2780 Cis-Pac resistant model stably expressing IGF1R-promoter-reporter.

IGF1R promoter-reporter activity were found to be decreased at late stage of resistance in both A2780 and OAW42 Cis-Pac resistant cellular models (Fig. 23A-C). The enhanced IGF1R promoter-reporter activity in A2780-dual<sup>ER</sup> and OAW42-dual<sup>ER</sup> cells corroborated with the increased IGF1R transcript levels in these cells compared to the respective sensitive cells.

To recognize the exact region/sequence of IGF1R promoter involved in oscillatory expression pattern of IGF1R gene, four deletion constructs were generated (Fig. 24A). The deletion constructs DEL-1 and DEL-2 which have either 5'-flanking region and 5'UTR respectively with TIS disrupted in both showed moderate decrease in promoter activity. DEL-1 showed 1.5, 1.6 and 1.4-fold decrease in promoter activity compared to full length promoter in A2780 sensitive, A2780-dual<sup>ER</sup> and A2780-dual<sup>LR</sup> cells respectively. Similarly, DEL-2 showed 1.5, 1.5 and 1.7-fold decrease in promoter activity compared to full length promoter in A2780 sensitive, A2780-dual<sup>ER</sup> and A2780-dual<sup>LR</sup> cells respectively (Fig. 24B).

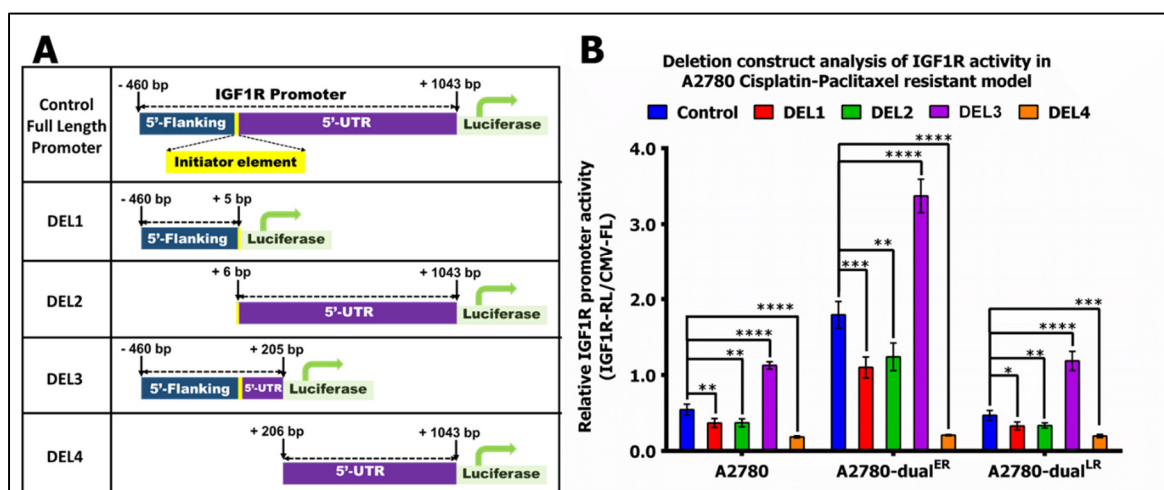


**Figure 24: IGF1R promoter activity resides in -460 to +205 bp region of promoter in EOC cells**

**A.** Pictorial representation different deletion constructs of IGF1R promoter. **B.** Deletion constructs, DEL-1 (-460 to +5 bp) and DEL-2 (+6 to +1043) showed moderate decrease in promoter activity across A2780 Cis-Pac resistant model, whereas DEL-3 (-460 to +205 bp) showed increase in IGF1R promoter activity compared to full length promoter at all stages of chemoresistance.

Surprisingly the DEL-3 construct with intact TIS and a part of 5-UTR, showed increased promoter activity compared to full length promoter at all stages of resistance, with 1.6, 1.7 and 2.0-fold increase in promoter activity in A2780 sensitive, A2780-dual<sup>ER</sup> and A2780-dual<sup>LR</sup> cells respectively, while construct DEL-4, which lacks 5'-flanking region and TIS both, showed a drastic attenuation of promoter activity (3.3, 10.5 and 3.4-fold decrease compared to full length promoter in A2780 sensitive, A2780-dual<sup>ER</sup> and A2780-dual<sup>LR</sup> cells respectively) (Fig. 24B). These results indicated that majority of IGF1R promoter activity resides in -460 to +205 bp region of the promoter in both sensitive and chemoresistant EOC cells and +206 to +1043 bp region of promoter might harbour a strong suppressive cis or trans acting element present in 5'UTR of IGF1R promoter since DEL-3 construct showed significant increase in promoter activity compared to the full length promoter (Fig. 24B).

### **2.3.2 Potential regulators of IGF1R promoter in chemoresistant EOC cells**

The modulation of IGF1R promoter activity during acquirement of chemoresistance is intriguing and indicates presence of a dynamic regulatory interaction of TF/s driving transcriptional surge at onset of chemoresistance development. In order to identify the putative regulators of IGF1R promoter, we performed a promoter-binding TF profiling plate array using nuclear extracts of A2780-dual<sup>ER</sup> cells and 1503bp promoter of IGF1R (Fig. 25A). The purity of nuclear lysates was checked by western blotting (Fig. 25B). A total nine putative transcriptional regulators binding to IGF1R promoter (>1.5 decrease in luminescence signal in TF binding with IGF1R-promoter competition) were identified by screening promoter-binding TF profiling plate array (consisting of total 96 TF probes) from nuclear extracts of A2780-dual<sup>ER</sup> cells, that comprised of Retinoid X receptor (RXR), SRY-Box 9 (SOX9), Vitamin D3 receptor (VDR), Growth Factor Independent 1 (GFI1), Retinoic acid related orphan receptors (ROR), SP1, Runt related transcription factor 1 (RUNX1), NK2 Homeobox 5 (NKX2.5) and SRY-Box 18 (SOX18) (Fig. 25C). Identification of SP1

(a previously reported TF binding to IGF1R promoter) as a binder and TFIID as a non-binder (IGF1R promoter lacks TATA-box) strengthened the promoter binding TF plate array data. RXR showed maximum binding to IGF1R promoter (4.6-fold decrease in luminescence signal), followed by SOX9 (3.7-fold decrease), VDR (3.1-fold decrease), GFI1 (3.1-fold decrease), ROR (2.8-fold decrease), SP1 (2.7-fold decrease), RUNX1 (2.3-

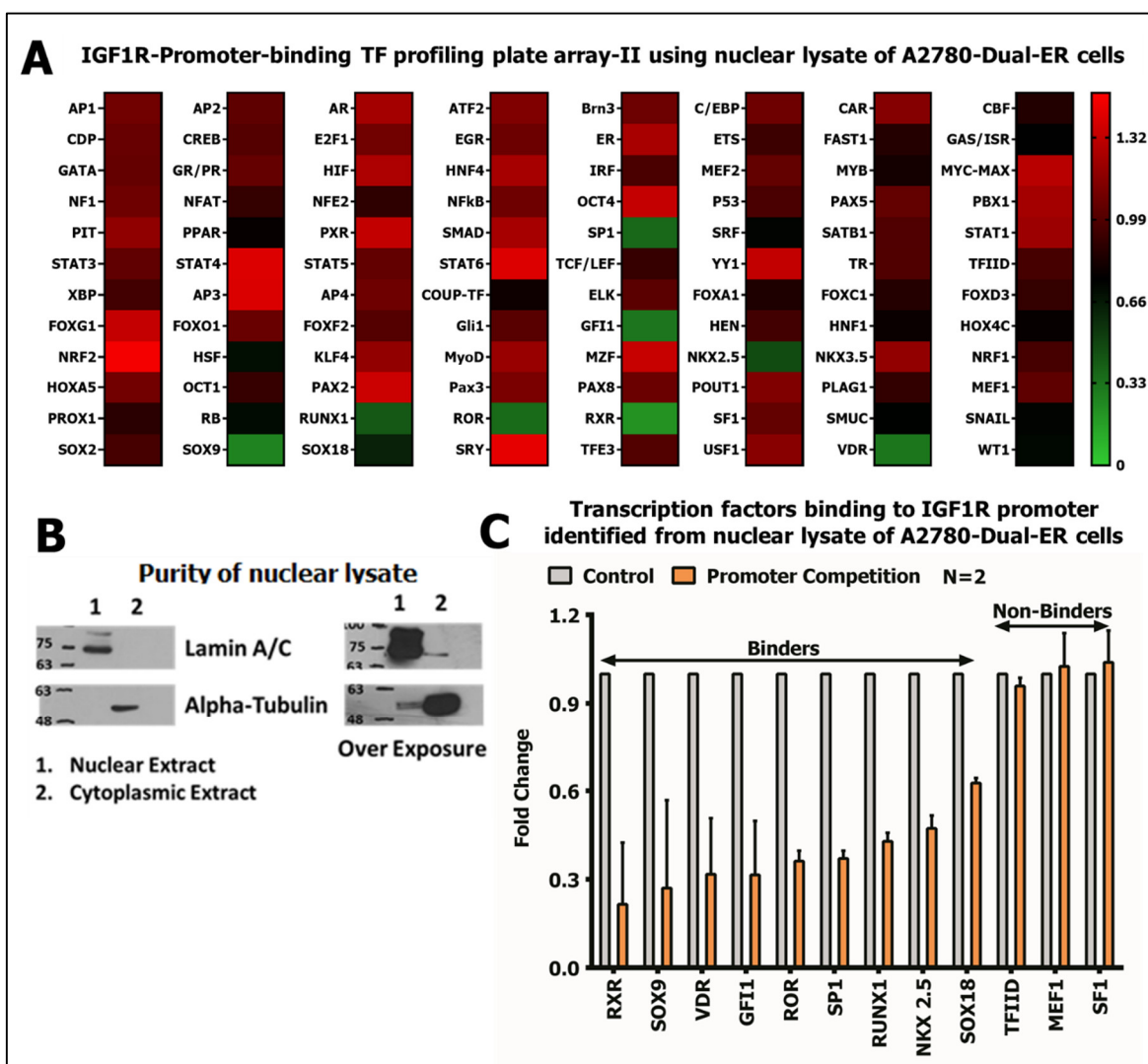


**Figure 25: IGF1R-Promoter-binding TF plate array in A2780-dual<sup>ER</sup> cells**

**A.** Heat map showing fold change in TF binding using IGF1R-promoter for competition in promoter-binding TF plate array using nuclear lysate of A2780-dual<sup>ER</sup> cells. **B.** Purity check of nuclear lysate of A2780-dual<sup>ER</sup> cells. **C.** Graphical representation of the identified IGF1R promoter binders and non-binders from promoter-binding TF plate array.

fold decrease), NKX2.5 (2.1-fold decrease) and SOX18 (1.6-fold decrease).

Next we performed an *in-silico* analysis of IGF1R promoter using JASPAR-TF binding profile database (<http://jaspar2016.genereg.net/>) to predict the presence of consensus

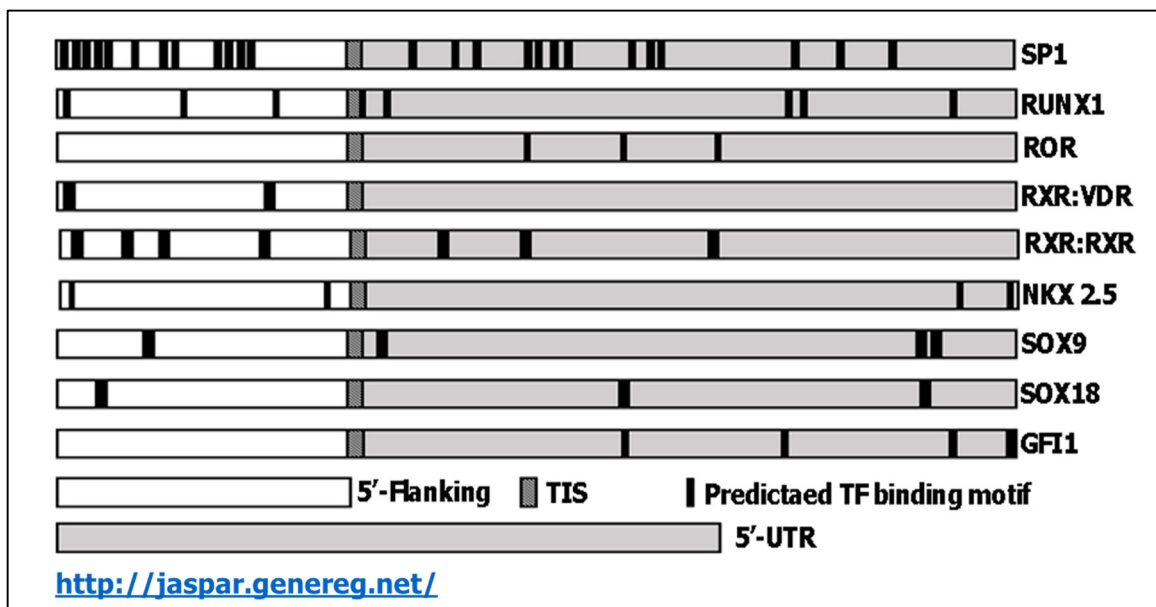


**Figure 26: Prediction of TF binding motifs using JASPAR-TF database**

Schematic representation of the predicted binding sites of the TFs on IGF1R promoter as predicted by JASPAR-TF database (threshold >75%).

binding motifs for each identified TF from TF plate array and for known TFs such as E2F1 and FOXO3a. Several consensus binding elements for each TF were predicted using JASPER-TF database at probability threshold score of >75%, which are distributed throughout the GC-rich IGF1R promoter on both 5' flanking and 5'UTR, while GFI1 has binding sites only on 5'UTR (+206 to +1043 bp) but not on 5'Flanking (Fig. 26 and Table 3). GFI1 functions as a transcriptional repressor as part of several complexes, including the EHMT2-GFI1-HDAC1, AJUBA-GFI1-HDAC1 and RCOR-GFI-KDM1A-HDAC1 that suppress the transcription by histone deacetylation. GFI1 could be the potential suppressive trans-acting element present in 5'UTR of IGF1R promoter, as DE3-4 construct (which lacks +206 to +1043 bp region that harbours the predicted GFI1 binding motifs) showed significant increase in promoter activity as compared to the full-length promoter (Fig. 24) and needs further investigation.

**Table 3: Number of the predicted binding sites of the TFs on IGF1R promoter as predicted by JASPAR-TF database (threshold>75%)**

Number of binding sites for TFs on IGF1R promoter			
TF Name	Number of binding sites	TF Name	Number of binding sites
RXR:RXR	7	RUNX1	8
RXR:ROR	2	NKX2.5	4
SOX9	4	SOX18	3
GFI1	4	FOXO3a	8
ROR	3	E2F1	9
SP1	25	TFIID	0

To validate the identified candidates, we employed an inducer/inhibitor-based approach and tested the retinoic acid family related (RXR and ROR) and VDR, which bind to DNA as homo/hetero-dimers (Fig. 27A). No change in IGF1R-promoter or human sodium-iodide-symporter-(hNIS)-promoter (a known RA target) [336] activity was observed in A2780 and A2780-dual<sup>ER</sup> cells treated with all-trans-RA retinoic acid derivative (ATRA) (Fig. 27B-C). However, ATRA upregulated hNIS-promoter and downregulated IGF1R-promoter in MCF-7 cells (Fig. 27B). Though SOX9 and GFI1 showed maximum binding in TF promoter binding TF array, due to unviability of suitable activator or inhibitor we choose RUNX1 for further validation. Strong DNA binding activity of RUNX1 requires hetero-dimerization with CBF $\beta$  which can be inhibited by a small molecule, Ro5-3335 (Fig. 27D) [337]. Treatment with Ro5-3335 led to decrease in IGF1R-promoter- reporter activity in A2780 and OAW42 Cis-Pac resistant models at all stages of resistance. This reduction was more profound in A2780-dual<sup>ER</sup> and OAW42-dual<sup>ER</sup> cells compared to the respective sensitive and late resistant cells, 2.0 and 1.7-fold reduction respectively (Fig. 27E-F). Thus, RA family member TFs RXR and ROR might not be true regulators of IGF1R promoter,

whereas hematopoietic transcription factor RUNX1 could be positive regulator of IGF1R promoter during acquirement of chemoresistance in EOC cells.

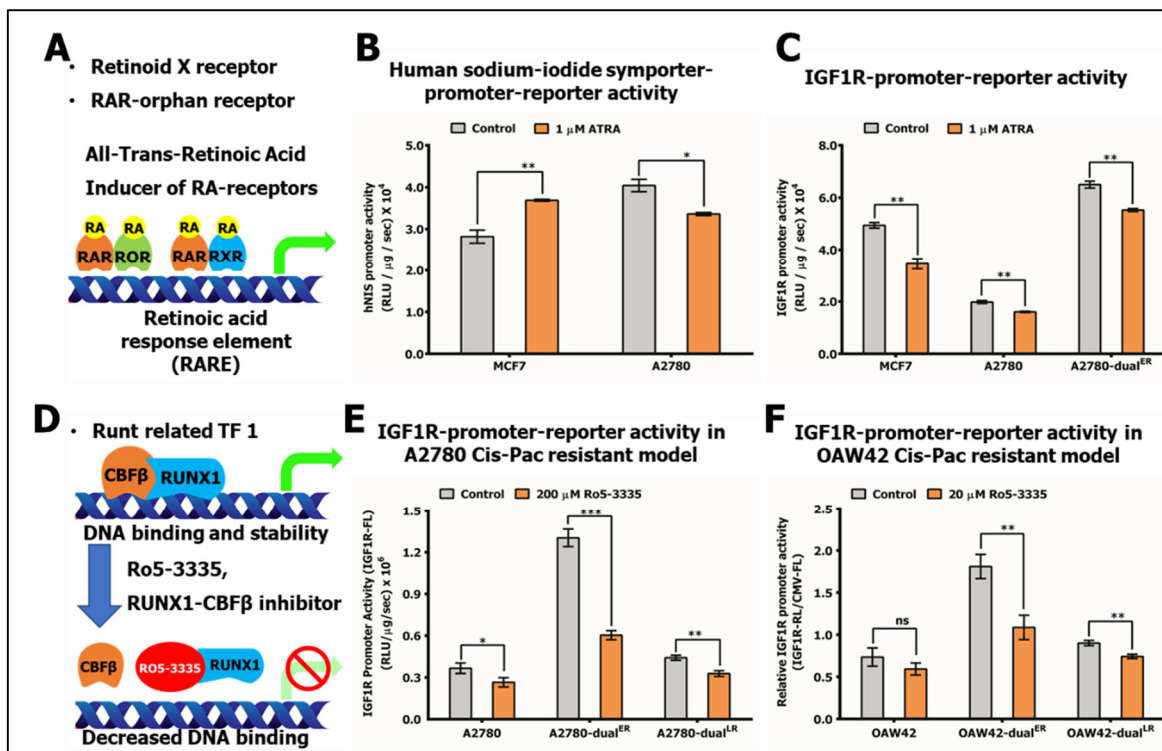


**Figure 27: Validation of IGF1R promoter binding TFs identified through Promoter-binding TF plate array**

**A.** Pictorial representation of retinoic acid derivative (ATRA) mediated binding of RAR and RXR to RARE on target genes. **B.** hNIS promoter activity in All-trans-RA treated MCF-7 and A2780 cells showing increase hNIS promoter only in MCF7. **C.** IGF1R promoter activity in All-trans-RA treated MCF7, A2780 and A2780-dualER cells showing no change in IGF1R promoter activity in A2780 and A2780-dualER cells. **D.** Pictorial representation of Ro5-3335 inhibiting RUNX1-CBF $\beta$  heterodimerization and DNA binding. **E-F.** Ro5-3335 (A2780=200 $\mu$ M and OAW42=20  $\mu$ M) reduced IGF1R-promoter activity in parental as well as chemoresistant cells with maximal effect in ER-cells of A2780 and OAW42 Cis-Pac resistant models.

### 2.3.3 RUNX1 a novel regulator of IGF1R promoter in EOC cells

RUNX1 is known as master regulator of haematopoiesis and serves as a pioneering TF that regulates DNA binding affinity and activity of other TFs involved in haematopoiesis [338-340]. RUNX1 is one of the most frequently mutated genes in a variety of haematological malignancies [341]. Aberrant expression and functional consequences of increased RUNX1 expression are increasingly reported in solid tumors [342]. In EOC patients, RUNX1 overexpression was found in primary and omental metastatic tumors, moreover increased RUNX1 expression post chemotherapy was attributed to hypomethylation of the gene [343-345]. Since, Ro5-3335 attenuated IGF1R promoter-reporter activity at early stages of resistance in both A2780 and OAW42 chemoresistant models, we further evaluated role of RUNX1 in regulation of IGF1R in chemoresistant EOC cells. Ro5-3335 treatment reduced endogenous IGF1R transcript levels by 1.7 and 1.9-fold in A2780-dual<sup>ER</sup> and cells OAW42-

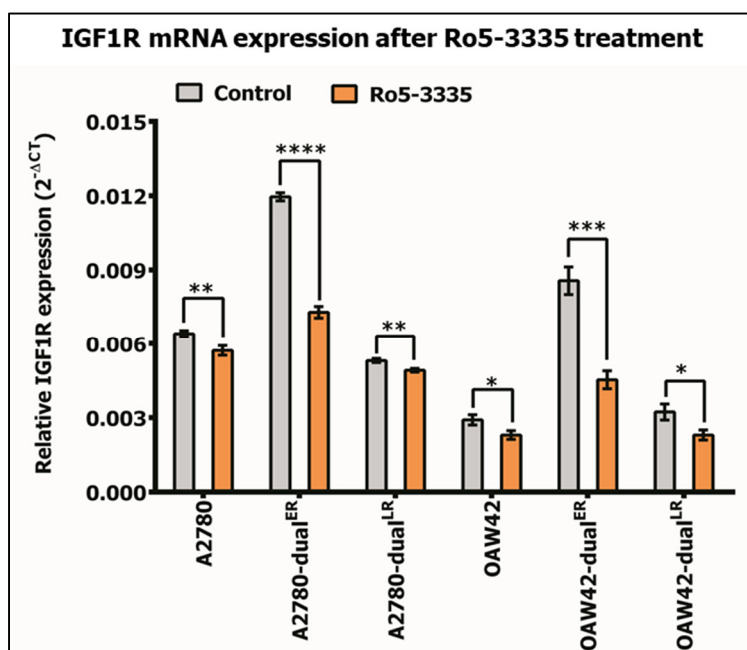


**Figure 28: RUNX1 inhibition downregulates IGF1R transcript levels in EOC cells**

Ro5-3335 (A2780=200 $\mu$ M and OAW42=20 $\mu$ M) reduced IGF1R transcript levels in parental as well as chemoresistant cells with maximal effect in ER-cells.

dual<sup>ER</sup> respectively, however no significant change was observed in sensitive and late resistant cells of both A2780 and OAW42 Cis-Pac resistant models (Fig. 28). Since both IGF1R promoter-reporter activity and IGF1R mRNA levels were significantly attenuated by Ro5-3335 treatment at early stages of chemoresistance we checked expression of RUNX1 and

other RUNX family members (RUNX2 and RUNX3) across resistant models. RUNX1 transcript levels were found to be increased in both early and late resistant cells (A2780-dual<sup>ER</sup>/A2780-dual<sup>LR</sup>/OAW42-dual<sup>ER</sup>/OAW42-dual<sup>LR</sup>) (Fig. 29A), whereas RUNX2 levels were significantly low in both A2780 and OAW42 Cis-Pac resistant models and RUNX3 transcript levels found to be only increased in late resistant cells (A2780-dual<sup>LR</sup>/OAW42-dual<sup>LR</sup>) (Fig. 29B). No change in transcript levels of RUNX1 binding partner CBF $\beta$  was

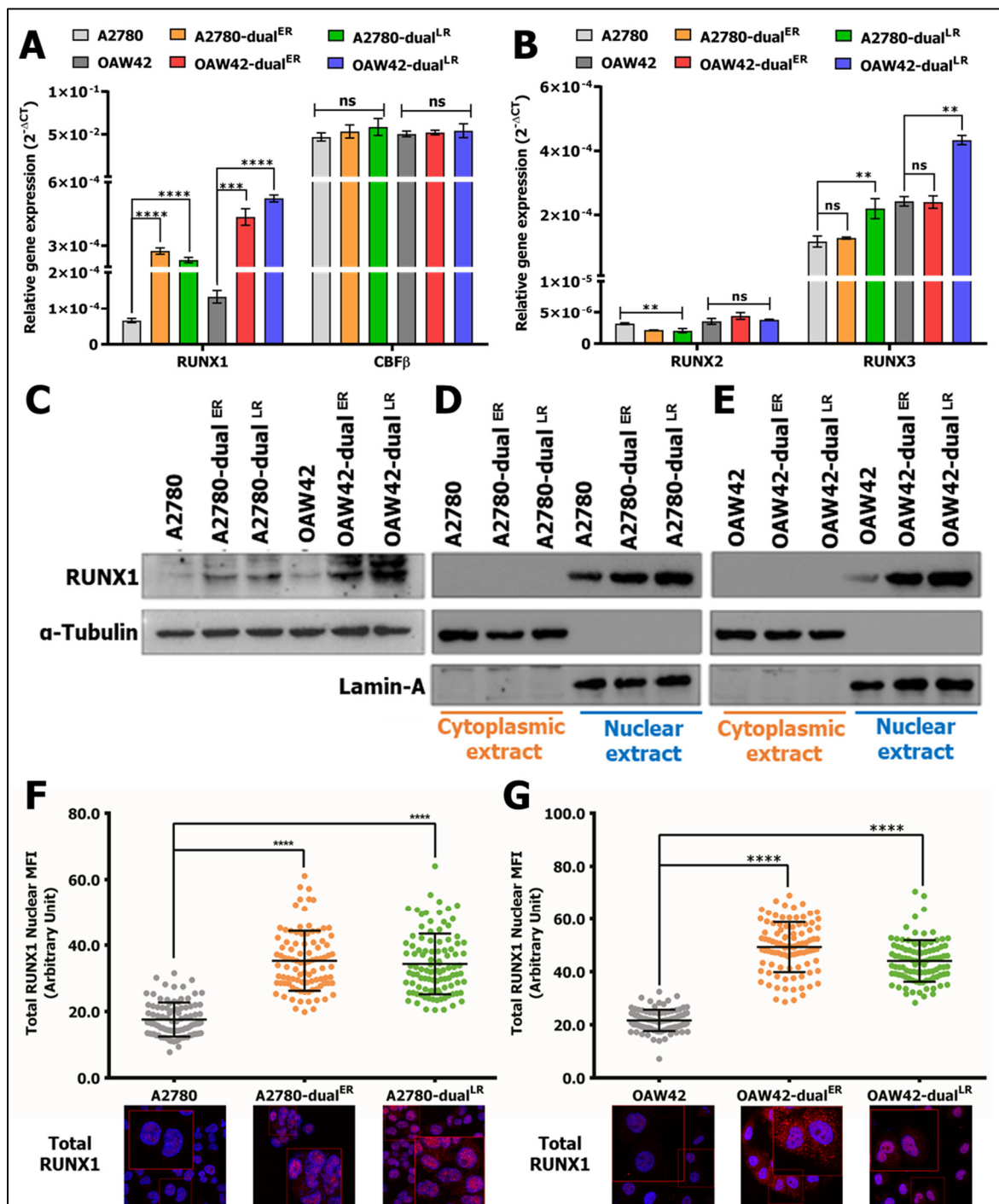


**Figure 29: RUNX1 shows enhanced expression in resistant EOC cells**

**A.** Real-time PCR showing increased transcript levels of RUNX1 in A2780-dual<sup>ER</sup>/A2780-dual<sup>LR</sup>/OAW42-dual<sup>ER</sup>/OAW42-dual<sup>LR</sup> cells, whereas no change in CBF $\beta$  transcript levels was seen across both A2780 and OAW42 Cis-Pac resistant models. **B.** Real-time PCR showing no change in transcript levels of RUNX2 across both A2780 and OAW42 Cis-Pac resistant models, and increased transcript levels of RUNX3 only in A2780-dual<sup>LR</sup>/OAW42-dual<sup>LR</sup> cells. **C-G.** Immunoblot and immunofluorescence shows increased expression and increased nuclear localization of RUNX1 in A2780-dual<sup>ER</sup>/A2780-dual<sup>LR</sup>/OAW42-dual<sup>ER</sup>/OAW42-dual<sup>LR</sup> cells.

seen across both A2780 and OAW42 Cis-Pac resistant models (Fig. 29A). RUNX1 mRNA, protein and nuclear localization were enhanced in both early and late stages of resistance (Fig. 29A, C-G), yet intriguingly Ro5-3335 treatment reduced IGF1R-promoter-reporter activity and transcript levels maximally at early stages of resistance. Hence, we further checked RUNX1 binding to IGF1R promoter by site specific ChIP across the resistant models for four predicted RUNX1 response elements on IGF1R promoter. Among the four predicted response elements (Fig. 30A), specific binding of RUNX1 was observed only on sites 1 and 2 but not on sites 3-4 on IGF1R promoter and RUNX1 occupancy on IGF1R

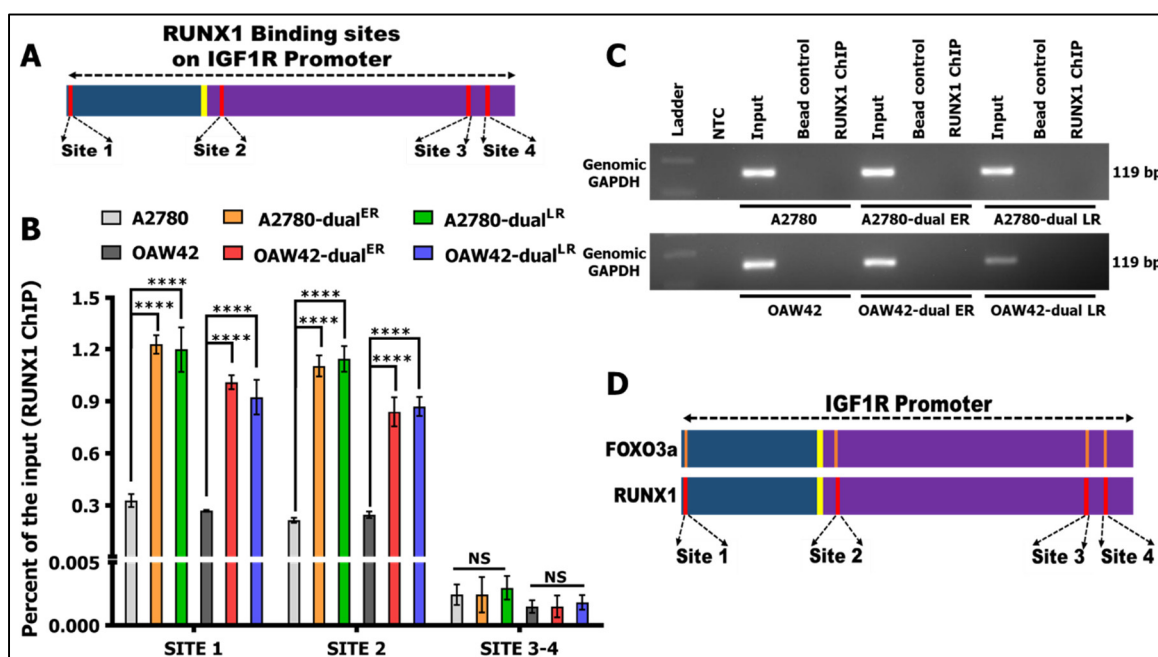


**Figure 30: RUNX1 ChIP across A2780 and OAW42 Cis-Pac resistant models**

**A.** Pictorial representation of predicted RUNX1 binding motifs on IGF1R promoter. **B.** RUNX1-ChIP shows increased binding of RUNX1 to IGF1R promoter on S1 and S2 but not on S3-4 in A2780-dual<sup>ER</sup>/A2780-dual<sup>LR</sup>/OAW42-dual<sup>ER</sup>/OAW42-dual<sup>LR</sup> cells (values were plotted as % binding of RUNX1 compared to input-DNA). **C.** Gel image showing amplification of genomic locus of GAPDH (lacking RUNX1 binding motifs) only in input DNA and not in bead control and RUNX1 ChIP DNA ensuring RUNX1 specific ChIP across A2780 (upper panel) and OAW42 (lower panel) Cis-Pac resistant model. **D.** Pictorial depiction of proximity of RUNX1 and FOXO3a predicted binding motifs of using JASPAR-TF database.

promoter was increased in both early and late resistant cells, as compared to sensitive counterparts of both A2780 and OAW42 Cis-Pac resistant models (Fig. 30B).

Though RUNX1 occupancy on IGF1R promoter remained comparable across the resistance stages, the effect of Ro5-3335 was more profound in ER-cells indicating possible involvement of other positive regulator/s in modulation of IGF1R during acquirement of chemoresistance. Intriguingly, RUNX1 binding sites were found to be in proximity of FOXO3a response elements (Fig. 30D), a known regulator which was not represented in the TF-array. We already have reported enhanced FOXO3a transcript levels in chemoresistant EOC cells [252]. The RUNX transcription factor family members in complex with the CBF $\beta$  co-factor produces a stable DNA binding complex which alone or in combination with other factors regulate gene expression. The direct physical interaction between RUNX1 and several other transcription factors stabilizes the final transcription complex and enhances the DNA binding affinity for each single factor [340]. We hypothesize that RUNX1 and FOXO3a might co-operatively control IGF1R expression during chemoresistance development in EOC cells.

### 2.3.4 FOXO3a and RUNX1 positively regulate IGF1R promoter at the onset of chemoresistance

FOXO3a, a member of Fork-Head-Box family transcription factors, which are commonly activated in stress conditions and assist cells to survive the stress or drive them towards apoptosis. Transcriptional activity of this family of proteins is modulated through differential phosphorylation either leading to its activation or degradation. To evaluate the role FOXO3a in regulation of IGF1R promoter, we first checked effect of mutating FOXO3a consensus motifs on IGF1R promoter at site 1 and 2. Mutating FOXO3a response elements at S1( $\Delta$ -S1)/S2( $\Delta$ -S2) individually or together decreased IGF1R promoter activity by 3.4-fold in A2780-dual<sup>ER</sup> cells, while it decreased only 1.7 and 1.5-fold in A2780 sensitive and A2780-Cis-Pac<sup>LR</sup> cells respectively (Fig. 31A). Similarly, IGF1R promoter activity decreased more significantly in OAW42-Cis-Pac<sup>ER</sup> cells when both FOXO3a binding sites were mutated together (Fig. 31B). RUNX1 inhibition by Ro5-3335 and perturbation of FOXO3a consensus motifs specifically attenuated IGF1R promoter activity in early resistant cells. Furthermore, FOXO3a protein levels (Fig. 32A) were found to be increased in A2780-

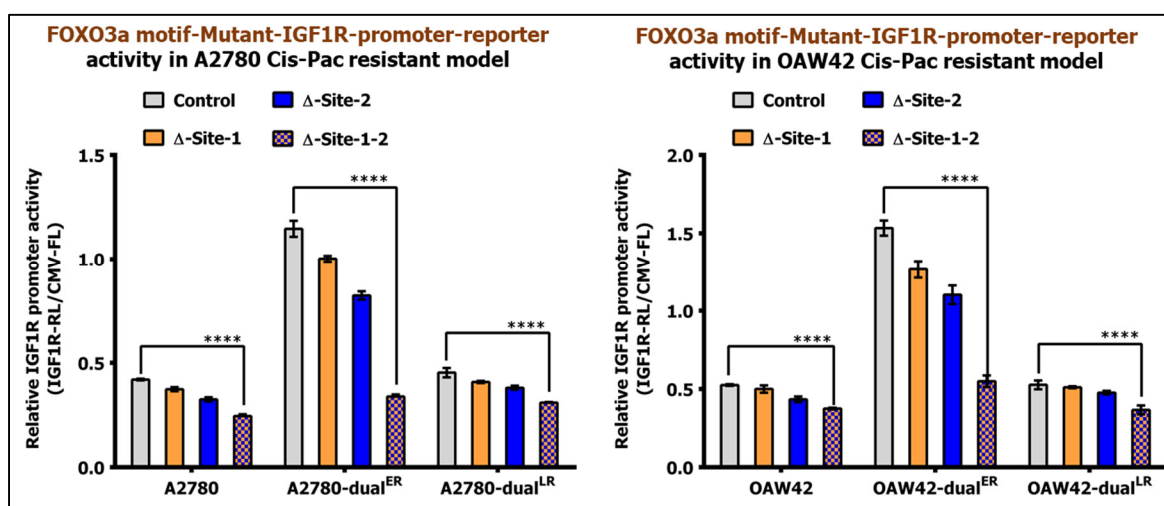


**Figure 31: FOXO3a positively regulates IGF1R promoter activity in EOC cells**

**A-B.** Mutating FOXO3a binding sites ( $\Delta$ -S1,  $\Delta$ -S2 and  $\Delta$ -S1-S2) decreased IGF1R-promoter activity in parental as well as chemoresistant cells with maximal effect in ER-cells of A2780 (A) and OAW42 (B) Cis-Pac resistant models.

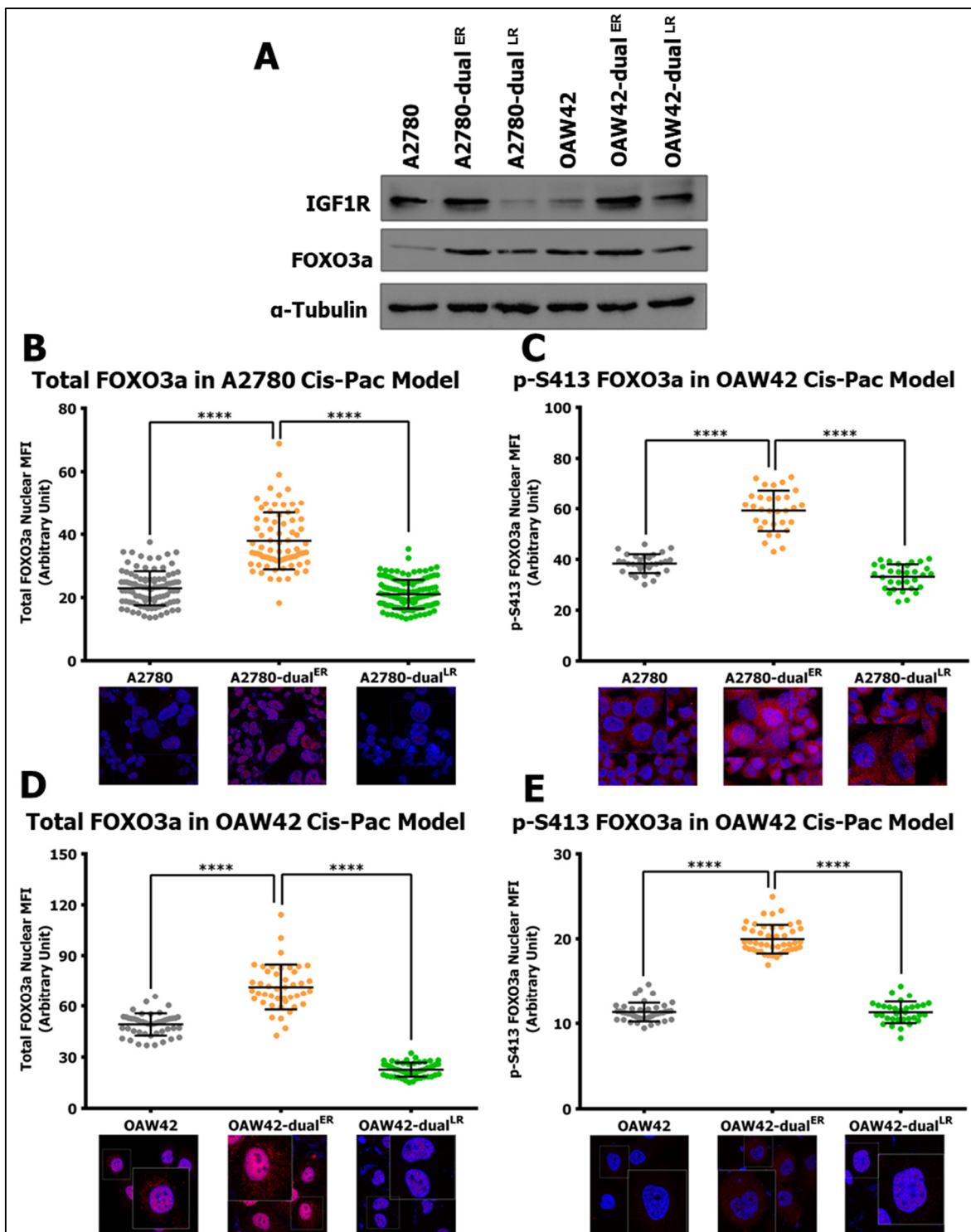


**Figure 32: Increased expression and activation of FOXO3a at early stage of chemoresistance development**

A-E. Immunoblot (A) and immunofluorescence show increased expression and enhanced nuclear localization of total (B and C) and phospho-S413 (D and E) (activation mark) FOXO3a in ER-cells of both A2780 and OAW42 Cis-Pac resistant models.

dual<sup>ER</sup> cells and OAW42-dual<sup>ER</sup> cells and showed enhanced nuclear localization for both

total and activated (p-S413) FOXO3a in A2780-dual<sup>ER</sup> cells and OAW42-dual<sup>ER</sup> cells as compared to their respective sensitive and late resistant counterparts (Fig. 32B-E). Hence, we next assessed the direct binding of FOXO3a by site specific ChIP across the resistant models for site1 and 2 on IGF1R promoter. ChIP assay showed highest occupancy of FOXO3a on S1 and S2 sites of IGF1R promoter (0.1235% and 0.2534% respectively) in A2780-dual<sup>ER</sup> cells which dropped below 0.05% in both A2780 and A2780-dual<sup>LR</sup> cells (Fig. 33A). Similarly, percent occupancy of FOXO3a on both the sites was higher in OAW42-dual<sup>ER</sup> cells compared to OAW42 and OAW42-dual<sup>LR</sup> cells (Fig. 33A). Since RUNX1 inhibition or mutation at FOXO3a response elements led to suboptimal decrease in IGF1R promoter activity, combinatorial effect for both these molecular alterations were

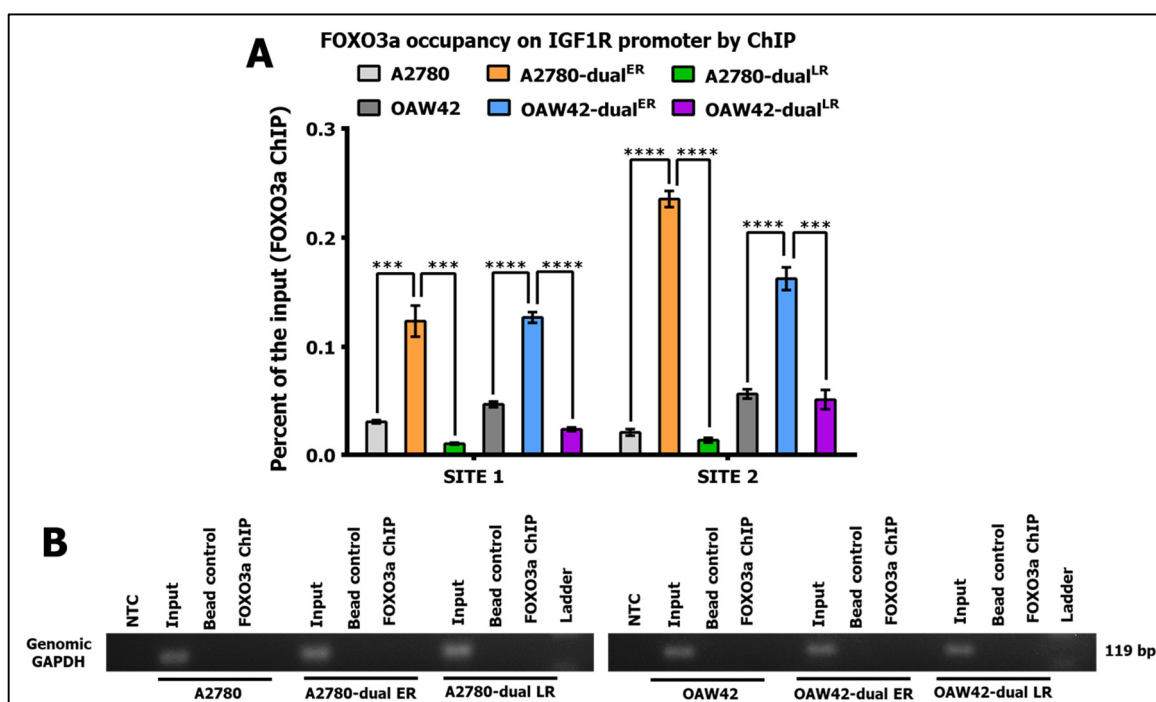


**Figure 33: FOXO3a ChIP across A2780 and OAW42 Cis-Pac resistant models**

Enhanced binding of FOXO3a to site1 and site2 was observed only in A2780-dual<sup>ER</sup>/OAW42-dual<sup>ER</sup> cells (values were plotted as % binding of FOXO3a compared to input-DNA). **B.** Gel image showing amplification of genomic locus of GAPDH (lacking FOXO3a binding motifs) only in input DNA and not in bead control and FOXO3a ChIP DNA ensuring FOXO3a specific ChIP across A2780 (left panel) and OAW42 (right panel) Cis-Pac resistant model.

tested in the models. IGF1R promoter activity was further reduced to 7.1 and 5.3-fold when compared to RUNX1 inhibition (2.0 and 2.1-fold) or mutant-promoter (2.8 and 2.3-fold) alone in A2780-dual<sup>ER</sup> and OAW42-dual<sup>ER</sup> cells respectively with minimal reduction in sensitive and LR cells (Fig. 34A-B). These results indicate that RUNX1 might cooperate with FOXO3a to orchestrate a transcriptional surge for IGF1R at the onset of resistance development in EOC cell lines.

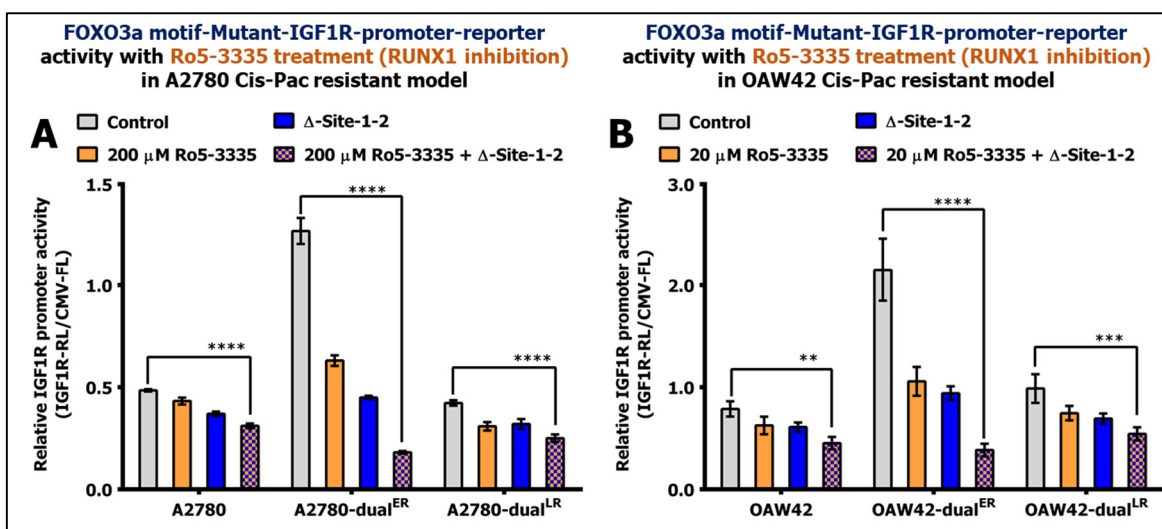


**Figure 34: RUNX1 and FOXO3a synergistically regulate IGF1R promoter activity in EOC cells during chemoresistant development**

$\Delta$ -S1-S2 mutant IGF1R promoter (FOXO3a site 1 and site 2 mutated) showed maximal reduction upon Ro5-3335 treatment (A2780=200 $\mu$ M and OAW42=20  $\mu$ M) in A2780-dual<sup>ER</sup> (A) and OAW42-dual<sup>ER</sup> (B) cells.

### 2.3.5 RUNX1 dictates FOXO3a binding to IGF1R promoter

The RUNX1 can influence the transcriptional dynamics through sequential or concurrent binding to its interacting partners. RUNX1 was shown to modulate the oncogenic Myb and Myc enhancer activity in T-cell acute lymphoblastic leukaemia cell lines and primary patient samples to regulate expression of TAL1- and NOTCH1 [346]. In B-cell acute lymphoblastic leukaemia FUBP1 and RUNX1 were shown to cooperate for upregulation of the oncogene c-KIT, promoting cell proliferation and resistance against c-KIT inhibitor imatinib mesylate [347]. RUNX1 is also shown to interact with FOXO3a during 3D breast epithelial acinar

morphogenesis, jointly regulating transcription of genes related to oxidative stress response and proliferation [348]. To assess whether RUNX1 and FOXO3a exist as complex in the EOC cells, IP of RUNX1 was performed from all the stages of A2780 Cis-Pac resistant model and probed for co-IP of FOXO3a. A significant interaction of FOXO3a with RUNX1 was observed only in the ER cells despite of incremented level of immune-precipitated RUNX1 with increasing resistance (Fig. 35). This data indicates that both FOXO3a and RUNX1 can exist as a complex and ER cells possess highest amount of such complex.

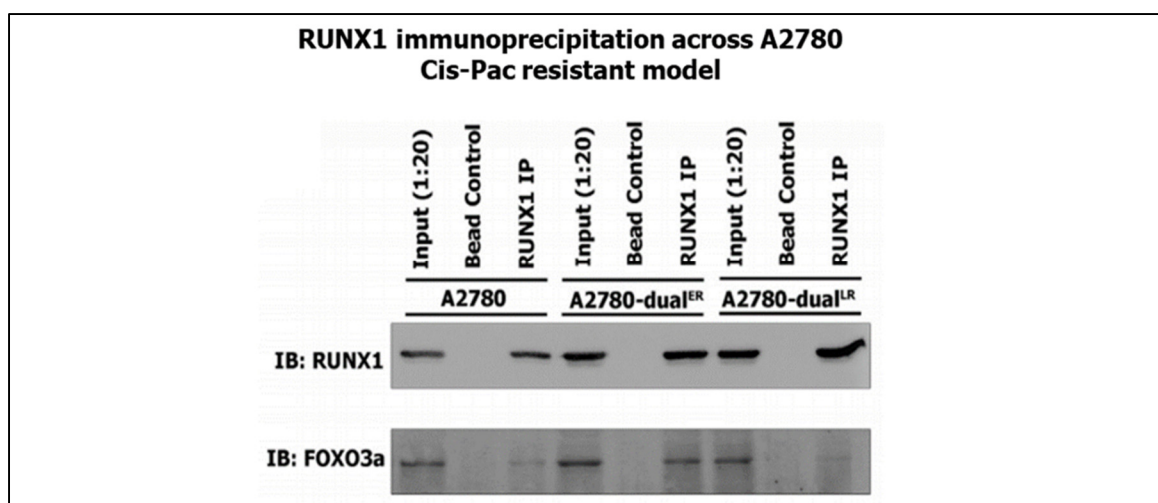


**Figure 35: RUNX1 and FOXO3a show enhanced interaction at early stage of chemoresistance development**

Co-immunoprecipitation across A2780-Cis-Pac resistance model showed maximum RUNX1-FOXO3a interaction in ER cells followed by A2780 cells and least in LR cells.

Since, both FOXO3a and RUNX1 possess DNA binding ability in their own capacity and in complementation with other transcriptional modulators, we aimed to understand the kinetics of cooperativity between RUNX1 and FOXO3a for IGF1R promoter occupancy. The sequential ChIP or ChIP-re-ChIP enables investigation of concurrently binding proteins on desired region of DNA sequence and enables to analyse the co-occupancy of transcription factors and DNA modifiers. ChIP-re-ChIP assay was performed in both combinations i.e., RUNX1-FOXO3a sequential ChIP or FOXO3a-RUNX1 sequential ChIP in A2780 Cis-Pac resistant model. Both the factors were able to co-occupy the IGF1R promoter at sensitive

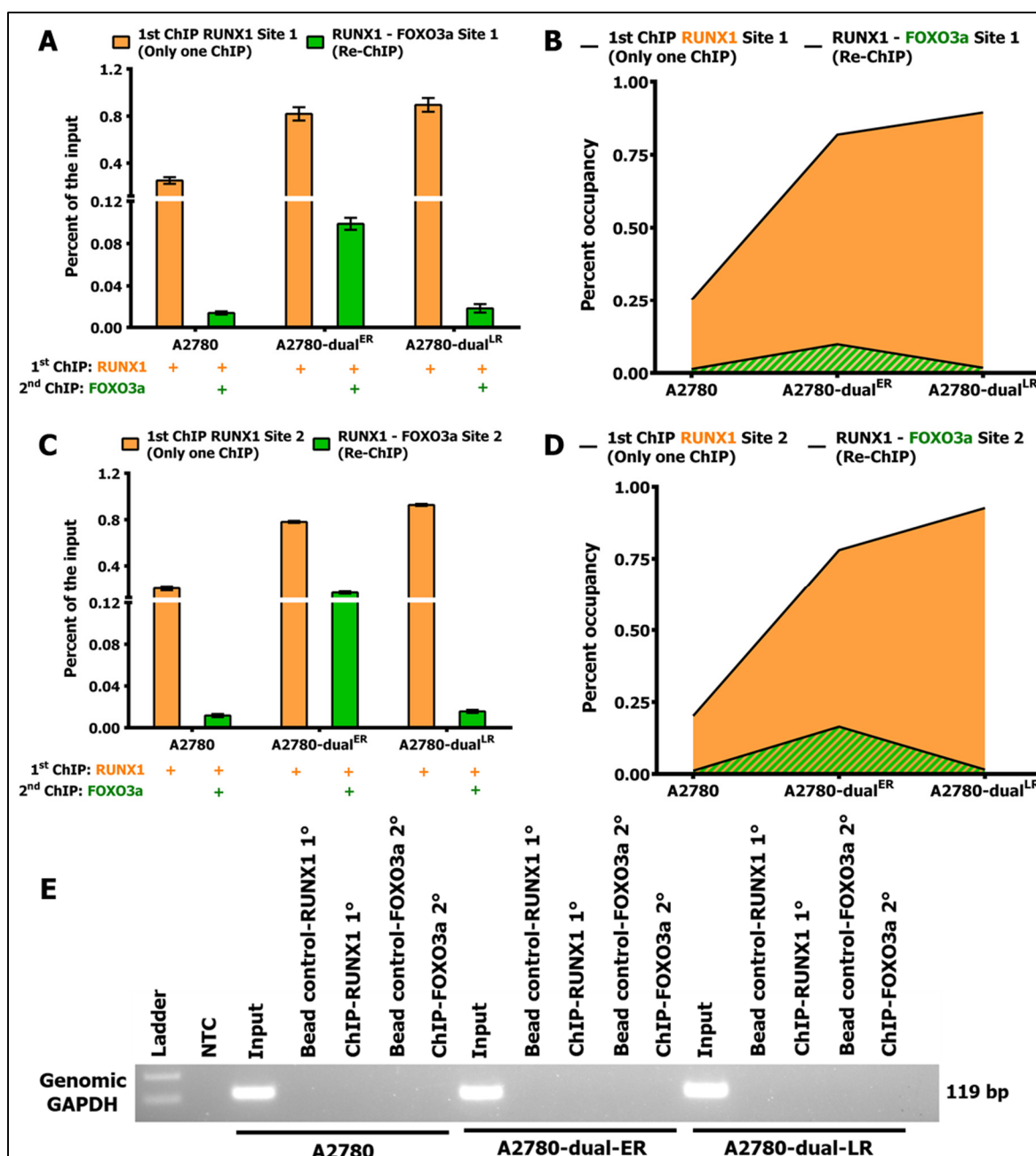


**Figure 36: RUNX1-FOXO3a (ChIP-re-ChIP) show enhanced co-occupancy on IGF1R promoter at early stage of chemoresistance development**

**A-D.** ChIP-re-ChIP of RUNX1 followed by FOXO3a on site 1 (A) and site 2 (C). Area plot (B&D) depicts the RUNX1 bound region co-occupied by FOXO3a. **E.** Gel image showing amplification of genomic locus of GAPDH only in input DNA and not in bead control and ChIP DNA.

and all stages of resistance, though the occupancy differed for each of them (Fig. 36 & Fig. 37). As observed previously RUNX1 conferred a much stronger binding in both early and late resistant cells after first round of RUNX1-ChIP (Fig. 36A&C), whereas in subsequent

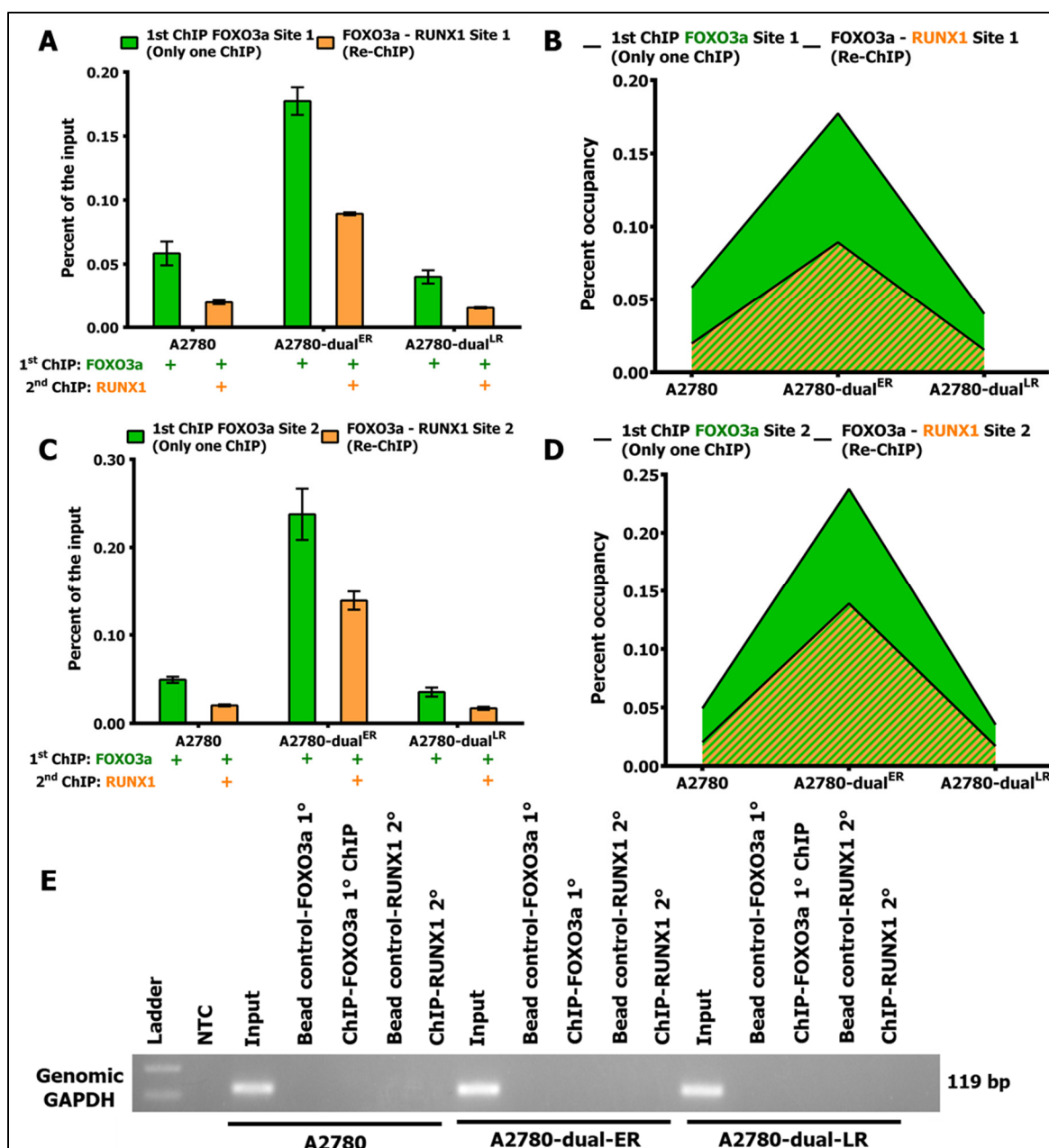


**Figure 37: FOXO3a-RUNX1 (ChIP-re-ChIP) show enhanced co-occupancy on IGF1R promoter at early stage of chemoresistance development**

**A-D.** ChIP-re-ChIP of FOXO3a followed by RUNX1 on site 1 (A) and site 2 (C). Area plot (B&D) depicts the FOXO3a bound region co-occupied by RUNX1. **E.** Gel image showing amplification of genomic locus of GAPDH only in input DNA and not in bead control and ChIP DNA.

second round of ChIP FOXO3a showed preferential higher binding only in early resistant cells as compared to sensitive and late resistant cells (Fig. 36 B&D), indicating higher co-occupancy of FOXO3a in RUNX1 bound IGF1R promoter specifically in early resistant

cells. Similarly, in FOXO3a-RUNX1- ChIP-re-ChIP also showed higher co-occupancy of FOXO3a and RUNX1 on IGF1R promoter at both the sites in early resistant cells (Fig. 37A-D). Irrespective of the combination of ChIP-re-ChIP, RUNX1 and FOXO3a showed enhanced co-occupancy in A2780-dual<sup>ER</sup> cells as compared to A2780-sensitive and A2780-dual<sup>LR</sup> cells on IGF1R promoter. Since RUNX1 and FOXO3a show augmented interaction and increased co-occupancy at early stage of resistance and co-operation between FOXO3 and RUNX1 is known to influence Bim promoter activity and expression [349] we asked whether RUNX1 plays a similar role for IGF1R promoter. We performed FOXO3a ChIP across A2780 and OAW42 Cis-Pac resistant model after RUNX1 inhibition using Ro5-3335. FOXO3a-ChIP in presence of Ro5-3555 showed that percent occupancy of FOXO3a on S1 and S2 remained unchanged in A2780-sensitive and A2780-dual<sup>LR</sup> cells, whereas in

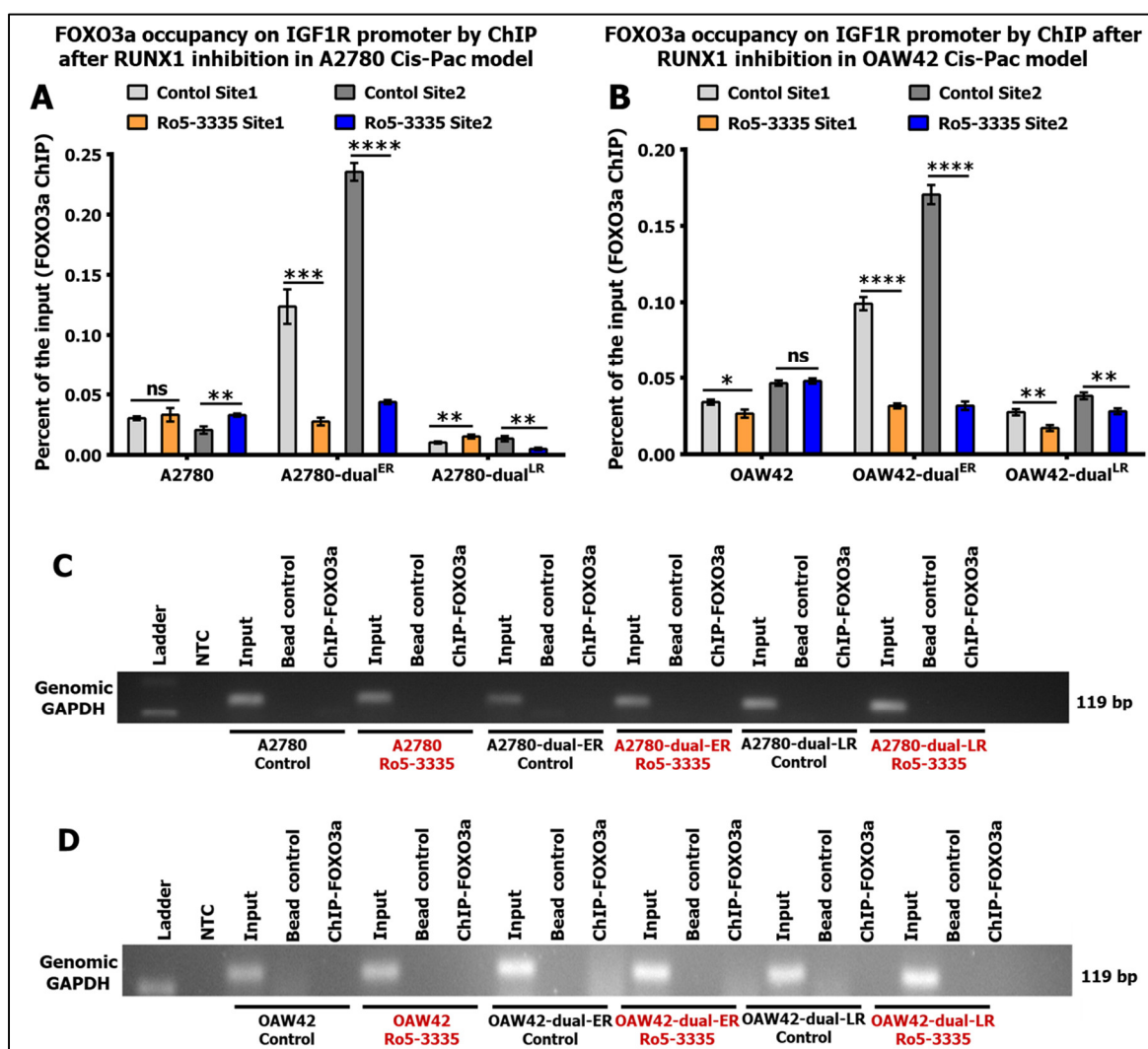


**Figure 38: RUNX1 inhibition attenuates FOXO3a binding to IGF1R promoter**

**A-B.** Ro5-3335 treatment specifically attenuated binding of FOXO3a to site1 and site2 in A2780-dual<sup>ER</sup>/OAW42-dual<sup>ER</sup> cells (Values were plotted as % binding compared to input-DNA). **C-D.** Gel image showing amplification of genomic locus of GAPDH (lacking FOXO3a binding motifs) only in input DNA and not in bead control and FOXO3a ChIP DNA ensuring FOXO3a specific ChIP across A2780 (C) and OAW42 (D) Cis-Pac resistant model.

A2780-dual<sup>ER</sup> cells percent occupancy of FOXO3a on S1 and S2 decreased significantly from 0.1236% to 0.0276% (4.5 fold) and 0.2354% to 0.0437% (5.4 fold) (Fig. 38A). Similarly, FOXO3a occupancy on both sites were decreased in OAW42-dual<sup>ER</sup> cells to 3.1 and 5.4-fold in presence of the RUNX1 inhibitor, no significant change was observed in OAW42-sensitive and OAW42-dual<sup>LR</sup> cells (Fig. 38B). To further confirm that the

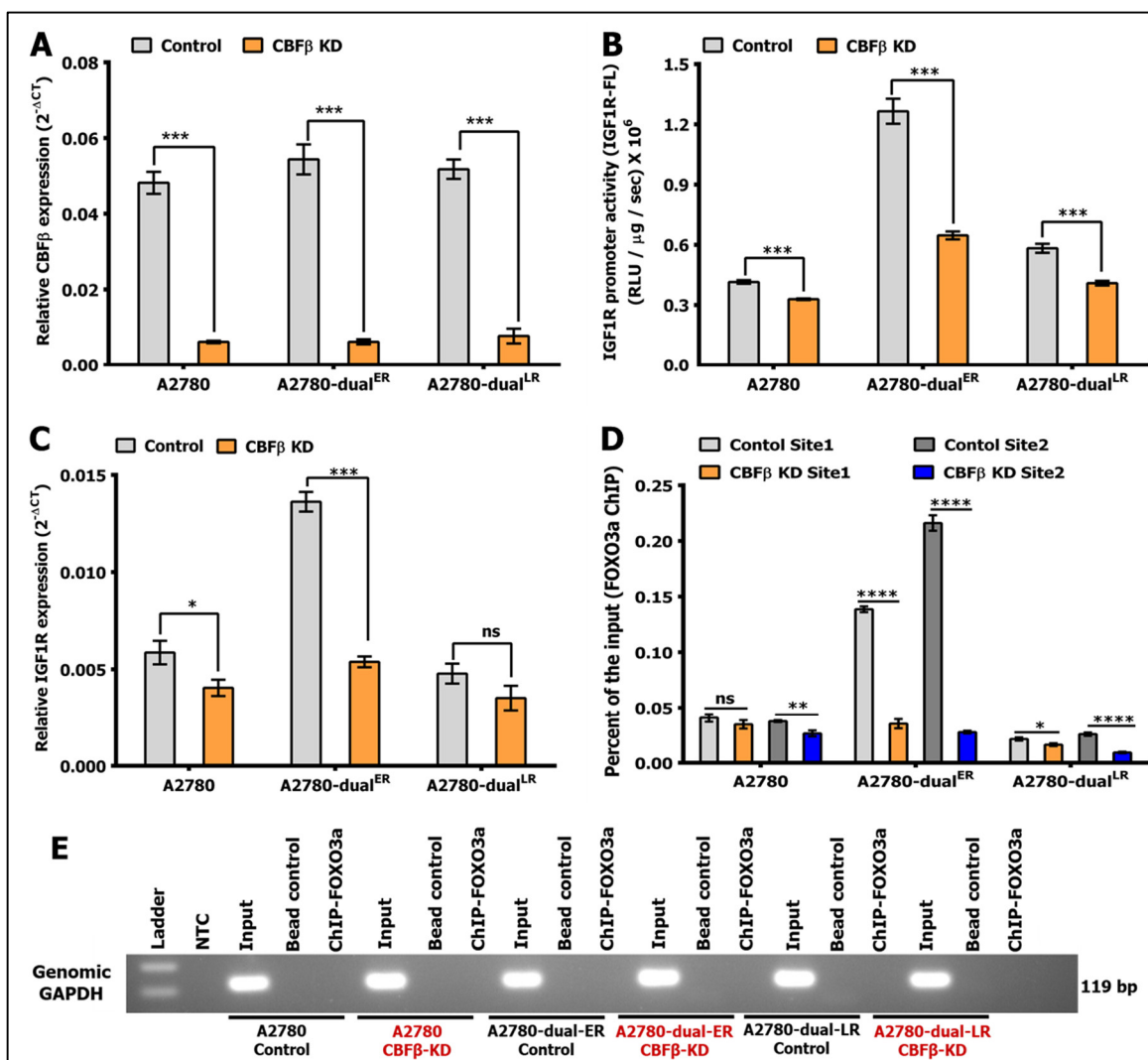


**Figure 39: RUNX1 dictates FOXO3a binding to IGF1R promoter**

**A.** Real-time PCR showing extent of knockdown of CBF $\beta$  in A2780 dual-resistant model. **B-C.** CBF $\beta$ -KD reduced IGF1R transcript level and attenuated IGF1R-promoter activity specifically and significantly in A2780-dual<sup>ER</sup> cells. **D.** CBF $\beta$ -KD specifically attenuated binding of FOXO3a to site1 and site2 in A2780-dual<sup>ER</sup> cells (Values were plotted as % binding compared to input-DNA). **E.** Gel image showing amplification of genomic locus of GAPDH (lacking FOXO3a binding motifs) only in input DNA and not in bead control and FOXO3a ChIP DNA ensuring FOXO3a specific ChIP across A2780 Cis-Pac resistant model.

cooperative interaction of RUNX1 and FOXO3a on IGF1R regulation occurs exclusively at the onset of resistance, CBF $\beta$  gene was silenced in A2780 Cis-Pac chemoresistant model (Fig. 39A). Silencing of CBF $\beta$  significantly attenuated IGF1R transcripts and promoter activity only in A2780-dual<sup>ER</sup> cells compared to their counterparts (Fig. 39B-C). FOXO3a-ChIP across CBF $\beta$ -KD A2780 Cis-Pac resistant model showed similar results observed with RUNX1 inhibitor Ro5-3335. Binding of FOXO3a was significantly affected in CBF $\beta$ -KD-A2780-dual<sup>ER</sup> cells (4.0-fold and 7.9-fold drop on S1 and S2 respectively). However, FOXO3a binding on those sites remained unchanged for CBF $\beta$ -KD-A2780 and CBF $\beta$ -KD-A2780-dual<sup>LR</sup> cells (Fig. 39D). Thus, not only RUNX1 and FOXO3a show stronger cooperation and occupancy, but RUNX1 also influences the binding of FOXO3a to IGF1R promoter driving transcriptional surge at onset of chemoresistant development in EOC cells.

**2.3.6 AKT-FOXO3a negative feedback loop leads to pulsatile expression of IGF1R**

Though RUNX1 levels did not alter between early and late resistant cells, the total Foxo3a protein level declined with concomitant decrease in IGF1R expression in late resistant stages. Multiple post transcriptional modifications (PTMs) such as, phosphorylation, acetylation, and ubiquitination, regulate both subcellular localization and transcriptional activity of the FOXO3a [350]. In response to growth factor signalling phosphorylation of FOXO3a by the downstream effector kinases, AKT, SGK, ERK, CK1, and IKK $\beta$  induce

cytoplasmic translocation of FOXO3a, and in contrast under stress conditions JNK, MST1, and AMPK promote nuclear localization and transcriptional activation of FOXO3a. Apart from phosphorylation, mono-ubiquitination and deacetylation by SIRT1/2 stabilize the

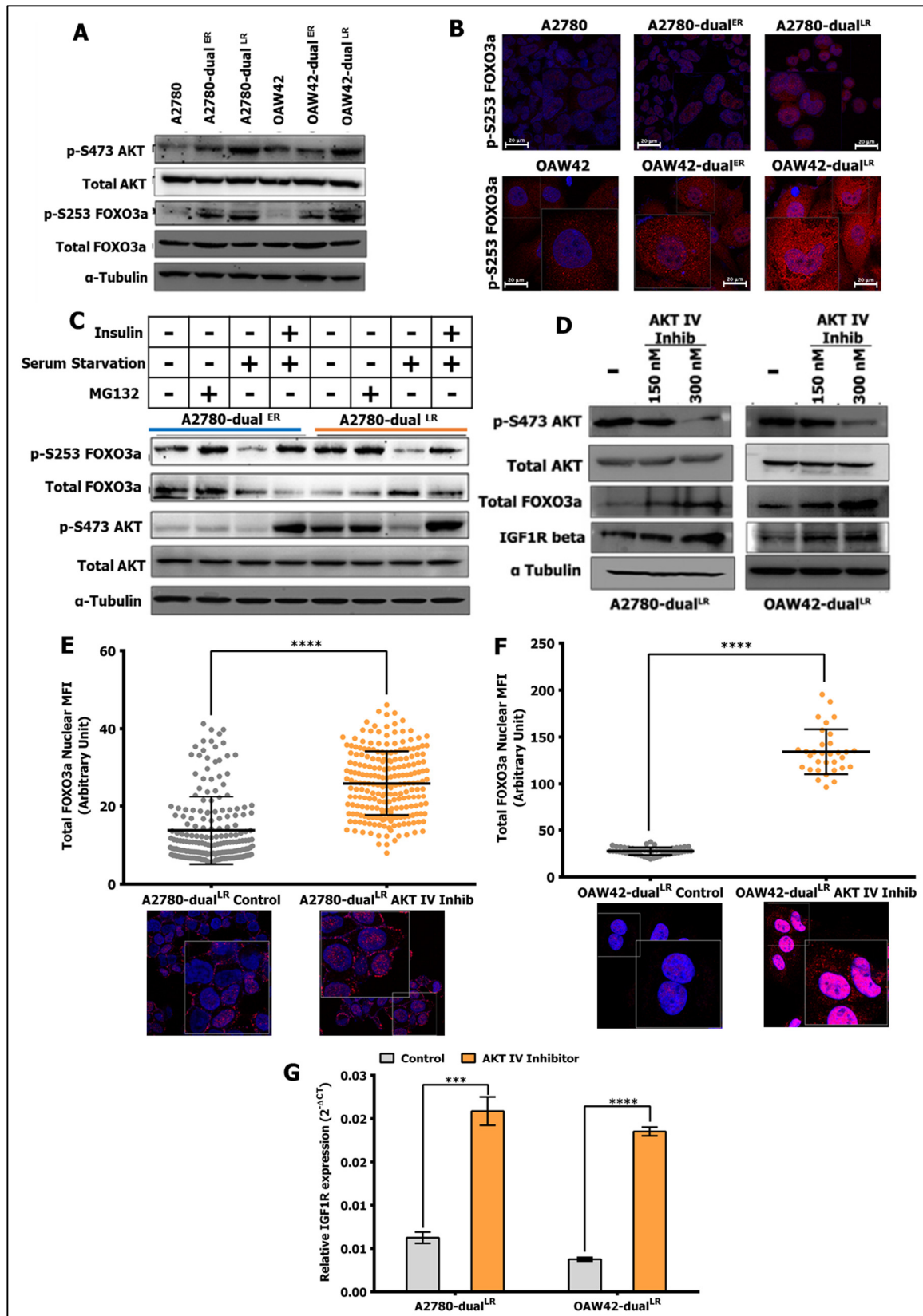


**Figure 40: AKT-FOXO3a feedback loop negatively regulates IGF1R expression at late-resistant stages**

**A-B.** Immunoblot (A) and immunofluorescence (B) showing incremental levels of p-S473-AKT and p-S253-FOXO3a with increasing resistance in A2780/OAW42 models. **C.** Serum starvation led to loss of both p-S473-AKT and p-S253-FOXO3a in A2780-dual<sup>ER</sup> and dual<sup>LR</sup> cells and increased FOXO3a levels in A2780-dual<sup>LR</sup> cells. Insulin stimulation led to sharp increase in p-S253-FOXO3a in both ER and LR cells. **D-G.** Effect of AKT-IV on FOXO3a and IGF1R. Increased nuclear localization (E&F) and total FOXO3a (D), decreased p-S473-AKT (D) and increased IGF1R mRNA (G) and IGF1R protein (D) were observed in A2780-dual<sup>LR</sup> and OAW42-dual<sup>LR</sup> cells.

FOXO3a protein levels and enhance the transcriptional activity of FOXO3a [350]. Both A2780 and OAW42 Cis-Pac resistant cellular models show increased FOXO3a nuclear localization of total and transcriptionally active (p-S413) at early stages of resistance which subsequently decreases in late resistant cells. To understand the underlying mechanism of the FOXO3a decline, we looked at the post-translational modifications which is known to control the stability of the protein. The late resistant cells are characterised by high level of activated AKT [351] which is known to promote FOXO3a degradation by phosphorylating the protein at S253 and T32 residues [352]. Indeed p-S253-FOXO3a levels were found gradually increasing with resistance, peaking at late stages in both A2780 and OAW42 Cis-Pac resistant models, which corroborated with increasing levels of p-S473-AKT (active) being highest in LR cells (Fig. 40A-B). MG132, a potent proteasome inhibitor, increased p-S253-FOXO3a levels in A2780-dual<sup>ER</sup> and A2780-dual<sup>LR</sup> cells indicating active degradation of FOXO3a is mediated through S253 phosphorylation (Fig. 40C). Consequently, A2780 Cis-Pac resistant model cells cultured in serum deprived media showed decreased p-S473-AKT levels and simultaneous loss of p-S253-FOXO3a in both A2780-dual<sup>ER</sup> and A2780-dual<sup>LR</sup> cells but increase in total FOXO3a was observed only in A2780-dual<sup>LR</sup> cells (Fig. 40C). Insulin stimulation in serum starved cells restored p-S473-

AKT levels causing increase in p-S253-FOXO3a and decrease in total FOXO3a levels in both A2780-dual<sup>ER</sup> and A2780-dual<sup>LR</sup> cells (Fig. 40C). Finally, treatment of an AKT inhibitor-IV increased FOXO3a expression (Fig. 40D), enhanced nuclear localization (Fig. 40E-F) and increased IGF1R transcript (Fig. 40G) and protein levels (Fig. 40D) in A2780-dual<sup>LR</sup> and OAW42-dual<sup>LR</sup> cells.

## **2.4 Discussion**

Acquired chemoresistance is a dynamic and multifactorial phenomenon governed by non-linear signalling cascades through aberrant gene regulatory networks that are instrumental drivers of tumorigenesis and are highly adaptive to rewire during therapy resistance development. Increasingly, the molecular regulators of these aberrant gene regulatory networks, DNA and histone modifiers, cis-acting regulatory regions and trans-acting transcription factors have revealed dependency of many cancer types including Ovarian cancer, to dysregulated transcriptional programs driving both tumorigenesis and chemotherapy resistance [353-356]. Many of these dysregulated transcriptional modulators such as, c-Myc, E2F1, FOXM1, BRD4, RUNX1, RUNX1-ETO are overexpressed in many cancer types, promoting tumor proliferation, cell cycle progression, replicative immortality, metabolism, and immune evasion. The pluripotency transcription factors (OCT4, SOX2 and NANOG) and epithelial mesenchymal transcription factors (SNAIL, ZEB, SLUG and TWIST) are shown to orchestrate the expression of large number of genes helping cancer cells to metastasize and survive the chemotherapy induced cell death. Unlike other receptor tyrosine kinases which prominently show oncogenic mutations and gene amplification, IGF1R is predominantly shown to be modulated by an array of transcription factors which includes both wild type and oncogenic mutant tumor suppressors and oncogenic fusion transcription factors. IGF1R signalling plays an important role in embryonic and neonatal development through two major signalling arms (PIK3CA/AKT and MAPK/ERK

pathways) which when dysregulated aid in oncogenic transformation, uncontrolled cellular proliferation, evasion of apoptosis, altered metabolism, self-renewal, differentiation, and therapy resistance. Strong association between elevated IGF1R expression with therapy resistance, in particular with chemoresistance is reported in colorectal [357], lung [358], renal [359], ovarian [250] and prostate [360] and other cancers. Chemoresistance has been a major hurdle for majority of the cancers including EOC. IGF1R not only confers resistance to conventional chemotherapy (Cisplatin & Paclitaxel) but also to targeted therapies such as PIK3CA inhibitors [361] and Trastuzumab in EOC [265, 362]. These studies focus on implications of therapy induced IGF1R expression on cancer cell survival and onetime relation between extent of resistance and level of IGF1R expression often undermining the underlying signalling cascades driving dynamic nature of chemoresistance development. We recently reported increased IGF1R expression (both transcript and protein levels) at the onset of chemoresistance which declines at late stages of the resistance in chemoresistant cellular models [252]. These isogenic models, which were established over a period of 4-5 months using pulse method, depict the progression of chemoresistance mimicking the clinical condition. Similarly, a therapy induced transcriptional surge in IGF1R expression was observed in paired neoadjuvant chemotherapy treated tumors of a small cohort of advanced stage high grade serous EOC patients. To date, the underlying mechanisms behind this undulating IGF1R expression during progression of resistance that points towards a complex regulatory circuit has not been deciphered. In the present study, we identified RUNX1 as a novel positive regulator of IGF1R gene using a promoter-binding transcription factor array, which in cooperation with FOXO3a induces transcriptional surge in IGF1R expression at the onset of Cisplatin-Paclitaxel resistance in EOC cells. Augmented interaction between RUNX1 and transcriptionally active FOXO3a at early stage of chemoresistance leads to heightened RUNX1-FOXO3a co-occupancy on IGF1R promoter

driving transcriptional activation of IGF1R; whereas, such cooperative interaction falls apart when cells acquire maximal resistance towards the drugs (late resistant cells) leading to downregulation of IGF1R expression. The hyperactive AKT in late resistant cells exerts an active negative feedback loop on FOXO3a (protein degradation), hindering the RUNX-FOXO3a interaction leading to lower FOXO3a occupancy even in the presence of an optimally bound RUNX1 on IGF1R promoter and thus led to dynamic oscillatory modulation of IGF1R expression during acquisition of chemoresistance. The observed molecular dynamics of the two critical transcriptional regulators (RUNX1 and FOXO3a) and their cooperative action to regulate IGF1R signalling pathway portrays the intricate molecular network associated with acquisition of chemoresistance in EOC cells.

In absence of mutational activation and rare instances of gene amplification, overexpression of IGF1R gene is attributed to transcriptional and epigenetic modulation [212]. Intriguingly, the high GC rich IGF1R promoter is a prospective site for rich epigenetic interactions but such epigenetic regulations are seldom reported [212]. Conspicuous absence of methylation by SAM, a methyl donor agent in Glioblastoma cells and in benign and metastatic Prostate cancer cells [311, 312] points toward a pre-dominant role of the transcriptional regulators. Around 16.5% of EOC cases of The Cancer Genome Atlas (TCGA) dataset show enhanced IGF1R transcription and 4% cases show gene amplification [209, 210]. The unique IGF1R promoter is comprised of a GC rich 5'-flanking region without the TATA or CAAT box sequences and is differentially regulated by several TFs either directly or indirectly through SP1 in various circumstances [212]. A 1503bp long IGF1R promoter (consisting of 5'-flanking region, transcription initiator sequence and 5'-UTR) driving luciferase reporter system showed enhanced IGF1R promoter-reporter activity at early stages of chemoresistance development (A2780-dual<sup>ER</sup> and OAW42-dual<sup>ER</sup> cells as compared to the respective sensitive and late resistant cells). The deletion construct analysis showed that

majority of IGF1R promoter activity resides within -460 to +205 bp region of promoter in sensitive and chemoresistant EOC cells and +206 to +1043 bp region of promoter harbours a strong suppressive cis or trans acting element possible present in 5'UTR of IGF1R promoter. Sarfstein. et. al. (2009), using biotinylated IGF1R promoter reported identification of c-jun, p53, WT1, SP1, E2F1, KLF6 and ER- $\alpha$  as IGF1R promoter binding TFs in ER+ and ER- breast cancer cells and validated ER $\alpha$  as an positive regulator of IGF1R promoter in breast cancer cells [363]. Apart from VHL loss in 5-Fluorouracil and etoposide resistant renal cell carcinoma and FOXO1 activation in Phosphatidylinositol-3-Kinase Catalytic Subunit delta (PI3K- $\delta$ ) inhibitor resistant murine model [275, 319], probable action of other transcriptional regulator/s in mediating cancer therapy resistance through IGF1R are unknown. Anticipating similar role of multiple TFs behind the undulating IGF1R expression in our chemoresistant models, we performed a promoter binding transcription factor plate array to identify the putative regulators of IGF1R promoter. A total nine putative transcriptional regulators binding to IGF1R promoter were identified by screening promoter-binding TF profiling plate array (consisting of total 96 TF probes) from nuclear extracts of A2780-dual<sup>ER</sup> cells, RXR, SOX9, VDR, GFI1, ROR, SP1, RUNX1, NKX2.5 and SOX18. Identification of SP1 (a previously reported TF binding to IGF1R promoter) as a binder and TFIID as a non-binder (IGF1R promoter lacks TATA-box) strengthened the promoter binding TF plate array data. SOX18 has been shown to positively regulate IGF1R expression in breast cancer cells (MCF7 and BT-474) and in hepatocellular carcinoma cells (MHCC-97H and HepG2) [364, 365], while IGF1R has been identified as a potential target gene for SOX9 through ChIP-seq analysis of E13.5 mouse and E90 bovine foetal testes [366]. The hematopoietic stem cell TF RUNX1 is shown to positively regulate IGF1R expression in T-cell acute lymphoblastic leukaemia [367] and ligand activated nuclear receptor RXR is shown to down regulate IGF1R mRNA levels in MCF7 breast cancer cells

after 9-cis-RA treatment [368]. However, none of these have been validated as IGF1R promoter binding TFs. Though transcription factor-promoter array analysis in this study identified several unique transcriptional regulators, perturbation of only RUNX1 activity (RUNX1-CBF $\beta$  inhibitor, Ro5-3335) significantly attenuated IGF1R transcriptional and promoter activity in both A2780 and OAW42 chemoresistant models and highest reduction was seen in early-resistant cells. The rest of the potential binders either were not able to modulate IGF1R expression (RXR/ROR) or were not feasible to test due to unavailability of specific activator/inhibitor and technical difficulties to create site specific mutations at seven lengthy binding sites.

RUNX1, a well-known master regulator of hematopoietic lineages gathered attention as a tumor suppressor for long in haematological cancers [341]. Recently, RUNX1 has been found to have a more widespread role in several cancers including EOC [342, 369]. In EOC patients, RUNX1 overexpression was found in primary as well as omental metastatic tumors and increased RUNX1 expression post chemotherapy was attributed to hypomethylation of the RUNX1 gene [343]. RUNX1-CBF $\beta$  complex is a central player in fine-tuning the balance among cell differentiation, proliferation, EMT and often acts in cooperation with other transcriptional regulators in lymphoma, breast, colorectal cancer and haematological malignancies [338, 347, 348, 370]. We find increased expression and nuclear localization of RUNX1 along with enhanced binding of RUNX1 to IGF1R promoter in both early and late resistant cells of A2780 and OAW42 Cis-Pac resistant models. Despite increased RUNX1 expression and functional activities (nuclear localization and enhanced binding on IGF1R promoter) across all stages of resistance, specific inhibition of IGF1R by Ro5-3335 was observed only in early-resistant cells but at sub-optimal level which signifies for contributory role of other regulator/s for optimal activation. RUNX1 is able to influence the binding of other transcription factors and promotes transactivation of specific genes [340].

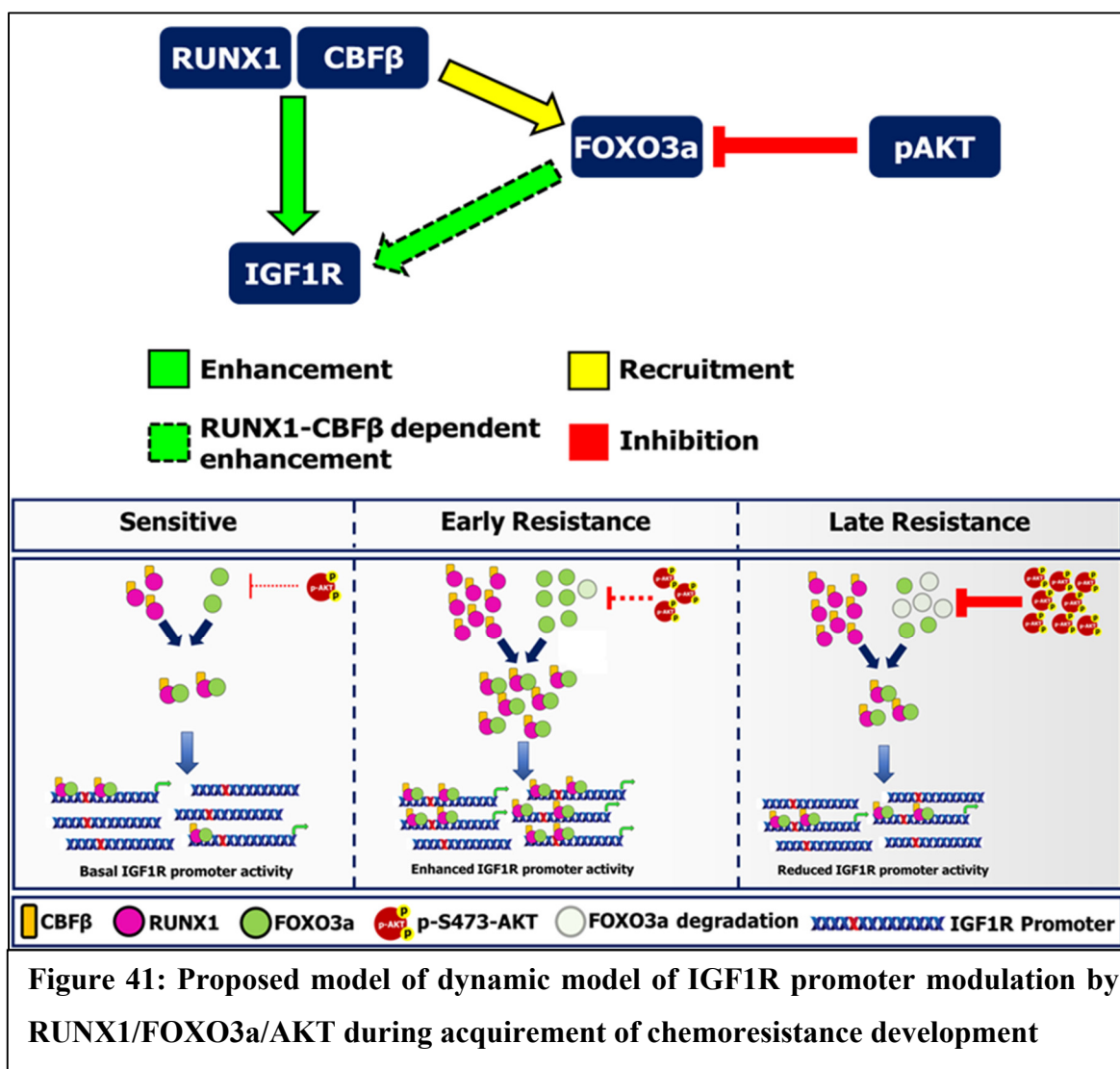
Using JASPAR, a TF binding prediction software we found that consensus binding sites of TFs identified from TF-array and previously reported IGF1R binding TFs are scattered throughout IGF1R promoter. Intriguingly, RUNX1 and FOXO3a (a known IGF1R regulator) [328] binding elements showed close proximity to each other on IGF1R promoter. FOXO3a is a member of Forkhead box transcription factors and controls a wide range of cellular functions, including cell cycle regulation, apoptosis, DNA repair, energy metabolism, ageing and oxidative stress defence. Differential phosphorylation of FOXO3a governs its activation (serine 413 phosphorylation) or degradation (S253 phosphorylation) and is commonly activated in stress conditions and assist cells to survive the stress or drive them towards apoptosis. Like RUNX1 inhibition, mutating FOXO3a response elements at S1( $\Delta$ -S1)/S2( $\Delta$ -S2) individually or together decreased IGF1R promoter activity significantly in early stages of chemoresistant in both A2780 and OAW42 Cis-Pac resistant models. Intriguingly, FOXO3a exhibited a similar pulsatile pattern like IGF1R across resistant stages with increased nuclear localization of both total and transcriptionally active FOXO3a (p-S413) and higher promoter occupancy in early resistant cells of both A2780 and OAW42 Cis-Pac resistant models. Further, mutating FOXO3a binding elements on IGF1R promoter in combination with Ro5-3335 treatment showed significant synergism in attenuating IGF1R promoter activity in early resistant cells as compared to FOXO3a binding element mutant IGF1R promoter or Ro5-3335 treatment alone, signifying synergistic role of both RUNX1 and FOXO3a in regulation of IGF1R promoter.

The RUNX1 can influence the transcriptional dynamics through sequential or concurrent binding to its interacting partners. In B-cell acute lymphoblastic leukaemia FUBP1 and RUNX1 were shown to cooperate for upregulation of the oncogene c-KIT, promoting cell proliferation and resistance against c-KIT inhibitor imatinib mesylate [347]. RUNX1 is also shown to interact with FOXO3a during 3D breast epithelial acinar morphogenesis, jointly

regulating transcription of genes related to oxidative stress response and proliferation [348]. The co-immunoprecipitation result demonstrated a stage specific interaction pattern between RUNX1 and FOXO3a which was highest in early resistant cells but minimal in sensitive and late resistant cells. This stage specific interaction pattern seems to influence their IGF1R promoter binding capacity as maximal RUNX1-FOXO3a co-occupancy was evident during onset of resistance which subsequently decreased at late-resistant stages as revealed by Chip-re-Chip assay. Irrespective of the combination of ChIP-re-ChIP, RUNX1 and FOXO3a showed enhanced co-occupancy in A2780-dual<sup>ER</sup> cells as compared to A2780-sensitive and A2780-dual<sup>LR</sup> cells on IGF1R promoter. Since RUNX1 and FOXO3a show augmented interaction and increased co-occupancy at early stage of resistance and cooperation between FOXO3 and RUNX1 is known to influence Bim promoter activity and expression [61] we asked whether RUNX1 plays a similar role for IGF1R promoter. This cooperative binding is critical for optimal IGF1R transcription as neither of the transcription factors could independently drive IGF1R expression. Both chemical and genetic inhibition of RUNX1 abolished FOXO3a binding in early-resistant cells indicating that RUNX1 binding is an obligatory step for FOXO3a occupancy specifically at the onset of resistance. Contrary to RUNX1, FOXO3a exhibited a poorer binding to IGF1R promoter and lower nuclear localization in late resistant cells thereby affecting the co-occupancy and transcriptional rate. Post translational modifications (PTMs) at various residues in FOXO3a predominantly control its transcriptional activity and nuclear localization. These PTMs majorly involve phosphorylation of FOXO3a at S253, T15 (AKT), S12, S284, S294 (ERK), S644 (IKK $\beta$ ), S574 (JNK), and S143 (AMPK) [350]. Accumulating evidence suggest presence of an feedback suppression loop between AKT and receptor tyrosine kinases through FOXO family of transcription factors and thus inhibiting AKT activity induces upregulation of HER3, IGF1R and Insulin receptor [371-373]. We find simultaneous

presence of hyperactivated AKT and p-S253-FOXO3a (a nuclear exclusion and degradation mark) in late-resistant cells. Indeed, AKT inactivation either through serum starvation or by an inhibitor led to decreased p-S253-FOXO3a levels and increased total FOXO3a and IGF1R expression in late resistant cells.

Altogether our data presents a complex story of IGF1R regulation through a sequential network of FOXO3a-RUNX1 interaction governed by FOXO3a stability and degradation kinetics required by cancer cells during acquirement of chemoresistance (Fig. 41). Here, for



the first time we report RUNX1 as a unique regulator of IGF1R promoter which exerts a nonlinear cooperative interaction with FOXO3a and dynamically modulate IGF1R expression during acquirement of chemoresistance in EOC cells. Genetic and

pharmacological inhibition followed by ChIP and ChIP-re-ChIP assay revealed that RUNX1 strengthened FOXO3a occupancy on IGF1R promoter, leading to a transcriptional surge during initiation of resistance which is lost at the late stages due to presence of an exclusive AKT-FOXO3a negative feedback loop. The observed cooperative action of two critical transcriptional regulators (RUNX1 and FOXO3a) to regulate an important (IGF1R) signalling pathway predicts a new avenue for targeting EOC through RUNX1-IGF1R axis during acquirement of chemoresistance.

## Chapter 3: Investigating the role of IGF1R signalling in maintenance of chemoresistance, tumorigenesis and cancer stem cell properties

### 3.1 Introduction

The IGF-axis plays vital role in embryonic and neonatal development; however, it is also important for postnatal growth and normal functioning of several other tissues and organs including ovary. The active IGF2/IGF1R signalling has been shown to be important for follicular development, where thecal cells in small antral follicles and granulosa cells in dominant follicles secrete IGF2 in both autocrine and paracrine manner as opposed to endocrine IGF1, which is primarily secreted by liver in adults [374-376]. Increased expression of IGF1R, IRS1 and IRS2 and decreased expression of PTEN in polycystic ovarian syndrome patients further strengthened importance of IGF1R in normal ovarian function [377]. The role of IGF1R signalling in ovarian cancer came into highlight with overexpression of IGF1R, IGF1 and IGF2 in human ovarian tumors were detected [378]. Hyperactivation of IGF1R signalling has been shown to induce proliferation and hyperplasia of ovarian surface epithelium and promote tumorigenesis in mouse models [379, 380]. More recently human ovulatory follicular fluid has been shown to induce tumorigenesis in mammary fat pad and fimbria carcinogenesis in Trp53-null mice. The IGFBP bound IGF2 and the IGFBP-lytic enzyme PAPP-A were shown to be abundantly present in FF, which activated IGF1R/AKT/mTOR and IGF1R/NANOG/OCT4 pathways leading to cell survival, stemness and malignant transformation of fimbrial epithelial cells in TP53<sup>-/-</sup>/Rb<sup>-/-</sup> mouse model [381]. In a cohort of 109 EOC patients, IGF2 mRNA level was strongly associated with the grade of disease and poor overall survival [249]. In a study involving 121 serous OC patients (Mutant-BRCA1, n=30; Wt-BRCA1, n=32; hypermethylated

BRCA1-promoter, n=28; and hypomethylated BRCA1-promoter, n=31), it was found that IGF1R is overexpressed in patients with Wt-BRCA1 as compared to the adjacent normal tissue and furthermore IGF1R levels were significantly more elevated in patients with mutant-BRCA1 or hypermethylated BRCA1 promoter. In addition, it was found that BRCA1 acts as negative regulator of IGF1R promoter and BRCA1 knockdown increased expression of IGF1R in OC cells[314]. Several other studies have reported IGF1R overexpression in OC patients and OC cell lines [382, 383]. Elisenda et. al. using orthotopic patient derived xenograft models showed that TGF $\beta$ /SMAD2 signalling induced IGF1R overexpression, promoted tumorigenesis, and inhibiting either TGF $\beta$  or IGF1R stalled tumor cell proliferation [384]. IGF1R overexpression also been strongly correlated with platinum-resistance in OC patients. In a study of twelve platinum resistant and 16 platinum sensitive patients, microarray analysis found IGF1 was most differentially expressed gene and found enrichment of 204 genes related to IGF1R/PI3K/NF $\kappa$ B/ERK gene signalling networks in platinum resistant patients [385]. PIK3CA/AKT and MAPK/ERK pathway activation downstream of IGF1/IGF2/IGF1R has been shown to essential for resistance against platinum based drugs in OC patients [250, 386]. Further studies revealed that hyperactive IGF1R signalling not only confers resistance against platinum-based drugs but also against other therapeutic agents used in treatment of OC. IGF1R or IGF2 overexpression conferred resistance to Cisplatin and Paclitaxel in OC lines HEY, OVCAR-8, SKOV-3, BG-1, and A2780-CP [250, 251]. We recently reported a pulsatile nature of IGF1R during acquirement of platinum alone, paclitaxel alone and platinum-taxol dual resistance in EOC cells [252]. The increased IGF1R expression at the onset of resistance plays an integral role in maintenance of drug resistance, while cells that achieved complete and irreversible resistance possess low level of IGF1R indicating active IGF1R signalling might be dispensable at late stages of resistance [252]. Drug induced enhancement of IGF1R

expression was also observed in a small cohort of advanced stage high grade serous EOC patients after 3-4 cycles of platinum-taxol treatment [252]. Also, upregulation of IGF1R expression has been found to confer resistance PIK3 inhibitors such as BYL719, Taselisib and Idelalisib in ovarian cancer, breast cancer and leukaemia [274-276]. IGF1R overexpression is shown to impart resistance against Herceptin (Trastuzumab) which has been approved for HER2 overexpressing breast cancer and preclinically tested for OC [265, 387, 388].

Apart from imparting chemoresistance IGF1R signalling has been shown to regulate CSC-phenotype in other cancer types but little is known in OC. Picropodophyllin, an IGF1R inhibitor blocked proliferation of leukaemia stem cells and induced apoptosis which was rescued by overexpression of pluripotency transcription factor Nanog [257]. Similarly, increased expression of IGF2 and IGF1R was shown to maintain CSCs in HCC primary cultures and imparted resistance against Sorafenib and Cisplatin [389]. Chemoresistance model developed against Oxaliplatin of HCC cell line (MHCC97H) both *invitro* and *invivo* identified IGF1/IGF1R signalling pathway that maintains cancer stem cell phenotype and Oxaliplatin resistance in these cells [258]. In HNSCC patient derived spheroids, which showed higher ALDH activity and increased expression of stem cell markers KLF4, SOX2 and Nanog, hyperactivation of EGFR and IGF1R were shown to maintain CSC phenotype and resistance to  $\gamma$ -radiation, 5-Flurouracil, Etoposide, and Cisplatin [390]. Human CRC cell lines (SW480, SW620, HCT116, HT29, and HCT15) derived SP population or ALDH<sup>+</sup> population showed IGF1 dependent CSC enrichment driven by  $\beta$ -Catenin and AKT. These IGF1 dependent CSCs were shown to be sensitive against anti-IGF1R antibody Figitumumab [391]. Constitutive activation of IGF1R has been shown to induce different lineages during mammary tumorigenesis through maintenance of progenitor populations through Snail and NF $\kappa$ B signalling pathways [392]. The IGF1R signalling plays important

role in OC tumorigenesis as well as chemoresistance and yet its role in regulation of OC CSC phenotype remains elusive. The OC stem cells either isolated by CSC markers (CD44<sup>+</sup>, CD177<sup>+</sup> and Nestin<sup>+</sup>) [393] or by functional assays such as side population (SP) [394] or spheroid assay [395] were shown to be highly tumorigenic. Subsequent studies revealed OC CSCs govern several biological features such as cancer progression, metastasis and most importantly chemoresistance [148, 396-398]. Elevated levels of HMGA1 were shown to maintain spheroid forming ability of A2780, SKOV3 and PA1 OC cells. These spheroid culture derived CSCs showed increased levels of drug transporters ABCB1 and ABCG2 that imparted resistance against Paclitaxel and Doxorubicin in tumor xenograft [399]. Similarly, CSC-like spheroid cells derived from human OC cells and primary cultures were shown to be highly tumorigenic, invasive, and resistant against Cisplatin and Paclitaxel [400, 401]. Our group using endogenously developed isogenic chemoresistance models of A2780 and OAW42 OC cells (Cisplatin-resistance, Paclitaxel-resistance, and Cisplatin + Paclitaxel-resistance) showed increased in CSC population with increasing resistance [253]. Our group and others also showed that the standard platinum-based treatment leads to enrichment of CSC-like cells in OC cells [297] and in residual tumors, resulting in increased chemoresistance and enhanced metastatic potential [394, 402, 403]. In addition, it has been reported that PARP inhibitors, an FDA approved only targeted therapy for OC, also increases CSC-like phenotype with enhanced DNA repair capability [404].

Chemoresistance continues to be a major hurdle in treatment of EOC. The five-year overall survival for EOC has not improved significantly in last four decades and remains low (40-45%), suggesting no significant improvement in diagnostics as well as the treatment modalities for EOC [7]. Hyperactivation of IGF1R signalling pathway in chemoresistance and ubiquitous overexpression of IGF1R and its ligands in many human malignancies has made IGF1R a prospective candidate for targeted therapy in cancers which solely depend

on chemotherapy, with limited or no targeted therapy options and face severe challenges due to chemoresistance such as EOC. However, several anti-IGF1R targeted therapies (anti-IGF1R and anti-IGF1/2 antibodies and IGF1R tyrosine kinase inhibitors) which have entered clinical trials did not meet clinical success due to complexity of the pathway involving the IGF binding proteins, high homology with Insulin receptor and trials in unselected patients [405]. Lessons learned from failures, and mounting evidence showing importance of IGF1R in both tumorigenesis and chemoresistance suggest that anti-IGF1R targeted therapies hold therapeutic potential [277-279] and possibly indirect approaches by targeting IGF1R transcription or translation rather than targeting the protein may result in more successful strategy. IGF1R expression has been shown to be primarily regulated at transcriptional level by plethora of transcription factors in different cancer types, however none of these studies have investigated potential of targeting IGF1R expression by inhibiting its transcription. Among the clinically approved targeted therapies very few have been approved to target transcription factors in cancer treatment. The oestrogen receptor modulators (Tamoxifen, Toremifene, Bazedoxifene and Raloxifene) and degraders (Fulvestrant, and Elacestrant) for treatment of oestrogen positive breast cancer patients [406], androgen receptor antagonists (Enzalutamide, Apalutamide and Darolutamide) for treatment of castration resistant prostate cancer patients [407] and EWS-FLI-1 fusion protein inhibitor (Efdispro) for treatment of Ewing sarcoma patients [408] are few of the clinically approved for drugs targeting transcription factors. Mutated or dysregulated transcription factors have emerged as an interesting druggable node due to their ability to rewire the aberrant gene expression patterns during tumorigenesis and therapy resistance development leading to pre-clinical and clinical development of targeted therapies against transcription factors such as STAT1/3, ETS1/2, wild type and mutant TP53, RUNX1, CBF $\beta$ -SMMHC, RUNX1-ETO and Myc-Max [409]. In the previous chapter we have

shown a complex regulatory machinery of transcription factors (RUNX1 and FOXO3a) along with hyperactive AKT modulate the IGF1R promoter activity during chemoresistance development. Inhibiting the RUNX1 transcriptional activity severely attenuated IGF1R promoter activity and reduced IGF1R expression at early stages of chemoresistance development. In this part of the study using A2780 Cisplatin-Paclitaxel resistance model, we aim to decipher the underlying role of IGF1R signaling in the crosstalk between two important aspects of OC biology, the CSCs phenotype and chemoresistance and explore the inhibition of RUNX1-FOXO3a axis to target IGF1R at early stages of chemoresistance development.

## **3.2 Methodology**

### **3.2.1 Development of Cisplatin-Paclitaxel resistant models of EOC cells**

A2780 and OAW42 isogenic Cisplatin-Paclitaxel resistant models were established using pulse method previously in the laboratory as described in section 2.2.1. The OC chemoresistant models used in this study are described below.

### **3.2.2 Quantitative real-time PCR**

Quantitative real-time PCR was performed following protocols described in section 5.4 using SYBR Green (Invitrogen) and appropriate gene specific primers. Relative expression of target genes was estimated by  $\Delta$ -Ct method using Glyceraldehyde 3-phosphate dehydrogenase (GAPDH) as normalisation control.

### **3.2.3 IGF1R and CBF $\beta$ silencing by lentiviral mediated sh-RNA construct**

IGF1R and CBF $\beta$  knock down lentiviral cassette were developed using a target sequence against IGF1R (5'-AGACCTGAAAGGAAGCGGAGA-3') [410] and CBF $\beta$  (5'-CCGCGAGTGTGAGATTAAGTA-3') [411] using standard cloning methods as described in section 5.3 and all constructs were verified by restriction digestion and sequencing.

Lentivirus particles were produced in HEK293FT and A2780, A2780-Dual<sup>ER</sup> and A2780-Dual<sup>LR</sup> cells were transduced with lentiviruses and stable cells were FACS sorted using eGFP as a marker using protocol described in section. 5.3.

### 3.2.4 Trypan blue exclusion assay for cell proliferation

Cells were seeded in a 6-well plate at density of  $2 \times 10^4$  cells/well and trypsinized after every 24 hours till 120 hours and viable cell count for each day was determined using 0.4% trypan blue dye. The doubling time was determined by using formula [412],

$$\text{Doubling time} = \frac{\text{Total duration of culture in hours} * \log(2)}{\text{Log}(10) \text{ Final cell count} - \text{Log}(10) \text{ Initial cell count}}$$

### 3.2.5 MTT cell cytotoxicity assay

Short term MTT cell cytotoxicity assay was performed as described in section 5.1.3.5.

Briefly cells were treated with appropriate drug concentrations as described below.

- A2780 and OAW42 Cisplatin-Paclitaxel resistant models were treated with Cisplatin + Paclitaxel (50ng/ml+8.5 ng/ml) for 72 hours.
- A2780 and OAW42 models Cisplatin-Paclitaxel resistant were treated with Ro5-3335 (A2780 = 200 $\mu$ M and OAW42 = 20 $\mu$ M) for 24 hours followed by Cisplatin + Paclitaxel (50ng/ml + 8.5 ng /ml) for 72 hours.

### 3.2.6 Long term survival clonogenic assay

Clonogenic assay was performed as described in section 5.1.3.9. Briefly cells were treated with appropriate drug concentrations as described below.

- A2780 and OAW42 Cisplatin-Paclitaxel resistant models were treated with Cisplatin + Paclitaxel (50ng/ml+8.5 ng/ml) for 24 hours.
- A2780 and OAW42 Cisplatin-Paclitaxel resistant models were treated with Ro5-3335 (A2780 = 200 $\mu$ M and OAW42 = 20 $\mu$ M) for 12 hours followed by Cisplatin + Paclitaxel (50ng/ml + 8.5 ng /ml) for 24 hours.

**3.2.7 Soft agar colony formation assay**

Anchorage independent growth and in-vitro tumorigenicity of was assayed by soft agar colony formation assay as described in section 5.1.3.6.

**3.2.8 Spheroid formation assay**

The self-renewable capacity of OC cells was assayed by spheroid formation assay that enriches CSC-like cells as described in section 5.1.3.8 [253].

**3.2.9 DyeCycle Violet side population assay**

Dye exclusion DyeCycle Violet side population assay was used to isolate the CSC like cells called the side population (SP) and non-CSCs called non-side population (NSP) form OC cells as described in section 5.1.3.8 [253].

**3.2.10 Western blotting**

Whole cell lysates were prepared and western blot was performed for IGF1R- $\beta$ , BCL-2, BCL-xL, BAD, cleaved-PARP, total AKT, p-S473-AKT, total ERK1/2, p-S-ERK1/2, Lamin-A,  $\beta$ -Actin, and  $\alpha$ -Tubulin following protocols described in section 5.6.

**3.2.11 Small animal bioluminescence imaging**

All experiments were approved by the Institutional Animal Ethics Committee at ACTREC and were performed as described in section 5.13. Briefly,  $4 \times 10^6$  cells of A2780-Dual<sup>ER</sup> cells stably expressing IGF1R-F12-TDT construct were subcutaneously injected in female non-obese diabetic-severe combined immunodeficient (NOD-SCID) mice and were followed for tumor growth. Animals were imaged at day 15 and divided into four groups (n=4/each), group-I: control, group-II: Cisplatin-Paclitaxel, group-III: Ro5-3335 and group-IV: Ro5-3335+Cisplatin-Paclitaxel. Group II and IV received 2mg/kg Ro5-3335 for 5days intravenously (day15-day19). On day 20 Group III and IV received a single dose of 2mg/kg-Cisplatin+1mg/kg-Paclitaxel intraperitoneally. For CBF $\beta$ -KD in-vivo study,  $4 \times 10^6$  cells of A2780-Dual<sup>ER</sup> and the CBF $\beta$ -KD counterpart stably expressing IGF1R-F12-TDT were

subcutaneously injected on upper and lower flanks of five female NOD-SCID mice. Animals were treated with 2mg/kg-Cisplatin+1mg/kg-Paclitaxel twice (day 35 and day 45) by intraperitoneal injection. Bioluminescence imaging and subsequent quantification was performed using Xenogen-IVIS and Living Image software 4.4 [253].

#### **Drug treatment in mice**

- Ro5-3335, diluted in normal saline at 2 mg/kg for 5 days intravenously.
- Single dose of chemotherapeutic agents Cisplatin + Paclitaxel diluted in normal saline at 2 mg/kg + 1 mg/kg respectively alone or after five days of Ro5-3335 treatment.

#### **3.2.12 Immunohistochemistry**

Immunohistochemistry of subcutaneous mouse xenografts was performed for Ki-67, IGF1R, and FOXO3a as described in section 5.12. Briefly, antigen retrieval for Ki67 and IGF1R was carried out in microwave at high power for 20 minutes, while that same for FOXO3a was done by boiling the slides in pressure cooker for 6 minutes. For both cases sodium citrate buffer (pH 6) was used. Staining was performed using IHC detection kit [413] and scored by an expert pathologist. The immunoreactivity score (IRS) was calculated using the formula: intensity  $\times$  extent of positivity [414].

### **3.3 Results**

#### **3.3.1 IGF1R regulates CSC phenotype and chemoresistance in EOC cells**

To understand the role of IGF1R signalling in maintaining chemoresistance in EOC cells, we made shRNA mediated knockdown of IGF1R in A2780 Cis-Pac resistance model and confirmed IGF1R silencing at transcript level (Fig. 42A). IGF1R silencing significantly sensitized the sensitive and early resistant cells to chemotherapeutic agents Cisplatin-Paclitaxel, whereas no change was observed in late resistant cells (Fig. 42B). Since, chemoresistant cells are shown to be enriched with CSC like cells and CSCs themselves are

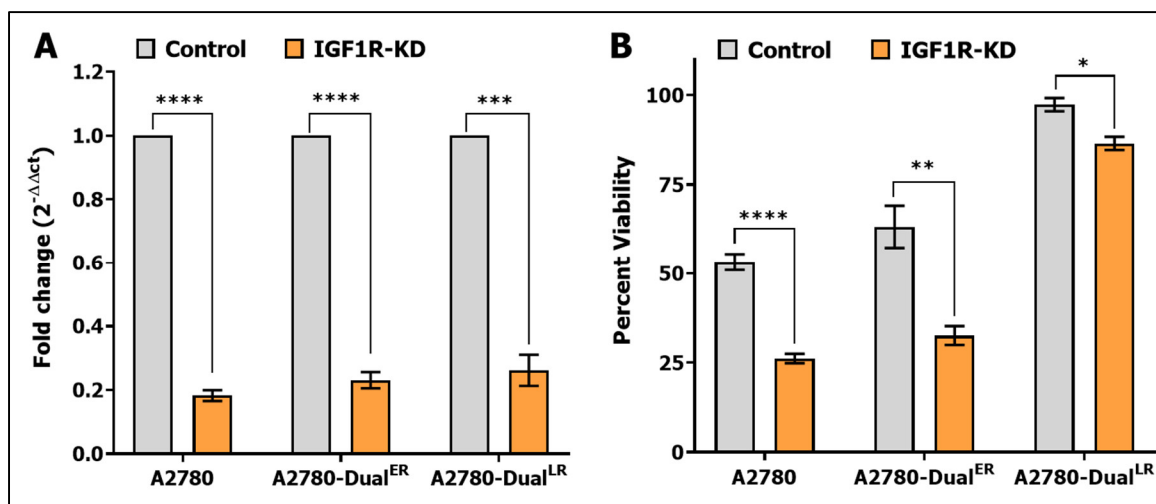


**Figure 42: IGF1R inhibition chemosensitize EOC cells to Cisplatin & Paclitaxel**

**A.** Real-time PCR showing extent of IGF1R knockdown at transcript and protein level in A2780, A2780-Dual<sup>ER</sup> and A2780-dual<sup>LR</sup> cells. **B.** MTT cell cytotoxicity assay showing increased sensitivity of A2780, A2780-Dual<sup>ER</sup> and A2780-dual<sup>LR</sup> cells to Cisplatin and Paclitaxel compared to respective control cells.

known to be intrinsically resistant to chemotherapeutic agents, we checked the effect of IGF1R silencing on CSCs in sensitive and early resistant cells [396]. Silencing IGF1R drastically decreased the levels of pluripotency transcription factors (SOX2, OCT4 and NANOG) as compared to control cells (Fig. 43A). Down regulation of pluripotency transcription factors after IGF1R knockdown significantly reduced both spheroid forming ability (A2780 sensitive, 2.5 fold; and A2780-Dual<sup>ER</sup> 3.1 fold) (Fig. 43B) and CSC-like SP phenotype (A2780 sensitive, 2.0 fold and A2780-Dual<sup>ER</sup>, 3 fold) of chemoresistant EOC cells (Fig. 43C). CSCs are known to be intrinsically resistant to wide range of chemotherapeutic agents (such as Doxorubicin, Cisplatin, Paclitaxel, Temozolomide, 5-Fluorouracil and Gemcitabine) mainly through higher expression of drug transporters or through hyperactivation of cell survival pathways [396]. Since, IGF1R seems to regulate both chemoresistance and CSC phenotype at early onset of chemoresistance development, we asked whether IGF1R has role in intrinsic chemoresistance of CSCs in our EOC chemoresistance models. The CSC-like SP cells isolated from parental A2780-sensitive and

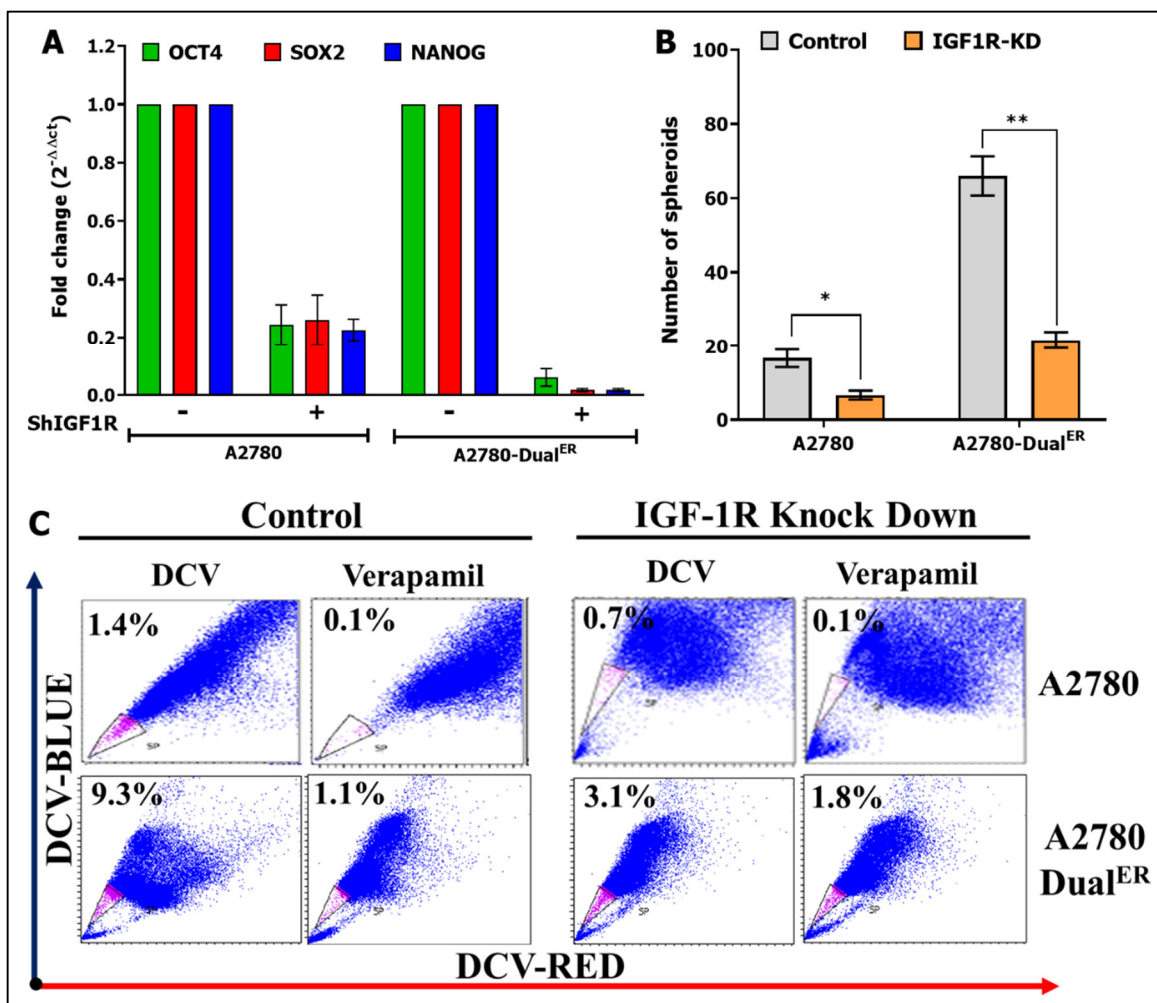


**Figure 43: IGF1R silencing abrogates CSC phenotype in sensitive and early resistant cells**

**A.** Real-time PCR showing drastic downregulation of pluripotency transcription factors (Oct4, Sox2 and Nanog) post IGF1R knockdown in A2780 and A2780-dual<sup>ER</sup> cells. **B-C.** IGF1R inhibition significantly decreases spheroid formation and SP population in A2780 and A2780-dual<sup>ER</sup> cells.

A2780-dual<sup>ER</sup> cells showed marked increased in chemoresistance as compared to their respective NSP and main population or parental cells (MP) (Fig. 44A-B). However, CSC-like SP cells isolated from IGF1R knockdown A2780-sensitive and A2780-dual<sup>ER</sup> cells showed enhanced chemosensitization to Cisplatin-Paclitaxel (Fig. 44A-B). Similar decrease in cell viability was seen in both NSP and MP (Fig. 44A-B). More importantly, SP cells isolated from IGF1R knockdown early resistant cells showed significantly higher chemosensitization than respective NSP and MP cells, whereas no such chemosensitization

was observed for SP cells isolated from IGF1R knockdown A2780 sensitive cells (Fig. 44C).

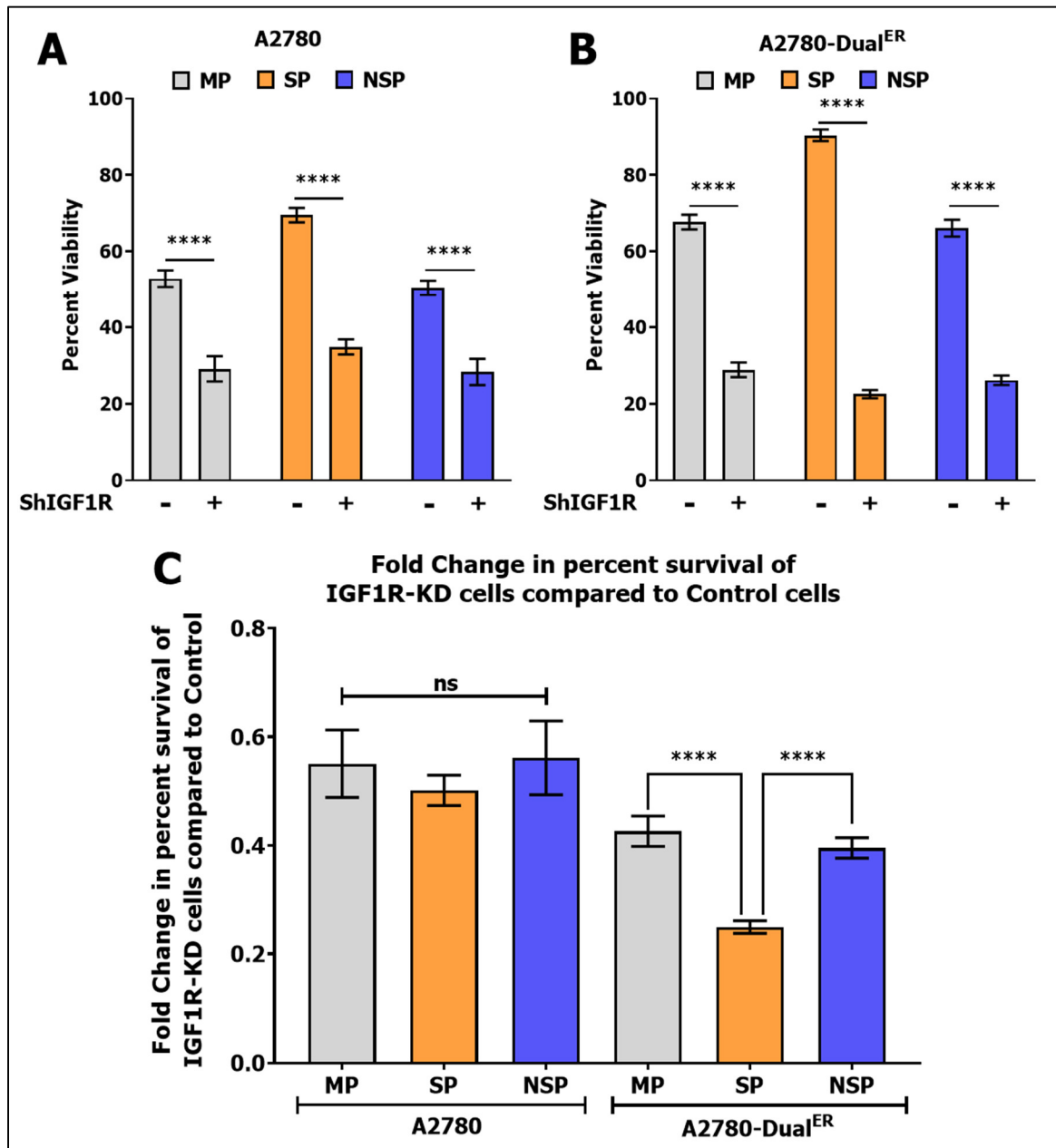


**Figure 44: IGF1R regulates chemoresistance of CSC-like SP cells in early resistant cells**

**A-B.** MTT cell cytotoxicity assay showing increased sensitivity of MP, SP and NSP cells to Cisplatin Paclitaxel post IGF1R knockdown in A2780 and A2780-dual<sup>ER</sup> cells. **C.** Graphical representation of fold change in percent survival of IGF1R knockdown cells compared to respective control cells, showing significantly higher chemosensitization of SP cells to Cisplatin and Paclitaxel compared to respective MP and NSP cells in A2780-dual<sup>ER</sup> cells, but not in A2780 sensitive.

### 3.3.2 IGF1R promotes cell proliferation and cell survival in early resistant cells

To further gain insights into IGF1R downstream signalling pathways we focused our study on Cisplatin-Paclitaxel dual resistance as it is more clinically relevant than single agent resistant models. The two major downstream signalling arms under activated IGF1R are PIK3CA/AKT and MAPK/ERK pathways, which primarily promote cellular proliferation and antagonize the apoptotic pathways (Fig. 45A) [415, 416]. A2780 Cisplatin-Paclitaxel resistant model showed gradual increase in phosphorylated AKT, whereas ERK1/2 phosphorylation was highest in ER cells (Fig. 45B). IGF1R knockdown in these cells showed no significant change in phosphorylation of AKT across the model (Fig. 45B). However, there was significant decrease in phosphorylated ERK1/2 in A2780 sensitive and A2780-dual<sup>ER</sup> cells which remained unchanged in A2780-dual<sup>LR</sup> cells (Fig. 45B). IGF1R signalling is known potent inducer of proliferation and inhibitor of apoptosis, hence next we

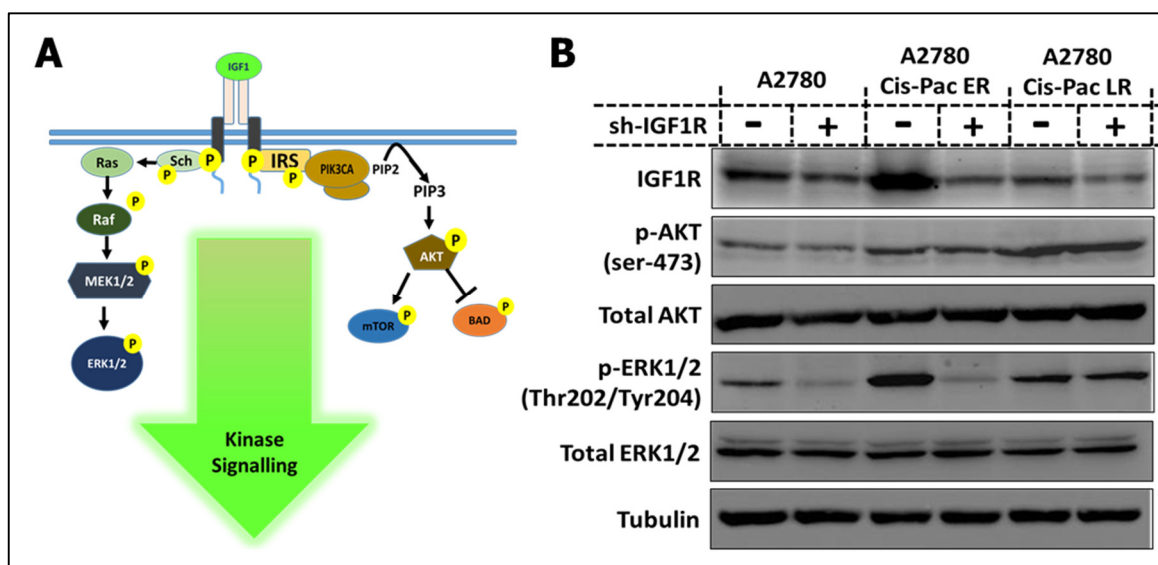


**Figure 45: IGF1R silencing abrogates MAPK/ERK pathway, but not PIK3CA/AKT pathway in A2780-Cis-Pac resistant model**

**A.** Pictorial representation of PIK3CA/AKT and MAPK/ERK pathway downstream of IGF1R. **B.** Immunoblot showing inhibition of ERK1/2 post IGF1R knockdown in A2780 sensitive and A2780-dual<sup>ER</sup> cells but not in A2780-Dual<sup>LR</sup> cells. No change in AKT activation was observed post IGF1R knockdown across the A2780-Cis-Pac resistant model.

checked the effect of IGF1R signalling on cellular proliferation and apoptosis in A2780-Cis-Pac resistant model. IGF1R knockdown significantly reduced cellular proliferation in A2780-Dual<sup>ER</sup> cells (Control =  $11.08 \times 10^5 \pm 0.56 \times 10^5$  cells/ml and IGF1R-KD =  $5.85 \times 10^5 \pm 0.51 \times 10^5$  cells/ml post 120 hours) followed by A2780-sensitive (Control =  $10.1 \times 10^5 \pm 0.63 \times 10^5$  cells/ml and IGF1R-KD =  $8.52 \times 10^5 \pm 0.35 \times 10^5$  cells/ml post 120 hours), whereas no effect was observed in A2780-Dual<sup>LR</sup> cells (Control =  $2.78 \times 10^5 \pm 0.30 \times 10^5$  cells/ml and IGF1R-KD =  $2.35 \times 10^5 \pm 0.35 \times 10^5$  cells/ml post 120 hours) (Fig. 46A). No significant change in doubling time of A2780-sensitive (Control =  $21.22 \pm 0.34$  hours and IGF1R-KD =  $22.18 \pm 0.24$  hours) and A2780-Dual<sup>LR</sup> cells (Control =  $31.67 \pm 1.29$  hours and IGF1R-KD =  $33.96 \pm 2.24$  hours) was observed post IGF1R knockdown, however doubling time of A2780-Dual<sup>ER</sup> cells significantly increased from  $20.73 \pm 0.27$  hours to  $27.91 \pm 0.71$  hours after IGF1R silencing (Fig. 46B). Since we did not observe any significant change in AKT and ERK activation post IGF1R knockdown in late resistant cells

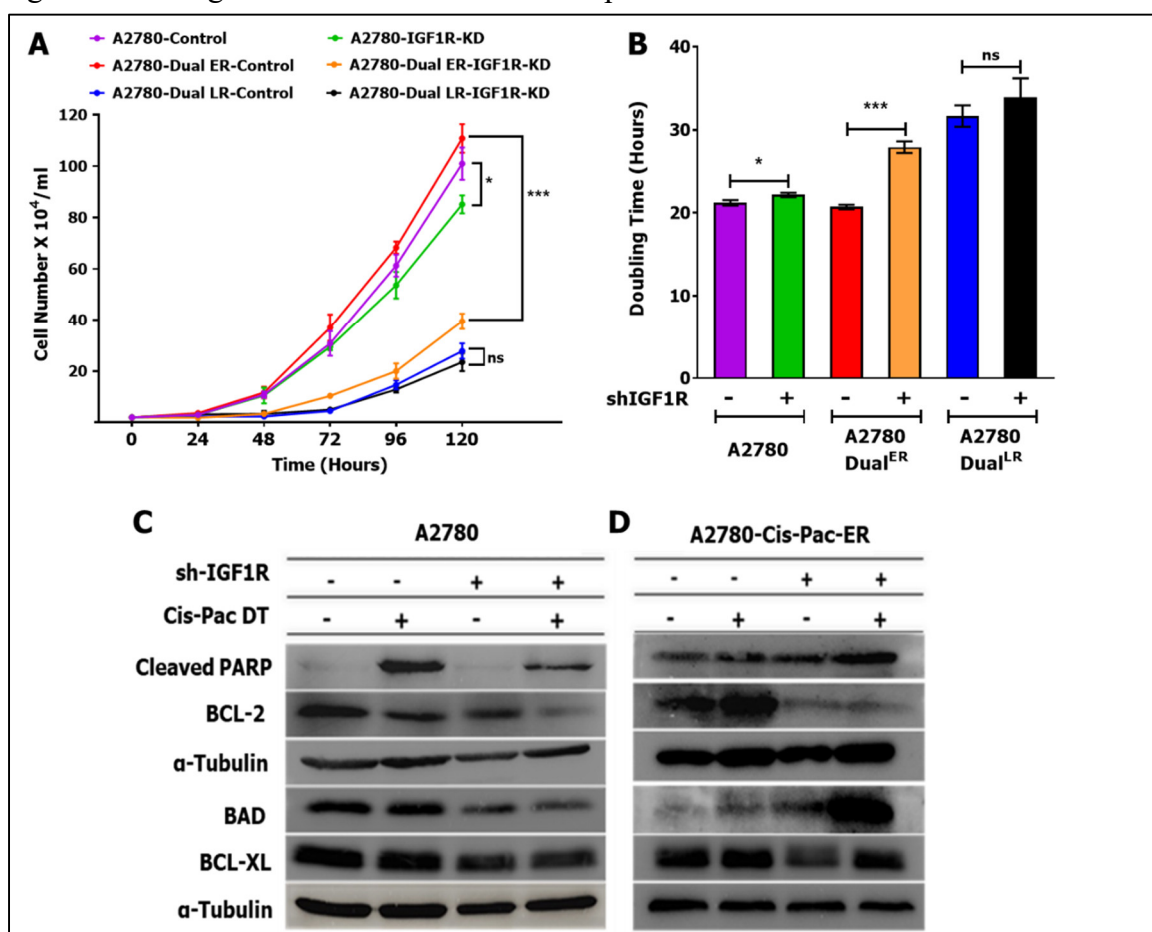


**Figure 46: IGF1R silencing inhibits proliferation and induces apoptosis in early resistant cells of A2780-Cis-Pac resistant model**

**A.** Graphical representation of trypan blue cell counting showing significant decrease in cellular proliferation of A2780 sensitive and A2780-dual<sup>ER</sup> cells post IGF1R knockdown. **B.** Graphical representation of doubling time calculated from trypan blue cell counting showing significant increase in doubling time of A2780-dual<sup>ER</sup> cells. **C-D.** Immunoblot of anti-apoptotic proteins (BCL-2 and BCL-XL) and pro-apoptotic protein (BAD) showing increased induction of apoptosis post Cisplatin-Paclitaxel treatment in IGF1R knockdown A2780 and A2780-dual<sup>ER</sup> cells.

we checked the effect of IGF1R silencing on apoptosis in sensitive and early resistant cells. The levels of anti-apoptotic proteins such as BCL-2 and BCL-XL decreased upon IGF1R knockdown in both A2780 sensitive and A2780-dual<sup>ER</sup> cells, whereas, levels of pro-apoptotic protein BAD remain unchanged (Fig. 46C-D). Upon treatment with Cisplatin-Paclitaxel, levels of BCL-2 and BCL-XL remained low in IGF1R knockdown cells as compared to their parental A2780-dual<sup>ER</sup> cells, while levels of BAD increased significantly in A2780-dual<sup>ER</sup> cells (Fig. 46C-D). In parental and IGF1R knockdown A2780 sensitive cells decrease in BCL-2 levels and no significant change in levels of BCL-XL and BAD were observed upon Cisplatin-Paclitaxel treatment (Fig. 46C). IGF1R knockdown A2780-dual<sup>ER</sup> cells showed marked increase in cleaved PARP compared to IGF1R knockdown A2780 sensitive cells (Fig. 46C-D). Thus, blocking IGF1R signaling sensitized the early resistant cells to Cisplatin-Paclitaxel and induced apoptosis by abrogating anti-apoptotic effects of BCL-2 and BCL-XL.

### **3.3.3 Impeding AKT inhibition induced IGF1R expression sensitizes the late resistant cells to AKT inhibition**

Increased expression of IGF1R is indispensable to maintain chemoresistance against Cisplatin-Paclitaxel at early stage of chemoresistance development, whereas hyperactive AKT suppressed IGF1R in late resistance stage. AKT inhibition has been shown to relieve

feedback suppression of IGF1R leading to resistance against PIK3CA, AKT and mTORC1 inhibitors [274, 276, 371, 417]. In the previous chapter, we have shown that inhibition of hyperactive AKT in late resistant cells relieved feedback inhibition loop on FOXO3a leading to increased expression of IGF1R. Thus, we asked, whether inhibiting IGF1R signalling post AKT inhibition could synergistically affect the chemoresistance of late resistant cells. Indeed, AKT inhibition upregulated IGF1R expression in A2780-Dual<sup>LR</sup> cells (Fig. 6A). As expected, IGF1R kinase inhibitor, Picropodophyllin, suppressed the AKT inhibition induced IGF1R expression in late resistant cells (Fig. 47A). The combination of IGF1R and AKT inhibitor at low dose (IC<sub>20</sub>) showed significantly higher cell death (~2 fold across all late resistant cells) as compared to AKT inhibitor IV or Picropodophyllin alone treatment (Fig. 47B). Thus, we show that inhibiting IGF1R in combination with AKT

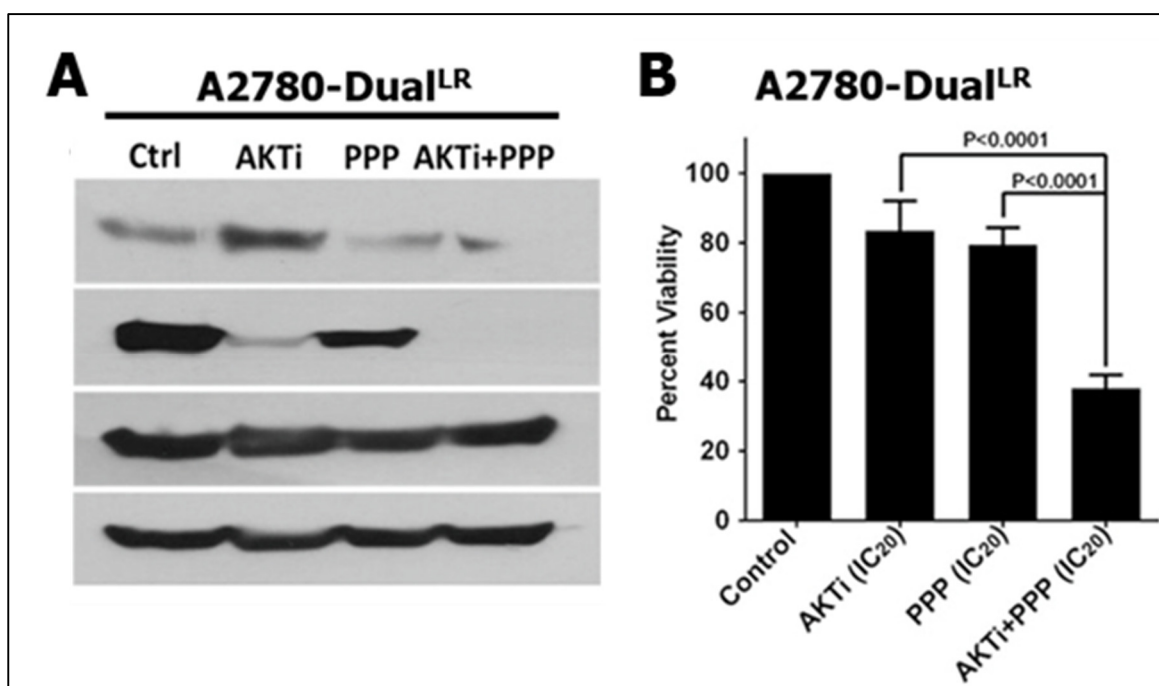


**Figure 47: Impeding AKT inhibition induced IGF1R expression sensitizes the late resistant cells to AKT inhibition**

**A.** Immunoblots showing increased expression of IGF1R post AKT inhibition which is suppressed by combining IGF1R inhibitor Picropodophyllin in A2780-Dual<sup>LR</sup> cells respectively. **B.** MTT cell viability assay showing synergetic effect of low dose AKT inhibitor IV and Picropodophyllin on viability of A2780-Dual<sup>LR</sup> cells respectively.

inhibition acts synergistically reducing cell survival in late resistant cells (highly resistant to Cisplatin-Paclitaxel) due to presence of an active AKT feedback inhibition loop on FOXO3a/IGF1R.

### **3.3.4 Inhibiting RUNX1/FOXO3a axis sensitizes early resistant to Cisplatin-Paclitaxel**

Despite strong association between IGF1R expression and therapy resistance in several cancers including EOC, therapeutic interventions targeting IGF1R did not meet success, thus alternative strategies are needed to target IGF1R. The growing body evidence suggest that aberrant IGF1R overexpression in many cancer types and therapy resistant cancers is primarily attributed to transcriptional activation of IGF1R promoter rather than to rare instances of gene amplification [212]. Till now, we have shown that RUNX1/FOXO3a mediated augmented IGF1R expression maintains chemoresistance at early stages, whereas in late resistance stage, abrogating AKT/FOXO3a negative feedback loop induced IGF1R expression by imparting resistance against AKT inhibition. Thus, we investigated the potential of blocking RUNX1/FOXO3a axis to assess the biological implication of this axis in targeting IGF1R at early onset of chemoresistance, where RUNX1/FOXO3a axis is predominantly active. Blocking RUNX1 transcriptional activity by CBF $\beta$  knockdown (RUNX1-CBF $\beta$  heterodimerization is essential for transcriptional activation of RUNX1), severely attenuated IGF1R protein levels in A2780-Dual<sup>ER</sup> cells (Fig. 48A). CBF $\beta$  knockdown mediated IGF1R downregulation significantly affected the chemoresistance properties of resistant cells. A2780-Dual<sup>ER</sup> cells showed maximum sensitization towards Cisplatin-Paclitaxel treatment in both MTT cell cytotoxicity assay (Control = 75.96% $\pm$ 2.51% and CBF $\beta$ -KD = 37.82% $\pm$ 1.56%) and long-term survival clonogenic assay (Control = 52.31% $\pm$ 1.67% and CBF $\beta$ -KD = 22.31% $\pm$ 2.24%) (Fig 48B-C). Surprisingly, A2780-Dual<sup>LR</sup> also showed significant decrease in cell viability in both MTT cell

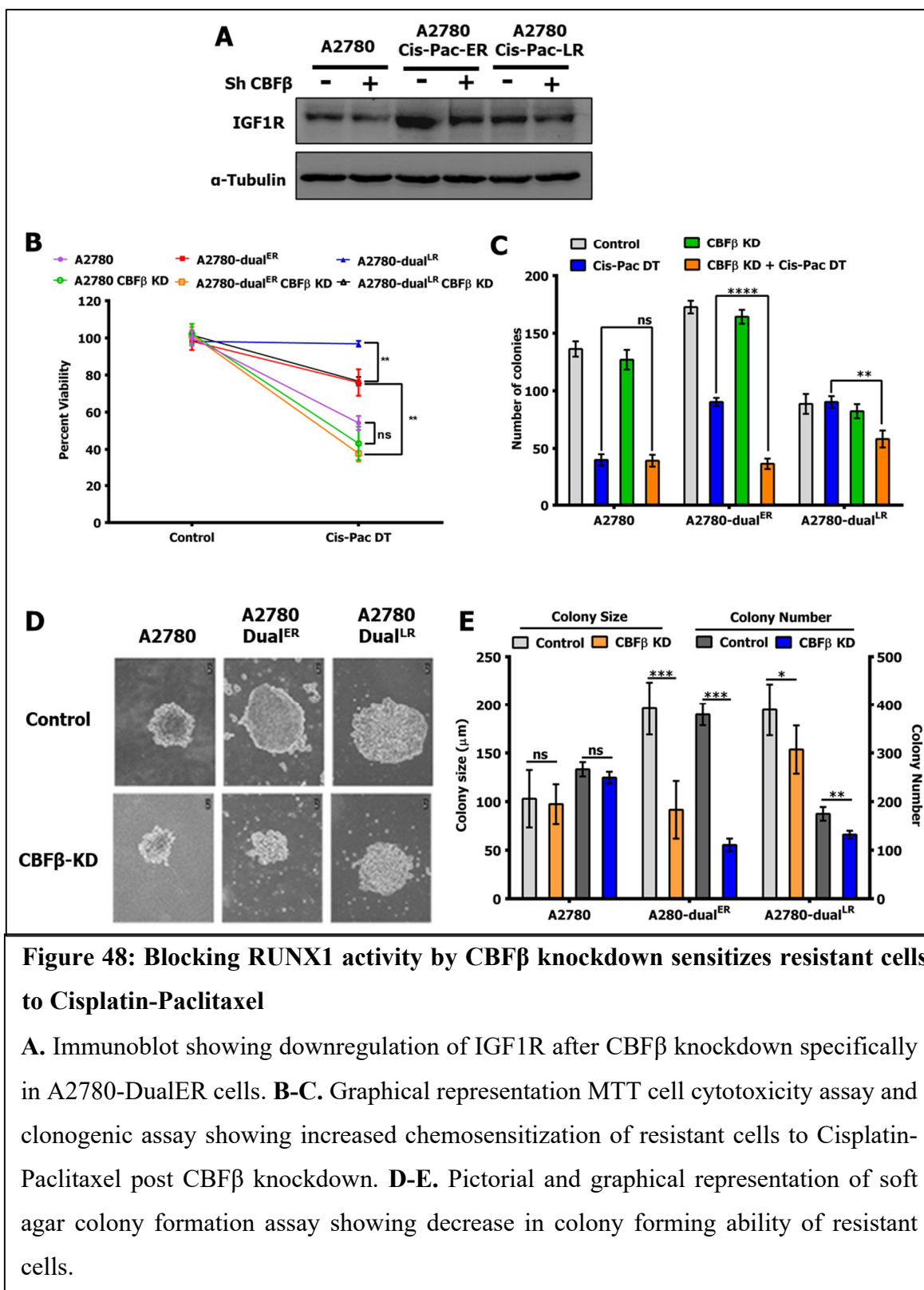


**Figure 48: Blocking RUNX1 activity by CBF $\beta$  knockdown sensitizes resistant cells to Cisplatin-Paclitaxel**

**A.** Immunoblot showing downregulation of IGF1R after CBF $\beta$  knockdown specifically in A2780-Dual<sup>ER</sup> cells. **B-C.** Graphical representation MTT cell cytotoxicity assay and clonogenic assay showing increased chemosensitization of resistant cells to Cisplatin-Paclitaxel post CBF $\beta$  knockdown. **D-E.** Pictorial and graphical representation of soft agar colony formation assay showing decrease in colony forming ability of resistant cells.

cytotoxicity assay (Control = 96.84% $\pm$ 1.54% and CBF $\beta$ -KD = 76.71% $\pm$ 1.81%) and long-term survival clonogenic assay (Control = 101.88% $\pm$ 4.63% and CBF $\beta$ -KD = 70.70% $\pm$ 7.25%), though not as drastic as seen for A2780-Dual<sup>ER</sup> cells (Fig. 48B-C). No

change cell viability was observed in A2780 sensitive cells (Fig. 48B-C). Since, IGF1R knockdown showed significant reduction in cellular proliferation, we next checked the tumorigenic properties of CBF $\beta$  knockdown cells by in vitro soft agar colony formation assay. CBF $\beta$  knockdown significantly affected anchorage independent growth sustainability in resistant cells but not in sensitive cells. A2780-Dual<sup>ER</sup> cells CBF $\beta$  knockdown drastically decreased both soft agar colony number from 274 to 61 and colony size from 196  $\mu$ M to 91  $\mu$ M (Fig. 48D-E). While in A2780-Dual<sup>LR</sup> cells CBF $\beta$  knockdown decreased soft agar colony size from 194  $\mu$ M to 153  $\mu$ M only, but soft agar colony number decreased significantly from 195 to 81 (Fig. 48D-E). No significant change in colony number and colony size was observed in A2780 sensitive cells (Fig. 48D-E).

To further validate our results that CBF $\beta$  knockdown mediated downregulation of IGF1R could chemosensitize the early resistant cells to Cisplatin-Paclitaxel, A2780- dual<sup>ER</sup> cells and their CBF $\beta$ -KD counterparts (Both stably expressing IGF1R promoter driven FL2-TDT

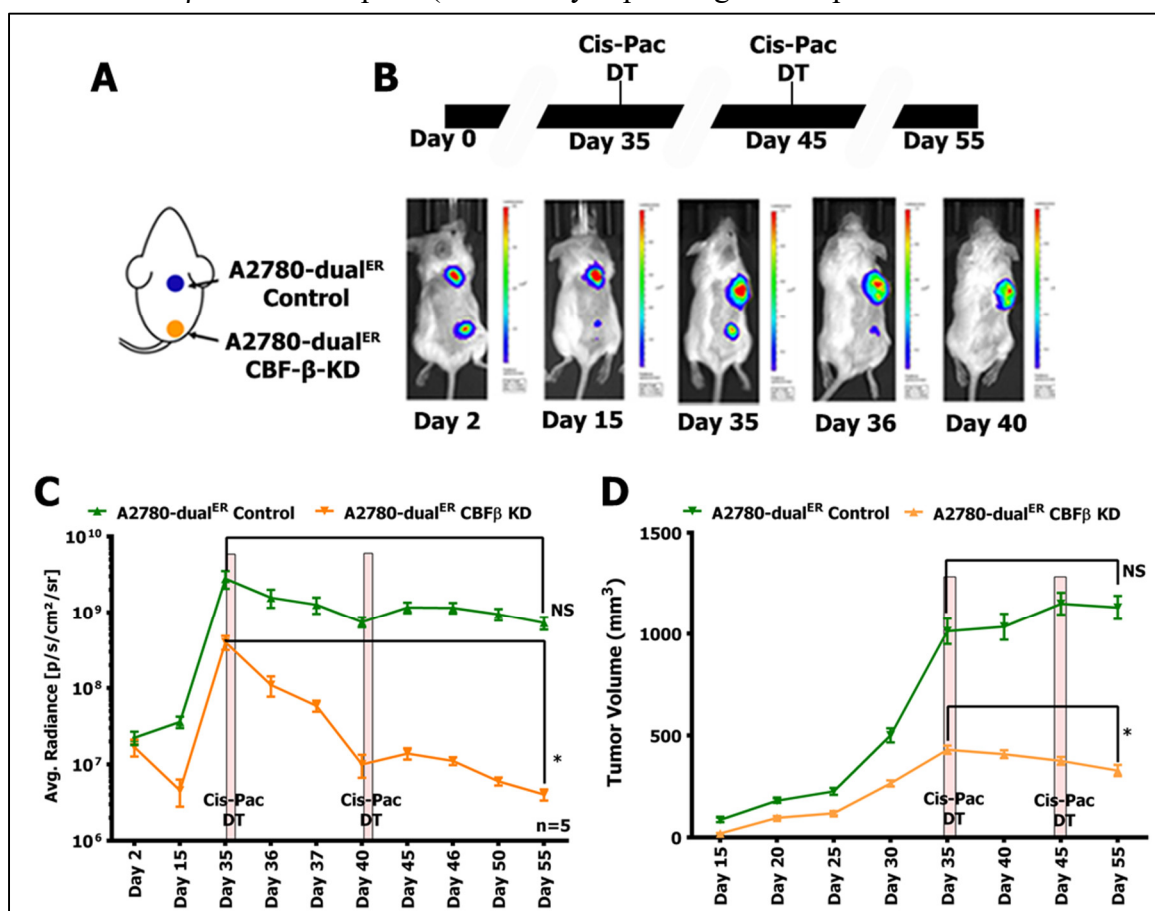
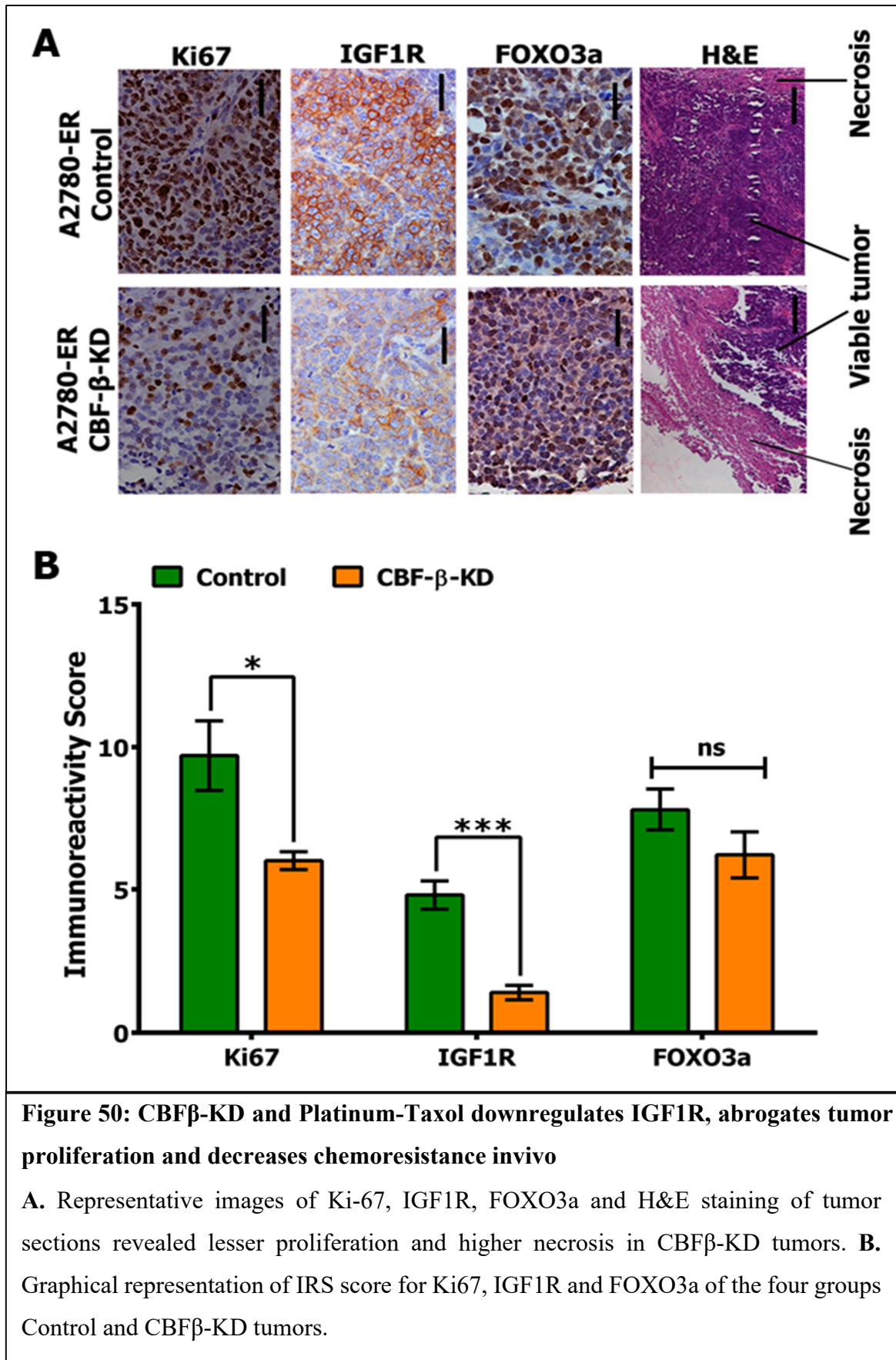


**Figure 49: CBF $\beta$ -KD and Platinum-Taxol attenuate IGF1R promoter activity and chemoresistance *in vivo***

**A-B.** Schematic diagram of treatment sequence, tumor implantation of A2780-dual<sup>ER</sup> and A2780-dual<sup>ER</sup> CBF $\beta$ -KD cells and representative bioluminescence images. **C.** Graphical representation of quantified bioluminescence signal (n=5/group) showing ~99-fold reduced IGF1R promoter activity. **D.** Graphical representation of tumor growth kinetics showing slower tumorigenesis and chemosensitization in CBF $\beta$ -KD tumors.

reporter) were subcutaneously implanted in the upper and lower flanks of NOD-SCID mice (n=5) (Fig. 49A). Despite implanting equal number of cells, the A2780-dual<sup>ER</sup> CBF $\beta$ -KD cells showed slower tumor growth compared to control (Fig. 49B-D). A 6.9-fold lower IGF1R-promoter activity was observed in CBF $\beta$ -KD tumors  $\{4.003 \times 10^8 \pm 8.397 \times 10^7 \text{ (p/s/cm}^2\text{/sr)}\}$  compared to the control tumors  $\{2.778 \times 10^9 \pm 7.307 \times 10^8 \text{ (p/s/cm}^2\text{/sr)}\}$  at day 35 (Fig. 49B-C). Animals were given two treatments of cisplatin-paclitaxel at 10 days interval. At day 55, a 99.5 fold drop in bioluminescence signal was observed in CBF $\beta$ -KD tumors  $\{4.003 \times 10^8 \pm 8.397 \times 10^7 \text{ to } 4.020 \times 10^6 \pm 667424 \text{ (p/s/cm}^2\text{/sr)}\}$ , compared to 3.9-fold drop in the control tumors  $\{2.778 \times 10^9 \pm 7.307 \times 10^8 \text{ to } 7.213 \times 10^8 \pm 1.357 \times 10^8 \text{ (p/s/cm}^2\text{/sr)}\}$  (Fig. 49B-C). The CBF $\beta$ -KD tumors showed slower growth rate, drug treatment led to 1.3-fold reduction in tumor volume at day 55 ( $430.3 \pm 20.11$  vs  $328.3 \pm 27.59$  mm<sup>3</sup>) which was not evident in the control group (Fig. 49D). Further, CBF $\beta$ -KD tumors showed decreased expression of IGF1R, low number of proliferating cells (Ki-67) and higher necrosis compared to control tumors (Fig. 50A-B).



### 3.3.5 Ro5-3335 and Cisplatin-Paclitaxel attenuate IGF1R promoter and chemoresistance *in vivo*

We showed that abrogating RUNX1 activity through CBF $\beta$  knockdown attenuated IGF1R expression and severely sensitized the early resistant cells to Cisplatin-Paclitaxel *in vivo*. Hence, we asked if the pharmacological inhibitor of RUNX1, Ro5-33335, could be used to indirectly target IGF1R by disrupting RUNX1/FOXO3a axis. Ro5-33335 dose was carefully selected after performing MTT assays (IC<sub>80-70</sub> at 200 $\mu$ M for A2780 and IC<sub>80-70</sub> at 20 $\mu$ M for OAW42 cells) for combination treatment with Cisplatin and Paclitaxel (Fig. 51A-B).

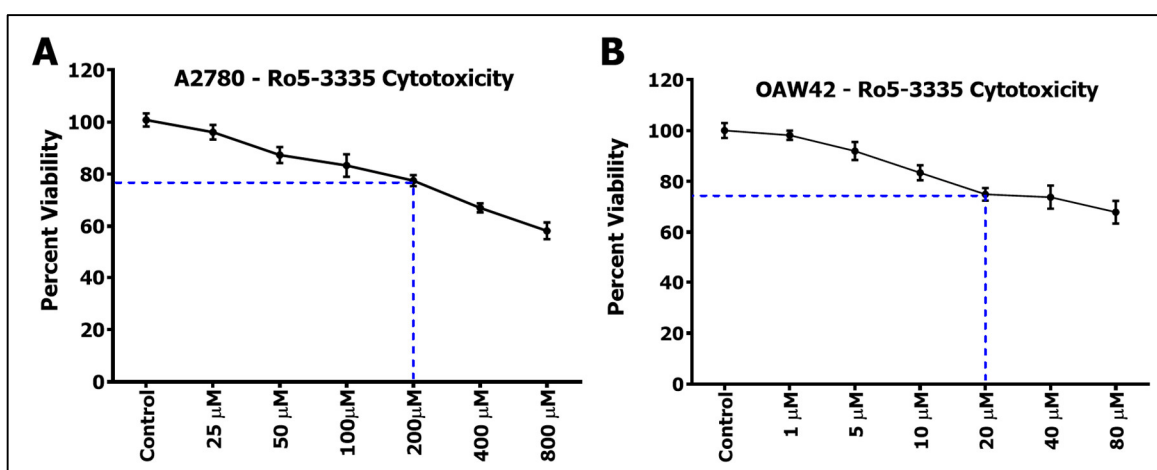
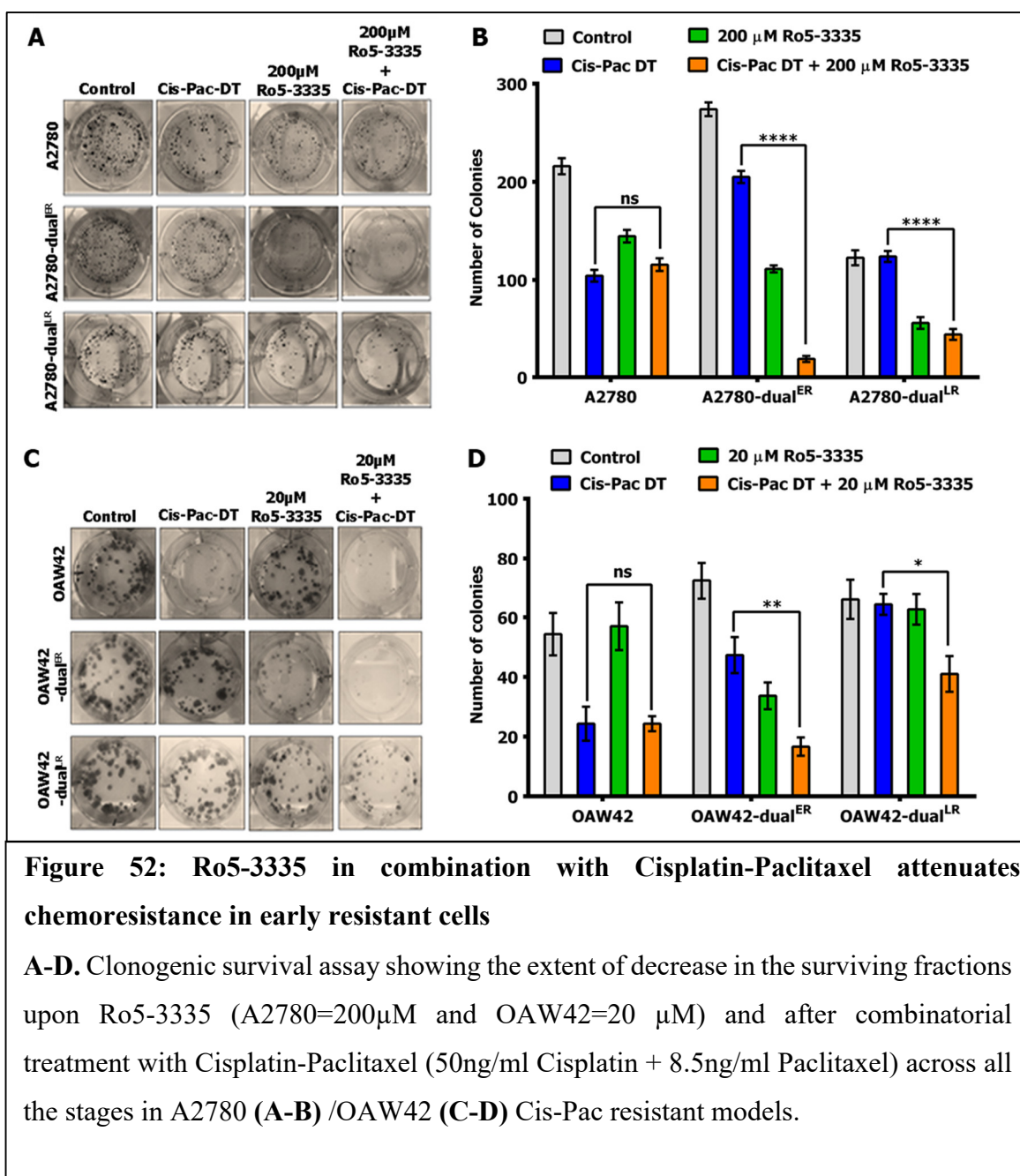


**Figure 51: Cytotoxicity of Ro5-3335 in A2780 and OAW42 cells across different concentration**

**A-B.** Cytotoxicity of Ro5-3335 in A2780 and OAW42 cells across different concentration respectively.

Ro5-3335 treatment alone significantly reduced the clonogenic potential of both the A2780-dual<sup>ER</sup> and OAW42-dual<sup>ER</sup> cells compared to respective sensitive and late resistant cells, however, this reduction was further increased when Ro5-3555 treatment was combined with platinum-taxol (Fig. 52A-D). In A2780-Cis-Pac resistant model, compared to Cisplatin-Paclitaxel alone, combination treatment (Ro5-3335 + Cisplatin-Paclitaxel) drastically reduced surviving fraction in A2780-dual<sup>ER</sup> cells (Cisplatin-Paclitaxel = 74.81% $\pm$ 2.28% reduced to Combination = 6.81% $\pm$ 1.11%) followed by A2780-dual<sup>LR</sup> cells (Cisplatin-Paclitaxel = 101.09% $\pm$ 4.53% reduced to Combination = 35.60% $\pm$ 4.49%), whereas no



change was observed in A2780 sensitive cells (Fig. 52A-B). Similar results were obtained with OAW42-Cis-Pac resistant model, combination treatment (Ro5-3335 + Cisplatin-Paclitaxel) drastically reduced surviving fraction in OAW42-dual<sup>ER</sup> cells (Cisplatin-Paclitaxel = 64.44%±8.33% reduced to Combination = 23.04%±4.22%) followed by OAW42-dual<sup>LR</sup> cells (Cisplatin-Paclitaxel = 97.47%±5.32% reduced to Combination = 62.12.60%±9.09%), whereas no change was observed in OAW42 sensitive cells (Fig. 52C-D).

Next, we checked the *in vivo* efficacy of Ro5-3335 to block IGF1R promoter activity and chemoresistance of A2780-dual<sup>ER</sup> cells by non-invasive optical imaging. Independent and combinatorial effects of Ro5-3335 and platinum-taxol treatment on IGF1R-promoter-luciferase activity and tumorigenicity were monitored in subcutaneous tumor xenograft of A2780-dual<sup>ER</sup> cells (stably expressing IGF1R promoter driven FL2-tdt reporter) by non-invasive optical imaging (Fig. 53A-C). Mice receiving Ro5-3335 showed 2-fold reduction in bioluminescence signal  $\{7.535 \times 10^7 \pm 1.539 \times 10^7$  to  $3.528 \times 10^7 \pm 5.873 \times 10^6$  (p/s/cm<sup>2</sup>/sr) at

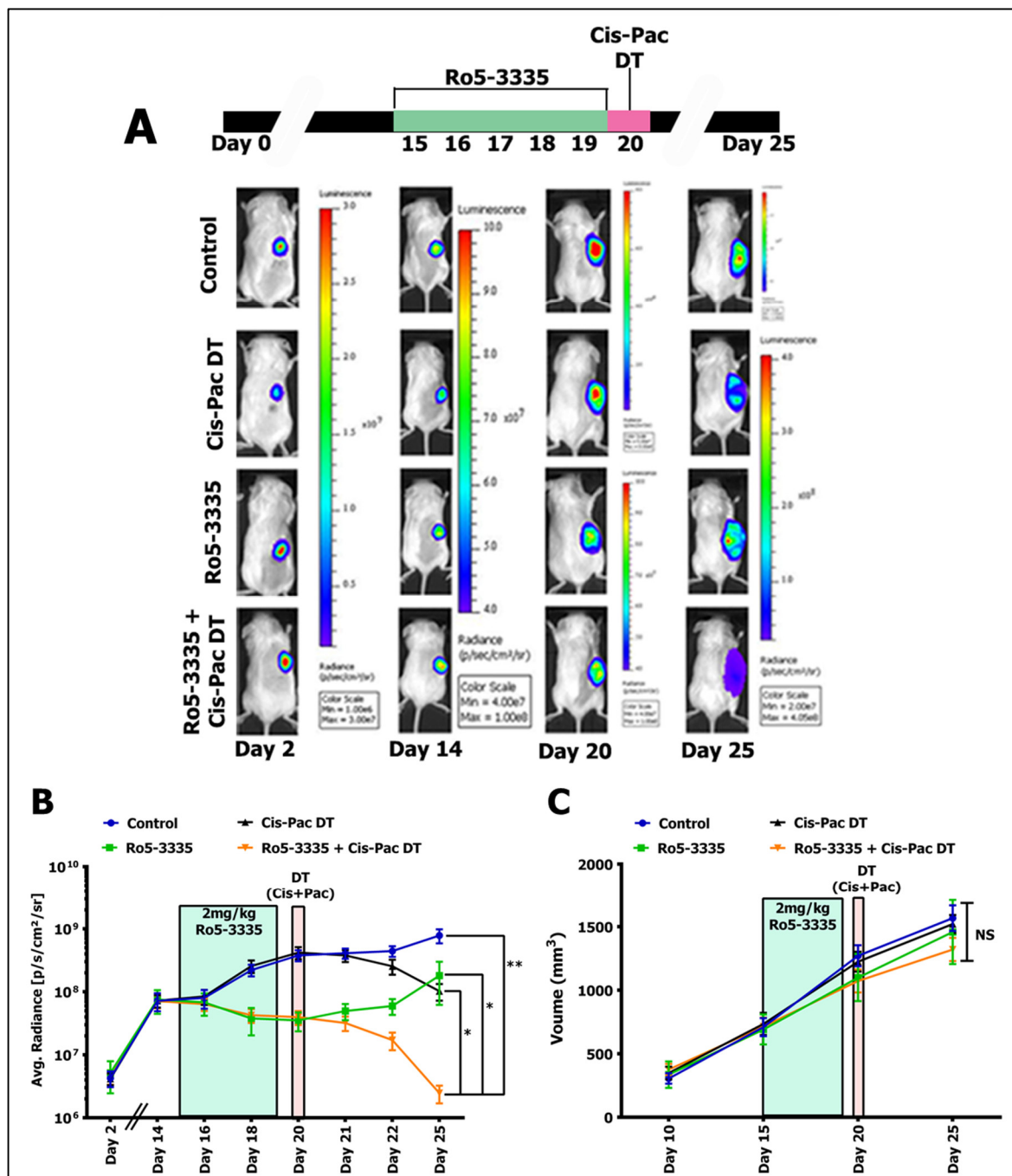


**Figure 53: Ro5-3335 mediated RUNX1 inhibition and Platinum-Taxol attenuate IGF1R promoter activity and chemoresistance *in vivo***

**A.** Ro5-3335 and Cisplatin-Paclitaxel treatment regime and representative bioluminescence images of A2780-dual<sup>ER</sup> tumor xenografts expressing IGF1R-FL2-TDT promoter-reporter treated with vehicle (control), Cisplatin-Paclitaxel, Ro5-3335 and Ro5-3335 with Cisplatin-Paclitaxel showing modulation in bioluminescence signal. **B.** Graphical representation of quantified bioluminescence signal (n=4/group) showing the trend in IGF1R promoter activity between the four groups. **C.** Graphical representation of tumor growth kinetics of the four groups.

end of the treatment (day-20) which then gradually increased to  $1.805 \times 10^8 \pm 5.932 \times 10^7$  (p/s/cm<sup>2</sup>/sr) (5.1-fold) at day-25 (Fig. 53A-B). Control group exhibited continuous increase in signal (10.9-fold) while Cisplatin-paclitaxel treatment group showed 4.1-fold reduction at day 25  $\{4.193 \times 10^8 \pm 9.138 \times 10^7$  to  $1.025 \times 10^8 \pm 3.028 \times 10^7$  (p/s/cm<sup>2</sup>/sr)}. The most drastic drop in IGF1R activity was observed in the group with combinatorial treatment (16.1-fold)  $\{3.959 \times 10^7 \pm 9.812 \times 10^6$  to  $2.468 \times 10^6 \pm 772284$  (p/s/cm<sup>2</sup>/sr)} at day-25 (Fig. 53A-B). Although no significant reduction in tumor volume was observed across the groups, slight decrease in tumor volume was noted between control and combinatorial groups ( $1567 \pm 101.4$  vs  $1321 \pm 90.84$  mm<sup>3</sup>) (Fig. 53C). Ki-67 staining and histological analysis showed decreased number of proliferating cells and higher necrosis in tumors of the combinatorial treatment group compared to the other groups (Fig. 54A-B). IGF1R staining among the groups showed maximal reduction in IGF1R in the combinatorial group compared to the rest of the groups (Fig. 54A-B), however, no significant change in FOXO3a staining was observed among the groups (Fig. 54A-B.). When statistical correlations were drawn among the groups comparing IGF1R staining with Ki67, FOXO3a, and tumor viability, only the IGF1R/FOXO3a exhibited lower correlation ( $R^2 = 0.688$ ) than the IGF1R/Ki67 ( $R^2 = 0.955$ ) and IGF1R/tumor viability ( $R^2 = 0.988$ ) (Fig 55A-C).

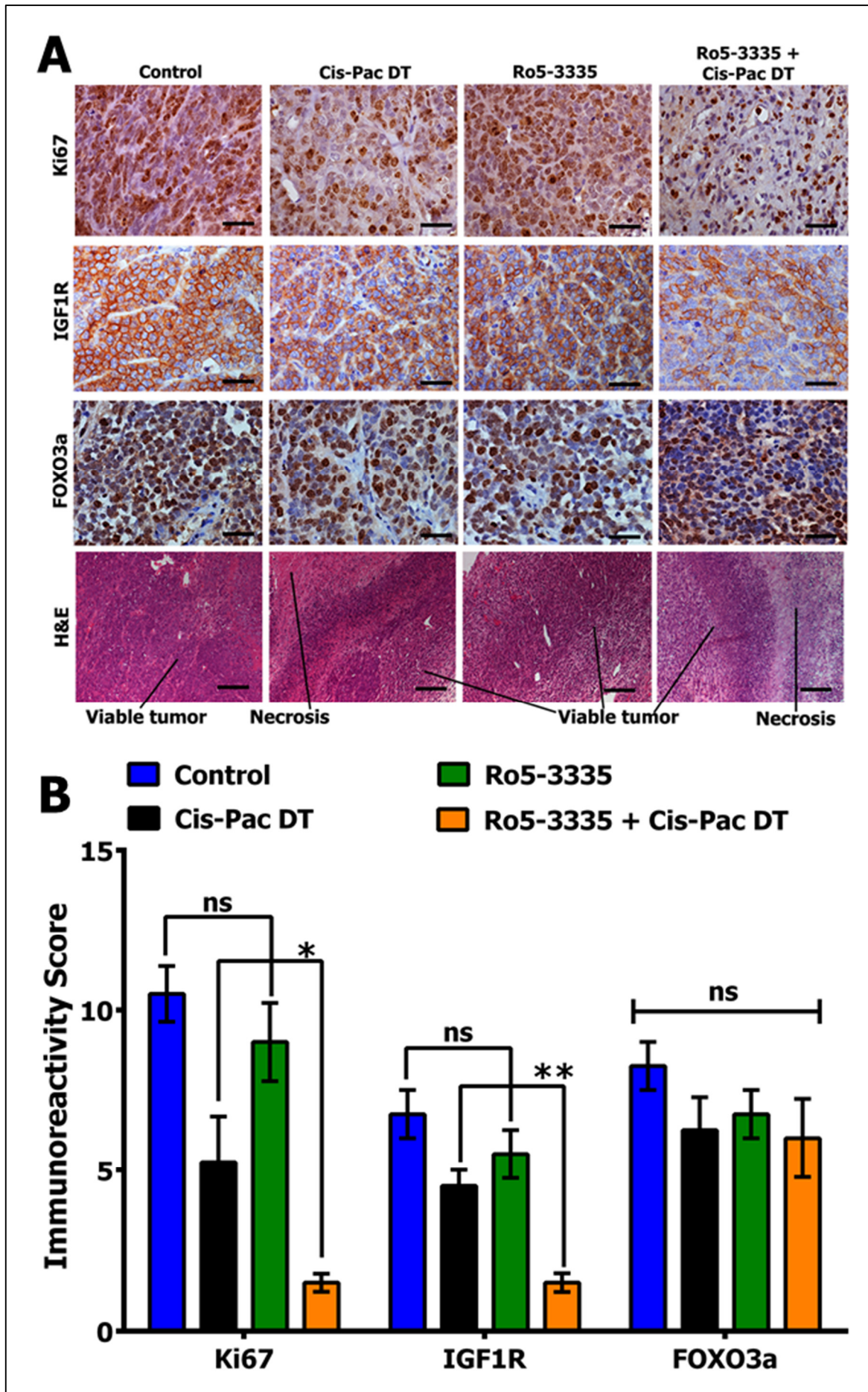


**Figure 55: Ro5-3335 and Platinum-Taxol downregulates IGF1R, abrogates tumor proliferation and decreases chemoresistance *in vivo***

**A-B.** Representative images (A) and graphical representation (B) of Ki-67, IGF1R, FOXO3a and H&E staining of tumor sections showing extent of cell proliferation and necrosis among the different treatment groups.

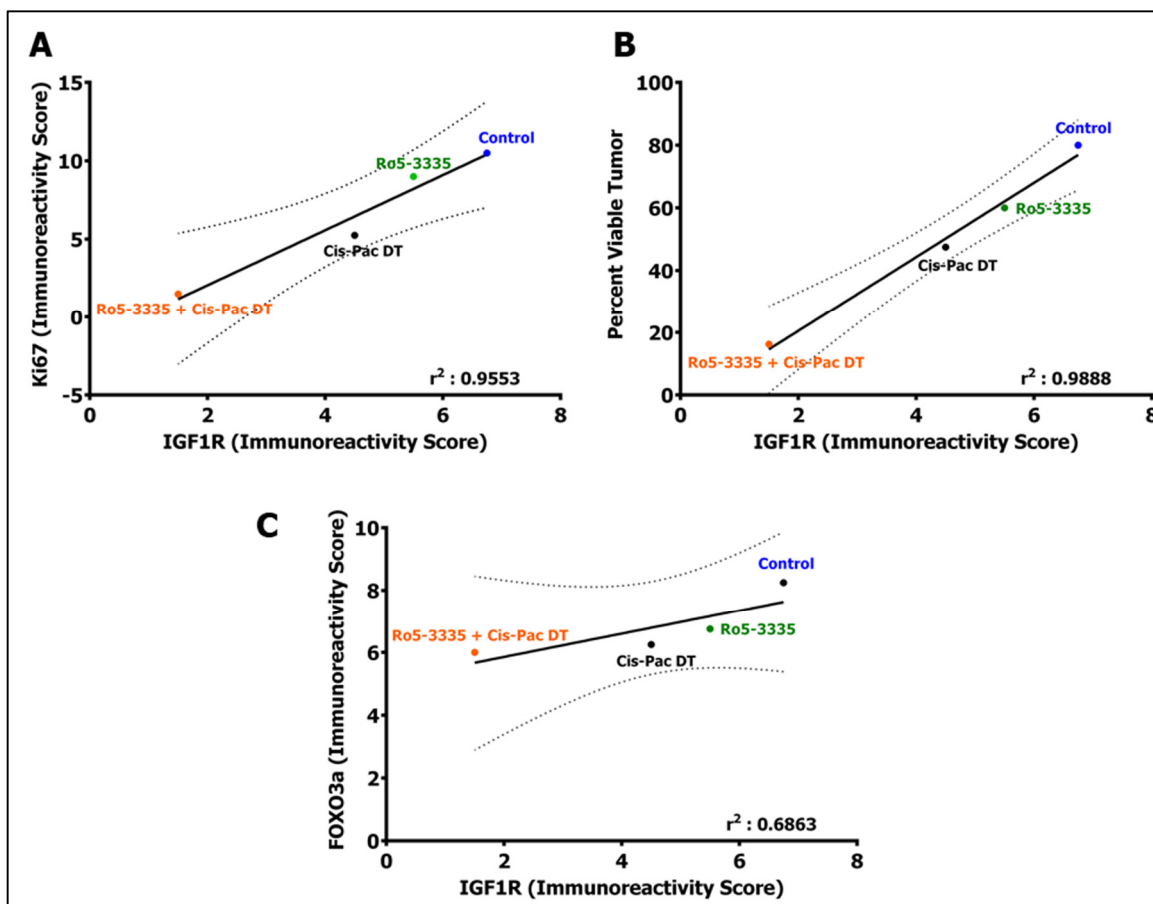


**Figure 54: IGF1R downregulation post Ro5-3335/Cisplatin-Paclitaxel/ combination treatment positively correlates with reduced tumor proliferation and increased necrosis**

**A-C.** Graphical representation the scatter plot and linear regression graphs depicting the coefficient of determination ( $R^2$ ) and statistical significance for correlation between Ki67 and IGF1R expression (A), tumor viability and IGF1R expression (B) and FOXO3a and IGF1R expression (C). The coefficient of correlation was calculated using Pearson's correlation coefficient test.

### 3.4 Discussion

Chemoresistance is a multifactorial phenomenon that enables cancer cells to evade apoptosis and promote cell survival. Underlying these mechanisms are aberrant gene regulatory networks and intricate network of signalling pathways that are activated by membrane receptors (growth factor receptors, G-protein-linked receptors, chemokine receptors and integrins) which are often deregulated in cancer and serve as interface between cancer cells and tumor microenvironment [204-208]. While majority of these receptors are overexpressed in different cancer types with high degree of genetic alterations (amplification, oncogenic fusions and activating mutations), IGF1R was found to be more commonly overexpressed across different cancer types with low level of amplification (3-6% in Sarcoma, Breast cancer, Ovarian cancer, Esophageal and Stomach adenocarcinoma) and lack of activating oncogenic mutations [209, 210]. Importance of IGF1R signalling in chemoresistance became evident with overexpression of IGF1R and its ligands (IGF1 and IGF2) in many cancer types including EOC imparting resistance against wide range of chemotherapeutic agents as well as targeted therapies. Moreover, IGF1R signalling pathway has been shown to be important for maintenance of a small fraction of self-renewable cancer stem cells that are shown to be inherently resistant to chemotherapeutic drugs. In the previous chapter we have shown that an intricate balance of RUNX1/FOXO3a interaction and a feedback inhibition loop of AKT on FOXO3a maintains a pulsatile nature of IGF1R expression through modulation of IGF1R promoter activity during acquirement of platinum-taxol resistance, however the direct role of IGF1R signaling in two important aspects of EOC biology, the CSC phenotype and chemoresistance are less explored.

IGF1R silencing significantly chemosensitized the early resistant cells to Cisplatin-Paclitaxel. More importantly IGF1R was shown to maintain CSC phenotype in early resistant cells through upregulation of pluripotency transcription factors SOX2, OCT4 and

NANOG. IGF1R silencing reduced the CSC-like SP population and self-renewal capacity of early resistant cells. The pluripotency transcription factor NANOG and IGF1R were shown to positively regulate each other leading sustained maintenance of CSCs in LC, AML, HNSCC and HCC [257, 389, 390, 418]. Similarly, IGF1R signalling was shown to regulate the intricate network of transcription factors involving SOX2 and OCT4 ( $\beta$ -Catenin/POU5F1/SOX2 and HIF-2a-OCT4/CXCR4) maintaining CSC phenotype [419-421]. Cancer stem cells are primarily characterized for their self-renewability, tumorigenicity as well as their intrinsic resistance towards the chemotherapeutic agents. Increased expression of drug transporter proteins such as MDR1, LRP, MRP1 and BCRP, enhanced activation of DNA repair pathways, slow cell cycling as well as cross-talk with EMT signalling pathway contribute to the intrinsic resistance of CSCs to chemotherapeutic drugs. The CSCs isolated from OC cells or patients have been shown to be highly tumorigenic, promoted metastasis and most importantly were shown to be chemoresistant [148, 396-398]. Majority of the studies have shown that CSCs contribute to the chemoresistance, however there is a growing body of evidence which indicate that therapeutic drugs also lead to enrichment of CSCs. The CSC-like SP cells isolated from A280-sensitive and A2780-dual<sup>ER</sup> cells were highly resistant to Cisplatin-Paclitaxel, as compared to the respective NSP and MP cells. Also, the SP cells isolated from IGF1R knockdown early resistant A2780-dual<sup>ER</sup> cells were comparatively more sensitive to Cisplatin-Paclitaxel than the respective NSP and MP cells. Active dependency on IGF1R signalling has shown that CSCs are sensitive to IGF1R inhibitors in Colorectal cancer, Neuroblastoma, Head and neck squamous cell cancer, Breast cancer and Glioblastoma [390, 391, 422, 423]. However, here we show that not only show that IGF1R helps in enriching and maintaining CSC-like SP cells in early resistant cells but also regulates the intrinsic chemoresistance of CSC-like SP cells isolated from early resistant EOC cells.

The two major signalling arms activated downstream of IGF1R are PIK3CA/AKT and MAPK/ERK pathways, which primarily promote cellular proliferation, cell survival, differentiation and antagonize the apoptotic pathways [415, 416]. The PIK3CA/AKT, showed gradual increase in AKT activation with increasing resistance, whereas, MAPK/ERK pathway showed highest ERK1/2 activation in only A2780-dau<sup>ER</sup> cells and remained low in both A2780-sensitive and A2780-Dual<sup>LR</sup> cells. IGF1R silencing significantly attenuated the ERK1/2 activation across the A2780 dual resistance model with most profound downregulation in A2780-Dual<sup>LR</sup> cells, whereas the PIK3CA/AKT signalling largely remains unaffected across the chemoresistance model. Despite the common notion that both PIK3CA/AKT and MAPK/ERK pathways are activated downstream of IGF1R, it has been observed that preferential activation of MAPK/ERK pathway can take place through a process known as biased signalling [424].  $\beta$ -arrestin1 a key mediator of G-protein-coupled receptors is shown to have high affinity for IGF1 bound IGF1R leading to sustained activation of MAPK/ERK pathway but not PIK3CA/AKT [425]. Figitumumab, an anti-IGF1R antibody was shown to fail in phase II clinical trials due to formation of IGF1R and IR hybrid receptor formation and biased IGF1R signalling activation [426]. Hypoxia and Akt induced Stem cell Factor and LL37 (a mature C-terminal peptide of the human cationic antimicrobial protein 18) were shown to bind to IGF1R and induce the biased activation of ERK1/2 over AKT [427], while such in depth understanding of IGF1R downstream signalling in chemoresistant EOC cells is warranted. Indeed, the MAPK/ERK pathway, which is highly active in early resistant cells, silencing IGF1R significantly decreased proliferation signifying importance of IGF1R/MAPK/ERK signalling in promoting cellular proliferation of early resistant cells. IGF1R signalling has also been shown to be strong inhibitor of apoptosis induced by chemotherapeutic agents, nutrient deprivation, anchorage independent growth and oxidative stress. The augmented

levels of IGF1R in early resistant cells were found to induce the levels of anti-apoptotic proteins BCL-2 and BCL-XL, whereas it antagonized the induction of pro-apoptotic protein BAD post Cisplatin-Paclitaxel treatment in A2780-Dual<sup>ER</sup> cells, augmented levels of IGF1R in early resistant cells were found to induce the levels of anti-apoptotic proteins BCL-2 and BCL-XL, whereas it antagonized the induction of pro-apoptotic protein BAD post Cisplatin-Paclitaxel treatment in A2780-Dual<sup>ER</sup> cells. The pro-apoptotic protein BAD which serve as a critical node between growth factor mediated survival signalling and inhibition of apoptosis. Upon activation of apoptotic cascade BAD binds to both BCL-2 and BCL-XL displacing the pro-apoptotic proteins BAX and BAK which induce mitochondrial depolarization. The growth factor mediated activation of cell survival signalling pathways PIK3CA//AKT and MAPK/ERK phosphorylate BAD at S136 and S112 respectively preventing binding of BAD to BCL-2 and BCL-XL, thus leading to suppression of apoptosis [428, 429]. Cisplatin-Paclitaxel treatment was shown to significantly upregulate anti-apoptotic proteins BCL-2 and BCL-XL in early resistant cells which was abrogated post IGF1R silencing. The active MAPK/ERK signalling was shown to positively regulate the anti-apoptotic proteins BCL-2, BCL-XL and MCL-1 in Pancreatic cancer, Acute myeloid leukaemia, Ovarian cancer and Endometroid cancer [430-435]. Since we observe both MAPK/ERK signalling and anti-apoptotic protein levels (BCL-2 and BCL-XL) going down in IGF1R knockdown early resistant cells leading to increased sensitivity to Cisplatin-Paclitaxel treatment, we postulate that IGF1R/MAPK/ERK pathway imparts chemoresistance in early resistant cells through modulation of anti-apoptotic proteins (BCL-2 and BCL-XL) and pro-apoptotic protein BAD.

Since IGF1R was shown to impart chemoresistance through both maintenance of CSC phenotype and activation MAPK/ERK pathway leading to suppression of apoptosis, IGF1R proves to be important molecule at early onset of chemoresistance development thus making

IGF1R an attractive molecule for targeted therapy. While IGF1R levels were significantly downregulated in late resistant cells through feedback inhibition loop on FOXO3a by activated AKT. Inhibiting AKT stabilized FOXO3a increasing IGF1R expression through transcriptional activation. Interestingly this AKT inhibition induced IGF1R could impart resistance against AKT inhibition, as dual inhibition of AKT and IGF1R significantly reduced cell survival of late resistant cells. The resistance against the PI3K/AKT/mTOR inhibitors are majorly through activation of redundant pathways, loss of feedback inhibition loops or through gain of function mutations leading to sustained activation of pathway. However, it has recently been found that inhibition of the PI3K/AKT/mTOR can rapidly induce overexpression or activation of RTKs such as HER2, HER3 IGF1R, and IR limiting the efficacy of these agents during treatment. The augmented levels of IGF1R imparting resistance against Cisplatin-Paclitaxel in early resistant cells and AKT inhibition induced IGF1R limiting efficacy of AKT inhibitor, both were regulated by transcriptional modulation of IGF1R promoter by RUNX1/FOXO3a. Moreover, overexpression of IGF1R in majority of cancer types has been strongly correlated with transcriptional activation of IGF1R rather than IGF1R gene amplification. Since, directing targeting of IGF1R by anti-IGF1R targeted agents (anti-IGF1R and anti-IGF1/2 antibodies and IGF1R tyrosine kinase inhibitors) have failed in clinical trials, we investigated potential of a new therapeutic window of targeting IGF1R transcription in chemoresistant EOC cells. Genetic ablation of RUNX1 transcriptional activity by CBF $\beta$  knockdown decreased IGF1R expression specifically in early resistant cells, which led to increased chemosensitization and reduced invitro tumorigenicity maximally in early resistant cells. To achieve similar effect, but using pharmacological means, we used the RUNX1 inhibitor, Ro5-3335. Like the CBF $\beta$  knockdown, pharmacological inhibition of RUNX1 showed enhanced chemosensitization of early resistant cells as compared to the sensitive and late resistant cells in both A2780

and OAW42 Cis-Pac resistant models. RUNX1, a master regulator of hematopoiesis, is one of the most frequently mutated gene in hematological malignancies [341]. RUNX1 in combination with FOXL2 was shown to maintain the fetal granulosa cell identity [436], whereas overexpression of RUNX1 either by hypomethylation of promoter or by loss of MicroRNA-302b has been shown to promote proliferation, migration, and invasion [344, 437]. Recently, RUNX1 has been found to have a more widespread role in several solid cancers [342, 438] but this is the first report of its role in regulation of IGF1R promoter activity and in development of chemoresistance. Both the Pharmacological (Ro5-3335) or genetic ablation (CBF $\beta$  knockdown) of RUNX1 activity decreased IGF1R expression, impaired tumor proliferation and showed enhanced chemosensitization to Cisplatin-Paclitaxel in tumor xenografts of A2780-Dual<sup>ER</sup> cells. Apart from VHL loss in 5-Fluorouracil and Etoposide resistant Renal cell carcinoma and FOXO1 activation in Phosphatidylinositol-3-Kinase Catalytic Subunit delta inhibitor resistant murine model [275, 319], probable action of other transcriptional regulator/s in mediating cancer therapy resistance through IGF1R are unknown. Such molecular knowledge is important to identify both therapeutic and diagnostic markers for the IGF1R addicted cancers including EOC. Continuous application of low dose Ro5-3335 showed attenuation of IGF1R promoter activity *in vivo* in tumor xenografts and with intermittent drug treatment led to significant decrease in IGF1R expression, thus establishing that disrupting the transcriptional activation of IGF1R promoter by RUNX1/FOXO3a can be a new window of therapeutic strategy to indirectly direct IGF1R. RUNX1 is indispensable for establishment of definitive hematopoiesis in vertebrates. However, no obvious illness was observed in long term use of 300mg/kg/day of Ro5-3335 in mice [337] and a single dose of 5mg/kg of Ro5-3555 protects LPS induced death in mice by reducing inflammation [439]. We applied similar low dose in fractionated manner (2mg/kg/day/5days) and observed that low dose RUNX1 inhibitor

with platinum-taxol could effectively delay resistance development. However, a detail dose dependent study is warranted to assess potential of RUNX1 inhibition combating the platinum-taxol resistance.

Altogether, our data strengthens the importance of augmented expression of IGF1R at onset of chemoresistance development, which imparts the chemoresistance against chemotherapeutic drugs Cisplatin and Paclitaxel in EOC cells. The hyperactive IGF1R signalling maintains the CSC phenotype, CSC chemoresistance, promotes cellular proliferation and antagonizes Cisplatin-Paclitaxel induced apoptosis in early resistant cells. Most importantly we show that perturbation of RUNX1 activity severely compromised IGF1R promoter activity and sensitized the tumors of early resistant cells to platinum-taxol treatment, as monitored by non-invasive imaging. Thus, an indirect approach by targeting IGF1R gene regulators, such as RUNX1, in IGF1R addicted cancer or in therapy resistant situation might arise as a viable option. This RUNX1-FOXO3a partnership most likely impacts other target genes required for resistance. Therefore, targeting RUNX1 in combination with chemotherapy might turn up as a new strategy to reverse or delay development on chemoresistance in EOC cells.

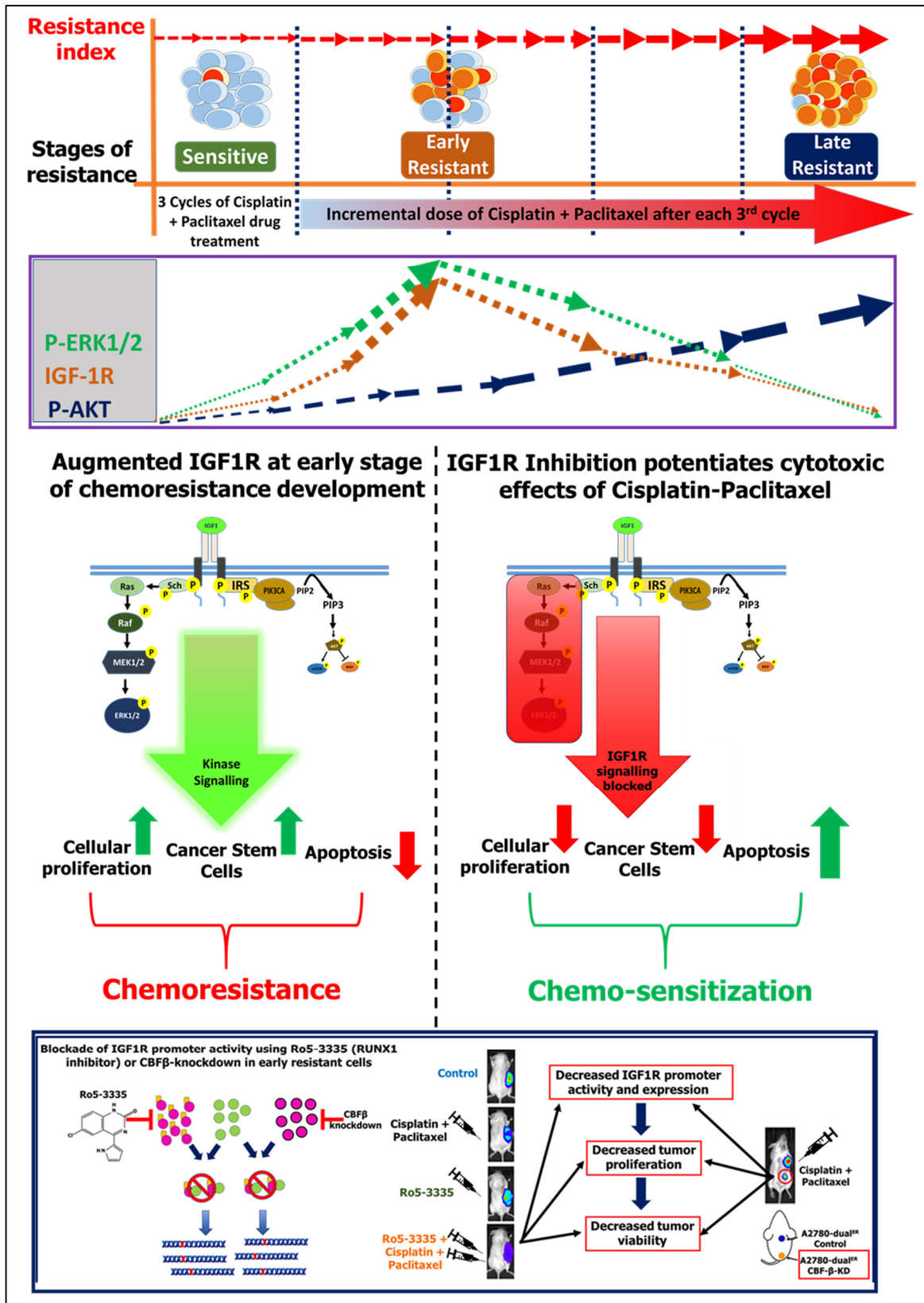


Figure 56: Proposed model of IGF1R/MAPK/ERK signalling mediated chemoresistance through maintenance of CSC phenotype and suppression of apoptosis at and for indirect targeting of the augmented expression of IGF1R at onset of chemoresistance development by blocking transcriptional regulators of IGF1R promoter in EOC cells

## Chapter 4: Summary and Conclusion

### 4.1 Summary

The race to develop anti-IGF1R targeted therapies for cancer has been hindered due to failure of clinical trials to yield clinical benefits. However, the mounting evidence suggest that not only IGF1R overexpression is ubiquitous across different cancer types but it is also a key signalling molecule underlying the resistance mechanisms against wide range of chemotherapeutic agents and targeted therapies [440]. The first anti-IGF1R targeted therapy (Teprotumumab) has been recently (January, 2020) approved, although not for cancer treatment, but for treatment of Graves' orbitopathy [441]. Several pre-clinical studies have started reevaluation of anti-IGF1R agents, not as a standalone treatment, but in combination with chemotherapeutic agents and other targeted therapies along with identification of predictive biomarkers to unlock the full potential of anti-IGF1R targeted therapies in cancer [440]. Using indigenously developed isogenic EOC chemoresistance models against Cisplatin/Paclitaxel/Cisplatin-Paclitaxel combination, we reported a pulsatile nature of IGF1R expression during acquirement of chemoresistance development. The augmented levels of IGF1R were shown to impart chemoresistance against Cisplatin-Paclitaxel at early stages of chemoresistance development; moreover, we observed similar therapy induced upregulation of IGF1R expression in tumors of a small cohort of high grade serous EOC patients [252]. The underlying mechanisms behind this undulating IGF1R expression during progression of chemoresistance has led to this investigation which deciphers two important questions pertaining the role of IGF1R signalling in chemoresistance development of EOC, A) unraveling the complex circuitry of modulators governing IGF1R expression and B) decoding the molecular mechanisms behind IGF1R mediated chemoresistance and identifying potential approach to indirectly target IGF1R through its regulators in IGF1R addicted or therapy resistant cancers.

IGF1R overexpression in many cancer types is significantly attributed to the transcriptional modulation rather than to rare instances of gene amplification, hence we used an IGF1R promoter driven bi-fusion (bioluminescence-fluorescence) reporter sensor to uncover the mechanisms behind this oscillating IGF1R expression during progression of resistance. The IGF1R-promoter-reporter sensor showed similar pulsatile nature as previously observed for endogenous IGF1R transcript and protein levels, significantly upregulated at early stages of chemoresistance and declined in late resistance stages. Next, using a transcription factor binding IGF1R promoter competition assay we identified eight new transcription factors (RXR, SOX9, VDR, GFI1, ROR, RUNX1, NKX2.5 and SOX18) along with SP1 (a known IGF1R regulator) as potential regulators of IGF1R promoter in chemoresistant EOC cell. Sarfstein. et. al. (2009), using biotinylated IGF1R promoter reported identification of several transcription factors binding to IGF1R promoter in breast cancer cells [363]. However, this is first report where we identify potential regulators of IGF1R promoter in chemoresistant cancer cells, apart from pVHL and FOXO1 regulating IGF1R in 5-Fluorouracil and etoposide resistant renal cell carcinoma and PI3K- $\delta$  inhibitor resistant chronic lymphocytic leukaemia respectively [300, 442]. Though transcription factor-promoter array analysis in this study identified several unique transcriptional regulators, perturbation of only RUNX1 activity (RUNX1-CBF $\beta$  inhibitor, Ro5-3335) significantly attenuated IGF1R transcriptional and promoter activity in chemoresistance models.

RUNX1, a significantly altered gene in acute myeloid leukaemia and functions as a pioneering transcription factor in haematopoiesis [341], showed increased expression and nuclear localization of RUNX1 along with enhanced binding of RUNX1 to IGF1R promoter at both early and late stages of chemoresistance. Despite increased RUNX1 expression and functional activities (nuclear localization and enhanced binding on IGF1R promoter) across both stages of chemoresistance, specific inhibition of IGF1R by Ro5-3335 was observed

only in early-resistant cells, which signifies for contributory role of other regulator/s for optimal activation. Using JASPAR, a TF binding prediction software we found that consensus binding sites of transcription factors identified from transcription factor array and previously reported IGF1R binding transcription factor are scattered throughout IGF1R promoter. Intriguingly, RUNX1 and FOXO3a (a known IGF1R regulator) [328] binding elements showed proximity to each other on IGF1R promoter. As opposed to RUNX1, FOXO3a exhibited a similar pulsatile pattern like IGF1R across resistant stages with increased nuclear localization of both total and transcriptionally active FOXO3a (p-S413) and higher IGF1R promoter occupancy in early resistant cells. Mutating FOXO3a binding elements on IGF1R promoter in combination with Ro5-3335 treatment showed significant synergism in attenuating IGF1R promoter activity in early resistant cells as compared to FOXO3a binding element mutant IGF1R promoter or Ro5-3335 treatment alone. Indeed, the co-immunoprecipitation results demonstrated a stage specific interaction pattern between RUNX1 and FOXO3a which was highest in early resistant cells but minimal in sensitive and late resistant cells. This stage specific interaction pattern seems to influence their IGF1R promoter binding capacity as maximal RUNX1-FOXO3a co-occupancy was evident during onset of resistance which subsequently decreased at late-resistant stages as revealed by Chip-re-Chip assay, thus signifying cooperativity between RUNX1 and FOXO3a in regulation of IGF1R promoter activity. This cooperativity became evident from genetic (CBF $\beta$  knockdown) and pharmacological inhibition (Ro5-3335 treatment) of RUNX1 activity, which abolished FOXO3a binding in early-resistant cells indicating that RUNX1 binding is an obligatory step for FOXO3a occupancy specifically at the onset of resistance. This cooperative interaction of RUNX1-FOXO3a, however falls apart as cells reach late resistant cells due to simultaneous presence of hyperactivated AKT, which downregulates FOXO3a by nuclear exclusion. Indeed, AKT inactivation either through

serum starvation or by an inhibitor restores FOXO3a levels in late resistant cells upregulating IGF1R expression.

Once, upstream molecular players regulating IGF1R expression were identified, we next checked the biological consequences of augmented IGF1R expression in maintaining chemoresistance properties of EOC cells. IGF1R silencing significantly chemosensitized the early resistant cells to chemotherapeutic agents Cisplatin-Paclitaxel alone. More importantly IGF1R was shown to maintain CSC phenotype in early resistant cells through upregulation of pluripotency transcription factors Sox2, Oct4 and Nanog. The CSC-like SP cells were highly resistant to Cisplatin-Paclitaxel compared to the respective NSP and MP cells, more importantly IGF1R knockdown showed enhanced chemosensitization of SP cells. Among the two major signalling arms, AKT showed gradual activation with increasing resistance, whereas, ERK1/2 showed highest activation in only early resistant cells. Silencing IGF1R revealed that the MAPK/ERK signalling arm is activated downstream of IGF1R, whereas PIK3CA/AKT signalling largely remains unaffected across the chemoresistant model. The increased levels of IGF1R in early resistant cells induced the levels of anti-apoptotic proteins BCL-2 and BCL-XL, whereas it antagonized the induction of pro-apoptotic protein BAD post Cisplatin-Paclitaxel treatment in early resistant cells, thus suppressing the Cisplatin-Paclitaxel induced apoptosis in early resistant cells. Interestingly, AKT inhibition in late resistant cells induced IGF1R, which was shown to impart resistance against AKT inhibition, as dual inhibition of AKT and IGF1R significantly reduced cell survival of late resistant cells. The augmented levels of IGF1R imparting resistance against Cisplatin-Paclitaxel in early resistant cells and AKT inhibition induced IGF1R limiting efficacy of AKT inhibitor, both were regulated by transcriptional modulation of IGF1R promoter by RUNX1/FOXO3a.

In present study we have shown that RUNX1/FOXO3a maintain augmented IGF1R promoter activity at onset of chemoresistance development in EOC cells leading to increased expression of IGF1R. Thus, we investigated the potential of blocking RUNX1/FOXO3a/IGF1R axis to assess the biological implication of this axis in targeting early onset of chemoresistance. Pharmacological (Ro5-3335 treatment) or genetic ablation (CBF $\beta$  knockdown) of RUNX1 activity attenuated IGF1R promoter activity, reduced IGF1R expression, impaired tumor proliferation and showed enhanced chemosensitization to Cisplatin-Paclitaxel both *invitro* and *invivo* in early resistant cells. RUNX1 is indispensable for establishment of definitive haematopoiesis in vertebrates. However, no obvious illness was observed in long term use of 300mg/kg/day of Ro5-3335 in mice [337] and a single dose of 5mg/kg of Ro5-3555 protects LPS induced death in mice by reducing inflammation [439]. We applied similar low dose in fractionated manner (2mg/kg/day/5days) and observed that low dose RUNX1 inhibitor with platinum-taxol could effectively delay resistance development. However, a detail dose dependent study is warranted to assess potential of RUNX1 inhibition combating the platinum-taxol resistance in cancers with augmented IGF1R expression.

## **4.2 Conclusion**

Here, for the first time we report RUNX1 as a unique regulator of IGF1R promoter which exerts a cooperative interaction with FOXO3a and dynamically modulate IGF1R expression during acquirement of chemoresistance in EOC cells. Genetic and pharmacological inhibition followed ChIP and ChIP-re-ChIP assay revealed that RUNX1 strengthened FOXO3a occupancy on IGF1R promoter, leading to a transcriptional surge during initiation of resistance which is lost at the late stages. Further an active AKT-FOXO3a negative feedback loop was shown to maintain the pulsatile behaviour of IGF1R and FOXO3a. We also showed that upregulated IGF1R at onset of resistance confers resistance to Cisplatin-

Paclitaxel through modulation of CSC phenotype and inhibition apoptosis by downstream IGF1R signalling. Perturbation of RUNX1 activity severely compromised IGF1R promoter activity and sensitized the tumors of early resistant cells to platinum-taxol treatment, as monitored by non-invasive imaging. Altogether our findings delineate a dynamic interplay between several molecular regulators (RUNX1/FOXO3a/AKT) driving pulsatile IGF1R expression and identifies a new avenue for targeting EOC through RUNX1-IGF1R axis during acquirement of chemoresistance.

## Chapter 5: Materials and Methods

### 5.1 Cell culture

#### 5.1.1 Reagents and chemicals

Sr. No.	Reagent name	Source
1	Media – DMEM, MEM and RPMI	Gibco, USA
2	Foetal bovine serum (FBS)	HiMedia, India
3	100X-Penicillin – Streptomycin (Pen-Strep)	HiMedia, India
4	Trypsin-0.25% –Ethylenediaminetetraacetic acid (EDTA)-0.02%	Sigma, USA
5	Phosphate buffered saline (PBS) pH7.4*	In-House
6	Dimethyl sulfoxide (DMSO)	Sigma, USA
7	G418	Sigma, USA
8	Puromycin	Sigma, USA
9	Superfect transfection reagent	Qiagen, USA
10	Lipofectamine 2000	Invitrogen, USA
11	Trypan blue solution (0.4%)	Sigma, USA
12	3-(4,5-dimethylthiazol-2-yl)-2,5-diphenyl tetrazolium bromide (MTT)	Sigma, USA
13	Low melting agarose	AMRESCO, USA
14	Agarose	Sigma, USA
15	Epidermal growth factor (EGF)	Sigma, USA
16	Fibroblast growth factor (FGF)	Sigma, USA
17	Insulin	Sigma, USA
18	Leukaemia inhibiting factor (LIF)	Thermo Fisher Scientific, USA
19	Vybrant DyeCycle Violet (DCV) stain	Thermo Fisher Scientific, USA
20	Verapamil hydrochloride	Sigma, USA
21	Methanol	Qualigens, India
22	Glacial acetic acid	Fischer Scientific, USA
23	Crystal violet	Sigma, USA
24	Polybrene	Sigma, USA

\*PBS: 137mM NaCl, 2.7mM KCl, 10mM Na<sub>2</sub>HPO<sub>4</sub> and 2mM KH<sub>2</sub>PO<sub>4</sub>, pH 7.4.

### 5.1.2 Cell lines

The cell lines used in the current study are listed below with their respective growth media.

Sr. No.	Cell line name	Origin	Source	Couture media
1	A2780	Ovarian cancer	ATCC	DMEM
2	OAW42	Ovarian cancer	ATCC	MEM
3	SKOV3	Ovarian cancer	ATCC	RPMI
4	MCF7	Ovarian cancer	ATCC	RPMI
5	HEK293FT	Human embryonic	ATCC	DMEM

### 5.1.3 Methods

All the cell lines used in current study were maintained in their respective media supplemented with the 10% FBS and 1% Pen-Strep and incubated under 5% CO<sup>2</sup> at 37°C and 90% humidity. Cells with 70-80% confluence were used for experiments.

#### 5.1.3.1 Sub-culture and maintenance

- a) Wash cells gently twice with sterile PBS after removing spent media.
- b) Add sterile trypsin-EDTA solution to the cell culture dish and incubate at 37°C till all cells detach from plate surface.

*Amount of trypsin as per cell culture dish size, 100mm: 1ml and 60mm: 0.5ml.*

- c) Collect cells by adding thrice the volume of sterile cell culture media and centrifuge at 800rpm for 5 minutes at 4°C.
- d) Discard the supernatant, resuspend cells in sterile PBS and centrifuge again at 800rpm for 5 minutes at 4°C.
- e) Discard the supernatant, resuspend cells in sterile culture media and make single cell suspension by pipetting.
- f) Count the cells using Neubauer chamber after diluting cells with trypan blue dye in 1:3 ratio. Estimate the viable cell count using formula,

$$\text{Viable cells per ml} = \frac{\text{Total number of cells counted}}{4} \times \text{Dilution factor} \times 10^4$$

- g) Sub-culture cells in 1:3 split ratio or according to experimental requirement.

#### 5.1.3.2 Cryopreservation of cells

- a) Briefly trypsinize cells as described in section 1.1.3.1 and determine viable cell count.
- b) Resuspend  $1-2 \times 10^6$ /ml cells in pre-chilled freezing media (sterile media with 50% FBS) and add sterile DMSO to this solution dropwise at final concentration of 10%.
- c) Aliquot 1ml of the above suspension to the cryo-vials (pre-labelled with cell line name, passage number and date of freezing) and freeze cells slowly (approximately at rate of  $1-2^\circ\text{C/hr}$ ) first at  $-20^\circ\text{C}$  for 2 hours and later at  $-80^\circ\text{C}$  overnight using mini-cooler. Next day store the frozen cryo-vials in liquid nitrogen.

#### 5.1.3.3 Revival of cryopreserved cells

- a) Thaw the frozen cryo-vial at  $37^\circ\text{C}$  in water bath. Transfer thawed cells to fresh 5ml sterile media and centrifuge at 800rpm for 5 minutes at  $4^\circ\text{C}$ .
- b) Discard the supernatant. Resuspend cells in sterile culture media, transfer to a 60mm cell culture dish and incubate the plate under 5%  $\text{CO}_2$  at  $37^\circ\text{C}$ .
- c) Next day cells wash cells once with sterile PBS and feed with fresh sterile media.

#### 5.1.3.4 Transfection of cells for transient/stable expression of transgenes

- a) One day prior to transfection trypsinize the cells, determine viable cell count and seed cells in appropriate number according to the experimental requirement.
- b) Wash the cells with sterile PBS once before adding DNA-transfection reagent complex to the cells.
- c) Prepare DNA-Superfect transfection reagent complex according to requirement of the experiment following manufacturer's instructions (See below).

<b>Culture format</b>	<b>Adherent cells to be seeded</b>	<b>DNA (<math>\mu\text{g}</math>)</b>	<b>Final volume of DNA to be diluted in serum free media (<math>\mu\text{l}</math>)</b>	<b>Volume of Superfect reagent (<math>\mu\text{l}</math>)</b>	<b>Volume of serum containing media (<math>\mu\text{l}</math>)</b>
24-Well	$2.0 - 8.0 \times 10^4$	1.0	60	5.0	350
12-Well	$0.4 - 2.0 \times 10^5$	1.5	75	7.5	400
6-Well	$0.9 - 4.0 \times 10^5$	2.0	100	10.0	600
60mm	$2.0 - 8.0 \times 10^5$	5.0	150	30.0	1000
100mm	$0.5 - 2.5 \times 10^6$	10	300	60.0	3000

- Dilute DNA in appropriate volume of sterile serum free media (containing no proteins or antibiotics) and mix well by gentle pipetting.
- Add appropriate volume of Superfect transfection reagent to above mixture and mix well by gentle pipetting.
- Incubate above mixture for 15-20 minutes at room temperature.
- After incubation add appropriate volume of sterile serum containing media.
- Mix the mixture gentle pipetting and immediately transfer it onto the cells to be transfected.

- d) Wash the cells with sterile PBS once before adding DNA-transfection reagent complex to the cells.
- e) Add DNA-transfection reagent complex onto the cells and incubate under 5% CO<sup>2</sup> at 37°C for three hours.
- f) Remove transfection complex after 3 hours of incubation, wash cells once with sterile PBS and process further according to the experimental requirements.
- g) Perform all transient transfection experiments within 72 hours of transfection.
- h) For stable transfection, cells trypsinize cells post 24 hours of transfection and subculture them in 100mm tissue culture dish maintaining single cell density post seeding.
- i) Maintain subcultured cells in sterile media containing appropriate quantity of drug selection marker (present in plasmid).

- j) Feed fresh sterile media with adequate quantity of drug selection marker every 72 hours.
- k) Once well isolated colonies emerge in cell culture dish, pick them up by point trypsinization and transfer to the 96-well plate and maintain them in sterile media containing appropriate quantity of drug selection marker.
- l) Screen each colony using appropriate method to identify cells expressing transgene.
- m) Maintain the established stable cells expressing transgene in sterile media containing appropriate quantity of drug selection marker during expansion.

#### 5.1.3.5 MTT cell viability assay

- a) Seed appropriate number of cells were in 96-well pate, 24 hours prior to the experiment.  
*A2780: 2000 cells/well and OAW42/SKOV3: 1000 cells/well*
- b) Treat cells with appropriate concentration of drugs as per the requirement of the experiment for 72 hours under 5% CO<sup>2</sup> at 37°C.
  - A2780 and OAW42 models Cisplatin + Paclitaxel (50ng/ml+8.5 ng/ml) for 72 hours
  - A2780 and OAW42 models Ro5-3335 (A2780 = 200µM and OAW42 = 20µM) for 24 hours followed by Cisplatin + Paclitaxel (50ng/ml + 8.5 ng /ml) for 72 hours
- c) Add 20µl of 5mg/ml of MTT solution to each well at the end of the incubation and incubate cell further for 2 hours under 5% CO<sup>2</sup> at 37°C.
- d) After two hours remove all media completely without disturbing the formazan crystals and dissolve crystals in 200µl of DMSO per well.
- e) Take optical density of solubilized formazan crystals at 560nm and 670nm.
- f) Determine percent cell viability using following formula,

$$\text{Percent cell viability} = \frac{\text{Test Absobance 560} - \text{Test Absobance 670}}{\text{Control Absobance 560} - \text{Control Absobance 670}} \times 100$$

#### 5.1.3.6 Soft agar colony formation assay

- a) Prewarm sterile 2X-cell culture media with 20% FBS at 37°C in water bath.

- b) Melt sterile 2% low melting agarose and keep it warm at 40°C in water bath.
- c) Mix equal amount of the 2X-cell sterile culture media with 20% FBS and sterile 2% low melting agarose.
- d) Coat 35mm culture dish with 1 ml of this mixture to form the bottom layer.
- e) Let the bottom layer solidify properly inside tissue culture hood for 40 minutes.
- f) Next trypsinize cells, make single cell suspension and determine viable cell count.
- g) Mix equal amount of the 2X-cell sterile culture media with 20% FBS and sterile 2% low melting agarose and add cells to this mixture at final concentration of 500cells/35mm dish. *Make sure that single cell suspension is achieved before pouring them. Seed control and test cells in triplicates.*
- h) Pour mixture containing cells on top of the bottom layer and let it solidify inside tissue culture hood for 40 minutes.
- i) Incubate soft agar plates under 5% CO<sup>2</sup> at 37°C.
- j) Every second day feed plates with 2-3 drops of the sterile 1X-media and monitor growth of the colonies.
- k) Count the number of colonies using compound microscope by using grid method. Also take multiple images of the colonies for determining average colony size.

#### 5.1.3.7 Spheroid formation assay

- a) Prepare sterile 10X-spheroid media with following composition and filter sterilize media using 0.2μ filter. Before use dilute 10X-spheroid with sterile incomplete media.

Stock concentration	Final concentration	10X-Spheroid media (10ml)
EGF (500ng/μl)	EGF (10ng/ml)	2μl
FGF(1000ng/μl)	FGF (20ng/ml)	2μl
Insulin (500ng/μl)	Insulin (10ng/ml)	2μl
LIF (100ng/μl)	LIF (10ng/ml)	10μl
Pen-Strep	Pen-Strep (1%)	100μl

- b) Prepare 24-well plates by coating them with sterile 1% agarose. Make sure the entire base gets properly coated with agarose.
- c) Let agarose layer solidify properly inside tissue culture hood for 40 minutes.
- d) Next trypsinize cells, make single cell suspension and determine viable cell count.
- e) Take required number of cells and resuspend them in sterile 1X-spheroid media such that final cell count is 2000cells/ml.

*Make sure that single cell suspension is achieved before pouring them. Seed control and test cells in triplicates.*

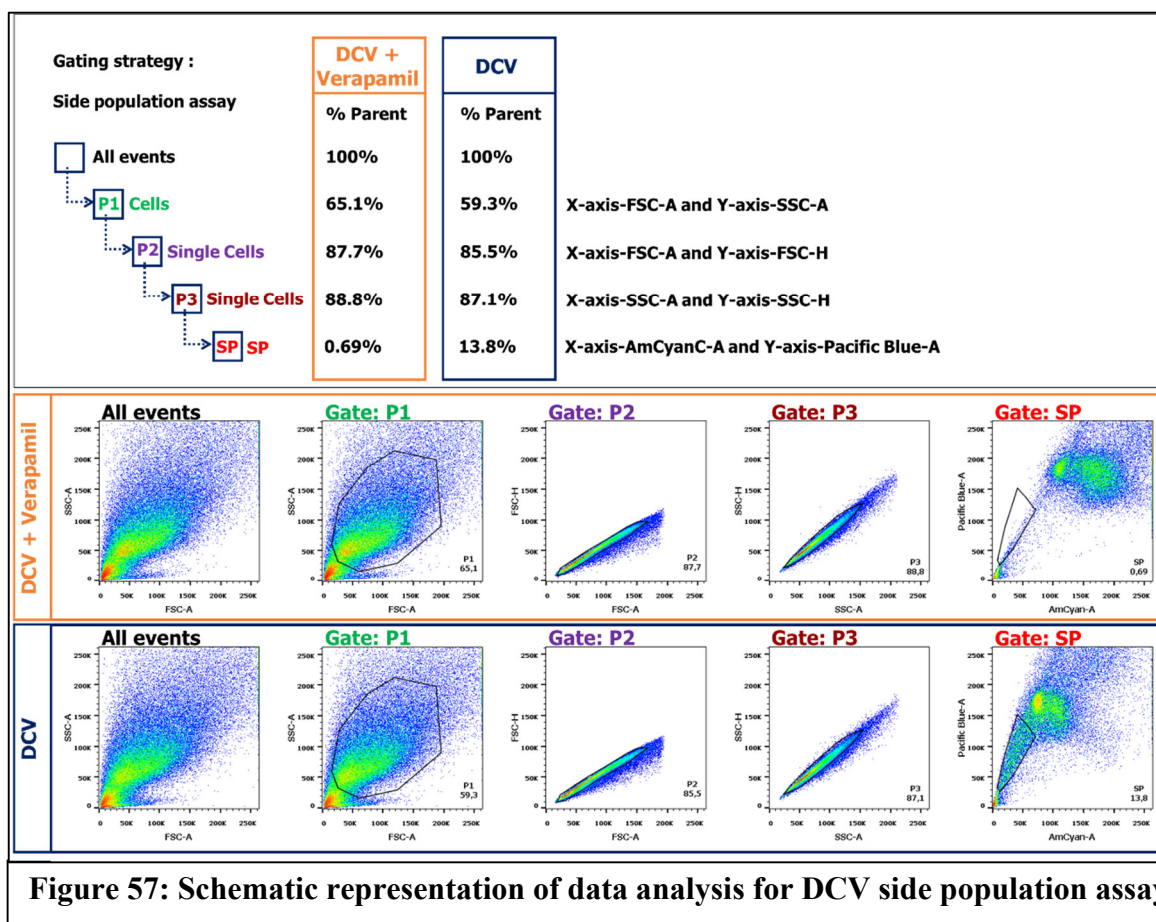
- f) Plate 1ml of above cell suspension per well in agarose coated 24-well plate in triplicates. Incubate plates under 5% CO<sub>2</sub> at 37°C.
- g) Feed spheroid plates after every 48 hours with sterile 10X-spheroid media such that final concentration becomes 1X. Monitor growth of the spheroids.
- h) Count number of spheroids using compound microscope by using grid method.
- i) To test self-renewal properties of cells spheroids must be serially passaged.
- j) Collect spheroids and centrifuge at 800rpm for 5 minutes at 4°C.
- k) Discard supernatant, resuspend spheroids in 200µl of sterile trypsin-EDTA and incubate for 2-3 minutes at 37°C.
- l) Neutralize trypsin by adding thrice the volume of sterile media containing FBS and centrifuge at 800rpm for 5 minutes at 4°C.
- m) Discard supernatant, resuspend in sterile PBS and centrifuge again at 800rpm for 5 minutes at 4°C.
- n) Resuspend cells in sterile spheroid media, make single cell suspension and determine viable cell count.
- o) Plate again the cells in agarose coated plates at density of 2000cells/well of 24-well plate as described previously and monitor the growth of the spheroids.

- p) Repeat assay for multiple passages to determine the maximum number of passages a cell can grow as spheroids.
- q) Count the number of spheroids at every passage.

#### 5.1.3.8 DyeCycle Violet side population assay

- a) DyeCycle Violet stain solution was used from Invitrogen (5mM-stock).
- b) Prepare Verapamil stock of 5mM in DMSO (Dissolve 1.23mg of Verapamil hydrochloride in 500 $\mu$ l of DMSO). Aliquot Verapamil stock (5mM), 50 $\mu$ l/tube and store at -20°C.
- c) Trypsinize cells, make single cell suspension and determine viable cell count.
- d) Resuspend cells in 1 ml of media as described below:
  - Verapamil control : 1-5x10<sup>6</sup> cells (DCV + Verapamil)
  - Test : 1-5x10<sup>6</sup> cells (DCV)
- e) Add 10 $\mu$ l of verapamil stock solution in control tube (final concentration 50 $\mu$ M) and incubate for 15 minutes at 37°C in water bath.
- f) After 15 minutes of incubation, add 1 $\mu$ l DyeCycle Violet stain solution (final concentration 5 $\mu$ M) to both the tubes (verapamil control and test) and incubate tubes for 90 minutes at 37°C in water bath in dark.
- g) Tap the tubes every 15 minutes.
- h) At the end of the incubation keep tubes on ice for 10 minutes and then centrifuge at 1000rpm for 5 minutes at 4°C.
- i) Discard the supernatant and resuspend cells in sterile PBS. Keep tubes on ice till acquired by flowcytometry.
- j) Analyse the acquired data as described below,
  - Gate cells (P1) in SSC-A Vs FSC-A scatter.

- Next identify single cell population first by FSC-H Vs FSC-A scatter in gate-P2 and then by SSC-H Vs SSC-A scatter in gate-P3.
- Finally identify the side population by Pacific Blue-A Vs AmCyanC-A scatter. Use Verapamil control to guide SP-gating.



### 5.1.3.9 Long term survival clonogenic assay

- Trypsinize cells, make single cell suspension and determine viable cell count.
- Seed 500cells/well in 6-well plates and incubate the plates under 5% CO<sup>2</sup> at 37°C.
- Next day treat cells with appropriate drugs for required time period.
- After drug treatment is done, remove drug containing media and add fresh media.
  - A2780 and OAW42 models Cisplatin + Paclitaxel (50ng/ml+8.5 ng/ml) for 24 hours

- A2780 and OAW42 models Ro5-3335 (A2780 = 200µM and OAW42 = 20µM) for 12 hours followed by Cisplatin + Paclitaxel (50ng/ml + 8.5 ng /ml) for 24 hours
- e) Incubate plates under 5% CO<sup>2</sup> at 37°C and observe the plates for colony formation. *Approximately till 7-10 days. Do not let the colonies merge.*
- f) At the end of the incubation wash plates once with PBS and fix carefully using pre-chilled fixative (90% methanol + 10% glacial acetic acid) at -20°C for 5 minutes.
- g) After 5 minutes remove the fixative and add staining solution (0.5% crystal violet in 90% methanol + 10% glacial acetic acid) to plates.
- h) Incubate plates in staining solution for 30-60minutes or till colonies get stained.
- i) Calculate the plating efficiency of control and treated cells using following formula,

$$\text{Plating efficiency} = \frac{\text{Number of colonies formed}}{\text{Number of cells seeded}} \times 100$$

- j) Calculate the surviving fraction using following formula,

$$\text{Surviving fraction} = \frac{\text{Plating efficiency of treated sample}}{\text{Plating efficiency of control sample}}$$

### 5.1.3.10 Preparation of lentilox virus particles

- a) One day prior to co-transfection seed 1X10<sup>6</sup> HEK293FT cells in a 60mm dish.
- b) Next day observe plate under microscope for uniform seeding and proceed further. If cells look like clumped at centre do not proceed.

*Uniform cell seeding is necessary for co-transfection.*

- c) Plasmids quantity required for co-transfection of one 60mm dish,

- VSVG : 2 µg
- PΔ : 4 µg
- pLL3.7-ShRNA : 6 µg

- d) Take required volume of plasmids in a 2ml sterile tube and make up the volume to 500µl using incomplete sterile media (media without FBS and antibiotics).

- e) In a second sterile 2ml tube take 30 $\mu$ l of Lipofectamine 2000 reagent and make up the volume to 500 $\mu$ l using incomplete sterile media (media without FBS and antibiotics).
- f) Incubate tubes at room temperature for 5 minutes. Later mix both the suspensions in 15ml sterile tube and incubate at 37°C for 20 minutes.
- g) At the end of incubation add 2ml of sterile complete media to the above mixture and mix gently twice.
- h) Remove spent media from cells to be transfected and add above 3ml mixture to cells carefully and incubate under 5% CO<sub>2</sub> at 37°C.
- i) Post 16-20 hours of transfection remove media containing transfection complex and feed fresh sterile complete media.
- j) Incubate plates under 5% CO<sub>2</sub> at 37°C for 48-60 hours. Daily observe cells for syncytia formation i.e. fusion of cells by observing GFP expression.  
*Syncytia is an indication of virus particle production.*
- k) Also observe media during 48-60 hours of incubation. Do not allow media to turn yellow as acidic pH may inactivate virus particles. If media looks exhausted add fresh 1-2ml of sterile complete media to on top of it gently.
- l) At the end of the 48-60 hours of incubation proceed to collect virus particles. Collect media into a 15 ml of sterile tube aseptically and discard cells.
- m) Centrifuge collected media at 2000 rpm for 10 minutes to pellet down cell debris. Next filter the supernatant through a 0.45 $\mu$  sterile syringe filter into a fresh tube.
- n) Ultra-centrifuge the 0.45 $\mu$  filtered supernatant at 30,000 rpm for 90 minutes at 4°C.  
*Acceleration: Full and Deceleration: No brake.*
- o) A white pellet will form. Discard the supernatant into hypo-chloride carefully without disturbing the pellet.

- p) Add fresh 0.5ml to 1.0ml of sterile complete media to pellet and gently tap such that pellet comes into media. *Do not pipette.*
- q) Keep tube for re-suspension of pellet at 4°C overnight. Next day use virus particles for transducing cells, if not using immediately aliquot the virus particles and store at -80°C.

### 5.1.3.11 Identification of viral titre

- a) Seed  $1 \times 10^5$  cells/well in a 12-well plate one day prior to the transduction.
- b) Dilute the viral stock in serial 2-fold dilutions as described below,

Serial dilution	Dilution factor	Serial dilution	Dilution factor
Neat	1	1:8	8
1:2	2	1:16	16
1:4	4	1:32	32

- c) Keep the final volume of all dilutions same.
- d) Determine the cell count of seeded cells before transduction with viral particles.
- e) Add diluted virus to the cells with 4µg/ml of polybrene and incubate cells under 5% CO<sub>2</sub> at 37°C for 48 hours.
- f) Post 48 hours of transduction analyse cells by flowcytometry for eGFP positive cells.
- g) Determine the viral titre for each dilution by formula,

*Viral transducing units (TU) per ml*

$$= \frac{\text{Number of cells transduced} \times \text{Percentage GFP positive cells}}{\text{Total volume of virus solution in ml} \times \text{Dilution factor}}$$

## 5.2 Bacterial culture

### 5.2.1 Reagents and chemicals

Sr. No.	Reagent name	Source
1	Luria-Bertani (LB) broth	HiMedia, India
2	Luria-Bertani (LB) agar	HiMedia, India
3	Yeast extract	HiMedia, India
4	Bactotryptone	HiMedia, India
5	Ampicillin	Sigma, USA
6	Kanamycin	Sigma, USA
7	Dimethyl sulfoxide (DMSO)	HiMedia, India
8	Sodium chloride	Qualigens, India
9	Potassium chloride	SDFCL, India
10	Magnesium sulphate	SRL, India
11	Magnesium chloride	HiMedia, India
12	4-(2-hydroxyethyl)-1-piperazineethanesulfonic acid (HEPES)	Sigma, USA
13	Calcium chloride	Sigma, USA
14	Manganese chloride	Sigma, USA
15	Potassium hydroxide	HiMedia, India
16	Glucose	HiMedia, India
17	Tris-Base	Sigma, USA
18	Sodium-EDTA	MP, India
19	NucleoSpin® Plasmid kit	Macherey-Nagel, Germany
20	Super optimal broth (SOB) media*	In-House
21	Transformation buffer (TB)**	In-House

\*SOB (100ml): 2g-bactotryptone, 0.5g-yeast extract, 50mg-Nal, 18.6mg-KCl. 1M- MgCl<sub>2</sub> (10 ml): 2.033g and 1M- MgSO<sub>4</sub> (10 ml): 2.465g. \*\*TB (120ml): 0.286g-HEPES (10mM), 0.265g-CaCl<sub>2</sub> (15mM), 2.237g-KCl (250mM). Dissolve all components and then adjust the pH to 6.7 using KOH, then add 1.306g-MnCl<sub>2</sub> (55mM) and make up the volume to 120ml.

### 5.2.2 Bacterial strains

Sr. No.	Bacterial strain	Source
1	Escherichia coli DH5 $\alpha$	ATCC
2	Escherichia coli stbale3	ATCC

### 5.2.3 Methods

All bacterial cultures were maintained aseptically in LB media with or without the antibiotics and incubated at 37°C for growth.

#### 5.2.3.1 Preparation of ultra-competent cells

- a) Prepare 100ml of SOB media\*, 1M-MgCl<sub>2</sub>\* and 1M-MgSO<sub>4</sub>\* separately one day prior and heat sterilize.
- b) Streak *E. coli DH5 $\alpha$*  or *E. coli stable3* on LB agar plate and incubate overnight at 37°C.
- c) Next day initiate starter culture by inoculating single colony from overnight grown plate in 1ml of LB broth and incubate for 4-6 hours in shaker incubator at 37°C and 200rpm.
- d) Add 1ml of each 1M-MgCl<sub>2</sub> and 1M-MgSO<sub>4</sub> to 100ml of SOB and pre-chill at 16°C.
- e) Inoculate pre-chilled SOB media (containing MgCl<sub>2</sub> and MgSO<sub>4</sub>) with 200 $\mu$ l of starter culture and incubate in shaker incubator at 16°C and 120rpm till optical density of culture reaches 0.4-0.5 at 600nm (approximately 48-60 hours).
- f) Prepare transformation buffer (TB)\*\* fresh the day which optical density reaches 0.4-0.5. Filter sterilize TB and pre-chill at 4°C before use.
- g) Pre-chill sterile 1.5ml micro-centrifuge tubes and 50ml centrifuge tubes. Now onwards all steps are performed on ice.
- h) Once optical density reaches 0.4-0.5 at 600nm, keep the flask on ice for 10 minutes.
- i) After 10 minutes transfer the bacterial culture to pre-chilled 50ml centrifuge tubes and centrifuge at 3000rpm for 10 mites at 4°C.

- j) Discard supernatant, resuspend pellet in pre-chilled TB and incubate on ice for 10 minutes.
- k) Centrifuge at 3000rpm for 10 minutes at 4°C. Discard the supernatant and resuspend the pellet in 1.86ml of pre-chilled TB.
- l) Add 0.14ml of DMSO to 1.86ml of culture and immediately transfer 100µl of this mixture to pre-chilled sterile 1.5ml micro-centrifuge tubes.
- m) Immediately snap freeze the culture containing micro-centrifuge tubes using liquid nitrogen. Store competent cells at -80°C. Check the competency using pUC19 vector.

### 5.2.3.2 Plasmid transformation into bacteria

- a) Thaw ultra-competent cells on ice and add 1-5ng of plasmid DNA<sup>@/##</sup> to it. Incubate on ice for 30 minutes.
- b) After 30 minutes give heat shock to above mixture at 42°C for 60 seconds and keep immediately on ice for 2 minutes.
- c) Add 900µl of SOC to above mixture and incubate for 1 hour in shaker incubator at 37°C and 200rpm.

*SOC: SOB + 1 mM Glucose*

- d) At the end of incubation dilute the 100µl of above transformed mixture<sup>@@/###</sup> 10 times and plate 100µl of diluted transformation mixture by spread plate method on LB agar containing appropriate antibiotic. Incubate plates overnight at 37°C.
- e) Modifications in bacterial transformation protocol for ligation and DpnI digested site-directed mutagenesis products.

- Ligation products:

*@Add 10-20µl of ligation product to competent cells for transformation.*

*@@Centrifuge the transformation mixture at 1500rpm for 5 minutes. Resuspend the pellet in 100µl of SOC and plate entire transformation mixture.*

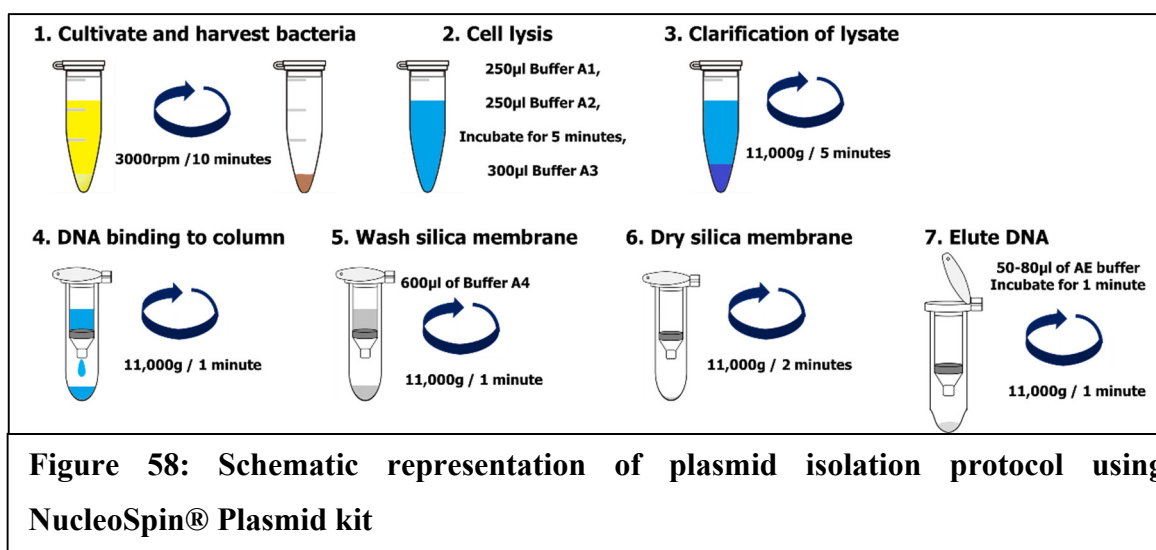
- DpnI digested site-directed mutagenesis products:

#Add 10 $\mu$ l of 1 DpnI digested site-directed mutagenesis products to competent cells for transformation.

##At the end of incubation plate undiluted 100-200 $\mu$ l of transformation mixture.

### 5.2.3.3 Isolation of plasmid DNA from bacteria

- Inoculate 5ml of sterile LB broth (containing appropriate antibiotic) with single colony from transformed bacteria and incubate for 12-16 hours in shaker incubator at 37°C and 200rpm.
- Centrifuge the overnight grown culture at 3000rpm for 10 minutes at 4°C. Discard the supernatant and use pellet to isolate plasmid DNA using NucleoSpin® Plasmid kit.
- Use the brief protocol describe below.



- Determine the purity and concentration of plasmid DNA by Nanodrop and store the plasmid DNA at -20°C.

## 5.3 Molecular cloning

### 5.3.1 Reagents and chemicals

Sr. No.	Reagent name	Source
1	Glacial acetic acid	Fischer Scientific, USA
2	Sodium-EDTA	MP, India
3	Tris base	Sigma, USA
4	Agarose	Sigma, USA
5	Ethidium bromide (EtBr)	Sigma, USA
6	6X DNA loading dye	NEB, USA
7	DNA markers: 100bp and 1kb DNA ladders	NEB, USA
8	NucleoSpin® Gel and PCR Clean-up kit	Macherey-Nagel, Germany
9	Restriction enzymes and buffers	NEB, USA
10	T4 DNA Ligase kit	NEB, USA
11	PrimeSTAR GXL DNA Polymerase	Clontech-Takara-Bio, USA
12	Tris acetate EDTA buffer (TAE)*	In-House

\*TAE buffer (1X-1L): 4.846g-Tris base (40mM), 1.21 ml- Glacial acetic (20mM), 0.372g-Sodium EDTA (1mM).

### 5.3.2 Methods

#### 5.3.2.1 DNA gel electrophoresis

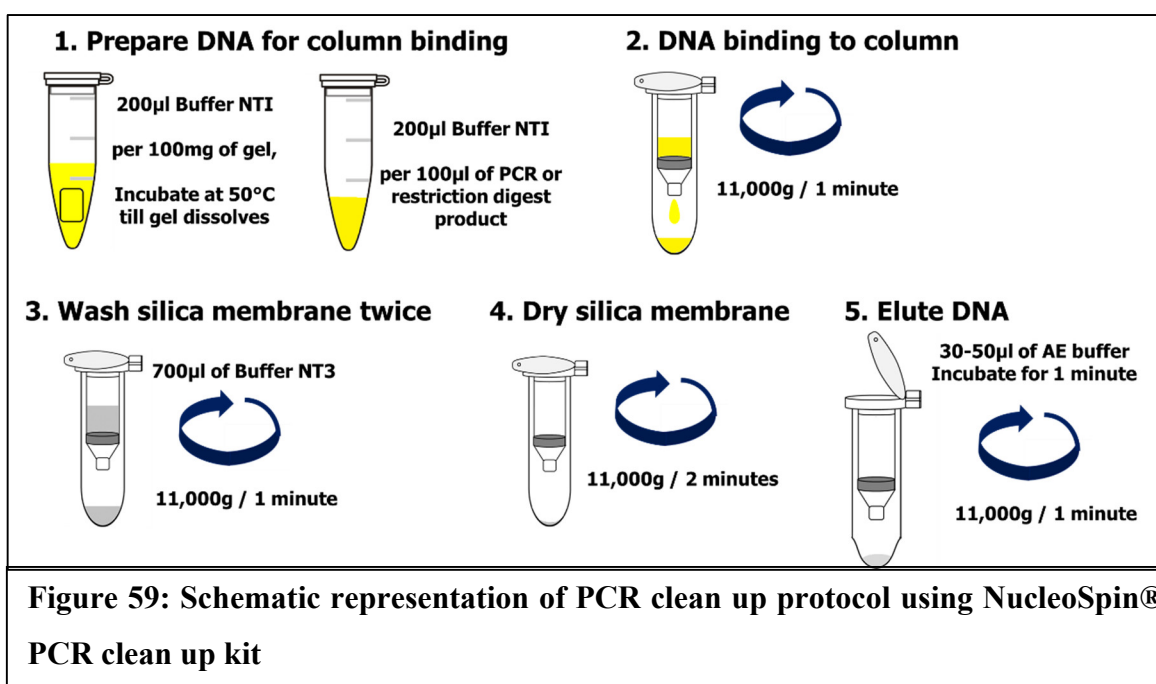
- a) Prepare agarose gel in 1X-TAE buffer according to the size of DNA to be resolved and downstream purpose. Add EtBr to molten agarose at final concentration of 0.2g/ml.

Agarose gel percentage	Range of effective separation (bp)
0.6-0.8	1,000-20,000
0.9-1.2	800-10,000
1.3-.15	300-7,000
1.6-2.0	100-3,000
2.0-3.0	25-1,000

- b) Transfer solidified agarose gel to electrophoresis tank and pour 1X-TAE buffer into electrophoresis tank. Wash the wells to remove residual agarose particles by pipetting.
- c) Mix the DNA samples such as PCR product and restriction digestion reactions with 6X-DNA loading dye and load the samples in gel along with appropriate DNA ladder.
- d) Run the samples at 60-80V till desired separation of DNA bands is achieved.
- e) Visualize and document the separated DNA bands using UV-gel documentation system.

### 5.3.2.2 DNA purification from gel, PCR product and restriction digestion reactions

- a) Cut the desired DNA fragment from agarose gel using clean scalpel under UV-illuminator. Use personal protective equipment.
- b) Collect the agarose piece containing DNA fragment in microfuge tube and determine the weight of the agarose piece.
- c) Purify DNA from gel, PCR and restriction digestion reactions using NucleoSpin® Gel and PCR Clean-up kit as per manufacturer's instructions.
- d) Use the brief protocol describe below.



- e) Determine the purity and concentration of purified DNA by Nanodrop and store the DNA at -20°C.

### 5.3.2.3 Restriction digestion

- a) Select appropriate restriction enzymes with compatible sites within both vector backbone plasmid and vector containing the insert DNA.
- b) Use NEBcloner (<http://nebcloner.neb.com/#!/redigest>) tool to determine the buffer system compatible for optimal functionality of restriction enzymes.
- c) Set restriction digestion as described below,

Component	50µl reaction
Plasmid DNA / PCR amplified DNA	1µg
10X-NEB restriction buffer	5µl (1X)
Restriction enzyme 1	10 units / 1µg of DNA
Restriction enzyme 2 ( <i>if required</i> )	10 units / 1µg of DNA
Nuclease free water	Make up the volume to 50µl

*Total amount of enzymes should be less than 10% of total reaction volume.*

- d) Incubate the reaction mixture at 37°C water bath for 16-20 hours.
- e) Analyze the restriction digestion by DNA gel electrophoresis.

### 5.3.2.4 Ligation

- a) Purify the vector backbone plasmid and insert DNA by NucleoSpin® Gel and PCR Clean-up kit
- b) Determine the purity and concentration of vector and insert plasmid DNA by Nanodrop.
- c) Set ligation reaction as described below, one test (vector + insert) and second vector control (only vector DNA). Use vector and insert DNA in 1:3 ratio.

Component	20µl reaction
Vector Plasmid DNA	50-100 ng
Insert plasmid DNA	150-300 ng
10X-NEB T4 DNA ligase buffer	2µl (1X)
T4 DNA Ligase enzyme	1µl
Nuclease free water	Make up the volume to 20µl

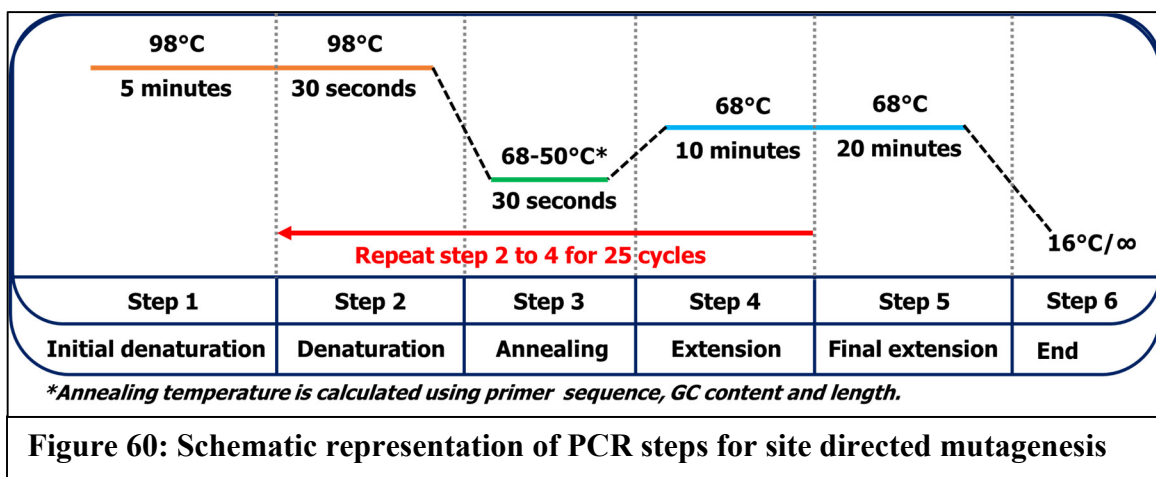
- d) Incubate the reaction mixture at 16°C water bath for 16-20 hours.
- e) Transform the ligation mixtures as described above. Screen the colonies using appropriate screening strategy. Verify the positive clone by restriction digestion and sanger sequencing.

### 5.3.2.5 Site directed mutagenesis

- a) Design mutagenesis primers, both forward and reverse with desired mutation approximately at centre of both primers.
- b) Set up SDM reaction as described below,

Component	50µl reaction
Plasmid DNA template	125 ng
Forward mutagenesis primer	125 ng
Reverse mutagenesis primer	125 ng
2.5 mM dNTPs mix	4µl (200µM each)
5X-Primestar GXL buffer	10µl (1X)
Primestar GXL enzyme (high fidelity)	1µl (1.25 units)
Nuclease free water	Make up the volume to 50µl

- c) Put the reaction in PCR machine and run the reactions as described below.



- d) Digest the original plasmid (used as template) and SDM-PCR product with DpnI restriction enzyme as described previously.

*DpnI endonuclease cuts the methylated and hemi-methylated DNA (5'-Gm6ATC-3'), thus will fragmentize the original plasmid (used as template) leaving behind only the newly synthesized plasmid with desired mutation.*

- e) Transform the ligation mixtures as described above. Isolate 5-10 colonies, grow them in LB broth and isolate plasmid DNA.
- f) Screen the colonies by Sanger sequencing for positive clones harbouring desired mutation.

**Table 4: List of SDM primers**

Primer Name	Sequence
FOXO3a Site 1 SDM For	CTGTTGTTGGGGGCAATGAACCTCTCCCAGCCC
FOXO3a Site 1 SDM Rev	TCATTGCCCCCAACAACAGAATTCCAAGATCTCCC
FOXO3a Site 2 SDM For	GGCTCTTGGGGACCAGCATTAACTCCGCTGA
FOXO3a Site 2 SDM Rev	TGCTGGTCCCCAAGAGCCCCAGCCTCG

## 5.4 Real time quantification of gene transcripts

### 5.4.1 Reagents and chemicals

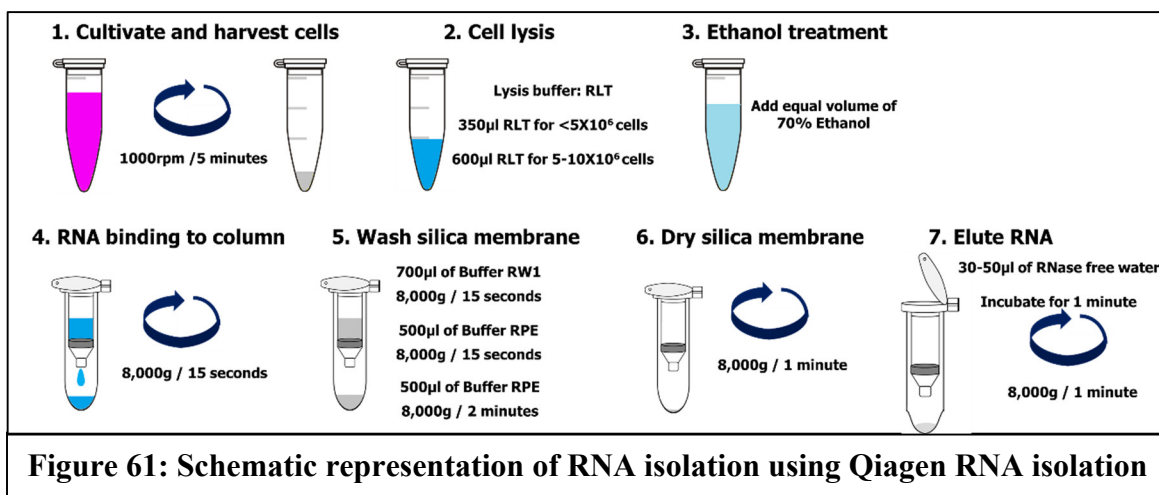
Sr. No.	Reagent name	Source
1	RNeasy total RNA isolation mini kit	Qiagen, Germany
2	SuperScript™ First-Strand cDNA Synthesis kit	Invitrogen, UK
3	PowerUp SYBR Green	Applied Biosystems, USA
4	Ethanol	Sigma, USA
5	Diethyl pyrocarbonate (DEPEC)	Sigma, USA
6	Sodium acetate	SRL, India
7	Sodium-EDTA	MP, India
8	Formaldehyde	Merck, India
9	Formamide	Sigma, USA
10	Ethidium bromide	Sigma, USA
11	6X-RNA loading dye	Sigma, USA
12	Agarose	Sigma, USA
13	3-(N-morpholino) propanesulfonic acid (MOPS) buffer*	In-House
14	Denaturation mix**	In-House
15	Gene specific primers	Sigma, India

\* MOPS buffer (1X-1L): 4.186g-MOPS (20mM), 0.411g-Sodium acetate (5mM), 0.372g-Sodium EDTA (1mM), adjust pH to 7.0 using NaOH. \*\*Denaturation mix (100µl): 13µl-37% Formaldehyde, 22µl-Formamide and, 65µl-10X-MOPS buffer.

### 5.4.2 Methods

#### 5.4.2.1 RNA isolation

- Trypsinize the cells, wash once with ice-cold PBS and centrifuge at 1000rpm for 5 minutes at 4°C.
- Discard the supernatant and use cell palette to isolate total RNA from cells using RNeasy mini kit following the brief protocol described below.



- c) Determine purity and concentration of purified RNA by Nanodrop and store at  $-80^{\circ}\text{C}$ .
- d) Prepare denaturing RNA gel<sup>@</sup> for checking quality of RNA.

<sup>@</sup>RNA gel: 0.32g-Agarose, 4ml-10X-MOPS buffer and 36ml DEPEC-ddH<sub>2</sub>O. Dissolve in microwave. Slowly add 0.72ml of 37%-Formaldehyde and 1-2µl of EtBr.

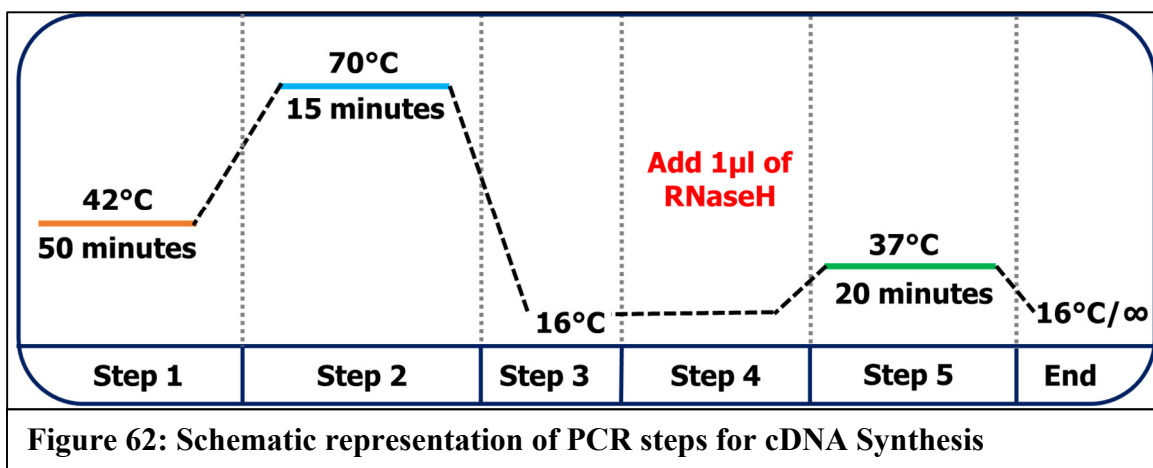
- e) Mix 1µg of RNA with 5µl of denaturation mix, 2µl of 6X-RNA loading dye and make the volume to 12µl with RNase free water.
- f) Heat the above mixture at  $65^{\circ}\text{C}$  for 10 minutes and load immediately on RNA gel.
- g) Run the gel at 60V for 30-45 minutes. Visualize and document the separated RNA bands using UV-gel documentation system.

#### 5.4.2.2 cDNA synthesis

- a) Prepare cDNA from total RNA using SuperScript™ First-Strand cDNA Synthesis kit.
- b) Prepare two reactions as described below,

Reaction 1		Reaction 2	
Component	Volume	Component	Volume
Total RNA (2µg)	(X) µl	10X-RT buffer	2 µl
10mM dNTP	1 µl	25 mM MgCl <sub>2</sub>	4 µl
Random hexamer primers	1 µl	0.1M DTT	2 µl
RNase free water	(X-8) µl	RNase OUT (40U/µl)	1
Total Volume	10 µl	Total Volume	9 µl

- c) Heat reaction 1 at 65°C for 5 minutes and then keep on ice for 1 minute.
- d) Mix reaction 1 and 2 and incubate at room temperature for 2 minutes.
- e) Add 1µl of SuperScript™II RT and incubate at room temperature for 10 minutes.
- f) Put the above mixture into PCR machine as described below.



- g) Store the cDNA at -20°C.

#### 5.4.2.3 Real time polymerase chain reaction assay

- a) Dilute the cDNA 1:10 using ddH<sub>2</sub>O and use diluted cDNA for real time PCR.
- b) Prepare real time PCR reaction as described below, one sample for each gene is set in triplicates on ice. No template control (NTC) for each gene is also set in triplicates.

One reaction		One gene/One sample (6+1 reactions= 3-sample and 3-NTC)	
Component	Volume	Component	Volume
ddH <sub>2</sub> O	2 µl	ddH <sub>2</sub> O	14 µl
2X-PowerUp SYBR Green	5 µl	2X-PowerUp SYBR Green	35 µl
5-pmol Forward primer	1 µl	5-pmol Forward primer	7 µl
5-pmol Forward primer	1 µl	5-pmol Forward primer	7 µl
1:10-Diluted cDNA	1 µl	1:10-Diluted cDNA	---
Total Volume	10 µl	Total Volume	63 µl

- c) Mix reaction mixture properly and distribute 31.5µl of above mixture into two different tubes.
- d) Add 3.5µl of 1:10-diluted cDNA to sample tube and 3.5µl of ddH<sub>2</sub>O in NTC tube.
- e) Distribute 10µl of both (sample and NTC) in triplicates in 384-well optical plate and run the PCR using comparative delta-Ct ( $\Delta$ -Ct) method.

#### 5.4.2.4 Data analysis

- a) Relative expression of target genes was estimated by  $\Delta$ -Ct method using GAPDH as normalisation control.
- b) Relative gene expression

$$\Delta Ct = Ct \text{ of gene} - Ct \text{ of GAPDH}$$

$$\text{Relative gene expression} = 2^{-\Delta Ct}$$

- c) Fold change

$$\Delta\Delta Ct = \Delta Ct \text{ of Control} - \Delta Ct \text{ of Test}$$

$$\text{Fold change} = 2^{-\Delta\Delta Ct}$$

**Table 5: List of real time primers**

Primer Name	Sequence
IGF1R Forward	CTGGACTCAGTACGCCGTTT
IGF1R Reverse	GGAAGTGAAGCATTGGTGCG
GAPDH Forward	TGCACCACCAACTGCTTAGC
GAPDH Reverse	GGCATGGACTGTGGTCATGAG
CBF $\beta$ Forward	GAGCCGCGAGTGTGAGATTA
CBF $\beta$ Reverse	GCCACAAAAGCGATTTCCGA

RUNX1 Forward	CAGGTTTGTCGGTCGAAGTG
RUNX1 Reverse	CCGATGTCTTCGAGGTTCTC
RUNX2 Forward	AGATGACATCCCCATCCATC
RUNX2 Reverse	GTGAGGGATGAAATGCTTGG
RUNX3 Forward	GCCGGCAATGATGAGAACTA
RUNX3 Reverse	AGGCCTTGGTCTGGTCTTCTAT
OCT4 Forward	GTGGAGAGCAACTCCGATG
OCT4 Reverse	TGCAGAGCTTTGATGTCCTG
SOX2 Forward	AACCCCAAGATGCACAACCTC
SOX2 Reverse	GCTTAGCCTCGTCGATGAAC
NANOG Forward	AAAGCTTGCCTTGCTTTGAA
NANOG Reverse	AAGTGGGTTGTTTGCCTTTG

## 5.5 Nuclear-Cytoplasmic fractionation

### 5.5.1 Reagents and chemicals

Sr. No.	Reagent name	Source
1	4-(2-hydroxyethyl)-1-piperazineethanesulfonic acid (HEPES)	Sigma, USA
2	Potassium chloride	Sigma, USA
3	Sodium chloride	Qualigens, India
4	Sodium-EDTA	MP, India
5	Glycerol	SDFCL, India
6	Nonidet P-40 (NP-40)	Sigma, USA
7	100X-Protease inhibitor cocktail	Sigma, USA
8	Sodium orthovanadate	Sigma, USA
9	Sodium fluoride	Sigma, USA

### 5.5.2 Buffers

Sr. No.	Buffer name and compositions
1	Cytoplasmic extraction (CE) buffer, <i>10m HEPES pH7.9, 10mM KCl and 0.1mM Na-EDTA.</i>
2	Cytoplasmic extraction (NE) buffer, <i>20mM HEPES pH7.9, 420mM NaKCl, 1mM Na-EDTA and 20%-Glycerol.</i>
3	10% NP-40 solution

### 5.5.3 Methods

- a) Trypsinize cells, wash once with ice cold PBS and centrifuge at 1000rpm at 4°C for 5 minutes. Discard the supernatant.
- b) Resuspend the cells in ice-cold CE-buffer five-times the volume of cell pellet and incubate on ice for 20-30 minutes (with gentle tapping in-between).
- c) At the end of incubation add protease inhibitor cocktail (final concentration-1X), Sodium orthovanadate (final concentration-1mM) and 5mM-Sodium fluoride (final concentration-5mM) to above mixture.

- d) Next add NP-40 to above mixture at final concentration of 0.3% and vortex with medium agitation for 5 seconds 3-5 times.
- e) Centrifuge at 5000-6000rpm at 4°C for 20 minutes. Carefully collect the supernatant as cytoplasmic lysate.
- f) Resuspend the nuclear pellet in 1ml of ice-cold CE-buffer, centrifuge at 5000-6000rpm at 4°C for 10 minutes and discard the supernatant. Repeat the washing of nuclear pellet 3-5 times with ice-cold CE-buffer.
- g) Further resuspend the nuclear pellet in equal volume of ice-cold NE-buffer (containing 1X-protease inhibitor cocktail, 1mM-Sodium orthovanadate and 5mM-Sodium fluoride), vortex rigorously for 5 seconds 3-5 times and incubate on ice for 20-30 minutes (with rigorous vortexing in-between).
- h) If necessary, sonicate the cell lysates (both cytoplasmic and nuclear lysates) using water cooled sonicator (Biorupter) at high amplitude for 6-10 cycles of 30-seconds-on/30-seconds-off.
- i) Centrifuge the lysates at 14000rpm for 30 minutes at 4°C. Collect the supernatant as cell lysates (cytoplasmic and nuclear) for further use. Always keep the lysates on ice. Aliquot the lysates and store at -20/-80°C.
- j) Check the purity of lysates (cytoplasmic and nuclear) for cross-contamination by western blotting.

## 5.6 Western blot

### 5.6.1 Reagents and chemicals

Sr. No.	Reagent name	Source
1	Bradford reagent	Sigma, USA
2	Tris-base	Sigma, USA
3	Sodium dodecyl sulphate (SDS)	Sigma, USA
4	$\beta$ -mercaptoethanol	Sigma, USA
5	100X-Protease inhibitor cocktail	Sigma, USA
6	Sodium orthovanadate	Sigma, USA
7	Sodium fluoride	Sigma, USA
8	Sodium chloride	Sigma, USA
9	Sodium EDTA	Sigma, USA
10	Sodium deoxycholate	HiMedia, India
11	Nonidet P-40 (NP-40)	MP, India
12	Triton-X-100	Sigma, USA
13	Acrylamide	Sigma, USA
14	Bis-acrylamide	Sigma, USA
15	Ammonium persulfate	Sigma, USA
16	Tetramethylethylenediamine (TEMED)	Sigma, USA
17	Pre-stained protein ladder	Sigma, USA
18	Methanol	Sigma, USA
19	Polyvinylidene difluoride (PVDF) membrane	Pall, USA
20	Bovine serum albumin (BSA)	HiMedia, India
21	Skimmed non-fat milk	Qualigens, India
22	Tween 20	Sigma, USA
23	Enhanced chemiluminescent substrate	Takara-Bio, USA
24	Primary antibodies	CST, Sigma, Abcam, Novus Biologicals
25	Horseradish peroxidase (HRP)-conjugated secondary antibodies	Sigma, USA

### 5.6.2 Buffers

Sr. No.	Buffer name and compositions
1	Radio immunoprecipitation assay (RIPA) buffer, 50mM Tris-HCl pH 8.0, 150mM NaCl, 1% Nonident P-40 or 1% Triton-X100, 0.5% Sodium deoxycholate and 0.1% SDS.
2	Laemmli buffer, 62.5mM Tris-HCl pH 6.8, 2% SDS, 10% Glycerol and 5% $\beta$ -mercaptoethanol.
3	Resolving gel buffer, 1.5 M Tris-HCl, pH 8.8.
4	Stacking gel buffer, 0.5 M Tris-HCl, pH 6.8.
5	5X-Protein loading buffer, 312.5mM Tris-HCl pH 6.8, 10% SDS, 50% Glycerol, 0.01% Bromophenol blue and 25% $\beta$ -mercaptoethanol.
6	Gel running buffer, 25mM Tris base, 190mM Glycine and 0.1% SDS.
7	30% Acryl amide mix, 29g Acryamide + 1g of Bis-acrylamide in 100ml double distilled water.
8	Transfer buffer*, 48mM Tris, 39mM glycine, 0.04% SDS and 20% methanol.
9	Tris-buffered saline (TBS), 20mM Tris, 150mM NaCl, pH 7.4.
10	Wash buffer (TBST), TBS with 0.1% Tween 20.
11	Blocking buffer, 5% BSA or 5% Skimmed-non-fat milk in TBST.
12	Stripping buffer, 62.5mM Trsi, 2% SDS and 0.8%- $\beta$ -mercaptoethanol.

\*Add methanol to transfer buffer just before use.

### 5.6.3 Methods

#### 5.6.3.1 Lysate preparation for western blotting

- Trypsinize cells, wash once with PBS and centrifuge at 1000rpm at 4°C for 5 minutes.
- Discard the supernatant and add required amount of the cell lysis buffer (RIPA buffer/ Laemmli buffer) with 1X-protease inhibitor cocktail, 1mM-Sodium orthovanadate and 5mM-Sodium fluoride, to cell palette and resuspend cells in lysis buffer.
- Incubate cells on ice resuspended in RIPA buffer for 30 minutes or at 37°C for 5 minutes for cells resuspended in Laemmli buffer.

- d) Sonicate the cell lysates using water cooled sonicator (Biorupter) at high amplitude for 6-10 cycles of 30-seconds-on/30-seconds-off.
- e) Centrifuge lysates at 14000rpm for 30 minutes at 4°C. Collect supernatant as cell lysates for further use. Always keep lysates on ice. Aliquot the lysates and store at -20/-80°C.
- f) Dilute the lysates 1:10 in PBS for protein estimation by Bradford reagent method.
- g) Add 5µl of diluted protein lysates in triplicates to 250µl of Bradford reagent in 96-well plate and mix well. Use 1:10 diluted lysis buffer for background absorbance.
- h) Measure absorbance at 595nm using plate reader. Estimate protein concentration using standard curve based on BSA. Calculate protein concentration using formula,

$$\text{Protein } (\mu\text{g}/\mu\text{l}) = \frac{\text{Absorbance} + y \text{ intercept of standrad curve}}{\text{slope of standard curve}} \times \text{Dilution factor}$$

- i) Mix 30-60µg of protein lysates with 5X-loading buffer (final concentration 1X) and heat lysates at 95°C for 5 minutes. Cool the lysates at RT and use for loading on gel.

### 5.6.3.2 Reducing-denaturing PAGE electrophoresis

- a) Prepare appropriate percentage of reducing poly-acrylamide gel for western blot as described below.

Resolving gel composition		Stacking gel composition	
Component	Volume	Component	Volume
Double distilled water	(4.41-X) ml	Double distilled water	1.21 ml
30% acryl amide mix	X ml	30% acryl amide mix	0.26 ml
Resolving gel buffer	1.5 ml	Stacking gel buffer	0.5 ml
10% SDS	60 µl	10% SDS	20 µl
10%-APS	30 µl	10%-APS	10 µl
TEMED	3 µl	TEMED	2 µl
Final volume	6 ml	Final volume	2 ml

Selection of gel percentage for protein of interest	
Protein size (kDa)	Gel percentage
10-60	12%
30-70	10%
40-120	8%

- b) Mount the gel in vertical gel electrophoretic apparatus and wash the wells of gel gently to remove any gel particles left inside wells.
- c) Load prepared samples into gel and run at 60V in stacking and at 80V in resolving.

#### 5.6.3.3 Semidry transfer of proteins to PVDF membrane

- a) Once gel run is complete, remove gel from electrophoretic apparatus and soak in pre-chilled transfer buffer (\*Add methanol to transfer buffer just before use) for 10 minutes.
- b) Soak the blotting pads with pre-chilled transfer buffer.
- c) Activate PVDF membrane by soaking it in 100% methanol for 60 seconds, wash with double distilled water thrice each for 60 seconds and soak in transfer buffer.
- d) Place two pre-soaked blotting pads in semi-dry transfer assembly and place activated PVDF membrane on them.
- e) Next place the gel on top of activated PVDF membrane. Make sure there are no air bubbles between PVDF membrane and gel. Again, place two pre-soaked blotting pads no top of PVDF membrane and gel.
- f) Close the apparatus and run transfer at 13-15V and 400mA for 30-60 minutes.

#### 5.6.3.4 Immuno probing of blots

- a) Once transfer is complete place the blotting pads containing PVDF membrane and gel in double distilled water to remove gel from PVDF membrane.
- b) Wash the blot thrice with TBST for 5 minutes and block the blot using appropriate blocking buffer for 60 minutes.

- c) At the end of the blocking, incubate blot with primary antibody for 16 hours at 4°C.
- d) Next wash the blot thrice with TBST for 10 minutes and incubate with HRP-conjugated secondary antibody for 2 hours at room temperature.
- e) At the end of incubation with secondary antibody again wash the blot thrice with TBST for 10 minutes and proceed for developing the blot.
- f) Add enhanced chemiluminescent substrate on blot and capture the chemiluminescence either by X-ray film or by gel documentation system.

### 5.6.3.5 Re- Immuno probing of blots

- a) To re-probe the blots with new antibody strip the blot of previously probed antibody by washing the blot in stripping buffer for 20 minutes.
- b) After stripping wash the blot five to six times with TBST for 10 minutes.
- c) Block the blot with blocking buffer and re-probe the blot with new antibody as described above.

**Table 6: List of antibody dilutions for western blot**

Antibody	Blocking	Dilution	Antibody	Blocking	Dilution
IGF1R	5% BSA	1:1000	Total ERK1/2	5% BSA	1:2000
RUNX1	5% Milk	1:2000	BCL2	5% BSA	1:1000
FOXO3a	5% Milk	1:2000	BCL-XL	5% BSA	1:1000
pS473-AKT	5% BSA	1:2000	BAD	5% BSA	1:1000
Total AKT	5% BSA	1:2000	Cleaved PARP	5% BSA	1:1000
pT202/Y204- ERK1/2	5% BSA	1:2000	pS253- FOXO3a	5% BSA	1:1000
$\alpha$ -Tubulin	5% BSA	1:2000	Lamin A/C	5% BSA	1:1000

## 5.7 Immunofluorescence

### 5.7.1 Reagents and chemicals

Sr. No.	Reagent name	Source
1	Paraformaldehyde	Sigma, USA
2	Methanol	Qualigens, India
3	Triton-X-100	Sigma, USA
4	Bovine serum albumin (BSA)	HiMedia, India
5	4',6-diamidino-2-phenylindole (DAPI)	Sigma, USA
6	Vectashield mounting medium	Vector Laboratories, USA
7	Primary antibodies	CST, Sigma, Abcam, Novus Biologicals
8	Fluorophore-conjugated secondary antibodies	Thermo Fischer Scientific, USA

### 5.7.2 Buffers

Sr. No.	Buffer name and compositions
1	Fixative, 4% Paraformaldehyde in PBS or 100% Methanol.
2	Permeabilization buffer, 0.1% Triton-X-100 in 4% paraformaldehyde.
3	Blocking buffer, 3% BSA.
4	Nuclear stain, 1mg/ml DAPI stock solution.

### 5.7.3 Methods

#### 5.7.3.1 Cell seeding

- a) Trypsinize cells, wash once with PBS and seed  $3-5 \times 10^4$  cells on sterile coverslip and incubate under 5% CO<sub>2</sub> at 37°C.
- b) Treat the cells if any drug treatment is to be given. Keep one coverslip for secondary antibody control.

#### 5.7.3.2 Immunostaining

- a) Remove media from coverslips and wash twice with PBS.

- b) Fix the cells with 4%-PFA for 10 minutes at 37°C or with pre-chilled 100%-Methanol for 2-3 minutes at -20°C.
- c) If necessary permeabilize the cells with permeabilization buffer for 5-10 minutes at room temperature
- d) Wash thrice with PBS after fixation and block coverslips using 3%-BSA for 30 minutes.
- e) After blocking incubate the coverslips with primary antibody (diluted in appropriate blocking buffer) for 16 hours at 4°C.

*Do not add primary antibody in secondary antibody control coverslip. Instead add blocking buffer.*

- g) Next day wash coverslips thrice with PBS for 5 minutes and incubate with fluorophore-conjugated secondary antibody (diluted in PBS or 3%-BSA) for 2 hours at room temperature in dark.
- h) At the end of incubation with secondary antibody again wash thrice with PBS for 5 minutes and stain the coverslips with nuclear stain DAPI for 5-10 seconds.
- i) Immediately wash again thrice with PBS for 5 minutes.
- f) Mount the coverslips using vectashield mounting medium and capture images using Carl Zeiss LSM780 microscope.
- g) Analyse the images using ImageJ software.

**Table 7: List of antibody dilutions for immunofluorescence**

Antibody	Fixation	Dilution	Antibody	Fixation	Dilution
IGF1R	Methanol	1:100	pS253-FOXO3a	4%PFA	1:100
RUNX1	4%PFA-Permeabilize	1:200	pS413-FOXO3a	4%PFA	1:100
FOXO3a	4%PFA-Permeabilize	1:200	pS473-AKT	4%PFA	1:200

## 5.8 Promoter binding transcription factor (TF) profiling array

### 5.8.1 Reagents and chemicals

Sr. No.	Reagent name	Source
1	TF Activation Profiling Plate Array II	Signosis
2	Cytoplasmic extraction buffer	In-house
3	Nuclear extraction buffer	In-house
4	100X-Protease inhibitor cocktail	Sigma, USA
5	Sodium orthovanadate	Sigma, USA
6	Sodium fluoride	Sigma, USA

### 5.8.2 Methods

#### 5.8.2.1 Nuclear lysate preparation

- a) Isolate nuclear lysates from cells using nuclear-cytoplasmic fractionation protocol described previously (section 1.5).
- b) Estimate protein concentration and check purity of nuclear lysates for contamination from cytoplasmic lysates by western blotting (section 1.3.2.2 and 1.6).

#### 5.8.2.2 Promoter fragment preparation

- a) Isolate promoter fragment of interest either by PCR amplification or restriction digestion, purify the promoter fragment by column purification as described previously.
- b) Determine the concentration of purified promoter fragment and check purity by DNA gel electrophoresis.

#### 5.8.2.3 Reagent preparation before starting

- a) Keep filter binding buffer and filter wash buffer on ice.
- b) Warm up plate hybridization and hybridization wash buffer at 42°C before use.
- c) Dilute 30ml of 5X plate hybridization wash buffer with 120 ml of ddH<sub>2</sub>O before use.
- d) Dilute 40ml of 5X detection wash buffer with 160 ml of ddH<sub>2</sub>O before use.

- e) Dilute 500 times of streptavidin-HRP with blocking buffer before use.

#### 5.8.2.4 Transcription factor and promoter DNA complex formation

- a) Mix the following components for each reaction in two different tubes,

Reagent	Volume	
	Control	Promoter competition
Transcription factor binding buffer mix	15 $\mu$ l	15 $\mu$ l
Transcription factor Probe mix	5 $\mu$ l	5 $\mu$ l
Promoter PCR fragment (0.1-0.5 $\mu$ M)	N/A	2-5 $\mu$ l
Nuclear extract (5 $\mu$ g-15 $\mu$ g)	X $\mu$ l	X $\mu$ l
ddH <sub>2</sub> O	Y $\mu$ l	Y $\mu$ l
Total volume	30 $\mu$ l	30 $\mu$ l

- b) Incubation at room temperature (20-23°C) for 30 minutes.

#### 5.8.2.5 Separation of TF-promoter DNA complex from free probes

- a) Equilibrate the isolation column by adding 200 $\mu$ l cold filter binding buffer, and centrifuge at 6000rpm for 1 minute at room temperature.
- b) Transfer the 30 $\mu$ l reaction mix directly onto the centre of the isolation column. Incubate on ice for 30 minutes.

*Don't incubate longer than 30 minutes, which results in high background.*

- c) Add 500 $\mu$ l cold filter wash buffer to the column, and incubate for 2-3 minutes on ice.
- d) Centrifuge at 6000rpm for 1 minute at 4°C, and discard the flow through.
- e) Wash the column by adding 500 $\mu$ l cold filter wash buffer to the column on ice.
- f) Centrifuge for 1 minute at 6000rpm at 4°C, and discard the flow through.
- g) Repeat the step e-f for additional 3-time washes.

#### 5.8.2.6 Elution of bound probes

- a) Add 100 $\mu$ l of Elution buffer onto the centre of column, and incubate at room temperature for 5 minutes.

- b) Put the column on a 1.5 ml microcentrifuge tube, and centrifuge at 10,000 rpm for 2 minutes at room temperature.
- c) Chill 500µl ddH<sub>2</sub>O in a 1.5ml microcentrifuge tube on ice for at least 10 minutes and keep on ice.
- d) Transfer eluted probe to a PCR tube and denature eluted probes at 98°C for 5 minutes.
- e) Immediately transfer the denatured probes to the chilled ddH<sub>2</sub>O and place on ice.
- f) The samples are ready for hybridization or store -20°C for the future use (the probe must be denatured again before use if frozen down).

#### **5.8.2.7 Hybridization of eluted probes with hybridization plate**

- a) Remove the sealing film from the plate.
- b) Add 10 ml warmed hybridization buffer to a dispensing reservoir (DNase free) and then add 600µl denatured probes. Mix them together by gently shaking the reservoir.
- c) Dispensing 100µl of the mixture into the corresponding wells immediately.
- d) Seal the wells with foil film securely and hybridize at 42°C overnight.

#### **5.8.2.8 Detection of hybridized probes**

- a) Remove the foil film and discard the contents of each well.
- b) Wash the plate 3-times by adding 200µl of pre-warmed 1X-plate hybridization wash buffer to each well. At each wash, incubate the plate for 5 minutes with gently shaking at room temperature.
- c) Complete removal of liquid at each wash by firmly tapping plate against paper towels.
- d) Add 200µl of blocking buffer to each well and incubate for 15 minutes at room temperature with gently shaking.
- e) Invert the plate over an appropriate container to remove blocking buffer.
- f) Add 40µl of streptavidin-HRP conjugate in 20ml blocking buffer (1:500) dilution, enough for two plates.

- g) Add 95µl of diluted streptavidin-HRP conjugate to each well and incubate for 45 min at room temperature with gently shaking.
- h) Wash the plate 3 times by adding 200µl 1X detection wash buffer to each well. At each wash, incubate the plate for 10 minutes gently shaking at room temperature.
- i) Completely remove liquid at each wash by firmly tapping the plate against clean paper towels. At the last wash, invert plate on clean paper towels for 1-2 minutes to remove excessive liquid.
- j) Freshly prepare the substrate solution,  
*For the whole plate: 1ml Substrate A + 1ml Substrate B + 8ml Substrate dilution buffer*
- k) Add 95µl substrate solution to each well and incubate for 1 min.
- l) Place the plate in the luminometer. Allow plate to sit inside machine for 5 min before reading.
- m) Set integration time to 1 second with no filter position. For the best results, read the plate within 5-20 minutes.
- n) If any TF is not present, it will not form a complex, leading to no detection of TF in the plate assay.
- o) If promoter-DNA fragment contains a TF binding sequence, it will compete with the biotin-labelled oligo to bind to the TF in the sample, leading to no or less complex formation and no or lower detection.
- p) Through comparison of chemiluminescence signal in the presence and absence of the competitor promoter-DNA fragment, putative TFs binding to promoter can be identified.

## 5.9 Luciferase reporter assay

### 5.9.1 Reagents and chemicals

Sr. No.	Reagent name	Source
1	5X-Passive lysis buffer	Promega, USA
2	Lar-II (Firefly luciferase substrate)	Promega, USA
3	1mg/ml Coelenterazine in 100%-Methanol (Renilla luciferase substrate)	Biosynth International Inc.

### 5.9.2 Methods

#### 5.9.2.1 Transfection, cell seeding and drug treatments

- a) Transfect the cells with desired reporter plasmids (Test reporter gene + constitutively active reporter gene in 9:1 ratio) as described previously and seed the transfected cells in triplicates in a 24-well plate or seed the stable cells expressing reporter genes in triplicates in a 24-well plate.
- b) Give the drug treatments in triplicate if necessary.
  - A2780 and OAW42 models Ro5-3335 (A2780 = 200 $\mu$ M and OAW42 = 20 $\mu$ M) for 24 hours
  - A2780 and MCF7 All-trans-RA (1 $\mu$ M) for 24 hours.

#### 5.9.2.2 Cell lysis

- a) Remove media, wash cells twice with PBS and add 80 $\mu$ l/well of 1X-Passive lysis buffer containing protease inhibitor.
- b) Incubate the plate with shaking at room temperature for 10 minutes.
- c) Collect the cell lysates and centrifuge the lysates at 14000rpm for 30 minutes at 4°C. Collect the supernatant as cell lysates for further use. Always keep the lysates on ice.

### 5.9.2.3 Measuring reporter activity

- a) Measure Firefly luciferase activity using Lar-II substrate.
- b) In a white 96-well plate put the 10-20 $\mu$ l of lysate and add 50 $\mu$ l of Lar-II substrate. Take the bioluminescence reading immediately using plate reader with open filter for 1 second each.
- c) Measure Renilla luciferase activity using Coelenterazine substrate. Dilute the Coelenterazine stock (1mg/ml) 1:50 in PBS just before use.
- d) In a white 96-well plate put the 10-20 $\mu$ l of lysate and add 50 $\mu$ l of diluted Coelenterazine substrate. Take the bioluminescence reading immediately using plate reader with open filter.
- e) Measure the protein content of lysates using Bradford reagent as described previously.
- f) Calculate relative reporter activity using formula described below,
  - Relative reporter activity from transient transfection experiment,

*Relative reporter activity*

$$= \frac{\text{Relative light units of test reporter gene/Protein}}{\text{Relative light units of constitutively active reporter gene/Protein}}$$

- Relative reporter activity from cells stably expressing reporter gene,

$$\text{Reporter activity (RLU}/\mu\text{g/sec)} = \frac{\text{Relative light units of test reporter gene}}{\text{Protein concentration of sample}}$$

## 5.10 Co-Immunoprecipitation (Co-IP)

### 5.10.1 Reagents and chemicals

Sr. No.	Reagent name	Source
1	Tris base	HiMedia, India
2	Sodium chloride	Qualigens, India
3	Nonidet P-40 (NP-40)	Sigma, India
4	Sodium-EDTA	MP, India
5	Sodium-EGTA	MP, India
6	Triton-X-100	Sigma, USA
7	100X-Protease inhibitor cocktail	Sigma, USA
8	Sodium dodecyl sulphate	HiMedia, India
9	$\beta$ -mercaptoethanol	Sigma, USA
10	Glycerol	Fischer Scientific, USA
11	Dithiothreitol (DTT)	Sigma, USA
12	Bovine serum albumin (BSA)	HiMedia, India

### 5.10.2 Buffers

Sr. No.	Buffer name and compositions
1	IP cell lysis buffer, <i>20mM Tris-HCl pH 7.4, 150mM NaCl, 1mM EDTA, 1mM EGTA, and 1% NP-40.</i>
2	IP wash buffer, <i>10mM Tris-HCl pH 7.4, 150mM NaCl, 1mM EDTA, 1mM EGTA, and 0.5%-Triton-X-100.</i>
3	IP blocking buffer, <i>0.1%-BSA in PBS.</i>
4	IP elution buffer, <i>125mM-Tris-HCl pH 6.8, 4% SDS, 20% Glycerol and 10% <math>\beta</math>-mercaptoethanol.</i>

### 5.10.3 Methods

#### 5.10.3.1 Lysate preparation

- a) Isolate nuclear pellets from cells ( $10^7$  cells) using nuclear-cytoplasmic fractionation protocol described previously (section 1.5).

- b) Add ice-cold IP cell lysis buffer (1ml for  $10^7$  cells) containing 1X-protease inhibitor cocktail, 1mM-Sodium orthovanadate and 5mM-Sodium fluoride, to nuclear pellet.
- c) Incubate for 30 minutes with constant agitation at 4°C. Centrifuge lysates at 14,000rpm for 30 minutes at 4°C and collect the supernatant as nuclear lysate for Co-IP.

#### **5.10.3.2 Immunoprecipitation**

- a) Add 40µl of Sepharose-G beads to 500µl of IP cell lysis buffer, wash the beads with agitation for 5 minutes and centrifuge at 4000rpm for 5 minutes at 4°C. Wash the beads with IP cell lysis buffer thrice.
- b) Block the washed beads with 0.1% BSA in PBS for 60 minutes with constant agitation.
- c) Resuspend the blocked beads in 200µl fresh IP cell lysis buffer containing 1X-protease inhibitor cocktail and store on ice.
- d) Add 2-10µg of primary antibody or as per recommended dilution to the blocked beads and incubate at 4°C for 4-6 hours with constant agitation.
- e) Next add 100-500µg of cell lysate to above mixture and again incubate at 4°C for 16 hours with constant agitation.

#### **5.10.3.3 Washing**

- a) Centrifuge tubes at 4000rpm for 5 minutes at 4°C. Discard supernatant and resuspend beads in 1ml IP wash buffer with 1X-protease inhibitors. Wash beads with IP wash buffer thrice. Carefully remove all IP wash buffer from beads and proceed for elution.

#### **5.10.3.4 Elution**

- a) Add 50µl of IP elution buffer to the beads and heat the mixture at 95°C for 5 minutes.
- b) Centrifuge the above mixture and pellet the beads. Collect the supernatant as first elute.
- c) Repeat the elution step once more and collect the second elute.
- d) Analyze the samples by western blot for IP and Co-IP.

## 5.11 Chromatin immunoprecipitation (ChIP) and sequential ChIP-re-

### ChIP

#### 5.11.1 Reagents and chemicals

Sr. No.	Reagent name	Source
1	Formaldehyde	Merck, India
2	Glycine	HiMedia, India
3	4-(2-hydroxyethyl)-1-piperazineethanesulfonic acid (HEPES)	Sigma, USA
4	Tris base	HiMedia, India
5	Bovine serum albumin (BSA-1mg/ml)	HiMedia, India
6	Salmon sperm DNA	Sigma, USA
7	Sodium chloride	Qualigens, India
8	Sodium-EDTA	MP, USA
9	Sodium-EGTA	MP, USA
10	100X-Protease inhibitor cocktail	Sigma, USA
11	Sodium dodecyl sulphate (SDS)	HiMedia, India
12	Sodium deoxycholate	Sigma, USA
13	Triton-X-100	Sigma, USA
14	Nonidet P-40 (NP-40)	Sigma, USA
15	Sodium bicarbonate	Amresco
16	RNase A (10mg/ml)	Sigma, USA
17	Proteinase K (20mg/ml)	Sigma, USA
18	Dithiothreitol (DTT-0.1M)	Sigma, USA

#### 5.11.2 Buffers

Sr. No.	Buffer name and compositions
1	ChIP lysis buffer, 50mM HEPES-KOH pH 7.5, 140mM NaCl, 1mM EDTA, 1mM EGTA, 1% Triton-X-100, 0.1% Sodium deoxycholate and 0.1% SDS.
2	RIPA buffer, 50mM Tris-HCl pH 8, 150mM NaCl, 1mM EDTA, 1mM EGTA, 1% NP-40, 0.5% Sodium deoxycholate and 0.1% SDS.
3	ChIP quenching buffer, 1.25M Glycine

4	ChIP low salt wash buffer, 20mM Tris-HCl pH 8, 150mM NaCl, 1mM EDTA, 1mM EGTA, and 0.1% Sodium dodecyl sulphate and 1% Triton-X-100.
5	ChIP high salt wash buffer, 20mM Tris-HCl pH 8, 500mM NaCl, 1mM EDTA, 1mM EGTA, and 0.1% SDS and 1% Triton-X-100.
6	ChIP elution buffer, 1% SDS and 100mM Sodium bicarbonate
7	ChIP-re-ChIP elution buffer, 10mM Tris-HCl pH8.0, 1mM EDTA, 1mM EGTA and 10mM DTT

### 5.11.3 Methods

#### 5.11.3.1 Lysate preparation

- a) Start with two-three 70-80% confluent 100mm tissue culture dishes ( $1-5 \times 10^7$  cells).  
Make sure each tissue culture dish has 10ml culture media.  
*For sequential ChIP-re-ChIP take six-eight 70-80% confluent 100mm tissue culture dishes ( $5-10 \times 10^7$  cells).*
- b) Cross-link the proteins to DNA by adding 37% Formaldehyde drop-wise directly to the media to a final concentration of 0.75% with gentle rotating motion at room temperature (203 $\mu$ l of 37% Formaldehyde to 10 ml of media). Incubate with gentle rotating motion at room temperature for 10 minutes.
- c) Add ice-cold 1.25M Glycine to a final concentration of 125mM to the media drop-wise with gentle rotating motion at room temperature (1ml of 1.25M Glycine to 10 ml of media). Incubate with gentle rotating motion at room temperature for 5 minutes.
- d) After 5 minutes keep plates on ice. Rinse the cells twice with 10ml of ice-cold PBS.
- e) Add 5ml of ice-cold PBS to plates and scrape the cells thoroughly with cell scraper and transfer to a 50ml centrifuge tube. Repeat the cell collection using ice-cold PBS.
- f) Centrifuge at 1000g, for 5 minutes at 4°C. Carefully decant the supernatant and resuspend the cell pellet in ChIP cell lysis buffer (750 $\mu$ l of ChIP cell lysis buffer per  $10^7$  cells) and incubate on ice for 30 minutes.

### 5.11.3.2 Sonication

- a) Sonicate lysate to shear DNA to an average fragment size of 200-1000bp using water cooled sonicator (Biorupter).

*Cross-linked lysate should be sonicated at different time course and different sonication cycles to identify the optimal sonication conditions to get desired fragment size of sonicated DNA. Purify the sonicated DNA as described in section and analyse the fragment size of DNA by running the samples on 1.5% agarose gel.*

- b) Pellet the cell debris by centrifugation at 8000g for 5 minutes at 4°C. Transfer the supernatant to a fresh tube. This chromatin preparation will be used for the immunoprecipitation.
- c) Remove the 50µl of each sonicated sample to determine the DNA concentration and fragment size. This 50µl will be used as input DNA.

### 5.11.3.3 Determination of DNA concentration

- a) Remove the 50µl of each sonicated sample to determine the DNA concentration.
- b) Add 70µl of elution buffer, 4.8µl of 5M NaCl and 2µl of 10mg/ml of RNase A to 50µl of sonicated sample and incubate at 65°C overnight with shaking.
- c) Next add 2µl of 20mg/ml of proteinase K and incubate at 60°C for 2 hours with shaking.
- d) Purify the DNA using column purification as described previously. Determine the DNA concentration of purified DNA and use it as input DNA.

### 5.11.3.4 Bead preparation

- a) Take 40µl of Sepharose G beads (20µl for IP and 20µl for bead control) in 1ml of RIPA buffer. Wash thrice the beads with RIPA buffer. After each wash centrifuge at 4000rpm for 5 minutes at 4°C.

- b) Add RIPA buffer to twice the volume of washed beads. Add single sheared salmon sperm DNA to a final concentration of 75ng/μl of beads and BSA to a final concentration of 0.1 μg/μl of beads.
- c) Incubate at room temperature for 30 minutes with constant shaking.
- d) Wash once with RIPA buffer and centrifuge at 4000rpm for 5 minutes at 4°C. Resuspend the beads in RIPA buffer to twice the volume of blocked beads.

#### 5.11.3.5 Immunoprecipitation

- a) Take 15-20μg of DNA (Sonicated lysate) and dilute the sample 1:5 with RIPA buffer and add 20μl of blocked beads.

*For sequential ChIP-re-ChIP begin first ChIP with 50-60μg of DNA (Sonicated lysate) and dilute the sample 1:5 with RIPA buffer and add 50μl of blocked beads.*

- b) Add 1-2μg of antibody per 20μg of DNA and incubate overnight at 4°C with constant rotation.

#### 5.11.3.6 Washing

- a) Centrifuge the immunoprecipitated samples at 4000rpm for 5 minutes and discard the supernatant.
- b) Wash the beads twice with ChIP low salt wash buffer with 1X-protease inhibitors and once with ChIP high salt wash buffer with 1X-protease inhibitors. After each wash centrifuge at 4000rpm for 5 minutes at 4°C.

#### 5.11.3.7 Elution and reverse cross-linking

- a) Resuspend the washed beads in 120μl of elution buffer and incubate for 30 minutes at 30°C with constant agitation.
- b) Centrifuge at 4000rpm for 5 minutes and collect the supernatant in fresh tube.

- c) Add 4.8µl of 5M NaCl and 5µl of 10mg/ml of RNase A and incubate at 65°C overnight with shaking.
- d) Next add 5µl of 20mg/ml of proteinase K and incubate at 60°C for 2 hours with shaking.
- e) Purify the DNA using column purification as described previously. This DNA is used as ChIP DNA.

#### 5.11.3.8 Elution of first ChIP DNA in ChIP-re-ChIP

- a) Resuspend the washed beads from first round of ChIP in 125µl of ChIP-re-ChIP elution buffer with 1X-protease inhibitors.
- b) Incubate for 60 minutes at 30°C with constant agitation.
- c) Centrifuge at 4000rpm for 5 minutes and collect the supernatant in fresh tube.
- d) Divide the elute in two fractions, first fraction (25µl) and second fraction (100µl).
- e) Proceed to reverse crosslinking of first fraction as described in section 1.11.3.7 (c-e).

This is ChIP DNA for first round of ChIP and input for second round of ChIP.

#### 5.11.3.9 Second ChIP round of ChIP-re-ChIP

- a) Dilute the second fraction 20 times with RIPA buffer and proceed for second round of ChIP as described in sections 1.11.3.4 to .11.3.7.

**Table 8: List of ChIP real time primers**

Primer Name	Sequence
Site 1 ChIP Forward	GCCGCATGCACGCATTTATT
Site 1 ChIP Reverse	GGCTGGGAGAGGTTTCATTGA
Site 2 ChIP Forward	GGGGCTCTTGTTTACCAGCA
Site 2 ChIP Reverse	CTCTCTCGAGTTCGCCTGGT
Site 3-4 ChIP Forward	GCCGCCTTCGGAGTATTGTT
Site 3-4 ChIP Reverse	CGGAGCCAGACTTCATTCT

## 5.12 Immunohistochemistry

### 5.12.1 Reagents and chemicals

Sr. No.	Reagent name	Source
1	Xylene	Qualigens, India
2	Ethanol	Qualigens, India
3	Sodium citrate	Sigma, USA
4	Tween 20	Sigma, USA
5	Mouse-rabbit specific HRP/DAB IHC detection kit	Abcam, UK
6	Tris base	HiMedia, India
7	Sodium chloride	Qualigens, India
8	Haematoxylin	Sigma, USA
9	DPX mountant	Sigma, USA

### 5.12.2 Buffers

Sr. No.	Buffer name and compositions
1	Sodium citrate buffer, <i>10mM Sodium citrate, 0.05% Tween 20, pH 6.0.</i>
2	Tris buffered saline (TBS), 20mM Tris-HCl and 140mMNaCl.
3	Wash buffer TBST, <i>TBS with 0.01% Tween 20.</i>

### 5.12.3 Methods

#### 5.12.3.1 Deparaffinization and rehydration

- Place slides with the paraffin-embedded sections at 65°C for 3-4 hours.
- Warm the Xylene solution 1. Deep the slides first in pre-warmed Xylene solution 1 followed by Xylene solution 2 and Xylene solution 3. Incubate for 10 minutes at room temperature for each Xylene deep.
- Next, Deep the slides first in 100% Ethanol followed by 90% Ethanol and 70% Ethanol. Incubate for 5 minutes at room temperature for each Ethanol deep.
- Place slides in running cold tap water for 10 minutes to rinse off ethanol. Keep the slides in the tap water until ready to perform antigen retrieval.

### 5.12.3.2 Blocking endogenous peroxidase activity

- a) Block endogenous peroxidase activity of tissue sections by incubating sections with peroxidase block (3% H<sub>2</sub>O<sub>2</sub>) for 10 minutes in dark at room temperature.
- b) Wash the slides thrice with TBS.

### 5.12.3.3 Heat induced antigen retrieval

- a) Sodium citrate buffer was used for heat induced antigen retrieval either by microwave or pressure cooker.
- b) *Microwave:* Add appropriate amount of antigen retrieval buffer in a microwave container and deep the slides in buffer. Boil the slides at 320V for 6 minutes followed by 650V for 4 minutes. Make sure sections remain submerged in buffer and do not peel off during process. Allow the slides to cooldown at room temperature.
- c) *Pressure cooker:* Add appropriate amount of antigen retrieval buffer in a cooker and boil the buffer. Deep the slides in pre-warmed buffer and close the lid. Once cooker reaches full pressure count 3 minutes. Switch off the hotplate and allow the cooker to cooldown at room temperature.

### 5.12.3.4 Immunostaining

- a) Wash the slides thrice with TBST and block the sections using protein block in moist chamber for 1 hour at room temperature.
- b) Drain the slides of protein block and wipe around the section with tissue paper.
- c) Incubate slide with primary antibody diluted in TBS overnight at 4°C in moist chamber.
- d) Wash the slides thrice with TBST and incubate the sections with anti-rabbit-HRP secondary antibody for two hours at room temperature in moist chamber.
- e) If primary antibody is mouse origin, then incubate the section first with mouse complement for 30 minutes followed by anti-rabbit-HRP secondary antibody for two hours at room temperature in moist chamber.

- f) Wash the slides thrice with TBST.
- g) Dilute 50X-DAB chromogen in DAB-substrate. Add diluted chromogen to section and incubate for 5-30 seconds at room temperature.
- h) Place immediately in tap water till counterstaining.

#### 5.12.3.5 Counterstaining and mounting

- a) Deep the slides in Haematoxylin stain for 30-60 seconds and rinse the slides under running tap water for 10 minutes followed by 2 minutes deep in ddH<sub>2</sub>O.
- b) Deep the slides first in 70% Ethanol followed by 90% Ethanol and 100% Ethanol to dehydrate the sections. Incubate for 5 minutes for each Ethanol deep.
- c) Next immerse the slides in Xylene for 60 minutes.
- d) Mount the slides using mounting medium (DPX). Dry the mounted slides at 37°C overnight.
- e) Grade the slides from pathologist and take respective microscopic images.

**Table 9: List of antigen retrieval conditions and antibody dilution for IHC**

Antibody	Antigen retrieval	Dilution
IGF1R	Sodium citrate buffer (pH 6), microwave 20 minutes	Undiluted
Ki67	Sodium citrate buffer (pH 6), microwave 20 minutes	1:100
FOXO3a	Sodium citrate buffer (pH 6), pressure cooker 6 minutes	1:100

### 5.13 Small animal bioluminescence imaging

#### 5.13.1 Reagents and chemicals

Sr. No.	Reagent name	Source
1	D-Luciferin	Biosynth International Inc.
2	Isoflurane	Baxter, USA

#### 5.13.2 Methods

##### 5.13.2.1 Cell preparation

- Ovarian cancer cells stably expressing firefly luciferase 2 (FL2) reporter plasmids were established and were grown in their respective media, until 70-80% confluence.
- Cells were trypsinized, viable cell count was determined using trypan blue and  $4 \times 10^6$  viable cells per mouse were used for implantation.
- According to the number of mice to be implanted viable cells were collected in sterile ice-cold PBS such that each 100 $\mu$ l of cell suspension contains  $4 \times 10^6$  viable cells.

##### 5.13.2.2 Cell implantation in mice

- All experiments were approved by Institutional Animal Ethics Committee at ACTREC.
- Non-obese diabetic-severe combined immunodeficient (NODSCID) mice were used for implantation of Ovarian cancer cells stably FL2 reporter plasmids.
- Mice were anesthetized by isoflurane euthanasia and fur was removed by razor to facilitate proper implantation of cells and optical imaging.
- Required number of cells ( $4 \times 10^6$ ) were taken in a 26-gauge needle, skin of the mice was lifted to make a tent using needle and cells were injected at the base to get subcutaneous injection.
- Mice were imaged one day after implantation and on subsequent days to monitor tumour growth as described below.

#### 5.13.2.3 Bioluminescence imaging of mice

- a) Mice were imaged using Xenogen-IVIS-Spectrum optical imager, which captures both bioluminescence and bright field images.
- b) D-luciferin (100 $\mu$ l of 30mg/ml/mouse i.e. 3mg/mouse) was injected intraperitoneally into mice and were euthanized by isoflurane.
- c) Mouse were put inside Xenogen-IVIS-Spectrum optical imager under isoflurane euthanasia and bioluminescence images were acquired using sequence mode.
- d) Bioluminescence images were analysed using LIVING IMAGE 4.4 software.

#### 5.13.2.4 Drug treatment in mice

- a) Ro5-3335, diluted in normal saline at 2 mg/kg for 5 days intravenously.
- b) Single dose of chemotherapeutic agents Cisplatin + Paclitaxel diluted in normal saline at 2 mg/kg + 1 mg/kg respectively alone or after five days of Ro5-3335 treatment.

### 5.14 Statistics

All the data represent the mean  $\pm$  SEM of at least three independent experiments and were analysed for significance using unpaired Student's t test. P value  $\leq$  0.05 was considered as significant. Pearson's correlation coefficient test was used to calculate the correlation between Ki-67, IGF1R, FOXO3a IRS scores from IHC and tumor viability.

## References

1. Cialdella-Kam, L., et al., *Implementing cancer prevention into clinical practice*. J Cancer Educ, 2012. **27**(2 Suppl): p. S136-43.
2. Emmons, K.M. and G.A. Colditz, *Realizing the Potential of Cancer Prevention - The Role of Implementation Science*. N Engl J Med, 2017. **376**(10): p. 986-990.
3. Force, U.S.P.S.T., et al., *Screening for Skin Cancer: US Preventive Services Task Force Recommendation Statement*. JAMA, 2016. **316**(4): p. 429-35.
4. Blatt, A.J., et al., *Comparison of cervical cancer screening results among 256,648 women in multiple clinical practices*. Cancer Cytopathol, 2015. **123**(5): p. 282-8.
5. Siu, A.L. and U.S.P.S.T. Force, *Screening for Breast Cancer: U.S. Preventive Services Task Force Recommendation Statement*. Ann Intern Med, 2016. **164**(4): p. 279-96.
6. Kanodra, N.M., et al., *Primary Care Provider and Patient Perspectives on Lung Cancer Screening. A Qualitative Study*. Ann Am Thorac Soc, 2016. **13**(11): p. 1977-1982.
7. Quaresma, M., M.P. Coleman, and B. Rachet, *40-year trends in an index of survival for all cancers combined and survival adjusted for age and sex for each cancer in England and Wales, 1971-2011: a population-based study*. Lancet, 2015. **385**(9974): p. 1206-18.
8. Roser, M. and H. Ritchie. *Cancer*. Cancer 2015 November 2019; Available from: <https://ourworldindata.org/cancer>.
9. Collaborators, G.B.D.M., *Global, regional, and national under-5 mortality, adult mortality, age-specific mortality, and life expectancy, 1970-2016: a systematic analysis for the Global Burden of Disease Study 2016*. Lancet, 2017. **390**(10100): p. 1084-1150.
10. Altorki, N. and S. Harrison, *What is the role of neoadjuvant chemotherapy, radiation, and adjuvant treatment in resectable esophageal cancer?* Ann Cardiothorac Surg, 2017. **6**(2): p. 167-174.
11. Zhao, X., et al., *Neoadjuvant chemotherapy versus neoadjuvant chemoradiotherapy for cancer of the esophagus or the gastroesophageal junction: A meta-analysis based on clinical trials*. PLoS One, 2018. **13**(8): p. e0202185.
12. Elies, A., et al., *The role of neoadjuvant chemotherapy in ovarian cancer*. Expert Rev Anticancer Ther, 2018. **18**(6): p. 555-566.
13. Vergote, I., et al., *Neoadjuvant chemotherapy versus debulking surgery in advanced tubo-ovarian cancers: pooled analysis of individual patient data from the EORTC 55971 and CHORUS trials*. Lancet Oncol, 2018. **19**(12): p. 1680-1687.
14. Lee, J.W., et al., *Radiotherapy with and without Concurrent Cisplatin for Unresectable or Inoperable Locally Advanced Triple Negative Breast Cancer*. International Journal of Radiation Oncology • Biology • Physics, 2017. **99**(2): p. E28-E29.
15. Crawford, S., *Is it time for a new paradigm for systemic cancer treatment? Lessons from a century of cancer chemotherapy*. Front Pharmacol, 2013. **4**: p. 68.
16. Ke, X. and L. Shen, *Molecular targeted therapy of cancer: The progress and future prospect*. Frontiers in Laboratory Medicine, 2017. **1**(2): p. 69-75.
17. Albain, K.S., et al., *Gemcitabine plus Paclitaxel versus Paclitaxel monotherapy in patients with metastatic breast cancer and prior anthracycline treatment*. J Clin Oncol, 2008. **26**(24): p. 3950-7.
18. Blackwell, K.L., et al., *Overall survival benefit with lapatinib in combination with trastuzumab for patients with human epidermal growth factor receptor 2-positive metastatic breast cancer: final results from the EGF104900 Study*. J Clin Oncol, 2012. **30**(21): p. 2585-92.
19. McGuire, W.P., et al., *Cyclophosphamide and cisplatin compared with paclitaxel and cisplatin in patients with stage III and stage IV ovarian cancer*. N Engl J Med, 1996. **334**(1): p. 1-6.
20. Bolis, G., et al., *Paclitaxel vs epidoxorubicin plus paclitaxel as second-line therapy for platinum-refractory and -resistant ovarian cancer*. Gynecol Oncol, 1999. **72**(1): p. 60-4.
21. Coleman, R.L., et al., *Bevacizumab and paclitaxel-carboplatin chemotherapy and secondary cytoreduction in recurrent, platinum-sensitive ovarian cancer (NRG Oncology/Gynecologic Oncology Group study GOG-0213): a multicentre, open-label, randomised, phase 3 trial*. Lancet Oncol, 2017. **18**(6): p. 779-791.
22. Posner, M.R., et al., *Cisplatin and fluorouracil alone or with docetaxel in head and neck cancer*. N Engl J Med, 2007. **357**(17): p. 1705-15.
23. Long, H.J., 3rd, et al., *Randomized phase III trial of cisplatin with or without topotecan in carcinoma of the uterine cervix: a Gynecologic Oncology Group Study*. J Clin Oncol, 2005. **23**(21): p. 4626-33.
24. Tewari, K.S., et al., *Improved survival with bevacizumab in advanced cervical cancer*. N Engl J Med, 2014. **370**(8): p. 734-43.

25. Falcone, A., et al., *Phase III trial of infusional fluorouracil, leucovorin, oxaliplatin, and irinotecan (FOLFOXIRI) compared with infusional fluorouracil, leucovorin, and irinotecan (FOLFIRI) as first-line treatment for metastatic colorectal cancer: the Gruppo Oncologico Nord Ovest*. J Clin Oncol, 2007. **25**(13): p. 1670-6.
26. Hurwitz, H., et al., *Bevacizumab plus irinotecan, fluorouracil, and leucovorin for metastatic colorectal cancer*. N Engl J Med, 2004. **350**(23): p. 2335-42.
27. Al-Batran, S.E., et al., *Perioperative chemotherapy with fluorouracil plus leucovorin, oxaliplatin, and docetaxel versus fluorouracil or capecitabine plus cisplatin and epirubicin for locally advanced, resectable gastric or gastro-oesophageal junction adenocarcinoma (FLOT4): a randomised, phase 2/3 trial*. Lancet, 2019. **393**(10184): p. 1948-1957.
28. Bang, Y.J., et al., *Trastuzumab in combination with chemotherapy versus chemotherapy alone for treatment of HER2-positive advanced gastric or gastro-oesophageal junction cancer (ToGA): a phase 3, open-label, randomised controlled trial*. Lancet, 2010. **376**(9742): p. 687-97.
29. Konieczkowski, D.J., C.M. Johannessen, and L.A. Garraway, *A Convergence-Based Framework for Cancer Drug Resistance*. Cancer Cell, 2018. **33**(5): p. 801-815.
30. Hediger, M.A., et al., *The ABCs of solute carriers: physiological, pathological and therapeutic implications of human membrane transport proteins* Introduction. Pflugers Arch, 2004. **447**(5): p. 465-8.
31. Holland, I.B., *ABC transporters, mechanisms and biology: an overview*. Essays Biochem, 2011. **50**(1): p. 1-17.
32. Linton, K.J. and C.F. Higgins, *Structure and function of ABC transporters: the ATP switch provides flexible control*. Pflugers Arch, 2007. **453**(5): p. 555-67.
33. Zhang, Y., et al., *The SLC transporter in nutrient and metabolic sensing, regulation, and drug development*. J Mol Cell Biol, 2019. **11**(1): p. 1-13.
34. Grant, D.M., *Detoxification pathways in the liver*. J Inherit Metab Dis, 1991. **14**(4): p. 421-30.
35. Liang, Y., S. Li, and L. Chen, *The physiological role of drug transporters*. Protein Cell, 2015. **6**(5): p. 334-50.
36. Li, Q. and Y. Shu, *Role of solute carriers in response to anticancer drugs*. Mol Cell Ther, 2014. **2**: p. 15.
37. Verma, H., et al., *Drug metabolizing enzymes-associated chemo resistance and strategies to overcome it*. Drug Metab Rev, 2019. **51**(2): p. 196-223.
38. Wilkens, S., *Structure and mechanism of ABC transporters*. F1000Prime Rep, 2015. **7**: p. 14.
39. Bai, X., T.F. Moraes, and R.A.F. Reithmeier, *Structural biology of solute carrier (SLC) membrane transport proteins*. Mol Membr Biol, 2017. **34**(1-2): p. 1-32.
40. Schaich, M., et al., *MDR1 and MRP1 gene expression are independent predictors for treatment outcome in adult acute myeloid leukaemia*. Br J Haematol, 2005. **128**(3): p. 324-32.
41. Benderra, Z., et al., *Breast cancer resistance protein and P-glycoprotein in 149 adult acute myeloid leukemias*. Clin Cancer Res, 2004. **10**(23): p. 7896-902.
42. Liu, B., et al., *Co-expression of ATP binding cassette transporters is associated with poor prognosis in acute myeloid leukemia*. Oncol Lett, 2018. **15**(5): p. 6671-6677.
43. Wuchter, C., et al., *Clinical significance of P-glycoprotein expression and function for response to induction chemotherapy, relapse rate and overall survival in acute leukemia*. Haematologica, 2000. **85**(7): p. 711-21.
44. Marcelletti, J.F., et al., *Evidence of a role for functional heterogeneity in multidrug resistance transporters in clinical trials of P-glycoprotein modulation in acute myeloid leukemia*. Cytometry B Clin Cytom, 2019. **96**(1): p. 57-66.
45. Lu, L., et al., *Expression of MDR1 in epithelial ovarian cancer and its association with disease progression*. Oncol Res, 2007. **16**(8): p. 395-403.
46. Hille, S., et al., *Anticancer drugs induce mdr1 gene expression in recurrent ovarian cancer*. Anticancer Drugs, 2006. **17**(9): p. 1041-4.
47. Tong, X., et al., *Expression levels of MRP1, GST-pi, and GSK3beta in ovarian cancer and the relationship with drug resistance and prognosis of patients*. Oncol Lett, 2019. **18**(1): p. 22-28.
48. Mo, L., et al., *Ascites Increases Expression/Function of Multidrug Resistance Proteins in Ovarian Cancer Cells*. PLoS One, 2015. **10**(7): p. e0131579.
49. He, M., et al., *Hypoxia-inducible factor-2alpha directly promotes BCRP expression and mediates the resistance of ovarian cancer stem cells to adriamycin*. Mol Oncol, 2019. **13**(2): p. 403-421.
50. Januchowski, R., et al., *Analysis of MDR genes expression and cross-resistance in eight drug resistant ovarian cancer cell lines*. J Ovarian Res, 2016. **9**(1): p. 65.

51. Chen, Y., M.M. Bieber, and N.N. Teng, *Hedgehog signaling regulates drug sensitivity by targeting ABC transporters ABCB1 and ABCG2 in epithelial ovarian cancer*. *Mol Carcinog*, 2014. **53**(8): p. 625-34.
52. Ricciardelli, C., et al., *Chemotherapy-induced hyaluronan production: a novel chemoresistance mechanism in ovarian cancer*. *BMC Cancer*, 2013. **13**: p. 476.
53. Vesel, M., et al., *ABCB1 and ABCG2 drug transporters are differentially expressed in non-small cell lung cancers (NSCLC) and expression is modified by cisplatin treatment via altered Wnt signaling*. *Respir Res*, 2017. **18**(1): p. 52.
54. Tsou, S.H., et al., *A critical dose of doxorubicin is required to alter the gene expression profiles in MCF-7 cells acquiring multidrug resistance*. *PLoS One*, 2015. **10**(1): p. e0116747.
55. Li, W., et al., *Overexpression of Snail accelerates adriamycin induction of multidrug resistance in breast cancer cells*. *Asian Pac J Cancer Prev*, 2011. **12**(10): p. 2575-80.
56. Chen, W.J., et al., *Multidrug resistance in breast cancer cells during epithelial-mesenchymal transition is modulated by breast cancer resistant protein*. *Chin J Cancer*, 2010. **29**(2): p. 151-7.
57. Zhu, K., et al., *Short hairpin RNA targeting Twist1 suppresses cell proliferation and improves chemosensitivity to cisplatin in HeLa human cervical cancer cells*. *Oncol Rep*, 2012. **27**(4): p. 1027-34.
58. Mato, E., et al., *ABCG2/BCRP gene expression is related to epithelial-mesenchymal transition inducer genes in a papillary thyroid carcinoma cell line (TPC-1)*. *J Mol Endocrinol*, 2014. **52**(3): p. 289-300.
59. Uchibori, K., et al., *Establishment and characterization of two 5-fluorouracil-resistant hepatocellular carcinoma cell lines*. *Int J Oncol*, 2012. **40**(4): p. 1005-10.
60. Ballesterio, M.R., et al., *Expression of transporters potentially involved in the targeting of cytostatic bile acid derivatives to colon cancer and polyps*. *Biochem Pharmacol*, 2006. **72**(6): p. 729-38.
61. Tatsumi, S., et al., *Organic cation transporter 2 and tumor budding as independent prognostic factors in metastatic colorectal cancer patients treated with oxaliplatin-based chemotherapy*. *Int J Clin Exp Pathol*, 2014. **7**(1): p. 204-12.
62. Zhang, S., et al., *Organic cation transporters are determinants of oxaliplatin cytotoxicity*. *Cancer Res*, 2006. **66**(17): p. 8847-57.
63. Yokoo, S., et al., *Significance of organic cation transporter 3 (SLC22A3) expression for the cytotoxic effect of oxaliplatin in colorectal cancer*. *Drug Metab Dispos*, 2008. **36**(11): p. 2299-306.
64. Thomas, J., et al., *Active transport of imatinib into and out of cells: implications for drug resistance*. *Blood*, 2004. **104**(12): p. 3739-45.
65. Gupta, S., et al., *Human organic cation transporter 1 is expressed in lymphoma cells and increases susceptibility to irinotecan and paclitaxel*. *J Pharmacol Exp Ther*, 2012. **341**(1): p. 16-23.
66. Heise, M., et al., *Downregulation of organic cation transporters OCT1 (SLC22A1) and OCT3 (SLC22A3) in human hepatocellular carcinoma and their prognostic significance*. *BMC Cancer*, 2012. **12**: p. 109.
67. Schaeffeler, E., et al., *DNA methylation is associated with downregulation of the organic cation transporter OCT1 (SLC22A1) in human hepatocellular carcinoma*. *Genome Med*, 2011. **3**(12): p. 82.
68. Lautem, A., et al., *Downregulation of organic cation transporter 1 (SLC22A1) is associated with tumor progression and reduced patient survival in human cholangiocellular carcinoma*. *Int J Oncol*, 2013. **42**(4): p. 1297-304.
69. Hashimoto, Y., et al., *Expression of organic anion-transporting polypeptide 1A2 and organic cation transporter 6 as a predictor of pathologic response to neoadjuvant chemotherapy in triple negative breast cancer*. *Breast Cancer Res Treat*, 2014. **145**(1): p. 101-11.
70. Svoboda, M., et al., *Expression of organic anion-transporting polypeptides 1B1 and 1B3 in ovarian cancer cells: relevance for paclitaxel transport*. *Biomed Pharmacother*, 2011. **65**(6): p. 417-26.
71. Teft, W.A., et al., *OATP1B1 and tumour OATP1B3 modulate exposure, toxicity, and survival after irinotecan-based chemotherapy*. *Br J Cancer*, 2015. **112**(5): p. 857-65.
72. Lee, Y.Y., et al., *Prognostic value of the copper transporters, CTR1 and CTR2, in patients with ovarian carcinoma receiving platinum-based chemotherapy*. *Gynecol Oncol*, 2011. **122**(2): p. 361-5.
73. Holzer, A.K., et al., *The copper influx transporter human copper transport protein 1 regulates the uptake of cisplatin in human ovarian carcinoma cells*. *Mol Pharmacol*, 2004. **66**(4): p. 817-23.
74. Yoshida, H., et al., *Association of copper transporter expression with platinum resistance in epithelial ovarian cancer*. *Anticancer Res*, 2013. **33**(4): p. 1409-14.
75. Sun, S., et al., *The association between copper transporters and the prognosis of cancer patients undergoing chemotherapy: a meta-analysis of literatures and datasets*. *Oncotarget*, 2017. **8**(9): p. 16036-16051.

76. Chen, H.H., et al., *Predictive and prognostic value of human copper transporter 1 (hCtr1) in patients with stage III non-small-cell lung cancer receiving first-line platinum-based doublet chemotherapy*. Lung Cancer, 2012. **75**(2): p. 228-34.
77. Kim, E.S., et al., *Copper transporter CTR1 expression and tissue platinum concentration in non-small cell lung cancer*. Lung Cancer, 2014. **85**(1): p. 88-93.
78. Ogane, N., et al., *Prognostic value of organic anion transporting polypeptide 1B3 and copper transporter 1 expression in endometrial cancer patients treated with paclitaxel and carboplatin*. Biomed Res, 2013. **34**(3): p. 143-51.
79. Cui, H., et al., *Copper transporter 1 in human colorectal cancer cell lines: Effects of endogenous and modified expression on oxaliplatin cytotoxicity*. J Inorg Biochem, 2017. **177**: p. 249-258.
80. Agarwal, D.P., et al., *Metabolism of Cyclophosphamide by Aldehyde Dehydrogenases*, in *Enzymology and Molecular Biology of Carbonyl Metabolism 5*, H. Weiner, R.S. Holmes, and B. Wermuth, Editors. 1995, Springer US: Boston, MA. p. 115-122.
81. Sládek, N.E., et al., *Cellular levels of aldehyde dehydrogenases (ALDH1A1 and ALDH3A1) as predictors of therapeutic responses to cyclophosphamide-based chemotherapy of breast cancer: a retrospective study*. Cancer Chemotherapy and Pharmacology, 2002. **49**(4): p. 309-321.
82. Friedman, H.S., et al., *Cyclophosphamide resistance in medulloblastoma*. Cancer Res, 1992. **52**(19): p. 5373-8.
83. Kim, D., et al., *High NRF2 level mediates cancer stem cell-like properties of aldehyde dehydrogenase (ALDH)-high ovarian cancer cells: inhibitory role of all-trans retinoic acid in ALDH/NRF2 signaling*. Cell Death Dis, 2018. **9**(9): p. 896.
84. Gasparetto, M., et al., *Aldehyde Dehydrogenases Play a Role in Acute Myeloid Leukemia and Have Prognostic and Therapeutic Significance*. Blood, 2014. **124**(21): p. 2238-2238.
85. Verma, H., et al., *Drug metabolizing enzymes-associated chemo resistance and strategies to overcome it*. Drug Metabolism Reviews, 2019. **51**(2): p. 196-223.
86. Fujita, K., *Cytochrome P450 and anticancer drugs*. Curr Drug Metab, 2006. **7**(1): p. 23-37.
87. Nowell, S.A., et al., *Association of genetic variation in tamoxifen-metabolizing enzymes with overall survival and recurrence of disease in breast cancer patients*. Breast Cancer Res Treat, 2005. **91**(3): p. 249-58.
88. Chen, X., Y.W. Wang, and P. Gao, *SPIN1, negatively regulated by miR-148/152, enhances Adriamycin resistance via upregulating drug metabolizing enzymes and transporter in breast cancer*. J Exp Clin Cancer Res, 2018. **37**(1): p. 100.
89. Raynal, C., et al., *Pregnane X Receptor (PXR) expression in colorectal cancer cells restricts irinotecan chemosensitivity through enhanced SN-38 glucuronidation*. Mol Cancer, 2010. **9**: p. 46.
90. Pasello, M., et al., *Overcoming glutathione S-transferase P1-related cisplatin resistance in osteosarcoma*. Cancer Res, 2008. **68**(16): p. 6661-8.
91. Geng, M., et al., *The association between chemosensitivity and Pgp, GST-pi and Topo II expression in gastric cancer*. Diagn Pathol, 2013. **8**: p. 198.
92. Huang, J., M. Gu, and C. Chen, *[Expression of glutathione S-transferase-pi in operative specimens as marker of chemoresistance in patients with ovarian cancer]*. Zhonghua Fu Chan Ke Za Zhi, 1997. **32**(8): p. 458-61.
93. Cheng, X., et al., *Glutathione S-transferase-pi expression and glutathione concentration in ovarian carcinoma before and after chemotherapy*. Cancer, 1997. **79**(3): p. 521-7.
94. Shah, M.A. and G.K. Schwartz, *Cell cycle-mediated drug resistance: an emerging concept in cancer therapy*. Clin Cancer Res, 2001. **7**(8): p. 2168-81.
95. Bae, T., et al., *Restoration of paclitaxel resistance by CDK1 intervention in drug-resistant ovarian cancer*. Carcinogenesis, 2015. **36**(12): p. 1561-71.
96. Ma, Y., et al., *B7-H3 promotes the cell cycle-mediated chemoresistance of colorectal cancer cells by regulating CDC25A*. J Cancer, 2020. **11**(8): p. 2158-2170.
97. Sun, Y., et al., *CDC25A Facilitates Chemo-resistance in Ovarian Cancer Multicellular Spheroids by Promoting E-cadherin Expression and Arresting Cell Cycles*. J Cancer, 2019. **10**(13): p. 2874-2884.
98. Achuthan, S., et al., *Drug-induced senescence generates chemoresistant stemlike cells with low reactive oxygen species*. J Biol Chem, 2011. **286**(43): p. 37813-29.
99. Zheng, H., et al., *WEE1 inhibition targets cell cycle checkpoints for triple negative breast cancers to overcome cisplatin resistance*. Sci Rep, 2017. **7**: p. 43517.
100. Osman, A.A., et al., *Wee-1 kinase inhibition overcomes cisplatin resistance associated with high-risk TP53 mutations in head and neck cancer through mitotic arrest followed by senescence*. Mol Cancer Ther, 2015. **14**(2): p. 608-19.
101. Wang, L., et al., *MiR-26b reverses temozolomide resistance via targeting Wee1 in glioma cells*. Cell Cycle, 2017. **16**(20): p. 1954-1964.

102. Wu, S., et al., *Activation of WEE1 confers resistance to PI3K inhibition in glioblastoma*. *Neuro Oncol*, 2018. **20**(1): p. 78-91.
103. Bukhari, A.B., et al., *Inhibiting Wee1 and ATR kinases produces tumor-selective synthetic lethality and suppresses metastasis*. *J Clin Invest*, 2019. **129**(3): p. 1329-1344.
104. Ma, H.T., et al., *Depletion of p31 comet protein promotes sensitivity to antimetabolic drugs*. *J Biol Chem*, 2012. **287**(25): p. 21561-9.
105. Habu, T. and T. Matsumoto, *p31 comet inactivates the chemically induced Mad2-dependent spindle assembly checkpoint and leads to resistance to anti-mitotic drugs*. *SpringerPlus*, 2013. **2**(1): p. 562.
106. Sun, H., et al., *Aurora-A controls cancer cell radio- and chemoresistance via ATM/Chk2-mediated DNA repair networks*. *Biochim Biophys Acta*, 2014. **1843**(5): p. 934-44.
107. Anand, S., S. Penrhyn-Lowe, and A.R. Venkitaraman, *AURORA-A amplification overrides the mitotic spindle assembly checkpoint, inducing resistance to Taxol*. *Cancer Cell*, 2003. **3**(1): p. 51-62.
108. Corcoran, N.M., et al., *Molecular Pathways: Targeting DNA Repair Pathway Defects Enriched in Metastasis*. *Clin Cancer Res*, 2016. **22**(13): p. 3132-7.
109. Dabholkar, M., et al., *Messenger RNA levels of XPAC and ERCC1 in ovarian cancer tissue correlate with response to platinum-based chemotherapy*. *J Clin Invest*, 1994. **94**(2): p. 703-8.
110. Li, W. and D.W. Melton, *Cisplatin regulates the MAPK kinase pathway to induce increased expression of DNA repair gene ERCC1 and increase melanoma chemoresistance*. *Oncogene*, 2012. **31**(19): p. 2412-22.
111. Olausson, K.A., et al., *DNA repair by ERCC1 in non-small-cell lung cancer and cisplatin-based adjuvant chemotherapy*. *N Engl J Med*, 2006. **355**(10): p. 983-91.
112. MA, E.L.B. and W.F. El Kashef, *ERCC1 Expression in Metastatic Triple Negative Breast Cancer Patients Treated with Platinum-Based Chemotherapy*. *Asian Pac J Cancer Prev*, 2017. **18**(2): p. 507-513.
113. Luo, S.S., X.W. Liao, and X.D. Zhu, *Prognostic Value of Excision Repair Cross-Complementing mRNA Expression in Gastric Cancer*. *Biomed Res Int*, 2018. **2018**: p. 6204684.
114. Hsu, D.S., et al., *Regulation of excision repair cross-complementation group 1 by Snail contributes to cisplatin resistance in head and neck cancer*. *Clin Cancer Res*, 2010. **16**(18): p. 4561-71.
115. Bellmunt, J., et al., *Gene expression of ERCC1 as a novel prognostic marker in advanced bladder cancer patients receiving cisplatin-based chemotherapy*. *Ann Oncol*, 2007. **18**(3): p. 522-8.
116. Abdel-Fatah, T.M.A., et al., *ERCC1 Is a Predictor of Anthracycline Resistance and Taxane Sensitivity in Early Stage or Locally Advanced Breast Cancers*. *Cancers (Basel)*, 2019. **11**(8).
117. Li, W. and D.W. Melton, *Cisplatin regulates the MAPK kinase pathway to induce increased expression of DNA repair gene ERCC1 and increase melanoma chemoresistance*. *Oncogene*, 2012. **31**(19): p. 2412-2422.
118. Liu, J., et al., *Functional characterization of a novel transcript of ERCC1 in chemotherapy resistance of ovarian cancer*. *Oncotarget*, 2017. **8**(49): p. 85759-85771.
119. Bi, X., *Mechanism of DNA damage tolerance*. *World J Biol Chem*, 2015. **6**(3): p. 48-56.
120. Chen, X., et al., *MicroRNA29a enhances cisplatin sensitivity in nonsmall cell lung cancer through the regulation of REV3L*. *Mol Med Rep*, 2019. **19**(2): p. 831-840.
121. Shi, T.Y., et al., *DNA polymerase zeta as a potential biomarker of chemoradiation resistance and poor prognosis for cervical cancer*. *Med Oncol*, 2013. **30**(2): p. 500.
122. Zhu, X., et al., *REV3L, the catalytic subunit of DNA polymerase zeta, is involved in the progression and chemoresistance of esophageal squamous cell carcinoma*. *Oncol Rep*, 2016. **35**(3): p. 1664-70.
123. Wang, H., et al., *REV3L confers chemoresistance to cisplatin in human gliomas: the potential of its RNAi for synergistic therapy*. *Neuro Oncol*, 2009. **11**(6): p. 790-802.
124. Lin, S., et al., *Intrinsic adriamycin resistance in p53-mutated breast cancer is related to the miR-30c/FANCF/REV1-mediated DNA damage response*. *Cell Death Dis*, 2019. **10**(9): p. 666.
125. Niimi, K., et al., *Suppression of REV7 enhances cisplatin sensitivity in ovarian clear cell carcinoma cells*. *Cancer Sci*, 2014. **105**(5): p. 545-52.
126. Liu, Z., et al., *Nonhomologous end joining key factor XLF enhances both 5-fluorouracil and oxaliplatin resistance in colorectal cancer*. *Onco Targets Ther*, 2019. **12**: p. 2095-2104.
127. Yang, S. and X.Q. Wang, *XLF-mediated NHEJ activity in hepatocellular carcinoma therapy resistance*. *BMC Cancer*, 2017. **17**(1): p. 344.
128. Abdel-Fatah, T., et al., *Clinicopathological and functional significance of XRCC1 expression in ovarian cancer*. *Int J Cancer*, 2013. **132**(12): p. 2778-86.
129. Zhang, T., J. Chai, and L. Chi, *Induction Of XLF And 53BP1 Expression Is Associated With Temozolomide Resistance In Glioblastoma Cells*. *Onco Targets Ther*, 2019. **12**: p. 10139-10151.

130. Muller, C., et al., *DNA-Dependent protein kinase activity correlates with clinical and in vitro sensitivity of chronic lymphocytic leukemia lymphocytes to nitrogen mustards*. *Blood*, 1998. **92**(7): p. 2213-9.
131. Elliott, S.L., et al., *Mitoxantrone in combination with an inhibitor of DNA-dependent protein kinase: a potential therapy for high risk B-cell chronic lymphocytic leukaemia*. *Br J Haematol*, 2011. **152**(1): p. 61-71.
132. Willmore, E., et al., *DNA-dependent protein kinase is a therapeutic target and an indicator of poor prognosis in B-cell chronic lymphocytic leukemia*. *Clin Cancer Res*, 2008. **14**(12): p. 3984-92.
133. Sun, G., et al., *PRKDC regulates chemosensitivity and is a potential prognostic and predictive marker of response to adjuvant chemotherapy in breast cancer patients*. *Oncol Rep*, 2017. **37**(6): p. 3536-3542.
134. Abdel-Fatah, T.M., et al., *ATM, ATR and DNA-PKcs expressions correlate to adverse clinical outcomes in epithelial ovarian cancers*. *BBA Clin*, 2014. **2**: p. 10-7.
135. Shin, K., et al., *Expression of Interactive Genes Associated with Apoptosis and Their Prognostic Value for Ovarian Serous Adenocarcinoma*. *Adv Clin Exp Med*, 2016. **25**(3): p. 513-21.
136. Heeke, A.L., et al., *Prevalence of Homologous Recombination-Related Gene Mutations Across Multiple Cancer Types*. *JCO Precis Oncol*, 2018. **2018**.
137. Helleday, T., *Homologous recombination in cancer development, treatment and development of drug resistance*. *Carcinogenesis*, 2010. **31**(6): p. 955-60.
138. Lord, C.J. and A. Ashworth, *Mechanisms of resistance to therapies targeting BRCA-mutant cancers*. *Nat Med*, 2013. **19**(11): p. 1381-8.
139. Cruz, C., et al., *RAD51 foci as a functional biomarker of homologous recombination repair and PARP inhibitor resistance in germline BRCA-mutated breast cancer*. *Ann Oncol*, 2018. **29**(5): p. 1203-1210.
140. Lok, B.H., et al., *RAD52 inactivation is synthetically lethal with deficiencies in BRCA1 and PALB2 in addition to BRCA2 through RAD51-mediated homologous recombination*. *Oncogene*, 2013. **32**(30): p. 3552-8.
141. Feng, Z., et al., *Rad52 inactivation is synthetically lethal with BRCA2 deficiency*. *Proc Natl Acad Sci U S A*, 2011. **108**(2): p. 686-91.
142. Yazinski, S.A., et al., *ATR inhibition disrupts rewired homologous recombination and fork protection pathways in PARP inhibitor-resistant BRCA-deficient cancer cells*. *Genes Dev*, 2017. **31**(3): p. 318-332.
143. Cramer-Morales, K., et al., *Personalized synthetic lethality induced by targeting RAD52 in leukemias identified by gene mutation and expression profile*. *Blood*, 2013. **122**(7): p. 1293-304.
144. Sullivan-Reed, K., et al., *Simultaneous Targeting of PARP1 and RAD52 Triggers Dual Synthetic Lethality in BRCA-Deficient Tumor Cells*. *Cell Rep*, 2018. **23**(11): p. 3127-3136.
145. Boumahdi, S. and F.J. de Sauvage, *The great escape: tumour cell plasticity in resistance to targeted therapy*. *Nat Rev Drug Discov*, 2020. **19**(1): p. 39-56.
146. Sato, R., et al., *Concise Review: Stem Cells and Epithelial-Mesenchymal Transition in Cancer: Biological Implications and Therapeutic Targets*. *Stem Cells*, 2016. **34**(8): p. 1997-2007.
147. Shibue, T. and R.A. Weinberg, *EMT, CSCs, and drug resistance: the mechanistic link and clinical implications*. *Nat Rev Clin Oncol*, 2017. **14**(10): p. 611-629.
148. Singh, A. and J. Settleman, *EMT, cancer stem cells and drug resistance: an emerging axis of evil in the war on cancer*. *Oncogene*, 2010. **29**(34): p. 4741-51.
149. Zhu, D.J., et al., *Twist1 is a potential prognostic marker for colorectal cancer and associated with chemoresistance*. *Am J Cancer Res*, 2015. **5**(6): p. 2000-11.
150. Sun, L., et al., *HES1 Promotes Colorectal Cancer Cell Resistance To 5-Fu by Inducing Of EMT and ABC Transporter Proteins*. *J Cancer*, 2017. **8**(14): p. 2802-2808.
151. Francescangeli, F., et al., *A pre-existing population of ZEB2(+) quiescent cells with stemness and mesenchymal features dictate chemoresistance in colorectal cancer*. *J Exp Clin Cancer Res*, 2020. **39**(1): p. 2.
152. Li, N., et al., *An FBXW7-ZEB2 axis links EMT and tumour microenvironment to promote colorectal cancer stem cells and chemoresistance*. *Oncogenesis*, 2019. **8**(3): p. 13.
153. Tsoumas, D., et al., *ILK Expression in Colorectal Cancer Is Associated with EMT, Cancer Stem Cell Markers and Chemoresistance*. *Cancer Genomics Proteomics*, 2018. **15**(2): p. 127-141.
154. Papadaki, M.A., et al., *Circulating Tumor Cells with Stemness and Epithelial-to-Mesenchymal Transition Features Are Chemoresistant and Predictive of Poor Outcome in Metastatic Breast Cancer*. *Mol Cancer Ther*, 2019. **18**(2): p. 437-447.
155. Mabe, N.W., et al., *Epigenetic silencing of tumor suppressor Par-4 promotes chemoresistance in recurrent breast cancer*. *J Clin Invest*, 2018. **128**(10): p. 4413-4428.

156. Zhang, Y., et al., *Nestin overexpression in hepatocellular carcinoma associates with epithelial-mesenchymal transition and chemoresistance*. J Exp Clin Cancer Res, 2016. **35**(1): p. 111.
157. Sreekumar, R., et al., *Protein kinase C inhibitors override ZEB1-induced chemoresistance in HCC*. Cell Death Dis, 2019. **10**(10): p. 703.
158. Siebzehnrubl, F.A., et al., *The ZEB1 pathway links glioblastoma initiation, invasion and chemoresistance*. EMBO Mol Med, 2013. **5**(8): p. 1196-212.
159. Lin, Z., et al., *Chemotherapy-Induced Long Non-coding RNA 1 Promotes Metastasis and Chemoresistance of TSCC via the Wnt/beta-Catenin Signaling Pathway*. Mol Ther, 2018. **26**(6): p. 1494-1508.
160. Xie, S.L., et al., *SOX8 regulates cancer stem-like properties and cisplatin-induced EMT in tongue squamous cell carcinoma by acting on the Wnt/beta-catenin pathway*. Int J Cancer, 2018. **142**(6): p. 1252-1265.
161. Cai, J., et al., *Simultaneous overactivation of Wnt/beta-catenin and TGFbeta signalling by miR-128-3p confers chemoresistance-associated metastasis in NSCLC*. Nat Commun, 2017. **8**: p. 15870.
162. Venkatesha, V.A., et al., *Sensitization of pancreatic cancer stem cells to gemcitabine by Chk1 inhibition*. Neoplasia, 2012. **14**(6): p. 519-25.
163. Latifi, A., et al., *Isolation and characterization of tumor cells from the ascites of ovarian cancer patients: molecular phenotype of chemoresistant ovarian tumors*. PLoS One, 2012. **7**(10): p. e46858.
164. Alvero, A.B., et al., *Molecular phenotyping of human ovarian cancer stem cells unravels the mechanisms for repair and chemoresistance*. Cell Cycle, 2009. **8**(1): p. 158-66.
165. Latifi, A., et al., *Cisplatin treatment of primary and metastatic epithelial ovarian carcinomas generates residual cells with mesenchymal stem cell-like profile*. J Cell Biochem, 2011. **112**(10): p. 2850-64.
166. Gao, Y., et al., *Up-regulation of CD44 in the development of metastasis, recurrence and drug resistance of ovarian cancer*. Oncotarget, 2015. **6**(11): p. 9313-26.
167. Srivastava, A.K., et al., *Enhanced expression of DNA polymerase eta contributes to cisplatin resistance of ovarian cancer stem cells*. Proc Natl Acad Sci U S A, 2015. **112**(14): p. 4411-6.
168. Joyce, J.A., *Therapeutic targeting of the tumor microenvironment*. Cancer Cell, 2005. **7**(6): p. 513-20.
169. Liu, T., et al., *Cancer-associated fibroblasts: an emerging target of anti-cancer immunotherapy*. J Hematol Oncol, 2019. **12**(1): p. 86.
170. Ebbing, E.A., et al., *Stromal-derived interleukin 6 drives epithelial-to-mesenchymal transition and therapy resistance in esophageal adenocarcinoma*. Proc Natl Acad Sci U S A, 2019. **116**(6): p. 2237-2242.
171. Shintani, Y., et al., *IL-6 Secreted from Cancer-Associated Fibroblasts Mediates Chemoresistance in NSCLC by Increasing Epithelial-Mesenchymal Transition Signaling*. J Thorac Oncol, 2016. **11**(9): p. 1482-92.
172. Ham, I.H., et al., *Targeting interleukin-6 as a strategy to overcome stroma-induced resistance to chemotherapy in gastric cancer*. Mol Cancer, 2019. **18**(1): p. 68.
173. Wang, Y., et al., *IL-6 mediates platinum-induced enrichment of ovarian cancer stem cells*. JCI Insight, 2018. **3**(23).
174. Yan, H., B.Y. Guo, and S. Zhang, *Cancer-associated fibroblasts attenuate Cisplatin-induced apoptosis in ovarian cancer cells by promoting STAT3 signaling*. Biochem Biophys Res Commun, 2016. **470**(4): p. 947-54.
175. Izumi, D., et al., *TIAM1 promotes chemoresistance and tumor invasiveness in colorectal cancer*. Cell Death Dis, 2019. **10**(4): p. 267.
176. Tang, Y.A., et al., *Hypoxic tumor microenvironment activates GLI2 via HIF-1alpha and TGF-beta2 to promote chemoresistance in colorectal cancer*. Proc Natl Acad Sci U S A, 2018. **115**(26): p. E5990-E5999.
177. Lin, Y., J. Xu, and H. Lan, *Tumor-associated macrophages in tumor metastasis: biological roles and clinical therapeutic applications*. J Hematol Oncol, 2019. **12**(1): p. 76.
178. Baghdadi, M., et al., *Chemotherapy-Induced IL34 Enhances Immunosuppression by Tumor-Associated Macrophages and Mediates Survival of Chemoresistant Lung Cancer Cells*. Cancer Res, 2016. **76**(20): p. 6030-6042.
179. Yin, Y., et al., *The Immune-microenvironment Confers Chemoresistance of Colorectal Cancer through Macrophage-Derived IL6*. Clin Cancer Res, 2017. **23**(23): p. 7375-7387.
180. Kuwada, K., et al., *The epithelial-to-mesenchymal transition induced by tumor-associated macrophages confers chemoresistance in peritoneally disseminated pancreatic cancer*. J Exp Clin Cancer Res, 2018. **37**(1): p. 307.

181. Kim, J., J. Kim, and J.S. Bae, *ROS homeostasis and metabolism: a critical liaison for cancer therapy*. *Exp Mol Med*, 2016. **48**(11): p. e269.
182. Sun, X., et al., *SIRT5 Promotes Cisplatin Resistance in Ovarian Cancer by Suppressing DNA Damage in a ROS-Dependent Manner via Regulation of the Nrf2/HO-1 Pathway*. *Front Oncol*, 2019. **9**: p. 754.
183. Li, X., et al., *The SLC34A2-ROS-HIF-1-induced up-regulation of EZH2 expression promotes proliferation and chemo-resistance to apoptosis in colorectal cancer*. *Biosci Rep*, 2019. **39**(5).
184. Parekh, A., et al., *Multi-nucleated cells use ROS to induce breast cancer chemo-resistance in vitro and in vivo*. *Oncogene*, 2018. **37**(33): p. 4546-4561.
185. Schimmer, A.D., *Inhibitor of apoptosis proteins: translating basic knowledge into clinical practice*. *Cancer Res*, 2004. **64**(20): p. 7183-90.
186. Warren, C.F.A., M.W. Wong-Brown, and N.A. Bowden, *BCL-2 family isoforms in apoptosis and cancer*. *Cell Death Dis*, 2019. **10**(3): p. 177.
187. Han, B., et al., *Small-Molecule Bcl2 BH4 Antagonist for Lung Cancer Therapy*. *Cancer Cell*, 2015. **27**(6): p. 852-63.
188. Pepper, C., T. Hoy, and P. Bentley, *Elevated Bcl-2/Bax are a consistent feature of apoptosis resistance in B-cell chronic lymphocytic leukaemia and are correlated with in vivo chemoresistance*. *Leuk Lymphoma*, 1998. **28**(3-4): p. 355-61.
189. Sharifi, S., et al., *Roles of the Bcl-2/Bax ratio, caspase-8 and 9 in resistance of breast cancer cells to paclitaxel*. *Asian Pac J Cancer Prev*, 2014. **15**(20): p. 8617-22.
190. Braga, L.D.C., et al., *Apoptosis-related gene expression can predict the response of ovarian cancer cell lines to treatment with recombinant human TRAIL alone or combined with cisplatin*. *Clinics (Sao Paulo)*, 2020. **75**: p. e1492.
191. Bairey, O., et al., *Bcl-2, Bcl-X, Bax, and Bak expression in short- and long-lived patients with diffuse large B-cell lymphomas*. *Clin Cancer Res*, 1999. **5**(10): p. 2860-6.
192. Huang, J.Y., et al., *MicroRNA-650 was a prognostic factor in human lung adenocarcinoma and confers the docetaxel chemoresistance of lung adenocarcinoma cells via regulating Bcl-2/Bax expression*. *PLoS One*, 2013. **8**(8): p. e72615.
193. Liu, J.-b., et al., *A microRNA-4516 inhibitor sensitizes chemo-resistant gastric cancer cells to chemotherapy by upregulating ING4*. *RSC Advances*, 2018. **8**(66): p. 37795-37803.
194. Williams, J., et al., *Expression of Bcl-xL in ovarian carcinoma is associated with chemoresistance and recurrent disease*. *Gynecol Oncol*, 2005. **96**(2): p. 287-95.
195. Cheng, J., et al., *High PGAM5 expression induces chemoresistance by enhancing Bcl-xL-mediated anti-apoptotic signaling and predicts poor prognosis in hepatocellular carcinoma patients*. *Cell Death Dis*, 2018. **9**(10): p. 991.
196. Maji, S., et al., *STAT3- and GSK3beta-mediated Mcl-1 regulation modulates TPF resistance in oral squamous cell carcinoma*. *Carcinogenesis*, 2019. **40**(1): p. 173-183.
197. Dong, X., et al., *Elevated expression of BIRC6 protein in non-small-cell lung cancers is associated with cancer recurrence and chemoresistance*. *J Thorac Oncol*, 2013. **8**(2): p. 161-70.
198. Miyamoto, M., et al., *X-chromosome-linked inhibitor of apoptosis as a key factor for chemoresistance in clear cell carcinoma of the ovary*. *Br J Cancer*, 2014. **110**(12): p. 2881-6.
199. Nestal de Moraes, G., et al., *FOXO1 targets XIAP and Survivin to modulate breast cancer survival and chemoresistance*. *Cell Signal*, 2015. **27**(12): p. 2496-505.
200. Jeon, Y.K., et al., *Pellino-1 confers chemoresistance in lung cancer cells by upregulating cIAP2 through Lys63-mediated polyubiquitination*. *Oncotarget*, 2016. **7**(27): p. 41811-41824.
201. Augello, C., et al., *Inhibitors of apoptosis proteins (IAPs) expression and their prognostic significance in hepatocellular carcinoma*. *BMC Cancer*, 2009. **9**: p. 125.
202. Engel, K., et al., *USP9X stabilizes XIAP to regulate mitotic cell death and chemoresistance in aggressive B-cell lymphoma*. *EMBO Mol Med*, 2016. **8**(8): p. 851-62.
203. Yang, X.H., et al., *Co-expression of XIAP and CIAP1 Play Synergistic Effect on Patient's Prognosis in Head and Neck Cancer*. *Pathol Oncol Res*, 2019. **25**(3): p. 1111-1116.
204. Kampen, K.R., *Membrane proteins: the key players of a cancer cell*. *J Membr Biol*, 2011. **242**(2): p. 69-74.
205. Lin, C.Y., et al., *Membrane protein-regulated networks across human cancers*. *Nat Commun*, 2019. **10**(1): p. 3131.
206. Lazennec, G. and A. Richmond, *Chemokines and chemokine receptors: new insights into cancer-related inflammation*. *Trends Mol Med*, 2010. **16**(3): p. 133-44.
207. Aoudjit, F. and K. Vuori, *Integrin signaling in cancer cell survival and chemoresistance*. *Chemother Res Pract*, 2012. **2012**: p. 283181.

208. Du, Z. and C.M. Lovly, *Mechanisms of receptor tyrosine kinase activation in cancer*. Mol Cancer, 2018. **17**(1): p. 58.
209. Cerami, E., et al., *The cBio cancer genomics portal: an open platform for exploring multidimensional cancer genomics data*. Cancer Discov, 2012. **2**(5): p. 401-4.
210. Gao, J., et al., *Integrative analysis of complex cancer genomics and clinical profiles using the cBioPortal*. Sci Signal, 2013. **6**(269): p. p11.
211. Ouban, A., et al., *Expression and distribution of insulin-like growth factor-1 receptor in human carcinomas*. Human Pathology, 2003. **34**(8): p. 803-808.
212. Werner, H. and R. Sarfstein, *Transcriptional and epigenetic control of IGF1R gene expression: implications in metabolism and cancer*. Growth Horm IGF Res, 2014. **24**(4): p. 112-8.
213. LeRoith, D., et al., *Insulin-like growth factors*. Biol Signals, 1992. **1**(4): p. 173-81.
214. Siddle, K., *Molecular basis of signaling specificity of insulin and IGF receptors: neglected corners and recent advances*. Front Endocrinol (Lausanne), 2012. **3**: p. 34.
215. Siddle, K., *Signalling by insulin and IGF receptors: supporting acts and new players*. J Mol Endocrinol, 2011. **47**(1): p. R1-10.
216. Duan, C., *Specifying the cellular responses to IGF signals: roles of IGF-binding proteins*. J Endocrinol, 2002. **175**(1): p. 41-54.
217. Allard, J.B. and C. Duan, *IGF-Binding Proteins: Why Do They Exist and Why Are There So Many?* Front Endocrinol (Lausanne), 2018. **9**: p. 117.
218. Martin-Kleiner, I. and K. Gall Troselj, *Mannose-6-phosphate/insulin-like growth factor 2 receptor (M6P/IGF2R) in carcinogenesis*. Cancer Lett, 2010. **289**(1): p. 11-22.
219. De Meyts, P. and J. Whittaker, *Structural biology of insulin and IGF1 receptors: implications for drug design*. Nat Rev Drug Discov, 2002. **1**(10): p. 769-83.
220. Kavran, J.M., et al., *How IGF-1 activates its receptor*. Elife, 2014. **3**.
221. Li, J., et al., *Structural basis of the activation of type 1 insulin-like growth factor receptor*. Nat Commun, 2019. **10**(1): p. 4567.
222. Kato, H., et al., *Essential role of tyrosine residues 1131, 1135, and 1136 of the insulin-like growth factor-1 (IGF-1) receptor in IGF-1 action*. Mol Endocrinol, 1994. **8**(1): p. 40-50.
223. Iams, W.T. and C.M. Lovly, *Molecular Pathways: Clinical Applications and Future Direction of Insulin-like Growth Factor-1 Receptor Pathway Blockade*. Clin Cancer Res, 2015. **21**(19): p. 4270-7.
224. Brooks, P.C., et al., *Insulin-like growth factor receptor cooperates with integrin alpha v beta 5 to promote tumor cell dissemination in vivo*. J Clin Invest, 1997. **99**(6): p. 1390-8.
225. Fujita, M., et al., *Cross-talk between integrin alpha6beta4 and insulin-like growth factor-1 receptor (IGF1R) through direct alpha6beta4 binding to IGF1 and subsequent alpha6beta4-IGF1-IGF1R ternary complex formation in anchorage-independent conditions*. J Biol Chem, 2012. **287**(15): p. 12491-500.
226. Dalle, S., et al., *Insulin and insulin-like growth factor I receptors utilize different G protein signaling components*. J Biol Chem, 2001. **276**(19): p. 15688-95.
227. Sell, C., et al., *Effect of a null mutation of the insulin-like growth factor I receptor gene on growth and transformation of mouse embryo fibroblasts*. Mol Cell Biol, 1994. **14**(6): p. 3604-12.
228. Datta, S.R., et al., *Akt phosphorylation of BAD couples survival signals to the cell-intrinsic death machinery*. Cell, 1997. **91**(2): p. 231-41.
229. Yamaguchi, H. and H.G. Wang, *The protein kinase PKB/Akt regulates cell survival and apoptosis by inhibiting Bax conformational change*. Oncogene, 2001. **20**(53): p. 7779-86.
230. Cardone, M.H., et al., *Regulation of cell death protease caspase-9 by phosphorylation*. Science, 1998. **282**(5392): p. 1318-21.
231. Mayo, L.D. and D.B. Donner, *A phosphatidylinositol 3-kinase/Akt pathway promotes translocation of Mdm2 from the cytoplasm to the nucleus*. Proc Natl Acad Sci U S A, 2001. **98**(20): p. 11598-603.
232. Dupont, J., et al., *The insulin-like growth factor axis in cell cycle progression*. Horm Metab Res, 2003. **35**(11-12): p. 740-50.
233. Blume-Jensen, P. and T. Hunter, *Oncogenic kinase signalling*. Nature, 2001. **411**(6835): p. 355-65.
234. Zhang, D., et al., *Dual regulation of MMP-2 expression by the type 1 insulin-like growth factor receptor: the phosphatidylinositol 3-kinase/Akt and Raf/ERK pathways transmit opposing signals*. J Biol Chem, 2004. **279**(19): p. 19683-90.
235. Peeper, D.S., et al., *Ras signalling linked to the cell-cycle machinery by the retinoblastoma protein*. Nature, 1997. **386**(6621): p. 177-81.
236. Ueda, T., et al., *Mnk2 and Mnk1 are essential for constitutive and inducible phosphorylation of eukaryotic initiation factor 4E but not for cell growth or development*. Mol Cell Biol, 2004. **24**(15): p. 6539-49.

237. Ma, L., et al., *Phosphorylation and functional inactivation of TSC2 by Erk implications for tuberous sclerosis and cancer pathogenesis*. Cell, 2005. **121**(2): p. 179-93.
238. Roux, P.P., et al., *Tumor-promoting phorbol esters and activated Ras inactivate the tuberous sclerosis tumor suppressor complex via p90 ribosomal S6 kinase*. Proc Natl Acad Sci U S A, 2004. **101**(37): p. 13489-94.
239. Girnita, L., A. Girnita, and O. Larsson, *Mdm2-dependent ubiquitination and degradation of the insulin-like growth factor I receptor*. Proc Natl Acad Sci U S A, 2003. **100**(14): p. 8247-52.
240. Vecchione, A., et al., *The Grb10/Nedd4 complex regulates ligand-induced ubiquitination and stability of the insulin-like growth factor I receptor*. Mol Cell Biol, 2003. **23**(9): p. 3363-72.
241. Sehat, B., et al., *Role of ubiquitination in IGF-1 receptor signaling and degradation*. PLoS One, 2007. **2**(4): p. e340.
242. Patel, B.B., et al., *Curcumin enhances the effects of 5-fluorouracil and oxaliplatin in mediating growth inhibition of colon cancer cells by modulating EGFR and IGF-1R*. Int J Cancer, 2008. **122**(2): p. 267-73.
243. Qian, X., et al., *MicroRNA-143 inhibits tumor growth and angiogenesis and sensitizes chemosensitivity to oxaliplatin in colorectal cancers*. Cell Cycle, 2013. **12**(9): p. 1385-94.
244. Solomon-Zemler, R., R. Sarfstein, and H. Werner, *Nuclear insulin-like growth factor-1 receptor (IGF1R) displays proliferative and regulatory activities in non-malignant cells*. PLoS One, 2017. **12**(9): p. e0185164.
245. Aleksic, T., et al., *Nuclear IGF1R Interacts with Regulatory Regions of Chromatin to Promote RNA Polymerase II Recruitment and Gene Expression Associated with Advanced Tumor Stage*. Cancer Res, 2018. **78**(13): p. 3497-3509.
246. Codony-Servat, J., et al., *Nuclear IGF-1R predicts chemotherapy and targeted therapy resistance in metastatic colorectal cancer*. Br J Cancer, 2017. **117**(12): p. 1777-1786.
247. Ireland, L., et al., *Chemoresistance in Pancreatic Cancer Is Driven by Stroma-Derived Insulin-Like Growth Factors*. Cancer Res, 2016. **76**(23): p. 6851-6863.
248. Tommelein, J., et al., *Radiotherapy-Activated Cancer-Associated Fibroblasts Promote Tumor Progression through Paracrine IGF1R Activation*. Cancer Res, 2018. **78**(3): p. 659-670.
249. Sayer, R.A., et al., *High insulin-like growth factor-2 (IGF-2) gene expression is an independent predictor of poor survival for patients with advanced stage serous epithelial ovarian cancer*. Gynecol Oncol, 2005. **96**(2): p. 355-61.
250. Eckstein, N., et al., *Hyperactivation of the insulin-like growth factor receptor I signaling pathway is an essential event for cisplatin resistance of ovarian cancer cells*. Cancer Res, 2009. **69**(7): p. 2996-3003.
251. Huang, G.S., et al., *Insulin-like growth factor 2 expression modulates Taxol resistance and is a candidate biomarker for reduced disease-free survival in ovarian cancer*. Clin Cancer Res, 2010. **16**(11): p. 2999-3010.
252. Singh, R.K., et al., *IGF-1R inhibition potentiates cytotoxic effects of chemotherapeutic agents in early stages of chemoresistant ovarian cancer cells*. Cancer Lett, 2014. **354**(2): p. 254-62.
253. Singh, R.K., et al., *An active IGF-1R-AKT signaling imparts functional heterogeneity in ovarian CSC population*. Scientific Reports, 2016. **6**: p. 36612.
254. Oliva, C.R., et al., *IGFBP6 controls the expansion of chemoresistant glioblastoma through paracrine IGF2/IGF-1R signaling*. Cell Commun Signal, 2018. **16**(1): p. 61.
255. Verhagen, H.J., et al., *IGFBP7 induces apoptosis of acute myeloid leukemia cells and synergizes with chemotherapy in suppression of leukemia cell survival*. Cell Death Dis, 2014. **5**: p. e1300.
256. Lee, H.-Y., et al., *Insulin-like Growth Factor Binding Protein-3 Inhibits the Growth of Non-Small Cell Lung Cancer*. Cancer Research, 2002. **62**(12): p. 3530-3537.
257. Xu, D.D., et al., *The IGF2/IGF1R/Nanog Signaling Pathway Regulates the Proliferation of Acute Myeloid Leukemia Stem Cells*. Front Pharmacol, 2018. **9**: p. 687.
258. Bu, Y., et al., *Maintenance of stemness in oxaliplatin-resistant hepatocellular carcinoma is associated with increased autocrine of IGF1*. PLoS One, 2014. **9**(3): p. e89686.
259. Osuka, S., et al., *IGF1 receptor signaling regulates adaptive radioprotection in glioma stem cells*. Stem Cells, 2013. **31**(4): p. 627-40.
260. Harris, L.N., et al., *Predictors of resistance to preoperative trastuzumab and vinorelbine for HER2-positive early breast cancer*. Clin Cancer Res, 2007. **13**(4): p. 1198-207.
261. Gallardo, A., et al., *Increased signalling of EGFR and IGF1R, and deregulation of PTEN/PI3K/Akt pathway are related with trastuzumab resistance in HER2 breast carcinomas*. Br J Cancer, 2012. **106**(8): p. 1367-73.

262. Cornelissen, B., et al., *The level of insulin growth factor-1 receptor expression is directly correlated with the tumor uptake of (111)In-IGF-1(E3R) in vivo and the clonogenic survival of breast cancer cells exposed in vitro to trastuzumab (Herceptin)*. Nucl Med Biol, 2008. **35**(6): p. 645-53.
263. Oliveras-Ferreras, C., et al., *Pathway-focused proteomic signatures in HER2-overexpressing breast cancer with a basal-like phenotype: new insights into de novo resistance to trastuzumab (Herceptin)*. Int J Oncol, 2010. **37**(3): p. 669-78.
264. Huang, X., et al., *Heterotrimerization of the growth factor receptors erbB2, erbB3, and insulin-like growth factor-1 receptor in breast cancer cells resistant to herceptin*. Cancer Res, 2010. **70**(3): p. 1204-14.
265. Jia, Y., et al., *IGF-1R and ErbB3/HER3 contribute to enhanced proliferation and carcinogenesis in trastuzumab-resistant ovarian cancer model*. Biochem Biophys Res Commun, 2013. **436**(4): p. 740-5.
266. Yeo, C.D., et al., *Expression of insulin-like growth factor 1 receptor (IGF-1R) predicts poor responses to epidermal growth factor receptor (EGFR) tyrosine kinase inhibitors in non-small cell lung cancer patients harboring activating EGFR mutations*. Lung Cancer, 2015. **87**(3): p. 311-7.
267. Kato, Y., et al., *The role of IGF-1R in EGFR TKI resistance in NSCLC using IHC and AQUA technology*. Journal of Clinical Oncology, 2011. **29**(15\_suppl): p. 10556-10556.
268. Park, J.H., et al., *Activation of the IGF1R pathway potentially mediates acquired resistance to mutant-selective 3rd-generation EGF receptor tyrosine kinase inhibitors in advanced non-small cell lung cancer*. Oncotarget, 2016. **7**(16): p. 22005-15.
269. Guix, M., et al., *Acquired resistance to EGFR tyrosine kinase inhibitors in cancer cells is mediated by loss of IGF-binding proteins*. J Clin Invest, 2008. **118**(7): p. 2609-19.
270. Zhou, J., et al., *Implication of epithelial-mesenchymal transition in IGF1R-induced resistance to EGFR-TKIs in advanced non-small cell lung cancer*. Oncotarget, 2015. **6**(42): p. 44332-45.
271. Jameson, M.J., et al., *Activation of the insulin-like growth factor-1 receptor induces resistance to epidermal growth factor receptor antagonism in head and neck squamous carcinoma cells*. Mol Cancer Ther, 2011. **10**(11): p. 2124-34.
272. Choi, J., et al., *Bidirectional signaling between TM4SF5 and IGF1R promotes resistance to EGFR kinase inhibitors*. Lung Cancer, 2015. **90**(1): p. 22-31.
273. Cortot, A.B., et al., *Resistance to irreversible EGF receptor tyrosine kinase inhibitors through a multistep mechanism involving the IGF1R pathway*. Cancer Res, 2013. **73**(2): p. 834-43.
274. Leroy, C., et al., *Activation of IGF1R/p110beta/AKT/mTOR confers resistance to alpha-specific PI3K inhibition*. Breast Cancer Res, 2016. **18**(1): p. 41.
275. Scheffold, A., et al., *IGF1R as druggable target mediating PI3K-delta inhibitor resistance in a murine model of chronic lymphocytic leukemia*. Blood, 2019. **134**(6): p. 534-547.
276. Zorea, J., et al., *IGF1R upregulation confers resistance to isoform-specific inhibitors of PI3K in PIK3CA-driven ovarian cancer*. Cell Death Dis, 2018. **9**(10): p. 944.
277. Osher, E. and V.M. Macaulay, *Therapeutic Targeting of the IGF Axis*. Cells, 2019. **8**(8).
278. Ochnik, A.M. and R.C. Baxter, *Combination therapy approaches to target insulin-like growth factor receptor signaling in breast cancer*. Endocr Relat Cancer, 2016. **23**(11): p. R513-R536.
279. Di Maio, M. and G.V. Scagliotti, *The lesson learned from figitumumab clinical program and the hope for better results in squamous lung cancer*. Transl Lung Cancer Res, 2015. **4**(1): p. 15-7.
280. Bray, F., et al., *Global cancer statistics 2018: GLOBOCAN estimates of incidence and mortality worldwide for 36 cancers in 185 countries*. CA Cancer J Clin, 2018. **68**(6): p. 394-424.
281. Ferlay, J., et al., *Estimating the global cancer incidence and mortality in 2018: GLOBOCAN sources and methods*. Int J Cancer, 2019. **144**(8): p. 1941-1953.
282. Ferlay J, E.M., Lam F, Colombet M, Mery L, Piñeros M, Znaor A, Soerjomataram I, Bray F *Global Cancer Observatory: Cancer Today*. Lyon, France: International Agency for Research on Cancer. 2018 [cited 2020 28/03/2020]; Available from: <https://geo.iarc.fr/today>.
283. Testa, U., et al., *Ovarian Cancers: Genetic Abnormalities, Tumor Heterogeneity and Progression, Clonal Evolution and Cancer Stem Cells*. Medicines (Basel), 2018. **5**(1).
284. Duska, L.R. and E.C. Kohn, *The new classifications of ovarian, fallopian tube, and primary peritoneal cancer and their clinical implications*. Ann Oncol, 2017. **28**(suppl\_8): p. viii8-viii12.
285. Dochez, V., et al., *Biomarkers and algorithms for diagnosis of ovarian cancer: CA125, HE4, RMI and ROMA, a review*. J Ovarian Res, 2019. **12**(1): p. 28.
286. Mathieu, K.B., et al., *Screening for ovarian cancer: imaging challenges and opportunities for improvement*. Ultrasound Obstet Gynecol, 2018. **51**(3): p. 293-303.
287. Bhatla, N. and L. Denny, *FIGO Cancer Report 2018*. Int J Gynaecol Obstet, 2018. **143** Suppl 2: p. 2-3.

288. Cristea, M., et al., *Practical considerations in ovarian cancer chemotherapy*. Ther Adv Med Oncol, 2010. **2**(3): p. 175-87.
289. Luvero, D., A. Milani, and J.A. Ledermann, *Treatment options in recurrent ovarian cancer: latest evidence and clinical potential*. Ther Adv Med Oncol, 2014. **6**(5): p. 229-39.
290. Mittica, G., et al., *PARP Inhibitors in Ovarian Cancer*. Recent Pat Anticancer Drug Discov, 2018. **13**(4): p. 392-410.
291. Oza, A.M., et al., *Standard chemotherapy with or without bevacizumab for women with newly diagnosed ovarian cancer (ICON7): overall survival results of a phase 3 randomised trial*. Lancet Oncol, 2015. **16**(8): p. 928-36.
292. Raja, F.A., N. Chopra, and J.A. Ledermann, *Optimal first-line treatment in ovarian cancer*. Ann Oncol, 2012. **23 Suppl 10**: p. x118-27.
293. Zhang, Y., et al., *Inhibition of XIAP increases carboplatin sensitivity in ovarian cancer*. Onco Targets Ther, 2018. **11**: p. 8751-8759.
294. Goncharenko-Khaider, N., et al., *Ovarian cancer ascites increase Mcl-1 expression in tumor cells through ERK1/2-Elk-1 signaling to attenuate TRAIL-induced apoptosis*. Mol Cancer, 2012. **11**: p. 84.
295. Shigemasa, K., et al., *Increased MCL-1 expression is associated with poor prognosis in ovarian carcinomas*. Jpn J Cancer Res, 2002. **93**(5): p. 542-50.
296. Thakur, B. and P. Ray, *p53 Loses grip on PIK3CA expression leading to enhanced cell survival during platinum resistance*. Mol Oncol, 2016. **10**(8): p. 1283-95.
297. Thakur, B. and P. Ray, *Cisplatin triggers cancer stem cell enrichment in platinum-resistant cells through NF-kappaB-TNFalpha-PIK3CA loop*. J Exp Clin Cancer Res, 2017. **36**(1): p. 164.
298. Liefers-Visser, J.A.L., et al., *IGF system targeted therapy: Therapeutic opportunities for ovarian cancer*. Cancer Treat Rev, 2017. **60**: p. 90-99.
299. Werner, H., et al., *Structural and functional analysis of the insulin-like growth factor I receptor gene promoter*. Mol Endocrinol, 1992. **6**(10): p. 1545-58.
300. Yuen, J.S., et al., *The VHL tumor suppressor inhibits expression of the IGF1R and its loss induces IGF1R upregulation in human clear cell renal carcinoma*. Oncogene, 2007. **26**(45): p. 6499-508.
301. Renato Baserga, M.P.a.T.Y., *Chapter 6: IGF1R Signaling in Health and Disease*. Springer US, Molecular Biology Intelligence Unit, 2003. **1**: p. 104-120.
302. Pollak, M., *Insulin and insulin-like growth factor signalling in neoplasia*. Nat Rev Cancer, 2008. **8**(12): p. 915-28.
303. Werner, H., *Tumor suppressors govern insulin-like growth factor signaling pathways: implications in metabolism and cancer*. Oncogene, 2012. **31**(22): p. 2703-14.
304. Peruzzi, F., et al., *Multiple signaling pathways of the insulin-like growth factor I receptor in protection from apoptosis*. Mol Cell Biol, 1999. **19**(10): p. 7203-15.
305. Yuan, J., et al., *Function of insulin-like growth factor I receptor in cancer resistance to chemotherapy*. Oncol Lett, 2018. **15**(1): p. 41-47.
306. Denduluri, S.K., et al., *Insulin-like growth factor (IGF) signaling in tumorigenesis and the development of cancer drug resistance*. Genes Dis, 2015. **2**(1): p. 13-25.
307. Cooke, D.W., et al., *Analysis of the human type I insulin-like growth factor receptor promoter region*. Biochem Biophys Res Commun, 1991. **177**(3): p. 1113-20.
308. Mamula, P.W. and I.D. Goldfine, *Cloning and characterization of the human insulin-like growth factor-I receptor gene 5'-flanking region*. DNA Cell Biol, 1992. **11**(1): p. 43-50.
309. Nikoshkov, A., et al., *Epigenetic DNA methylation in the promoters of the Igf1 receptor and insulin receptor genes in db/db mice*. Epigenetics, 2011. **6**(4): p. 405-9.
310. Meyer, K.F., et al., *The fetal programming effect of prenatal smoking on Igf1r and Igf1 methylation is organ- and sex-specific*. Epigenetics, 2017. **12**(12): p. 1076-1091.
311. Schayek, H., et al., *Progression to metastatic stage in a cellular model of prostate cancer is associated with methylation of the androgen receptor gene and transcriptional suppression of the insulin-like growth factor-I receptor gene*. Exp Cell Res, 2010. **316**(9): p. 1479-88.
312. Ola, R., et al., *S-Adenosylmethionine - induced cytotoxicity in glioblastoma cells does not affect the IGF-1R methylation*. Revista Romana de Medicina de Laborator, 2010. **18**.
313. Abramovitch, S., et al., *BRCA1-Sp1 interactions in transcriptional regulation of the IGF-1R gene*. FEBS Letters, 2003. **541**(1-3): p. 149-154.
314. Liu, B., D. Li, and Y.F. Guan, *BRCA1 regulates insulin-like growth factor I receptor levels in ovarian cancer*. Oncol Lett, 2014. **7**(5): p. 1733-1737.
315. Maor, S.B., et al., *BRCA1 suppresses insulin-like growth factor-I receptor promoter activity: potential interaction between BRCA1 and Sp1*. Mol Genet Metab, 2000. **69**(2): p. 130-6.
316. Maor, S., et al., *Elevated insulin-like growth factor-I receptor (IGF-1R) levels in primary breast tumors associated with BRCA1 mutations*. Cancer Lett, 2007. **257**(2): p. 236-43.

317. Schayek, H., et al., *Tumor suppressor BRCA1 is expressed in prostate cancer and controls insulin-like growth factor I receptor (IGF-IR) gene transcription in an androgen receptor-dependent manner.* Clin Cancer Res, 2009. **15**(5): p. 1558-65.
318. Amichay, K., et al., *BRCA1 is expressed in uterine serous carcinoma (USC) and controls insulin-like growth factor I receptor (IGF-IR) gene expression in USC cell lines.* Int J Gynecol Cancer, 2012. **22**(5): p. 748-54.
319. Yuen, J.S., et al., *Validation of the type I insulin-like growth factor receptor as a therapeutic target in renal cancer.* Mol Cancer Ther, 2009. **8**(6): p. 1448-59.
320. Werner, H., et al., *Increased expression of the insulin-like growth factor I receptor gene, IGF1R, in Wilms tumor is correlated with modulation of IGF1R promoter activity by the WT1 Wilms tumor gene product.* Proc Natl Acad Sci U S A, 1993. **90**(12): p. 5828-32.
321. Werner, H., et al., *Wild-type and mutant p53 differentially regulate transcription of the insulin-like growth factor I receptor gene.* Proc Natl Acad Sci U S A, 1996. **93**(16): p. 8318-23.
322. Abramovitch, S. and H. Werner, *Functional and physical interactions between BRCA1 and p53 in transcriptional regulation of the IGF-IR gene.* Horm Metab Res, 2003. **35**(11-12): p. 758-62.
323. Idelman, G., et al., *WT1-p53 interactions in insulin-like growth factor-I receptor gene regulation.* J Biol Chem, 2003. **278**(5): p. 3474-82.
324. Maor, S., et al., *Estrogen receptor regulates insulin-like growth factor-I receptor gene expression in breast tumor cells: involvement of transcription factor Sp1.* J Endocrinol, 2006. **191**(3): p. 605-12.
325. Aiello, A., et al., *HMGAI protein is a positive regulator of the insulin-like growth factor-I receptor gene.* Eur J Cancer, 2010. **46**(10): p. 1919-26.
326. Schayek, H., et al., *Transcription factor E2F1 is a potent transactivator of the insulin-like growth factor-I receptor (IGF-IR) gene.* Growth Horm IGF Res, 2010. **20**(1): p. 68-72.
327. Rubinstein, M., et al., *Transcriptional activation of the insulin-like growth factor I receptor gene by the Kruppel-like factor 6 (KLF6) tumor suppressor protein: potential interactions between KLF6 and p53.* Endocrinology, 2004. **145**(8): p. 3769-77.
328. Huo, X., et al., *GSK3 protein positively regulates type I insulin-like growth factor receptor through forkhead transcription factors FOXO1/3/4.* J Biol Chem, 2014. **289**(36): p. 24759-70.
329. Karnieli, E., et al., *The IGF-I receptor gene promoter is a molecular target for the Ewing's sarcoma-Wilms' tumor I fusion protein.* J Biol Chem, 1996. **271**(32): p. 19304-9.
330. Finkelton, I., et al., *Transcriptional regulation of IGF-I receptor gene expression by novel isoforms of the EWS-WT1 fusion protein.* Oncogene, 2002. **21**(12): p. 1890-8.
331. Werner, H., et al., *A novel EWS-WT1 gene fusion product in desmoplastic small round cell tumor is a potent transactivator of the insulin-like growth factor-I receptor (IGF-IR) gene.* Cancer Lett, 2007. **247**(1): p. 84-90.
332. Meisel Sharon, S., et al., *TMPRSS2-ERG fusion protein regulates insulin-like growth factor-I receptor (IGF1R) gene expression in prostate cancer: involvement of transcription factor Sp1.* Oncotarget, 2016. **7**(32): p. 51375-51392.
333. Mancarella, C., et al., *ERG deregulation induces IGF-1R expression in prostate cancer cells and affects sensitivity to anti-IGF-1R agents.* Oncotarget, 2015. **6**(18): p. 16611-22.
334. Ayalon, D., T. Glaser, and H. Werner, *Transcriptional regulation of IGF-I receptor gene expression by the PAX3-FKHR oncoprotein.* Growth Horm IGF Res, 2001. **11**(5): p. 289-97.
335. Shahrabani-Gargir, L., T.K. Pandita, and H. Werner, *Ataxia-telangiectasia mutated gene controls insulin-like growth factor I receptor gene expression in a deoxyribonucleic acid damage response pathway via mechanisms involving zinc-finger transcription factors Sp1 and WT1.* Endocrinology, 2004. **145**(12): p. 5679-87.
336. Kogai, T., et al., *Retinoic acid induces sodium/iodide symporter gene expression and radioiodide uptake in the MCF-7 breast cancer cell line.* Proc Natl Acad Sci U S A, 2000. **97**(15): p. 8519-24.
337. Cunningham, L., et al., *Identification of benzodiazepine Ro5-3335 as an inhibitor of CBF leukemia through quantitative high throughput screen against RUNX1-CBFbeta interaction.* Proc Natl Acad Sci U S A, 2012. **109**(36): p. 14592-7.
338. Gilmour, J., et al., *The Co-operation of RUNX1 with LDB1, CDK9 and BRD4 Drives Transcription Factor Complex Relocation During Haematopoietic Specification.* Scientific Reports, 2018. **8**(1): p. 10410.
339. Knezevic, K., et al., *A Runx1-Smad6 rheostat controls Runx1 activity during embryonic hematopoiesis.* Mol Cell Biol, 2011. **31**(14): p. 2817-26.
340. Pencovich, N., et al., *Dynamic combinatorial interactions of RUNX1 and cooperating partners regulates megakaryocytic differentiation in cell line models.* Blood, 2011. **117**(1): p. e1-14.
341. Sood, R., Y. Kamikubo, and P. Liu, *Role of RUNX1 in hematological malignancies.* Blood, 2017. **129**(15): p. 2070-2082.

342. Riggio, A.I. and K. Blyth, *The enigmatic role of RUNX1 in female-related cancers - current knowledge & future perspectives*. FEBS J, 2017. **284**(15): p. 2345-2362.
343. Keita, M., et al., *Global methylation profiling in serous ovarian cancer is indicative for distinct aberrant DNA methylation signatures associated with tumor aggressiveness and disease progression*. Gynecol Oncol, 2013. **128**(2): p. 356-63.
344. Keita, M., et al., *The RUNX1 transcription factor is expressed in serous epithelial ovarian carcinoma and contributes to cell proliferation, migration and invasion*. Cell Cycle, 2013. **12**(6): p. 972-86.
345. Ge, T., et al., *MicroRNA-302b Suppresses Human Epithelial Ovarian Cancer Cell Growth by Targeting RUNX1*. Cellular Physiology and Biochemistry, 2014. **34**(6): p. 2209-2220.
346. Choi, A., et al., *RUNX1 is required for oncogenic Myb and Myc enhancer activity in T-cell acute lymphoblastic leukemia*. Blood, 2017. **130**(15): p. 1722-1733.
347. Debaize, L., et al., *Interplay between transcription regulators RUNX1 and FUBP1 activates an enhancer of the oncogene c-KIT and amplifies cell proliferation*. Nucleic Acids Res, 2018. **46**(21): p. 11214-11228.
348. Wang, L., J.S. Brugge, and K.A. Janes, *Intersection of FOXO- and RUNX1-mediated gene expression programs in single breast epithelial cells during morphogenesis and tumor progression*. Proc Natl Acad Sci U S A, 2011. **108**(40): p. E803-12.
349. Wildey, G.M. and P.H. Howe, *Runx1 is a co-activator with FOXO3 to mediate transforming growth factor beta (TGFbeta)-induced Bim transcription in hepatic cells*. J Biol Chem, 2009. **284**(30): p. 20227-39.
350. Wang, X., S. Hu, and L. Liu, *Phosphorylation and acetylation modifications of FOXO3a: Independently or synergistically?* Oncol Lett, 2017. **13**(5): p. 2867-2872.
351. Gaikwad, S.M., et al., *Differential activation of NF-kappaB signaling is associated with platinum and taxane resistance in MyD88 deficient epithelial ovarian cancer cells*. Int J Biochem Cell Biol, 2015. **61**: p. 90-102.
352. Tzivion, G., M. Dobson, and G. Ramakrishnan, *FoxO transcription factors; Regulation by AKT and 14-3-3 proteins*. Biochim Biophys Acta, 2011. **1813**(11): p. 1938-45.
353. Bao, J., et al., *Integrated high-throughput analysis identifies super enhancers associated with chemoresistance in SCLC*. BMC Med Genomics, 2019. **12**(1): p. 67.
354. Vera-Ramirez, L., et al., *Transcriptional shift identifies a set of genes driving breast cancer chemoresistance*. PLoS One, 2013. **8**(1): p. e53983.
355. Sharma, S.V., et al., *A chromatin-mediated reversible drug-tolerant state in cancer cell subpopulations*. Cell, 2010. **141**(1): p. 69-80.
356. Shang, S., et al., *Chemotherapy-Induced Distal Enhancers Drive Transcriptional Programs to Maintain the Chemoresistant State in Ovarian Cancer*. Cancer Res, 2019. **79**(18): p. 4599-4611.
357. Dallas, N.A., et al., *Chemoresistant colorectal cancer cells, the cancer stem cell phenotype, and increased sensitivity to insulin-like growth factor-I receptor inhibition*. Cancer Res, 2009. **69**(5): p. 1951-7.
358. Sun, Y., et al., *Role of insulin-like growth factor-1 signaling pathway in cisplatin-resistant lung cancer cells*. Int J Radiat Oncol Biol Phys, 2012. **82**(3): p. e563-72.
359. Bielen, A., et al., *Dependence of Wilms tumor cells on signaling through insulin-like growth factor I in an orthotopic xenograft model targetable by specific receptor inhibition*. Proc Natl Acad Sci U S A, 2012. **109**(20): p. E1267-76.
360. Rochester, M.A., et al., *Silencing of the IGF1R gene enhances sensitivity to DNA-damaging agents in both PTEN wild-type and mutant human prostate cancer*. Cancer Gene Therapy, 2005. **12**(1): p. 90-100.
361. Zorea, J., et al., *IGF1R upregulation confers resistance to isoform-specific inhibitors of PI3K in PIK3CA-driven ovarian cancer*. Cell Death & Disease, 2018. **9**(10): p. 944.
362. Bookman, M.A., et al., *Evaluation of monoclonal humanized anti-HER2 antibody, trastuzumab, in patients with recurrent or refractory ovarian or primary peritoneal carcinoma with overexpression of HER2: a phase II trial of the Gynecologic Oncology Group*. J Clin Oncol, 2003. **21**(2): p. 283-90.
363. Sarfstein, R., A. Belfiore, and H. Werner, *Identification of Insulin-Like Growth Factor-I Receptor (IGF-IR) Gene Promoter-Binding Proteins in Estrogen Receptor (ER)-Positive and ER-Depleted Breast Cancer Cells*. Cancers (Basel), 2010. **2**(2): p. 233-61.
364. Wang, G., et al., *Knockdown of SOX18 inhibits the proliferation, migration and invasion of hepatocellular carcinoma cells*. Oncol Rep, 2015. **34**(3): p. 1121-8.
365. Zhang, J., et al., *Suppression of SOX18 by siRNA inhibits cell growth and invasion of breast cancer cells*. Oncol Rep, 2016. **35**(6): p. 3721-7.

366. Rahmoun, M., et al., *In mammalian foetal testes, SOX9 regulates expression of its target genes by binding to genomic regions with conserved signatures*. *Nucleic Acids Res*, 2017. **45**(12): p. 7191-7211.
367. Jenkins, C.R., et al., *Collaboration Between RUNX and NOTCH Pathways in T-Cell Acute Lymphoblastic Leukemia*. *Blood*, 2012. **120**(21): p. 1279-1279.
368. Rubin, M., et al., *9-Cis retinoic acid inhibits growth of breast cancer cells and down-regulates estrogen receptor RNA and protein*. *Cancer Res*, 1994. **54**(24): p. 6549-56.
369. Scheitz, C.J.F., et al., *Defining a tissue stem cell-driven Runx1/Stat3 signalling axis in epithelial cancer*. *The EMBO Journal*, 2012. **31**(21): p. 4124-4139.
370. Li, Q., et al., *RUNX1 promotes tumour metastasis by activating the Wnt/ $\beta$ -catenin signalling pathway and EMT in colorectal cancer*. *Journal of Experimental & Clinical Cancer Research*, 2019. **38**(1): p. 334.
371. Chandarlapaty, S., et al., *AKT inhibition relieves feedback suppression of receptor tyrosine kinase expression and activity*. *Cancer Cell*, 2011. **19**(1): p. 58-71.
372. Rodrik-Outmezguine, V.S., et al., *mTOR kinase inhibition causes feedback-dependent biphasic regulation of AKT signaling*. *Cancer Discov*, 2011. **1**(3): p. 248-59.
373. Chakrabarty, A., et al., *Feedback upregulation of HER3 (ErbB3) expression and activity attenuates antitumor effect of PI3K inhibitors*. *Proc Natl Acad Sci U S A*, 2012. **109**(8): p. 2718-23.
374. el-Roeiy, A., et al., *Expression of insulin-like growth factor-I (IGF-I) and IGF-II and the IGF-I, IGF-II, and insulin receptor genes and localization of the gene products in the human ovary*. *J Clin Endocrinol Metab*, 1993. **77**(5): p. 1411-8.
375. Baumgarten, S.C., et al., *IGFIR Expression in Ovarian Granulosa Cells Is Essential for Steroidogenesis, Follicle Survival, and Fertility in Female Mice*. *Endocrinology*, 2017. **158**(7): p. 2309-2318.
376. Ipsa, E., et al., *Growth Hormone and Insulin-Like Growth Factor Action in Reproductive Tissues*. *Front Endocrinol (Lausanne)*, 2019. **10**: p. 777.
377. He, T., et al., *Comprehensive assessment the expression of core elements related to IGFIR/PI3K pathway in granulosa cells of women with polycystic ovary syndrome*. *Eur J Obstet Gynecol Reprod Biol*, 2019. **233**: p. 134-140.
378. Amutha, P. and T. Rajkumar, *Role of Insulin-like Growth Factor, Insulin-like Growth Factor Receptors, and Insulin-like Growth Factor-binding Proteins in Ovarian Cancer*. *Indian J Med Paediatr Oncol*, 2017. **38**(2): p. 198-206.
379. King, S.M., et al., *Insulin and insulin-like growth factor signaling increases proliferation and hyperplasia of the ovarian surface epithelium and decreases follicular integrity through upregulation of the PI3-kinase pathway*. *J Ovarian Res*, 2013. **6**(1): p. 12.
380. Coppola, D., et al., *The insulin-like growth factor 1 receptor induces transformation and tumorigenicity of ovarian mesothelial cells and down-regulates their Fas-receptor expression*. *Cancer Res*, 1999. **59**(13): p. 3264-70.
381. Hsu, C.F., et al., *IGF-axis confers transformation and regeneration of fallopian tube fimbria epithelium upon ovulation*. *EBioMedicine*, 2019. **41**: p. 597-609.
382. Beck, E.P., et al., *Identification of insulin and insulin-like growth factor I (IGF I) receptors in ovarian cancer tissue*. *Gynecol Oncol*, 1994. **53**(2): p. 196-201.
383. Yee, D., et al., *Expression of insulin-like growth factor I, its binding proteins, and its receptor in ovarian cancer*. *Cancer Res*, 1991. **51**(19): p. 5107-12.
384. Alsina-Sanchis, E., et al., *The TGF $\beta$  pathway stimulates ovarian cancer cell proliferation by increasing IGFIR levels*. *Int J Cancer*, 2016. **139**(8): p. 1894-903.
385. Koti, M., et al., *Identification of the IGF1/PI3K/NF kappaB/ERK gene signalling networks associated with chemotherapy resistance and treatment response in high-grade serous epithelial ovarian cancer*. *BMC Cancer*, 2013. **13**: p. 549.
386. Beltran, P.J., et al., *Ganitumab (AMG 479) inhibits IGF-II-dependent ovarian cancer growth and potentiates platinum-based chemotherapy*. *Clin Cancer Res*, 2014. **20**(11): p. 2947-58.
387. Browne, B.C., et al., *Inhibition of IGFIR activity enhances response to trastuzumab in HER-2-positive breast cancer cells*. *Ann Oncol*, 2011. **22**(1): p. 68-73.
388. Fiszman, G.L. and M.A. Jasnis, *Molecular Mechanisms of Trastuzumab Resistance in HER2 Overexpressing Breast Cancer*. *Int J Breast Cancer*, 2011. **2011**: p. 352182.
389. Shan, J., et al., *Nanog regulates self-renewal of cancer stem cells through the insulin-like growth factor pathway in human hepatocellular carcinoma*. *Hepatology*, 2012. **56**(3): p. 1004-14.
390. Leong, H.S., et al., *Targeting cancer stem cell plasticity through modulation of epidermal growth factor and insulin-like growth factor receptor signaling in head and neck squamous cell cancer*. *Stem Cells Transl Med*, 2014. **3**(9): p. 1055-65.

391. Hart, L.S., et al., *Human colon cancer stem cells are enriched by insulin-like growth factor-1 and are sensitive to figitumumab*. *Cell Cycle*, 2011. **10**(14): p. 2331-8.
392. Farabaugh, S.M., et al., *IGF1R constitutive activation expands luminal progenitors and influences lineage differentiation during breast tumorigenesis*. *Dev Biol*, 2020. **463**(1): p. 77-87.
393. Zhang, S., et al., *Identification and characterization of ovarian cancer-initiating cells from primary human tumors*. *Cancer Res*, 2008. **68**(11): p. 4311-20.
394. Hu, L., C. McArthur, and R.B. Jaffe, *Ovarian cancer stem-like side-population cells are tumourigenic and chemoresistant*. *Br J Cancer*, 2010. **102**(8): p. 1276-83.
395. Bapat, S.A., et al., *Stem and progenitor-like cells contribute to the aggressive behavior of human epithelial ovarian cancer*. *Cancer Res*, 2005. **65**(8): p. 3025-9.
396. Abdullah, L.N. and E.K. Chow, *Mechanisms of chemoresistance in cancer stem cells*. *Clin Transl Med*, 2013. **2**(1): p. 3.
397. Maugeri-Sacca, M., P. Vigneri, and R. De Maria, *Cancer stem cells and chemosensitivity*. *Clin Cancer Res*, 2011. **17**(15): p. 4942-7.
398. Li, F., et al., *Beyond tumorigenesis: cancer stem cells in metastasis*. *Cell Res*, 2007. **17**(1): p. 3-14.
399. Kim, D.K., et al., *Crucial role of HMGAI in the self-renewal and drug resistance of ovarian cancer stem cells*. *Exp Mol Med*, 2016. **48**: p. e255.
400. Liao, J., et al., *Ovarian cancer spheroid cells with stem cell-like properties contribute to tumor generation, metastasis and chemotherapy resistance through hypoxia-resistant metabolism*. *PLoS One*, 2014. **9**(1): p. e84941.
401. Eyre, R., et al., *Reversing paclitaxel resistance in ovarian cancer cells via inhibition of the ABCB1 expressing side population*. *Tumour Biol*, 2014. **35**(10): p. 9879-92.
402. Abubaker, K., et al., *Short-term single treatment of chemotherapy results in the enrichment of ovarian cancer stem cell-like cells leading to an increased tumor burden*. *Mol Cancer*, 2013. **12**: p. 24.
403. Wiechert, A., et al., *Cisplatin induces stemness in ovarian cancer*. *Oncotarget*, 2016. **7**(21): p. 30511-22.
404. Bellio, C., et al., *PARP Inhibition Induces Enrichment of DNA Repair-Proficient CD133 and CD117 Positive Ovarian Cancer Stem Cells*. *Mol Cancer Res*, 2019. **17**(2): p. 431-445.
405. Crudden, C., A. Girnita, and L. Girnita, *Targeting the IGF-1R: The Tale of the Tortoise and the Hare*. *Front Endocrinol (Lausanne)*, 2015. **6**: p. 64.
406. Masoud, V. and G. Pages, *Targeted therapies in breast cancer: New challenges to fight against resistance*. *World J Clin Oncol*, 2017. **8**(2): p. 120-134.
407. Imamura, Y. and M.D. Sadar, *Androgen receptor targeted therapies in castration-resistant prostate cancer: Bench to clinic*. *Int J Urol*, 2016. **23**(8): p. 654-65.
408. Cidre-Aranaz, F. and J. Alonso, *EWS/FLI1 Target Genes and Therapeutic Opportunities in Ewing Sarcoma*. *Front Oncol*, 2015. **5**: p. 162.
409. Bushweller, J.H., *Targeting transcription factors in cancer - from undruggable to reality*. *Nat Rev Cancer*, 2019. **19**(11): p. 611-624.
410. Chen, Y., et al., *Lentivirus-mediated short-hairpin RNA targeting IGF-1R inhibits growth and lymphangiogenesis in breast cancer*. *Oncol Rep*, 2012. **28**(5): p. 1778-84.
411. Greer, A.H., et al., *Knockdown of core binding factor beta alters sphingolipid metabolism*. *J Cell Physiol*, 2013. **228**(12): p. 2350-64.
412. V., R. *Doubling Time Computing*. 2006 [cited 2020; Available from: <http://www.doubling-time.com/compute.php>].
413. Deo, A., et al., *IGF1R predicts better survival in high-grade serous epithelial ovarian cancer patients and correlates with hCtr1 levels*. *Biomark Med*, 2019. **13**(7): p. 511-521.
414. Fedchenko, N. and J. Reifenrath, *Different approaches for interpretation and reporting of immunohistochemistry analysis results in the bone tissue - a review*. *Diagn Pathol*, 2014. **9**: p. 221.
415. Larsson, O., A. Girnita, and L. Girnita, *Role of insulin-like growth factor 1 receptor signalling in cancer*. *British Journal of Cancer*, 2005. **92**(12): p. 2097-2101.
416. Chitnis, M.M., et al., *The type 1 insulin-like growth factor receptor pathway*. *Clin Cancer Res*, 2008. **14**(20): p. 6364-70.
417. Muranen, T., et al., *Inhibition of PI3K/mTOR leads to adaptive resistance in matrix-attached cancer cells*. *Cancer Cell*, 2012. **21**(2): p. 227-39.
418. Chen, W.J., et al., *Cancer-associated fibroblasts regulate the plasticity of lung cancer stemness via paracrine signalling*. *Nat Commun*, 2014. **5**: p. 3472.
419. Xu, C., et al., *beta-Catenin/POU5F1/SOX2 transcription factor complex mediates IGF-1 receptor signaling and predicts poor prognosis in lung adenocarcinoma*. *Cancer Res*, 2013. **73**(10): p. 3181-9.

420. Kuo, Y.C., et al., *IGF-1R Promotes Symmetric Self-Renewal and Migration of Alkaline Phosphatase(+) Germ Stem Cells through HIF-2 $\alpha$ -OCT4/CXCR4 Loop under Hypoxia*. Stem Cell Reports, 2018. **10**(2): p. 524-537.
421. Cheng, C.L., et al., *CXCL14 Maintains hESC Self-Renewal through Binding to IGF-1R and Activation of the IGF-1R Pathway*. Cells, 2020. **9**(7).
422. Wang, X.H., et al., *IGF1R facilitates epithelial-mesenchymal transition and cancer stem cell properties in neuroblastoma via the STAT3/AKT axis*. Cancer Manag Res, 2019. **11**: p. 5459-5472.
423. Chang, W.W., et al., *The expression and significance of insulin-like growth factor-1 receptor and its pathway on breast cancer stem/progenitors*. Breast Cancer Res, 2013. **15**(3): p. R39.
424. Crudden, C., et al., *Below the Surface: IGF-1R Therapeutic Targeting and Its Endocytic Journey*. Cells, 2019. **8**(10).
425. Suleymanova, N., et al., *Functional antagonism of beta-arrestin isoforms balance IGF-1R expression and signalling with distinct cancer-related biological outcomes*. Oncogene, 2017. **36**(41): p. 5734-5744.
426. Zheng, H., et al., *beta-Arrestin-biased agonism as the central mechanism of action for insulin-like growth factor 1 receptor-targeting antibodies in Ewing's sarcoma*. Proc Natl Acad Sci U S A, 2012. **109**(50): p. 20620-5.
427. Bareja, A., et al., *Understanding the mechanism of bias signaling of the insulin-like growth factor 1 receptor: Effects of LL37 and HASF*. Cell Signal, 2018. **46**: p. 113-119.
428. Yang, E., et al., *Bad, a heterodimeric partner for Bcl-XL and Bcl-2, displaces Bax and promotes cell death*. Cell, 1995. **80**(2): p. 285-91.
429. Kale, J., E.J. Osterlund, and D.W. Andrews, *BCL-2 family proteins: changing partners in the dance towards death*. Cell Death Differ, 2018. **25**(1): p. 65-80.
430. Iavarone, C., et al., *Combined MEK and BCL-2/XL Inhibition Is Effective in High-Grade Serous Ovarian Cancer Patient-Derived Xenograft Models and BIM Levels Are Predictive of Responsiveness*. Mol Cancer Ther, 2019. **18**(3): p. 642-655.
431. Yang, Y., et al., *Reversing platinum resistance in ovarian cancer multicellular spheroids by targeting Bcl-2*. Onco Targets Ther, 2019. **12**: p. 897-906.
432. Galante, J.M., et al., *ERK/BCL-2 pathway in the resistance of pancreatic cancer to anoikis*. J Surg Res, 2009. **152**(1): p. 18-25.
433. Wang, C., et al., *Up-regulation of Bcl-2 by CD147 Through ERK Activation Results in Abnormal Cell Survival in Human Endometriosis*. J Clin Endocrinol Metab, 2015. **100**(7): p. E955-63.
434. Boucher, M.J., et al., *MEK/ERK signaling pathway regulates the expression of Bcl-2, Bcl-X(L), and Mcl-1 and promotes survival of human pancreatic cancer cells*. J Cell Biochem, 2000. **79**(3): p. 355-69.
435. Vitagliano, O., et al., *The Bcl-2/Bax and Ras/Raf/MEK/ERK signaling pathways: implications in pediatric leukemia pathogenesis and new prospects for therapeutic approaches*. Expert Rev Hematol, 2013. **6**(5): p. 587-97.
436. Nicol, B., et al., *RUNX1 maintains the identity of the fetal ovary through an interplay with FOXL2*. Nat Commun, 2019. **10**(1): p. 5116.
437. Ge, T., et al., *MicroRNA-302b suppresses human epithelial ovarian cancer cell growth by targeting RUNX1*. Cell Physiol Biochem, 2014. **34**(6): p. 2209-20.
438. Taniuchi, I., M. Osato, and Y. Ito, *Runx1: no longer just for leukemia*. EMBO J, 2012. **31**(21): p. 4098-9.
439. Luo, M.C., et al., *Runt-related Transcription Factor 1 (RUNX1) Binds to p50 in Macrophages and Enhances TLR4-triggered Inflammation and Septic Shock*. J Biol Chem, 2016. **291**(42): p. 22011-22020.
440. Werner, H., R. Sarfstein, and I. Bruchim, *Investigational IGF1R inhibitors in early stage clinical trials for cancer therapy*. Expert Opin Investig Drugs, 2019. **28**(12): p. 1101-1112.
441. Dolgin, E., *IGF-1R drugs travel from cancer cradle to Graves'*. Nat Biotechnol, 2020. **38**(4): p. 385-388.
442. Klein, U., *Resolving PI3K-delta inhibitor resistance in CLL*. Blood, 2019. **134**(6): p. 496-498.

**Re-Prints of Publications**



# Decoding molecular interplay between RUNX1 and FOXO3a underlying the pulsatile IGF1R expression during acquirement of chemoresistance

Ajit C. Dhadve<sup>a,c</sup>, Kishore Hari<sup>d</sup>, Bharat Rekhi<sup>e</sup>, Mohit Kumar Jolly<sup>d</sup>, Abhijit De<sup>b,c</sup>, Pritha Ray<sup>a,c,\*</sup>

<sup>a</sup> Imaging Cell Signaling & Therapeutics Lab, Advanced Centre for Treatment, Research and Education in Cancer, Tata Memorial Centre, Kharghar, Navi Mumbai, India

<sup>b</sup> Molecular Functional Imaging Lab, Advanced Centre for Treatment, Research and Education in Cancer, Tata Memorial Centre, Kharghar, Navi Mumbai, India

<sup>c</sup> Homi Bhabha National Institute, Anushakti Nagar, Mumbai, India

<sup>d</sup> Centre for BioSystems Science and Engineering, Indian Institute of Science, Bengaluru, India

<sup>e</sup> Tata Memorial Hospital, Dr. E Borges Road, Parel, Mumbai, Maharashtra, India

## ARTICLE INFO

### Keywords:

IGF1R regulation  
RUNX1  
FOXO3a  
Chemoresistance  
Ovarian Cancer

## ABSTRACT

Hyperactive Insulin like growth factor-1-receptor (IGF1R) signalling is associated with development of therapy resistance in many cancers. We recently reported a pulsatile nature of IGF1R during acquirement of platinum-taxol resistance in Epithelial Ovarian Cancer (EOC) cells and a therapy induced upregulation in IGF1R expression in tumors of a small cohort of high grade serous EOC patients. Here, we report Runt-related transcription factor 1 (RUNX1) as a novel transcriptional regulator which along with another known regulator Forkhead Box O3 (FOXO3a), drives the dynamic modulation of IGF1R expression during platinum-taxol resistance development in EOC cells. RUNX1-FOXO3a cooperatively bind to IGF1R promoter and produce a transcriptional surge during onset of resistance and such co-operativity falls apart when cells attain maximal resistance resulting in decreased IGF1R expression. The intriguing descending trend in IGF1R and FOXO3a expressions is caused by a Protein Kinase B (AKT)-FOXO3a negative feedback loop exclusively present in the highly resistant cells eliciting the pulsatile behaviour of IGF1R and FOXO3a. *In vivo* molecular imaging revealed that RUNX1 inhibition causes significant attenuation of the IGF1R promoter activity, decreased tumorigenicity and enhanced drug sensitivity of tumors of early resistant cells. Altogether our findings delineate a dynamic interplay between several molecular regulators driving pulsatile IGF1R expression and identify a new avenue for targeting EOC through RUNX1-IGF1R axis during acquirement of chemoresistance.

## 1. Introduction

Aberrant regulatory gene networks are instrumental drivers of tumorigenesis and are adaptive to rewire during therapy resistance development. The fundamental dynamic nature of acquired resistance is driven by oscillatory signalling cascades. We recently reported a pulsatile nature of Insulin like growth factor-1-receptor (IGF1R) during acquirement of platinum-taxol resistance in Epithelial Ovarian Cancer (EOC) cells [1]. The increased IGF1R expression at the onset of resistance plays an integral role in maintenance of drug resistance, cancer stem cells and tumorigenicity, while cells that achieved complete and irreversible resistance possess low level of IGF1R indicating active IGF1R signalling might be dispensable at late stages of resistance [1,2]. Drug induced enhancement of IGF1R expression was also observed in a small cohort of advanced stage high grade serous EOC patients after 3–4 cycles of platinum-taxol treatment [1]. A subset of these patients

having higher IGF1R expression at metastatic sites showed better overall survival and disease free survival and a positive correlation with the platinum transporter gene, human copper transporter 1 (hCtr1) than those with lower IGF1R expression [1,3]. To date, the underlying mechanisms behind this undulating IGF1R expression during progression of resistance that points towards a complex regulatory circuit has not been deciphered.

Association of dysregulated IGF1R signalling *via* phosphatidylinositol-3-kinase catalytic subunit alpha (PIK3CA)/protein kinase B (AKT) and mitogen-activated protein kinase (MAPK)/extracellular signal-regulated kinase (ERK) pathways is well established in oncogenic transformation, proliferation and chemoresistance [4,5]. Activating mutations in IGF1R are rare in incidence while copy number amplification has been found in 3–6% cases of sarcoma, EOC, breast, oesophageal and stomach adenocarcinoma [6,7]. Intriguingly, transcriptional activation of IGF1R without any significant change in copy

\* Corresponding author at: Imaging Cell Signaling & Therapeutics Lab, Advanced Centre for Treatment, Research and Education in Cancer, Tata Memorial Centre, Kharghar, Navi Mumbai, India.

E-mail address: [pray@actrec.gov.in](mailto:pray@actrec.gov.in) (P. Ray).

<https://doi.org/10.1016/j.bbadis.2020.165754>

Received 9 October 2019; Received in revised form 11 February 2020; Accepted 28 February 2020

Available online 03 March 2020

0925-4439/ © 2020 Elsevier B.V. All rights reserved.

number, is a common feature for many cancers [8–10] signifying existence of an intricate transcriptional regulation. The complex promoter activity is either regulated directly by specificity protein 1 (SP1), E2F transcription factor 1 (E2F1), Wilms tumor protein 1 (WT1), Runt-related transcription factor 1 (RUNX1) and Forkhead Box O3 (FOXO3a) or in conjunction with SP1 to induce {estrogen receptor alpha (ER $\alpha$ ), Krueppel-like factor 6 (KLF6) and high mobility group AT-hook 1 (HMGA1)} or repress {breast cancer type 1 susceptibility protein (BRCA1), tumor protein p53 (TP53) and Von Hippel–Lindau tumor suppressor (VHL)} IGF1R expression in variety of cancer cells in different circumstances [11–13]. Epigenetic regulation of this GC-rich promoter is seldom reported with conspicuous absence of methylation by S-adenosylmethionine (SAM), a methyl donor agent in glioblastoma cells and in benign and metastatic prostate cancer cells [14,15].

Despite strong association between IGF1R expression and therapy resistance in several cancers including EOC [16–21], therapeutic intervention targeting IGF1R did not meet success due to strong homology with insulin receptor and shared modulators [22]. Since acquirement of chemoresistance remains a clinical obstacle for EOC treatment, comprehending the principal molecular network underlying IGF1R signalling in therapy resistant cancer cells might lead to better therapeutic targets.

Here, for the first time we report RUNX1 as a unique regulator of IGF1R promoter which exerts a nonlinear cooperative interaction with FOXO3a and dynamically modulate IGF1R expression during acquirement of chemoresistance in EOC cells. Genetic and pharmacological inhibition followed by chromatin immunoprecipitation (ChIP) and ChIP-re-ChIP assay revealed that RUNX1 strengthened FOXO3a occupancy on IGF1R promoter, leading to a transcriptional surge during initiation of resistance which is lost at the late stages due to presence of an exclusive AKT-FOXO3a negative feedback loop. Perturbation of RUNX1 activity severely compromised IGF1R promoter activity and sensitized the tumors of early resistant cells to platinum-taxol treatment, as monitored by non-invasive imaging. The observed cooperative action of two critical transcriptional regulators (RUNX1 and FOXO3a) to regulate an important (IGF1R) signalling pathway predicts a new avenue for targeting EOC through RUNX1-IGF1R axis during acquirement of chemoresistance.

## 2. Materials and methods

### 2.1. Reagents and antibodies

Cisplatin, paclitaxel, G418, all-trans retinoic acid (ATRA),  $\beta$ -actin,  $\alpha$ -tubulin, anti-mouse and anti-rabbit tagged with horseradish peroxidase (HRP) were purchased from Sigma-Aldrich (USA). IGF1R- $\beta$ , p-S413-FOXO3a, p-S473-AKT and FOXO3a antibodies were procured from CST (CA, USA) and Novus biologicals (CO, USA). RUNX1, Lamin-A, Ki67, p-S253-FOXO3a were purchased from Abcam (UK). Ro5-3335 and Akt inhibitor IV were purchased from Merck Millipore (NJ, USA).

MC7f, core binding factor beta (CBF $\beta$ ) knock down A2780-platinum-taxol resistant model, A2780 and OAW42 platinum taxol resistant models were cultured as described earlier. The models were categorized into sensitive cells (parental), cisplatin-paclitaxel early resistant cells (dual<sup>ER</sup>), and cisplatin-paclitaxel late resistant cells (dual<sup>LR</sup>) stages based on their resistant indices [1].

### 2.2. Construction of IGF1R-promoter-reporter sensor, deletion and SDM plasmids

IGF1R-promoter-reporter construct was procured from Genecopoeia (MD, USA) and cloned upstream of Firefly Luciferase 2-Tandem Dimeric Tomato (FL2-TDT) or humanised Renilla Luciferase-enhanced Green Fluorescent Protein (hRL-eGFP) bi-fusion reporter protein separately in pCDNA 3.1 vector. FOXO3a response element mutants were made by site directed mutagenesis (SDM) in hRL-eGFP background and labelled

as  $\Delta$ -S1 (FOXO3a-Site1),  $\Delta$ -S2 (FOXO3a-Site2) and  $\Delta$ -S1-S2 (FOXO3a-Site1-2).

### 2.3. Promoter binding transcription factor profile plate array

A promoter-binding transcription factor (TF) profiling plate array-II, commercially available from Signosis (USA) was used to identify probable binders in nuclear lysate of A2780-dual<sup>ER</sup> cells following the manufacturer's instruction.

### 2.4. Transfection and luciferase reporter assay

All the transient and stable transfections with wild type/mutant IGF1R-promoter-reporter, human sodium iodide symporter (h-NIS)-promoter-reporter and cytomegalovirus (CMV)-beta-galactosidase ( $\beta$ gal)/CMV-FL2 (normalization vectors) were performed following previous protocols [23].

### 2.5. Immunofluorescence and western blotting

Immunofluorescence was performed for RUNX1, FOXO3a, p-S413-FOXO3a and p-S253-FOXO3 antibodies and images were acquired using Carl Zeiss, LSM 780 microscope. Mean fluorescence intensity value from entire nucleus of an individual cell and a minimum of 30 cells were quantified for each group using ImageJ software [1]. Whole cell, nuclear and cytosolic lysates were prepared as described earlier [24] and western blotting was performed for IGF1R- $\beta$ , FOXO3a, p-S253-FOXO3a, AKT, p-S413-AKT, RUNX1, Lamin-A and  $\alpha$ -tubulin [1,23].

### 2.6. Co-immunoprecipitation assay (Co-IP)

Nuclear cell pellets were prepared using nuclear-cytoplasmic fractionation procedure as described earlier [24] and nuclear cell lysates for immunoprecipitation (IP) were prepared in IP lysis buffer (20 mM Tris, pH 7.5, 150 mM NaCl, 1 mM EDTA, 1 mM EGTA, 1% NP-40) with protease inhibitors. Cell lysates (500  $\mu$ g) were incubated overnight at 4 °C with 10  $\mu$ g of anti-RUNX1 antibody in IP lysis buffer containing protein G-sepharose beads. The immune complexes were collected by centrifugation and washed four times in IP lysis buffer and eluted in 2  $\times$  Laemmli buffer. The presence of RUNX1 and FOXO3a in the Co-IP complexes was detected by western blotting using VeriBlot detection reagent (HRP) from Abcam (UK), which only recognize native (non-reduced) antibodies thereby minimizing detection of heavy and light chains if Co-IP complex is fully reduced.

### 2.7. Chromatin immunoprecipitation assay

ChIP was performed using 25  $\mu$ g chromatin with either RUNX1 or FOXO3a specific antibody following earlier protocol [23]. For ChIP-re-ChIP, 50  $\mu$ g of sonicated DNA was immunoprecipitated with one antibody (either RUNX1 or FOXO3a) and 1/4th of precipitated chromatin was reverse-crosslinked and processed for real time-polymerase chain reaction (RT-PCR). Rest was used for second round of immunoprecipitation with the other antibody [25] and analysed by RT-PCR. Non-immunoprecipitated chromatin was used as input control. A schematic diagram for the protocol of ChIP-re-ChIP is presented in Supplementary Fig. 1.

### 2.8. Quantitative real-time PCR

RT-PCR was performed using SYBR Green (Invitrogen) using appropriate gene specific primers (Supplementary Table 1) and Glyceraldehyde 3-phosphate dehydrogenase (GAPDH) was used for normalization [1].

## 2.9. CBF $\beta$ silencing by lentiviral mediated sh-RNA constructs

CBF $\beta$ - knock down lentiviral cassette was developed using a target sequence against CBF $\beta$  (5'-CCGCGAGTGTGAGATTAAGTA-3') [26]. A2780, A2780-dual<sup>ER</sup> and A2780-dual<sup>LR</sup> cells were transduced with lentiviruses and stable cells were FACS sorted using eGFP as a marker [2].

## 2.10. Cell cytotoxicity, clonogenic and soft agar assay

Cytotoxicity {3-(4,5-dimethylthiazol-2-yl)-2,5-diphenyl tetrazolium bromide (MTT)} and clonogenic assays for Ro5-3335 alone or in combinations with cisplatin-paclitaxel were performed following published protocols [1,24].

Soft agar assays were performed by plating single cell suspensions of various groups (500 cells/well of six-well dish) in 0.5% upper layer of low melting agarose in complete media. Resultant colonies after 7 days were counted using inverted microscope.

## 2.11. Bioluminescence imaging

All experiments were approved by the Institutional Animal Ethics Committee at ACTREC.  $4 \times 10^6$  cells of A2780-dual<sup>ER</sup> cells stably expressing IGF1R-Fl2-TDT construct were subcutaneously injected in female non-obese diabetic-severe combined immunodeficient (NOD-SCID) mice and were followed for tumor growth. Animals were imaged at day 15 and divided into four groups (n = 4/each), group-I: control, group-II: cisplatin-paclitaxel, group-III: Ro5-3335 and group-IV: Ro5-3335 + cisplatin-paclitaxel. Group III and IV received 2 mg/kg Ro5-3335 for 5 days intravenously (day 15–day 19). On day 20 Group II and IV received a single dose of 2 mg/kg-cisplatin + 1 mg/kg-paclitaxel intraperitoneally. For CBF $\beta$ -KD *in-vivo* study,  $4 \times 10^6$  cells of A2780-Cis-Pac-ER and the CBF $\beta$ -KD counterpart stably expressing IGF1R-Fl2-TDT were subcutaneously injected on upper and lower flanks of five female NOD-SCID mice. Animals were treated with 2 mg/kg-cisplatin + 1 mg/kg-paclitaxel twice (day 35 and day 45) by intraperitoneal injection. Bioluminescence imaging and subsequent quantification was performed using Xenogen-IVIS and Living Image software 4.4 [2].

## 2.12. Immunohistochemistry

Antigen retrieval for Ki67 and IGF1R was carried out in microwave at high power for 20 min, while that same for FOXO3a was done by boiling the slides in pressure cooker for 6 min. For both cases sodium citrate buffer (pH 6) was used. Staining was performed using IHC detection kit (Abcam, UK) [3] and scored by an expert pathologist. The immunoreactivity score (IRS) was calculated using the formula: intensity  $\times$  extent of positivity [27].

## 2.13. Statistical analysis

All the data represent the mean  $\pm$  SEM of at least three independent experiments and were analysed for significance using unpaired Student's *t*-test. *p* value  $\leq$  0.05 was considered as significant. Pearson's correlation coefficient test was used to calculate the correlation between Ki-67, IGF1R, FOXO3a IRS scores from IHC and tumor viability.

## 3. Results

### 3.1. RUNX1 acts as novel regulator of IGF1R during development of chemoresistance

Our previous results showed an association of dynamic modulation in IGF1R gene expression with acquirement of chemoresistance in

cisplatin-paclitaxel resistant cellular models developed in A2780 and OAW42 EOC cells, which were categorized into early (ER) and late (LR) resistant stages based on their resistance indices [1]. To identify the underlying molecular players, activity of a 1503 bp long IGF1R promoter driving a fusion reporter (FL2-TDT or hRL-eGFP) were tested and observed to be maximal at ER-stages compared to the respective sensitive and LR-stages in A2780 and OAW42 models (Supplementary Fig. S2A–C). Next, nine putative transcriptional regulators were identified by screening a promoter binding TF-plate-array from nuclear extracts of A2780-dual<sup>ER</sup> cells (Fig. 1A) that comprised of retinoid X receptor (RXR), SRY-Box transcription factor 9 (SOX9), vitamin D receptor (VDR), growth factor independent 1 transcriptional repressor (GFI1), retinoic acid receptor-related orphan receptor (ROR), SP1, RUNX1, NK2 homeobox 5 (NKX2.5) and SRY-box transcription factor 9 (SOX18) whose predicted binding motifs were found throughout the GC-rich IGF1R promoter using JASPAR database (probability score > 75%) (Fig. 1B and Table 1). Identification of SP1 as a binder and TATA-box binding transcription factor IID (TFIID) as a non-binder (IGF1R promoter lacks TATA-box) strengthened the promoter binding TF-plate-array data.

To validate the identified candidates, we employed an inducer/inhibitor based approach and treated ER-cells with Retinoic acid (RA) derivative to assess potential of RXR, ROR and VDR proteins in IGF1R regulation. RXR, ROR and VDR belong to superfamily of nuclear-receptors that homo/hetero-dimerize upon activation with RA/RA-derivatives and bind to RA response elements. No change in IGF1R-promoter or hNIS-promoter (a known RA target) [28] activity was observed in A2780 and A2780-dual<sup>ER</sup> cells treated with all-trans-RA (ATRA). However, ATRA could upregulate NIS-promoter in agreement with earlier report [29,30] but downregulated IGF1R-promoter in MCF-7 cells (Supplementary Fig. S2D–E) indicating inability of RXR, ROR and VDR in direct regulation of IGF1R promoter in our chemoresistant model.

Enhanced stabilization and DNA binding ability of RUNX1 requires hetero-dimerization with CBF $\beta$  co-factor which can be interrupted by a small molecule, Ro5-3335 [31]. While RUNX1 mRNA, protein and nuclear localization were enhanced in both stages of resistance (Fig. 1C–H), Ro5-3335 reduced IGF1R-promoter-reporter activity and transcript levels maximally in A2780-dual<sup>ER</sup> and OAW42-dual<sup>ER</sup> cells (Fig. 1I–K). Ro5-3335 dose was carefully selected after performing MTT assays (IC<sub>80–70</sub> at 200  $\mu$ M for A2780 and IC<sub>80–70</sub> at 20  $\mu$ M for OAW42 cells) (Supplementary Fig. S2F–G) which showed little toxicity but significant reduction in the promoter activity. Interestingly, among the four predicted response elements (Fig. 1B), specific binding of RUNX1 was observed only on sites 1 and 2 but not on sites 3–4 (Fig. 1L).

Though RUNX1 occupancy on IGF1R promoter remained comparable across the resistance stages, the effect of Ro5-3335 was more profound in ER-cells indicating possible involvement of other positive regulator/s. Intriguingly, RUNX1 binding sites were found to be in close proximity of FOXO3a response elements (Fig. 1B), a known regulator which was not represented in the TF-array. The RUNX family members are known to interact and enhance DNA binding affinity of other transcription factors [32]. We hypothesize that RUNX1 and FOXO3a might collectively control IGF1R expression during development of chemoresistance in EOC cells.

### 3.2. FOXO3a and RUNX1 cooperatively and positively regulate IGF1R promoter at the onset of resistance

The early resistant cells were found to possess enhanced nuclear localization of both total and activated (p-S413) FOXO3a (Fig. 2A–E). Mutating FOXO3a response elements at S1( $\Delta$ -S1)/S2( $\Delta$ -S2) individually or together decreased IGF1R promoter activity by 3.4 and 2.8 fold in A2780-dual<sup>ER</sup> and OAW42-dual<sup>ER</sup> cells respectively (Fig. 2G–H). ChIP assay showed highest occupancy of FOXO3a on S1 and S2 sites of IGF1R promoter (0.1235% and 0.2534% respectively) in A2780-dual<sup>ER</sup> cells

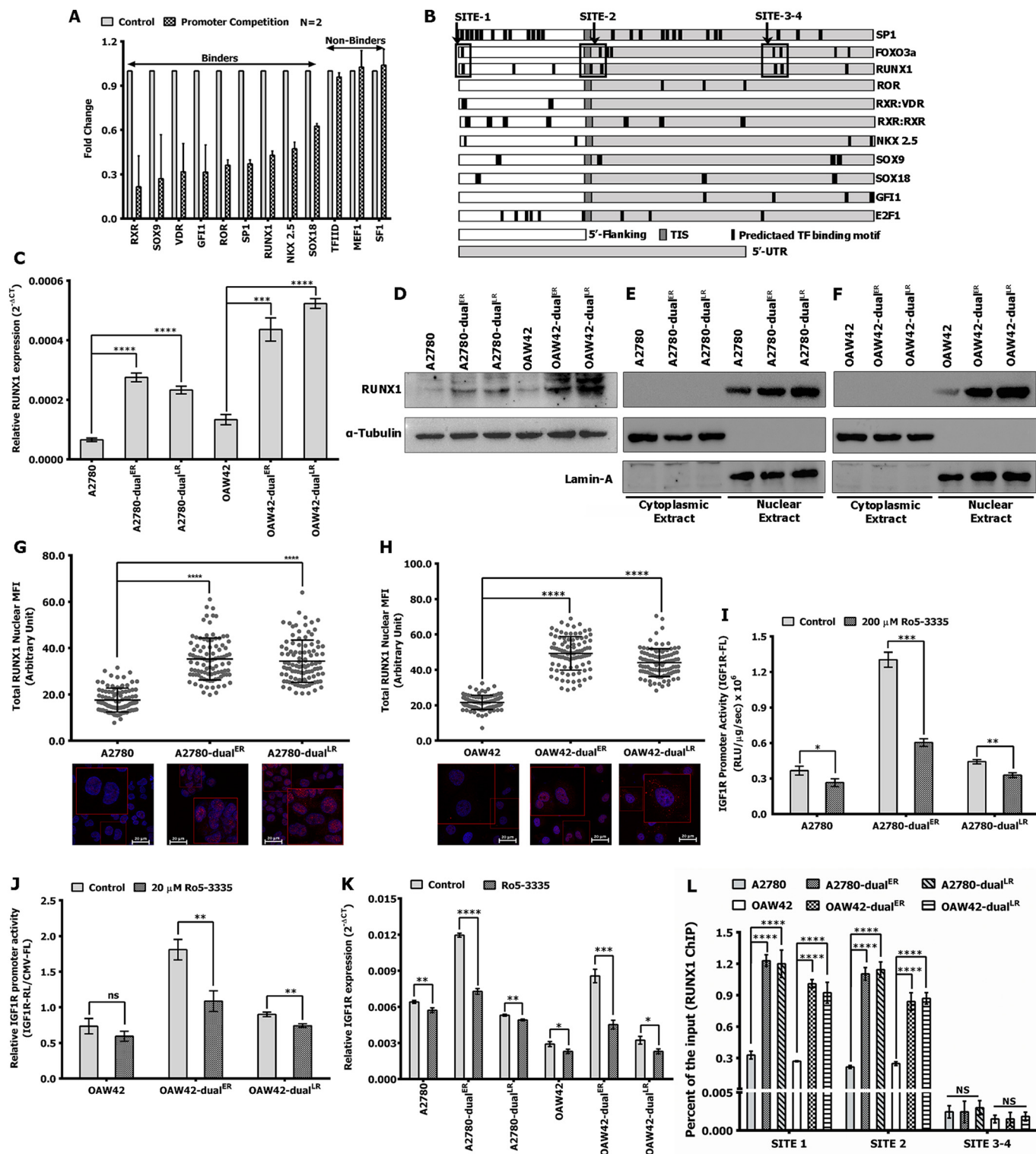


Fig. 1. RUNX1 positively regulates IGF1R promoter in A2780 and OAW42 dual resistant models.

A. Graphical representation of the identified IGF1R promoter binders and non-binders from TF-plate-array. B. Schematic representation of the predicted binding sites of the TFs on IGF1R promoter as predicted by JASPAR-TF database (threshold > 75%). C–H. Real-time PCR, immunoblot and immunofluorescence shows increased expression and increased nuclear localization of RUNX1 in A2780-dual<sup>ER</sup>/A2780-dual<sup>LR</sup>/OAW42-dual<sup>ER</sup>/OAW42-dual<sup>LR</sup> cells. I–K. Ro5-3335 (A2780 = 200  $\mu$ M and OAW42 = 20  $\mu$ M) reduced IGF1R-promoter activity and transcript levels in parental as well as chemoresistant cells with maximal effect in ER-cells. L. ChIP shows increased binding of RUNX1 to IGF1R promoter on S1 and S2 but not on S3–4 in A2780-dual<sup>ER</sup>/A2780-dual<sup>LR</sup>/OAW42-dual<sup>ER</sup>/OAW42-dual<sup>LR</sup> cells (values were plotted as % binding of RUNX1 compared to input-DNA). \*p  $\leq$  0.05, \*\*p  $\leq$  0.01, \*\*\*p  $\leq$  0.001, \*\*\*\*p  $\leq$  0.0001.

**Table 1**

Number of the predicted binding sites of the TFs on IGF1R promoter as predicted by JASPAR-TF database (threshold > 75%).

Number of binding sites for TFs on IGF1R promoter			
TF name	Number of binding sites	TF name	Number of binding sites
RXR:RXR	7	RUNX1	8
RXR:ROR	2	NKX2.5	4
SOX9	4	SOX18	3
GF11	4	FOXO3a	8
ROR	3	E2F1	9
SP1	25	TFIID	0

which dropped below 0.05% in both A2780 and A2780-dual<sup>LR</sup> cells. Similarly, percent occupancy of FOXO3a on both the sites was higher in OAW42-dual<sup>ER</sup> cells compared to OAW42 and OAW42-dual<sup>LR</sup> cells (Fig. 2F).

Since RUNX1 inhibition or mutation at FOXO3a response elements led to suboptimal decrease in IGF1R promoter activity, combinatorial effect for both these molecular alterations were tested in the models. IGF1R promoter activity was further reduced to 7.1 and 5.3 fold when compared to RUNX1 inhibition (2.0 and 2.1 fold) alone or mutant-promoter (2.8 and 2.3 fold) in A2780-dual<sup>ER</sup> and OAW42-dual<sup>ER</sup> cells respectively with minimal reduction in sensitive and LR cells (Fig. 2I–J). These results indicate that RUNX1 cooperates with FOXO3a to orchestrate a transcriptional surge for IGF1R at the onset of resistance development in EOC cell lines.

### 3.3. RUNX1 dictates FOXO3a binding to IGF1R promoter at the onset of resistance

The master regulator RUNX1 can influence the transcriptional dynamics through sequential or concurrent binding to its interacting partners. To assess whether RUNX1 and FOXO3a exist as complex in the A2780 cellular model of resistance, Co-IP of FOXO3a along with RUNX1 was performed from all the stages. A significant interaction of FOXO3a to RUNX1 was observed only in the ER cells despite of incremented level of RUNX1 with increasing resistance (Fig. 3A). This data indicates that both FOXO3a and RUNX1 can exist as a complex and ER cells possess highest amount of such complex.

Since both FOXO3a and RUNX1 possess DNA binding ability in their own capacity and in complementation with other transcriptional modulators, we aimed to understand the kinetics of cooperativity between RUNX1 and FOXO3a for IGF1R promoter occupancy. ChIP-re-ChIP assay (Supplementary Fig. 1) was performed in both combinations *i.e.*, RUNX1-FOXO3a-ChIP or FOXO3a-RUNX1-ChIP in A2780-dual-resistant model. Both the factors were able to co-occupy the IGF1R promoter at sensitive and all stages of resistance, though the occupancy differed for each of them. RUNX1 conferred a much stronger binding in both early and late resistant cells, while FOXO3a binding was preferentially higher in early and almost negligible in late resistant cells (Fig. 3B–I).

Though concurrent binding of RUNX1 and FOXO3a were evident from ChIP-re-ChIP, the occupancy of FOXO3a on S1 and S2 decreased 4.5-fold and 5.4-fold respectively after Ro5-3555 treatment only in A2780-dual<sup>ER</sup> cells, while percent occupancy on S1 and S2 remained unchanged in A2780 and A2780-dual<sup>LR</sup> cells. Similarly, FOXO3a occupancy on both sites were decreased in OAW42-dual<sup>ER</sup> cells in presence of Ro5-3555 (Fig. 3J–K).

To further confirm that the cooperative interaction of RUNX1 and FOXO3a on IGF1R regulation occurs exclusively at the onset of resistance, CBF $\beta$  gene was silenced in A2780 chemoresistant model. Silencing of CBF $\beta$  (Supplementary Fig. S3A) significantly attenuated IGF1R transcripts and promoter activity as well as the  $\Delta$ -S1-S2-mutant-IGF1R-promoter only in A2780-dual<sup>ER</sup> cells compared to their

counterparts (Supplementary Fig. S3B–C, Fig. 3M). The further attenuation in  $\Delta$ -S1-S2-mutant-IGF1R-promoter activity in CBF $\beta$ -KD cells may be due to presence of low level of active RUNX1 protein pool (since knocking down of CBF $\beta$  was unable to produce a complete ~100% reduction in active RUNX1-CBF $\beta$  pool). Binding of FOXO3a was significantly affected in CBF $\beta$ -KD-A2780-dual<sup>ER</sup> cells (4.0-fold and 7.9-fold drop on S1 and S2 respectively). However, FOXO3a binding on those sites remained unchanged for CBF $\beta$ -KD-A2780 and CBF $\beta$ -KD-A2780-dual<sup>LR</sup> cells (Fig. 3L). Real time expression analysis showed negligible levels of RUNX2 but high levels of RUNX3 at different stages of both the A2780 and OAW42 models. Following the similar trend of RUNX1, RUNX3 expression was maximal at late resistant stages (Supplementary Fig. 3D).

### 3.4. AKT-FOXO3a negative feedback loop influences IGF1R expression in late-resistant cells

Given the pulsatile dynamics of IGF1R and FOXO3a (Fig. 2E), we hypothesized that there can be a negative feedback loop operating either directly or indirectly on both IGF1R and FOXO3a. Such roles of negative feedback loops in enabling pulsatile behaviour have already proposed earlier [33,34]. A literature search revealed the possibility of such a negative feedback loop to FOXO3a mediated by AKT, where FOXO3a can activate AKT, which, in turn, can promote FOXO3a degradation by phosphorylation of the S253 residue [35]. Interestingly, a mathematical model developed to represent these interactions strengthened the proposed crucial role of AKT-FOXO3a negative feedback loop in enabling IGF1R pulsatile dynamics (Fig. 4A–C & Supplementary Fig. 4). Integration of both transcriptional and epigenetic regulators in the model showed that an AKT-FOXO3a negative feedback loop is indeed crucial to generate the pulsatile dynamics (Supplementary Fig. 5).

Following the model predictions, we looked at the post-translational modifications which are known to control the stability of FOXO3a [35]. The late resistant cells are characterised by high level of activated AKT [1]. Indeed phospho-S253-FOXO3a (a nuclear export and degradation mark) levels increased gradually with increasing resistance, peaking at late stages in both the cellular models (Fig. 4D–E). In serum deprived media, decreased phospho-S473-AKT levels were associated with loss of phospho-S253-FOXO3a in both A2780-dual<sup>ER</sup> and dual<sup>LR</sup> cells but increase in total FOXO3a was observed only in A2780-dual<sup>LR</sup> cells. Insulin stimulation in serum starved cells restored phospho-S473-AKT levels causing increased phospho-S253-FOXO3a and decreased total FOXO3a levels in both A2780-dual<sup>ER</sup> and dual<sup>LR</sup> cells (Fig. 4F). Finally, AKT inhibition using an AKT inhibitor (AKT-IV) increased FOXO3a expression, enhanced nuclear localization and increased IGF1R transcript and protein levels (Fig. 4G–J).

### 3.5. Combinatorial treatment of Ro5-3335 and platinum-taxol attenuates IGF1R-promoter activity and chemoresistance in-vivo

To assess the biological implication of RUNX1 guided FOXO3a binding to IGF1R promoter and subsequent IGF1R transcriptional up-regulation, we investigated chemoresistance and tumorigenic properties of the ER cells. Ro5-3335 treatment alone reduced the clonogenic potential of both the A2780-dual<sup>ER</sup> (2.5-fold) and OAW42-dual<sup>ER</sup> (2.2-fold) cells compared to their corresponding counterparts. Intriguingly, when Ro5-3555 treatment was combined with platinum-taxol, 11-fold and 2.8-fold reduction in colony formation were observed in A2780-dual<sup>ER</sup> and OAW42-dual<sup>ER</sup> cells compared to drug treatment alone. In contrast, only 2.8- and 1.6-fold differences were observed for A2780-dual<sup>LR</sup> and OAW42-dual<sup>LR</sup> cells with no changes in sensitive cells for the similar conditions (Fig. 5A–D). In CBF $\beta$ -KD cells, maximal chemosensitization was observed in ER cells compared to the respective CBF $\beta$ -KD counterparts as evidenced by a 2-fold decrease in cell viability (Fig. 5E). Both sensitive and LR cells showed nominal (~1.2-fold)

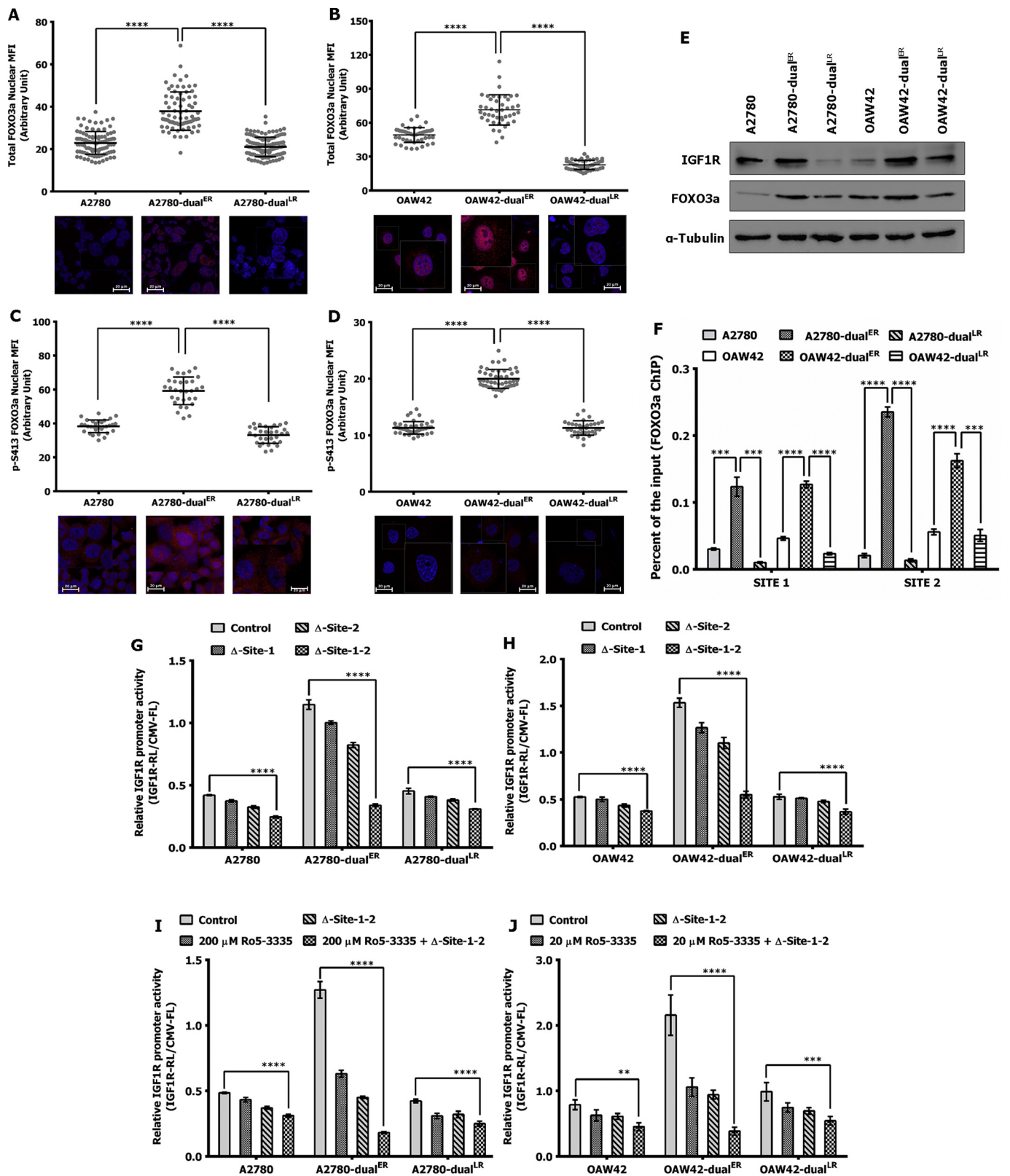
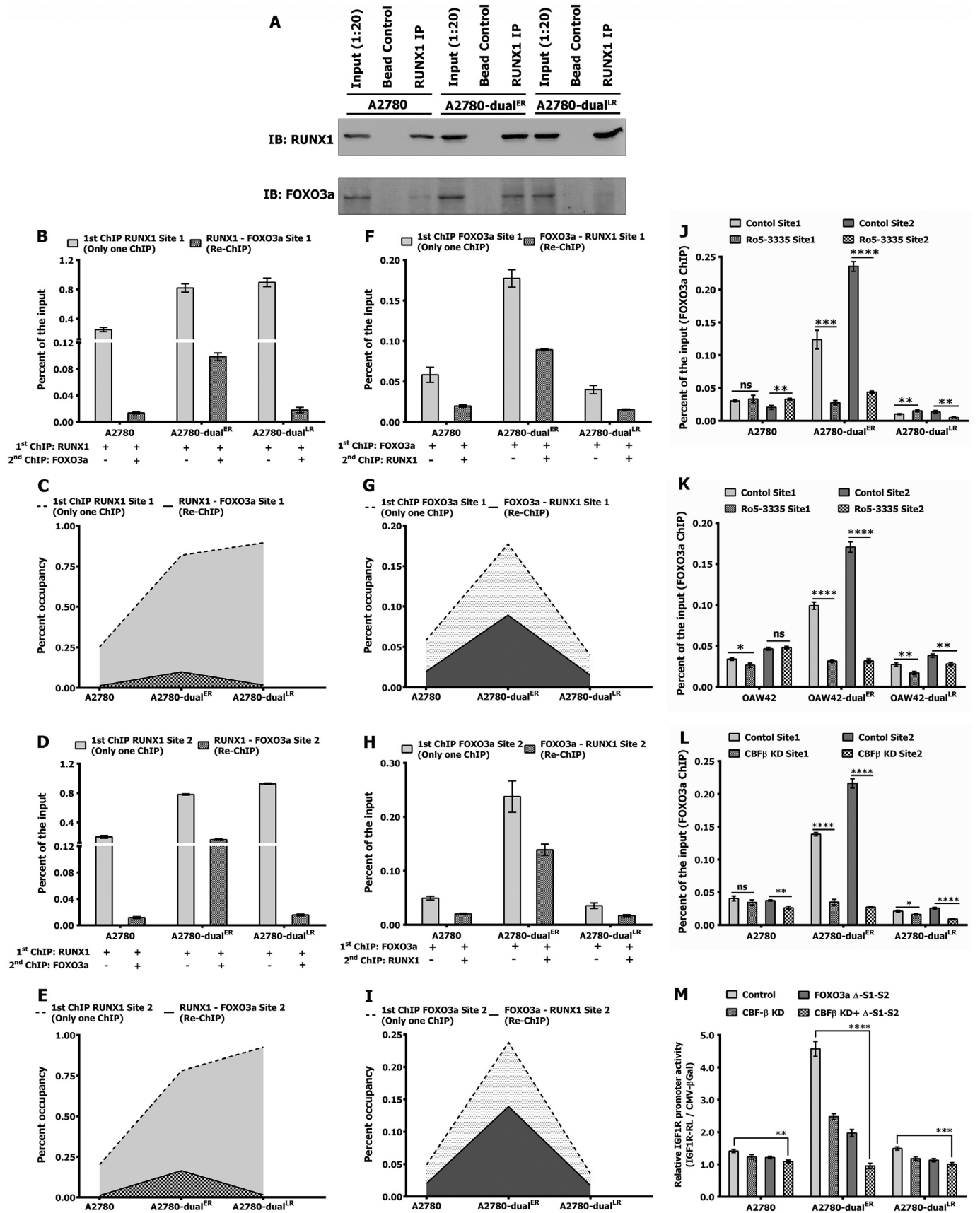


**Fig. 2.** Increased expression of FOXO3a controls IGF1R promoter activity in early-resistant stages. A–E. Immunofluorescence and Immunoblot show increased expression, enhanced nuclear localization of total and phospho-S473 (activation mark) FOXO3a in ER-cells. G–H. Mutating FOXO3a binding sites ( $\Delta$ -S1-S2) decreased IGF1R-promoter activity in A2780/OAW42 models. F. Enhanced binding of FOXO3a to site1 and site2 was observed only in A2780-dual<sup>ER</sup>/OAW42-dual<sup>ER</sup> cells (values were plotted as % binding of FOXO3a compared to input-DNA). I–J.  $\Delta$ -S1-S2 mutant IGF1R promoter showed maximal reduction upon Ro5-3335 treatment (A2780 = 200  $\mu$ M and OAW42 = 20  $\mu$ M) in A2780-dual<sup>ER</sup> and OAW42-dual<sup>ER</sup> cells. \*\*p  $\leq$  0.01, \*\*\*p  $\leq$  0.001, \*\*\*\*p  $\leq$  0.0001.



(caption on next page)

**Fig. 3.** Assessment of RUNX1 and FOXO3a binding sequence on IGF1R promoter.

A. Co-immunoprecipitation across A2780-Cis-Pac resistance model showed maximum RUNX1-FOXO3a interaction in ER cells followed by A2780 cells and least in LR cells. B-E. ChIP-re-ChIP of RUNX1 followed by FOXO3a on site 1 (B) and site 2 (D). Area plot (C & E) depicts the RUNX1 bound region co-occupied by FOXO3a. F-I. Chip-Re-Chip of FOXO3a followed by RUNX1 on site 1 (F) and site 2 (H). Area plot (G & I) depicts the FOXO3a bound region co-occupied by RUNX1. J-L. Ro5-3335 treatment (J and K) and CBF $\beta$ -KD (L) specifically attenuated binding of FOXO3a to site1 and site2 in A2780-dual<sup>ER</sup>/OAW42-dual<sup>ER</sup> cells (Values were plotted as % binding compared to input-DNA). M. Drastic attenuation in  $\Delta$ S1-S2-IGF1R-promoter activity was observed in CBF $\beta$ -KD-A2780-dual<sup>ER</sup> cells. \*p  $\leq$  0.05, \*\*p  $\leq$  0.01, \*\*\*p  $\leq$  0.001, \*\*\*\*p  $\leq$  0.0001.

decrease in viability after CBF $\beta$  knock down. Drug treatment in CBF $\beta$ -KD cells again showed maximal (2.5-fold) drop in colony formation in ER cells compared to the other counterparts (Fig. 5F). Similarly, highest reduction in both number and sizes were evident in CBF $\beta$ -KD-A2780-dual<sup>ER</sup> cells by soft agar colony formation assay (Fig. 5G-H). All these data suggest that both pharmacological and genetic inhibition of CBF $\beta$ -RUNX1 complex along with drug treatment exert maximal effects on chemoresistant and tumorigenic properties at the onset of resistance.

Next, independent and combinatorial effects of Ro5-3335 and platinum-taxol treatment on IGF1R-promoter-luciferase activity and tumorigenicity were monitored in subcutaneous tumor xenograft of A2780-dual<sup>ER</sup> cells by non-invasive optical imaging. Mice receiving Ro5-3335 showed 2-fold reduction in bioluminescence signal  $\{7.535 \times 10^7 \pm 1.539 \times 10^7$  to  $3.528 \times 10^7 \pm 5.873 \times 10^6$  (p/s/cm<sup>2</sup>/sr)} at end of the treatment (day-20) which then gradually increased to  $1.805 \times 10^8 \pm 5.932 \times 10^7$  (p/s/cm<sup>2</sup>/sr) (5.1-fold) at day-25 (Fig. 6A-B). Control group exhibited continuous increase in signal (10.9-fold) while cisplatin-paclitaxel treatment group showed 4.1-fold reduction at day 25  $\{4.193 \times 10^8 \pm 9.138 \times 10^7$  to  $1.025 \times 10^8 \pm 3.028 \times 10^7$  (p/s/cm<sup>2</sup>/sr)}. The most drastic drop in IGF1R activity was observed in the group with combinatorial treatment (16.1-fold)  $\{3.959 \times 10^7 \pm 9.812 \times 10^6$  to  $2.468 \times 10^6 \pm 772,284$  (p/s/cm<sup>2</sup>/sr)} at day-25 (Fig. 6A-B). Although no significant reduction in tumor volume was observed across the groups, slight decrease in tumor volume was noted between control and combinatorial groups ( $1567 \pm 101.4$  vs  $1321 \pm 90.84$  mm<sup>3</sup>) (Fig. 6C). Ki-67 staining and histological analysis showed decreased number of proliferating cells and higher necrosis in tumors of the combinatorial treatment group compared to the other groups (Fig. 6D-G and Supplementary Fig. S6A). IGF1R staining among the groups showed maximal reduction in IGF1R in the combinatorial group compared to the rest of the groups (Fig. 6E and Supplementary Fig. S6A), however, no significant change in FOXO3a staining was observed among the groups (Fig. 6F and Supplementary Fig. S6A). When statistical correlations were drawn among the groups comparing IGF1R staining with Ki67, FOXO3a, and tumor viability, only the IGF1R/FOXO3a exhibited lower correlation ( $R^2 = 0.688$ ) than the IGF1R/Ki67 ( $R^2 = 0.955$ ) and IGF1R/tumor viability ( $R^2 = 0.988$ ) (Supplementary Fig. S6B-D).

To investigate the chemo-sensitization effect of the genetically disrupted RUNX1-CBF $\beta$  complex, A2780-dual<sup>ER</sup> cells and their CBF $\beta$ -KD counterparts were subcutaneously implanted in the upper and lower flanks of NOD-SCID mice (n = 5). Despite implanting equal number of cells, the A2780-dual<sup>ER</sup> CBF $\beta$ -KD cells showed slower tumor growth. A 6.9-fold lower IGF1R-promoter activity was observed in CBF $\beta$ -KD tumors  $\{4.003 \times 10^8 \pm 8.397 \times 10^7$  (p/s/cm<sup>2</sup>/sr)} compared to the control tumors  $\{2.778 \times 10^9 \pm 7.307 \times 10^8$  (p/s/cm<sup>2</sup>/sr)} at day 35 (Fig. 7A-B). Animals were given two treatments of cisplatin-paclitaxel at 10 days interval. At day 55, a 99.5 fold drop in bioluminescence signal was observed in CBF $\beta$ -KD tumors  $\{4.003 \times 10^8 \pm 8.397 \times 10^7$  to  $4.020 \times 10^6 \pm 667,424$  (p/s/cm<sup>2</sup>/sr)}, compared to 3.9-fold drop in the control tumors  $\{2.778 \times 10^9 \pm 7.307 \times 10^8$  to  $7.213 \times 10^8 \pm 1.357 \times 10^8$  (p/s/cm<sup>2</sup>/sr)} (Fig. 7A-B). Though the CBF $\beta$ -KD tumors showed slower growth rate, drug treatment led to 1.3-fold reduction in tumor volume at day 55 ( $430.3 \pm 20.11$  vs  $328.3 \pm 27.59$  mm<sup>3</sup>) which was not evident in the control group (Fig. 7C). Further, CBF $\beta$ -KD tumors showed decreased expression of IGF1R, low number of proliferating cells (Ki67) and higher necrosis

compared to control tumors (Fig. 7D-G and Supplementary Fig. S6E-H).

#### 4. Discussion

Dysregulated signalling network underlying the acquired chemoresistance are mediated by cooperative interaction of various transcription factors and are often intrinsically non-linear in nature. Association of hyperactive IGF1R signalling with chemo/radio/targeted therapy resistance has been reported in several cancers including Epithelial Ovarian Cancer [16-21]. These studies report a onetime relation between the extent of resistance and level of IGF1R expression often undermining the transcriptional dynamicity during acquirement of resistance. We, for the first time, have reported a transcriptional surge in IGF1R expression at the onset of chemoresistance which declines at late stages of resistance and was inversely related to AKT activation in platinum-taxol resistant EOC cells [1]. Similarly a therapy induced transcriptional surge in IGF1R expression was observed in paired neoadjuvant chemotherapy treated tumors of a small cohort of advanced stage high grade serous EOC patients [3]. However, the underlying factors for this transcriptional surge and subsequent decay were unknown. In this study, we identified RUNX1 as a novel transcriptional regulator of IGF1R gene which in cooperation with FOXO3a induces IGF1R transcription at the onset of platinum-taxol resistance in EOC cells. Such interaction falls apart when the cells acquired maximal resistance towards the drugs leading to downregulation of IGF1R expression. Lower FOXO3a occupancy in presence of an optimally bound RUNX1 on IGF1R promoter at late resistant stages was due to AKT mediated degradation which resulted in debilitated IGF1R transcription and could be reversed by an AKT inhibitor. This undulating behaviour of IGF1R appeared due to a dynamic interplay between RUNX1, FOXO3a and AKT, at different stages of resistance. We further showed that pharmacological or genetic inhibition of RUNX1 decreased resistance and tumorigenicity of the early resistant cells.

In absence of mutational activation and rare instances of gene amplification, overexpression of IGF1R gene is attributed to transcriptional and epigenetic modulation [12]. Only 16.5% of EOC cases of The Cancer Genome Atlas (TCGA) dataset show enhanced IGF1R transcription and 4% cases show gene amplification [6,7]. The unique IGF1R promoter is comprised of a GC rich 5'-flanking region without the TATA or CAAT box sequences and is differentially regulated by several TFs either directly or indirectly through SP1 in various circumstances [12]. Intriguingly, the high GC rich IGF1R promoter is a prospective site for rich epigenetic interactions but such epigenetic regulations are seldom reported [12]. Rather conspicuous absence of methylation by SAM, a methyl donor agent in Glioblastoma cells and in benign and metastatic Prostate cancer cells [14,15] points towards a pre-dominant role of the transcriptional regulators. Apart from VHL loss in 5-Fluorouracil and etoposide resistant renal cell carcinoma and FOXO1 activation in phosphatidylinositol-3-kinase catalytic subunit delta (PI3K- $\delta$ ) inhibitor resistant murine model [36,37], probable action of other transcriptional regulator/s in mediating cancer therapy resistance through IGF1R are unknown. Such molecular knowledge is important to identify both therapeutic and diagnostic markers for the IGF1R addicted cancers including EOC. Though transcription factor-promoter array analysis in this study identified several unique transcriptional regulators (SOX9, SOX18, RUNX1, RXR, ROR and VDR),

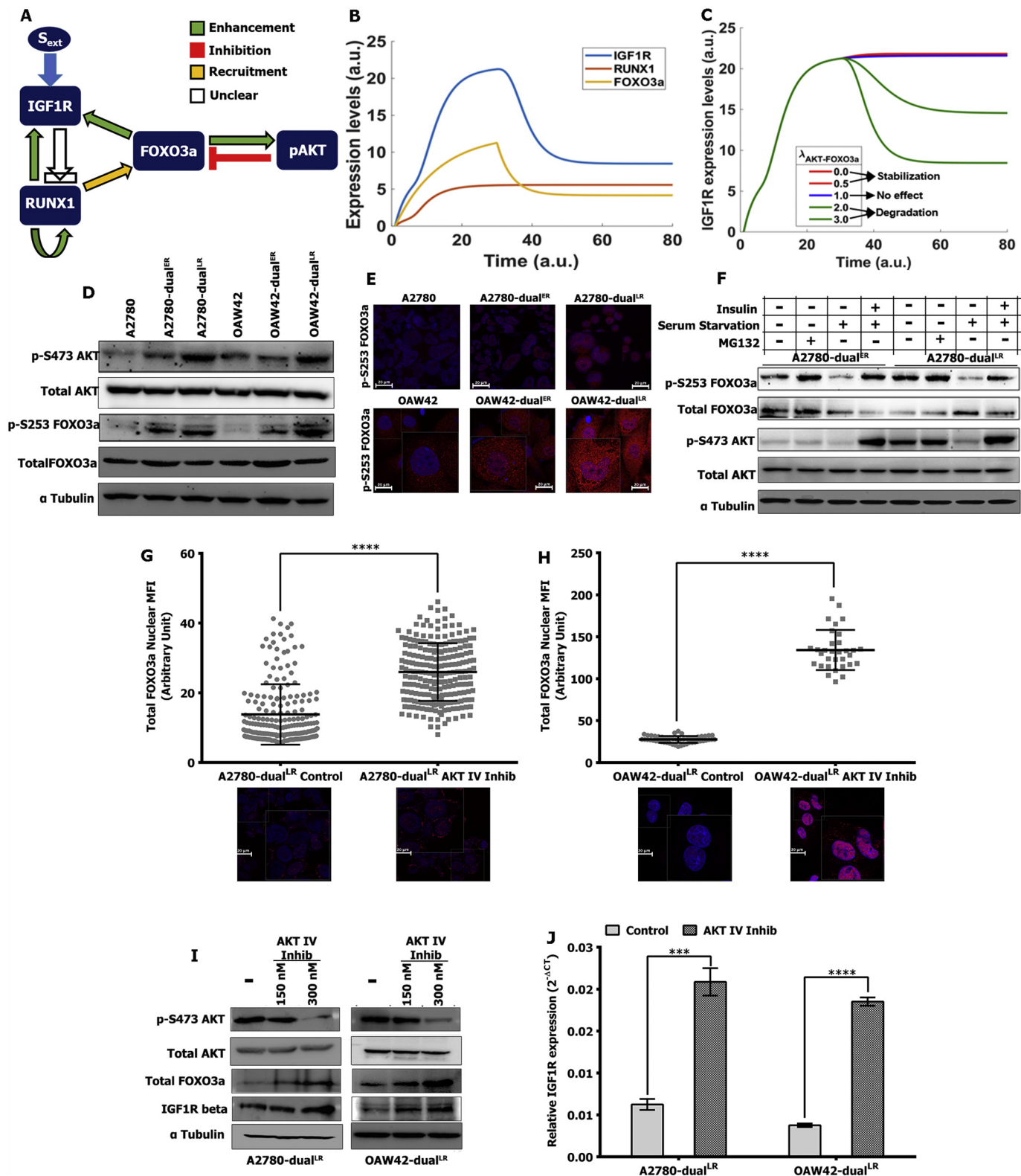


**Fig. 4.** AKT-FOXO3a feedback loop negatively regulate IGF1R expression at late-resistant stages.

A. Network constructed to explain IGF1R pulsatile dynamics. B. Dynamics of RUNX1, FOXO3a and IGF1R obtained by mathematical simulation of the network. C. Effect of AKT mediated FOXO3a degradation on IGF1R dynamics. D–E. Immunoblot and immunofluorescence showing incremental levels of p-S473-AKT and p-S253-FOXO3a with increasing resistance in A2780/OAW42 models. F. Serum starvation led to loss of both p-S473-AKT and p-S253-FOXO3a in A2780-dual<sup>ER</sup> and dual<sup>LR</sup> cells and increased FOXO3a levels in A2780-dual<sup>LR</sup> cells. Insulin stimulation led to sharp increase in p-S253-FOXO3a in both ER and LR cells. G–J. Effect of AKT-IV on FOXO3a and IGF1R. Increased nuclear localization (G & H) and total FOXO3a (I), decreased p-S473-AKT (I) and increased IGF1R mRNA (J) and IGF1R protein (I) were observed in A2780-dual<sup>LR</sup> and OAW42-dual<sup>LR</sup> cells. \*\*\*p ≤ 0.001, \*\*\*\*p ≤ 0.0001.

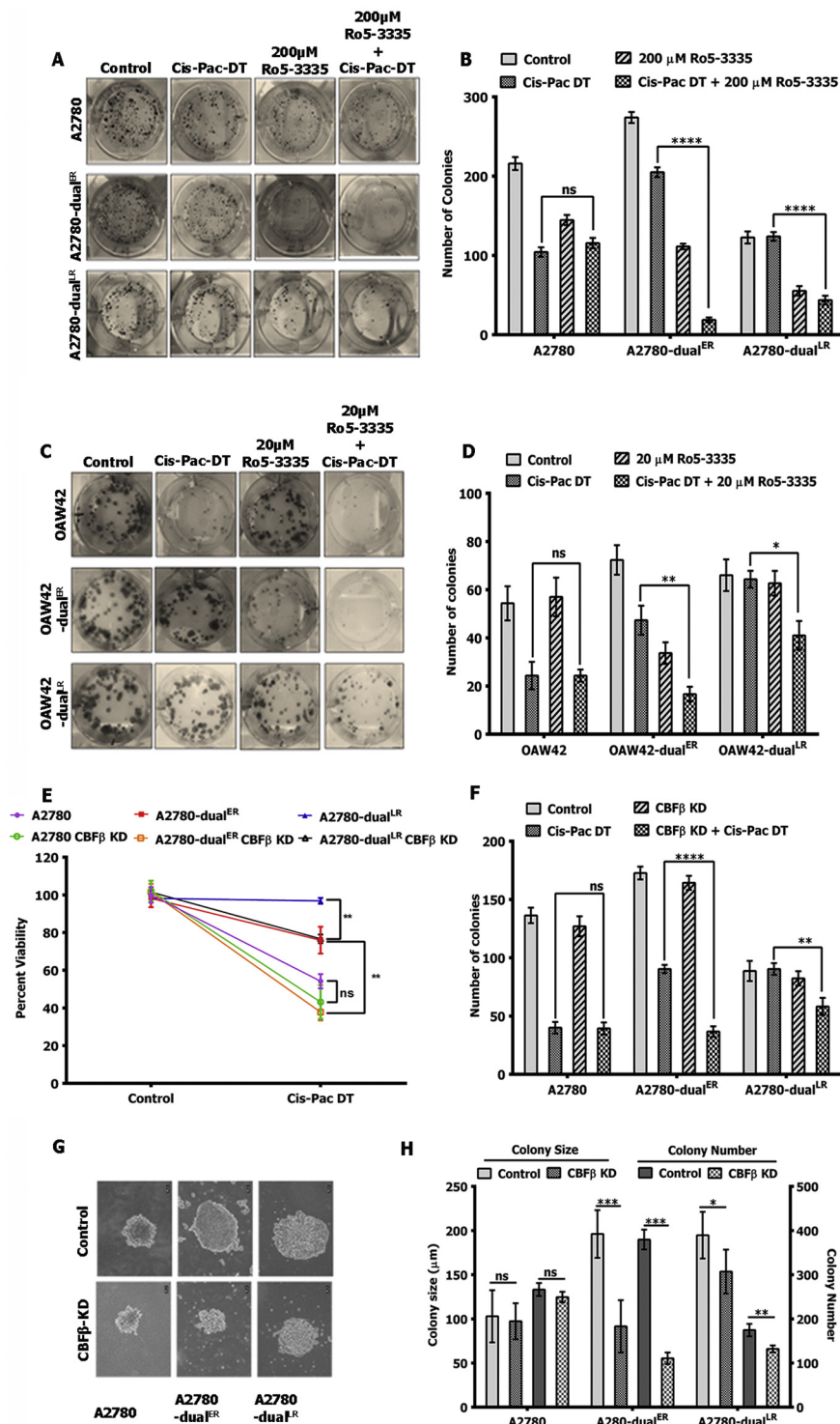


**Fig. 5.** RUNX1 inhibition affects chemoresistant properties of EOC cells.

A–D. Clonogenic survival assay showing the extent of decrease in the surviving fractions upon Ro5-3335 (A2780 = 200 µM and OAW42 = 20 µM) and after combinatorial treatment with cisplatin-paclitaxel across all the stages in A2780/OAW42 models (50 ng cisplatin + 8.5 ng paclitaxel/ml). E–H. MTT (E), clonogenic (F) and soft agar assay (G–H) showing decrease in surviving fractions upon cisplatin-paclitaxel treatment in CBFβ-KD cells compared to the controls in A2780-dual resistant model. \*p ≤ 0.05, \*\*p ≤ 0.01, \*\*\*p ≤ 0.001, \*\*\*\*p ≤ 0.0001.

perturbation of only RUNX1 activity significantly attenuated IGF1R transcriptional and promoter activity in both A2780 and OAW42 chemoresistant models and highest reduction was seen in early-resistant cells. The rest of the potential binders either were not able to modulate IGF1R expression (RXR/ROR/VDR) or were not feasible to test due to absence of specific activator/inhibitor and technical difficulties to

create site specific mutations at seven lengthy binding sites (SOX9/SOX18). RUNX1, a well-known master regulator of hematopoietic lineages gathered attention as a tumor suppressor for long in haematological cancers [38]. Recently, RUNX1 has been found to have a more widespread role in several cancers [39,40] but this is the first report of its association with development of chemoresistance. RUNX1-CBFβ

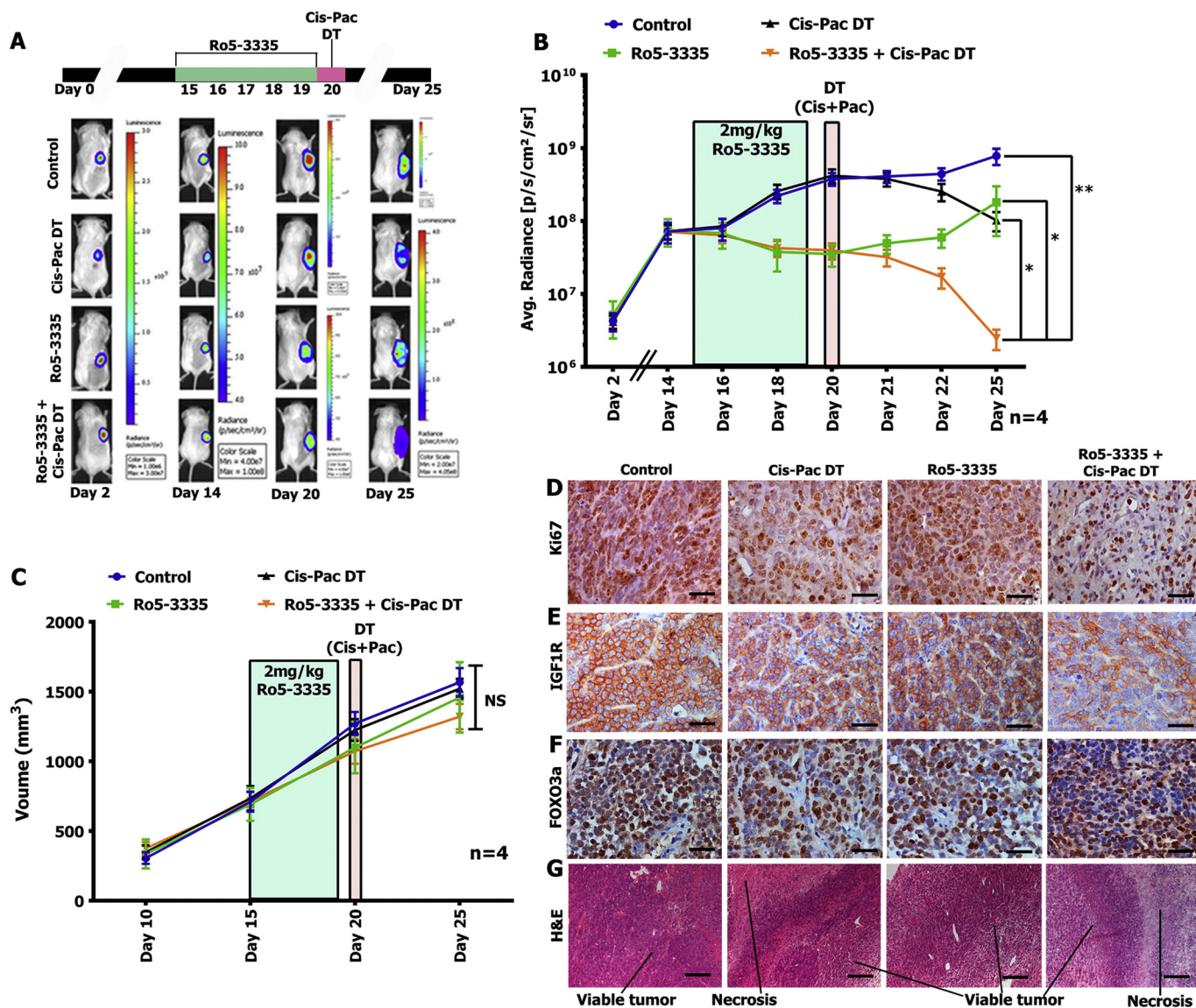


**Fig. 6.** Ro5-3335 mediated RUNX1 inhibition and platinum-taxol attenuate IGF1R promoter activity and chemoresistance *in vivo*. A. Ro5-3335 and cisplatin-paclitaxel treatment regime and representative bioluminescence images of A2780-dual<sup>ER</sup> tumor xenografts expressing IGF1R-FL2-TDT promoter-reporter treated with vehicle (control), cisplatin-paclitaxel, Ro5-3335 and Ro5-3335 with cisplatin-paclitaxel showing modulation in bioluminescence signal. B. Graphical representation of quantified bioluminescence signal (n = 4/group) showing the trend in IGF1R promoter activity between the four groups. C. Graphical representation of tumor growth kinetics of the four groups. D–G. Representative images of Ki-67, IGF1R, FOXO3a and H&E staining of tumor sections showing extent of cell proliferation and necrosis among the groups. \*p ≤ 0.05, \*\*p ≤ 0.01.

complex is a central player in fine-tuning the balance among cell differentiation, proliferation, EMT and often acts in cooperation with other transcriptional regulators [40–43]. Such functional cooperativity of RUNX1 with other transcription factors is reported in lymphoma, breast, colorectal cancer and haematological malignancies [42–45]. In spite of increased RUNX1 expression and functional activities (nuclear localization and enhanced binding at sites 1–2) across all stages of resistance, specific inhibition of IGF1R by Ro5-3335 was observed only in early-resistant cells and signifies for contributory role of other regulator/s for optimal activation. FOXO3a [43,46], a known IGF1R regulator is found to share overlapping binding motifs with RUNX1 (site 1 and 2) on IGF1R promoter and also exhibited a similar pulsatile pattern like IGF1R across resistant stages with highest promoter occupancy in early resistant cells. Both RUNX1 and FOXO3a function as transcriptional modulator individually and in conjunction with each other [32,43–46]. The co-immunoprecipitation result demonstrated a stage specific interaction pattern between RUNX1 and FOXO3a which was

highest in early resistant cells but minimal in sensitive and late resistant cells. This stage specific interaction pattern seems to influence their IGF1R promoter binding capacity as maximal RUNX1-FOXO3a co-occupancy was evident during onset of resistance which subsequently decreased at late-resistant stages as revealed by Chip-re-Chip assay. This cooperative binding is critical for optimal IGF1R transcription as neither of the transcription factor could independently drive IGF1R expression. Both chemical and genetic inhibition of RUNX1 abolished FOXO3a binding in early-resistant cells indicating that RUNX1 binding is an obligatory step for FOXO3a occupancy specifically at the onset of resistance. Contrary to RUNX1, FOXO3a exhibited a poorer binding to IGF1R promoter and lower nuclear localization in late resistant cells thereby affecting the co-occupancy and transcriptional rate.

These intriguing dynamics prompted us to construct a network and mathematically analyse the interactions leading towards IGF1R and FOXO3a pulsatile dynamics which occurs as a result of adaptation to the drug induction. Our mathematical analysis which considered both

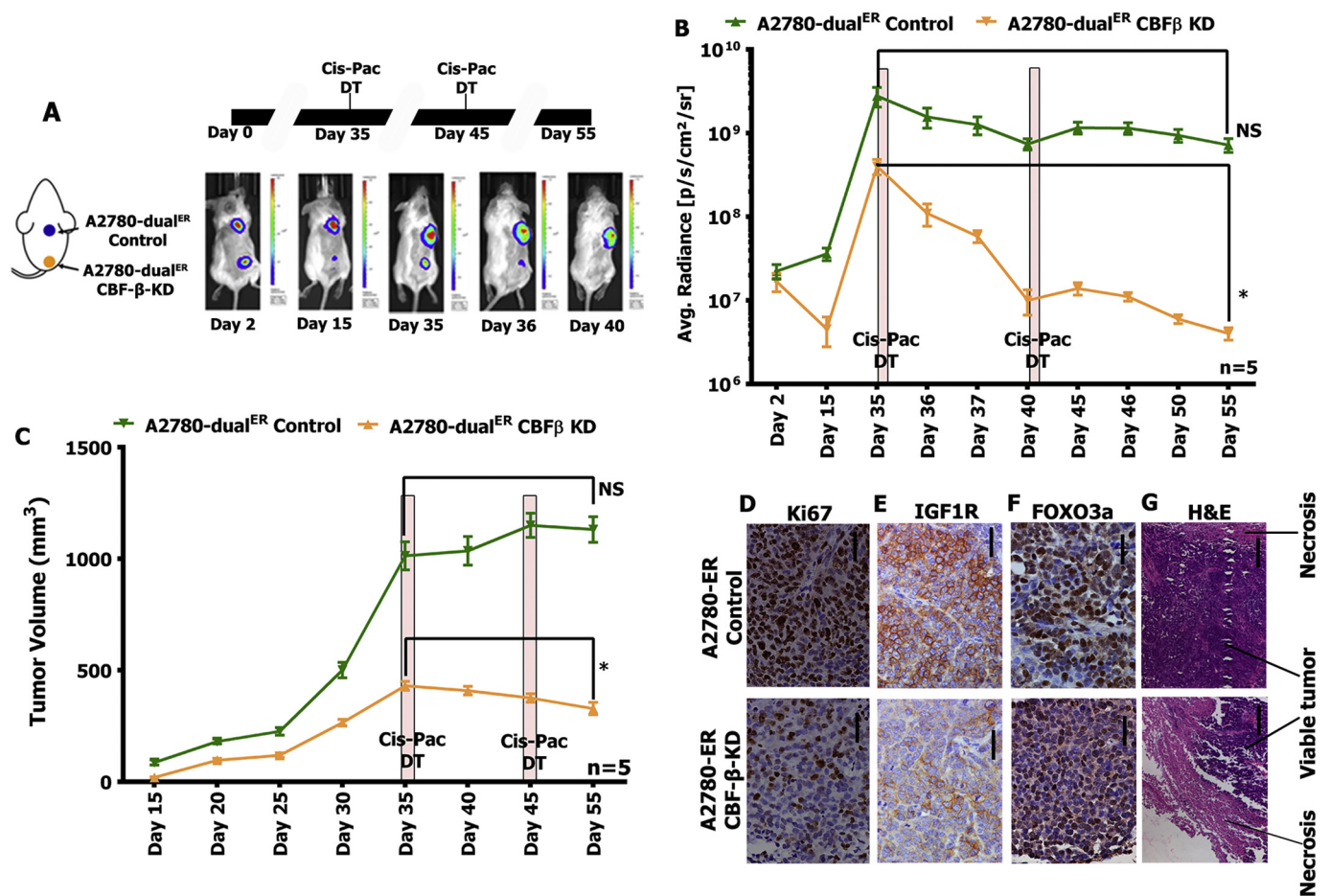


Fig. 7. CBF $\beta$ -KD and platinum-taxol attenuate IGF1R promoter activity and chemoresistance *in-vivo*.

A. Schematic diagram of treatment sequence, tumor implantation of A2780-dual<sup>ER</sup> and A2780-dual<sup>ER</sup> CBF $\beta$ -KD cells and representative bioluminescence images. B. Graphical representation of quantified bioluminescence signal (n = 5/group) showing ~99 fold reduced IGF1R promoter activity. C. Graphical representation of tumor growth kinetics showing slower tumorigenesis and chemosensitization in CBF $\beta$ -KD tumors. D–G. Representative images of Ki-67, IGF1R, FOXO3a and H&E staining of tumor sections revealed lesser proliferation and higher necrosis in CBF $\beta$ -KD tumors. \*p  $\leq$  0.05.

transcriptional and epigenetic factors suggested a crucial role of a negative feedback loop between FOXO3a and AKT in the pulsatile dynamics of IGF1R and FOXO3a. Indeed, AKT inactivation either through serum starvation or by an inhibitor led to decreased p-S253-FOXO3a levels and increased total FOXO3a and IGF1R expression in late resistant cells. Our *in-silico* analysis also suggested that while methylation events on IGF1R promoter can indeed affect the duration and amplitude of the IGF1R pulse, the qualitative dynamics of the fall of IGF1R concentration, which is crucial for the definition of a pulse, is independent of such methylation events. However, a delay between the expression of IGF1R and the activation of FOXO3a-Akt negative feedback loop was found to be a necessary component of the model, which raises the possibility of involvement of additional factors in FOXO3a-Akt negative feedback loop or the presence of other negative feedback loops interacting with FOXO3a, acting in timescales larger than FOXO3a-Akt feedback loop. Such possibilities require further exploration.

Pharmacological or genetic ablation of RUNX1 imparted chemosensitization and reduced colony formation maximally in ER cells, thus indicating blockade of RUNX1-FOXO3a mediated IGF1R upregulation renders the early resistant stage cells sensitive to cisplatin-paclitaxel. Continuous application of low dose Ro5-3335 or genetic perturbation of RUNX1 with intermittent drug treatment led to significant decrease in IGF1R expression, stalled tumor cell proliferation and induction of necrosis in tumor xenograft models of early-resistant cells. RUNX1 is indispensable for establishment of definitive haematopoiesis in vertebrates. However, no obvious illness was observed in long term use of

300 mg/kg/day of Ro5-3335 in mice [31] and a single dose of 5 mg/kg of Ro5-3555 protects LPS induced death in mice by reducing inflammation [47]. We applied similar low dose in fractionated manner (2 mg/kg/day/5 days) and observed that low dose RUNX1 inhibitor with platinum-taxol could effectively delay resistance development. However, a detail dose dependent study is warranted to assess potential of RUNX1 inhibition combating the platinum-taxol resistance.

Though recognized as a promising target, clinical benefits of IGF1R-targeting agents are not found for patients with breast, pancreatic, non-small cell lung cancers and ovarian cancers [22]. Possible reasons for such failure result from the strong homology between IGF1R and Insulin receptor and shared ligands (IGF1, IGF2 and insulin) and ligand binding proteins (IGFBPs) between the two pathways. Thus, an indirect approach by targeting IGF1R gene regulators in IGF1R addicted cancer or in therapy resistant situation might arise as a viable option. This RUNX1-FOXO3a partnership most likely impacts other target genes required for resistance. Therefore, targeting RUNX1 in combination with chemotherapy might turn up as a new strategy to reverse or delay development on chemoresistance in EOC cells.

Supplementary data to this article can be found online at <https://doi.org/10.1016/j.bbadis.2020.165754>.

#### CRediT authorship contribution statement

Ajit C. Dhadve: Investigation, Writing - original draft, Writing - review & editing. Kishore Hari: Methodology, Writing - original draft,

Writing - review & editing. **Bharat Rekhi:** Investigation, Writing - original draft, Writing - review & editing. **Mohit Kumar Jolly:** Methodology, Writing - original draft, Writing - review & editing. **Abhijit De:** Formal analysis, Writing - original draft, Writing - review & editing. **Pritha Ray:** Conceptualization, Methodology, Supervision, Formal analysis, Writing - original draft, Writing - review & editing.

#### Declaration of competing interest

The authors declare that they have no known competing financial interests or personal relationships that could have appeared to influence the work reported in this paper.

#### Acknowledgments

We acknowledge funding support from Advanced Centre for Treatment, Research and Education in Cancer, Tata Memorial Centre, Council of Scientific and Industrial Research, India grant 27/(0314)/16/EMR-II and Advanced Centre for Treatment, Research and Education in Cancer, Tata Memorial Centre for fellowship to ACD. MKJ was supported by Ramanujan Fellowship provided by Science and Engineering Research Board, Department of Science and Technology (SB/S2/RJN-049/2018). We acknowledge support from Molecular Imaging Facility at ACTREC.

#### References

- [1] R.K. Singh, S.M. Gaikwad, A. Jinager, S. Chaudhury, A. Maheshwari, P. Ray, IGF-1R inhibition potentiates cytotoxic effects of chemotherapeutic agents in early stages of chemoresistant ovarian cancer cells, *Cancer Lett.* 354 (2014) 254–262.
- [2] R.K. Singh, A. Dhadve, A. Sakpal, A. De, P. Ray, An active IGF-1R-AKT signaling imparts functional heterogeneity in ovarian CSC population, *Sci. Rep.* 6 (2016) 36612.
- [3] A. Deo, S. Chaudhury, S. Kannan, B. Rekhi, A. Maheshwari, S. Gupta, P. Ray, IGF1R predicts better survival in high-grade serous epithelial ovarian cancer patients and correlates with hCtr1 levels, *Biomark. Med* 13 (2019) 511–521.
- [4] M.M. Chitnis, J.S. Yuen, A.S. Protheroe, M. Pollak, V.M. Macaulay, The type 1 insulin-like growth factor receptor pathway, *Clin. Cancer Res.* 14 (2008) 6364–6370.
- [5] O. Larsson, A. Girmita, L. Girmita, Role of insulin-like growth factor 1 receptor signalling in cancer, *Br. J. Cancer* 92 (2005) 2097–2101.
- [6] E. Cerami, J. Gao, U. Dogrusoz, B.E. Gross, S.O. Sumer, B.A. Aksoy, A. Jacobsen, C.J. Byrne, M.L. Heuer, E. Larsson, Y. Antipin, B. Reva, A.P. Goldberg, C. Sander, N. Schultz, The cBio cancer genomics portal: an open platform for exploring multidimensional cancer genomics data, *Cancer Discov.* 2 (2012) 401–404.
- [7] J. Gao, B.A. Aksoy, U. Dogrusoz, G. Dresdner, B. Gross, S.O. Sumer, Y. Sun, A. Jacobsen, R. Sinha, E. Larsson, E. Cerami, C. Sander, N. Schultz, Integrative analysis of complex cancer genomics and clinical profiles using the cBioPortal, *Sci. Signal.* 6 (2013) p11.
- [8] J.S. Kim, E.S. Kim, D. Liu, J.J. Lee, C. Behrens, S.M. Lippman, W.K. Hong, I.I. Wistuba, E. Lee, H.Y. Lee, Activation of insulin-like growth factor 1 receptor in patients with non-small cell lung cancer, *Oncotarget* 6 (2015) 16746–16756.
- [9] G. Peiro, E. Adrover, L. Sanchez-Tejada, E. Lerma, M. Planelles, J. Sanchez-Paya, F.I. Aranda, D. Giner, F.J. Gutierrez-Avino, Increased insulin-like growth factor-1 receptor mRNA expression predicts poor survival in immunophenotypes of early breast carcinoma, *Mod. Pathol.* 24 (2011) 201–208.
- [10] A. Ouban, P. Muraca, T. Yeatman, D. Coppola, Expression and distribution of insulin-like growth factor-1 receptor in human carcinomas, *Hum. Pathol.* 34 (2003) 803–808.
- [11] C.E. Jenkins, S. Gusscott, R.J. Wong, O.O. Shevchuk, G. Rana, V. Giambra, K. Tyshchenko, R. Islam, M. Hirst, A.P. Weng, RUNX1 promotes cell growth in human T-cell acute lymphoblastic leukemia by transcriptional regulation of key target genes, *Exp. Hematol.* 64 (2018) 84–96.
- [12] H. Werner, R. Sarfstein, Transcriptional and epigenetic control of IGF1R gene expression: implications in metabolism and cancer, *Growth Hormon. IGF Res.* 24 (2014) 112–118.
- [13] X. Huo, S. Liu, T. Shao, H. Hua, Q. Kong, J. Wang, T. Luo, Y. Jiang, GSK3 protein positively regulates type I insulin-like growth factor receptor through forkhead transcription factors FOXO1/3/4, *J. Biol. Chem.* 289 (2014) 24759–24770.
- [14] H. Schayek, I. Bentov, S. Sun, S.R. Plymate, H. Werner, Progression to metastatic stage in a cellular model of prostate cancer is associated with methylation of the androgen receptor gene and transcriptional suppression of the insulin-like growth factor-1 receptor gene, *Exp. Cell Res.* 316 (2010) 1479–1488.
- [15] R. Ola, I. Berindan-Neagoie, O. Balacescu, M. Banicioiu, A. Dricu, S-adenosylmethionine-induced cytotoxicity in glioblastoma cells does not affect the IGF-1R methylation, *Revista Romana de Medicina de Laborator* 18 (2010).
- [16] N.A. Dallas, L. Xia, F. Fan, M.J. Gray, P. Gaur, G. van Buren 2nd, S. Samuel, M.P. Kim, S.J. Lim, L.M. Ellis, Chemoresistant colorectal cancer cells, the cancer stem cell phenotype, and increased sensitivity to insulin-like growth factor-I receptor inhibition, *Cancer Res.* 69 (2009) 1951–1957.
- [17] Y. Sun, S. Zheng, A. Torossian, C.K. Speirs, S. Schleicher, N.J. Giacalone, D.P. Carbone, Z. Zhao, B. Lu, Role of insulin-like growth factor-1 signaling pathway in cisplatin-resistant lung cancer cells, *Int. J. Radiat. Oncol. Biol. Phys.* 82 (2012) e563–e572.
- [18] A. Bielen, G. Box, L. Perryman, L. Bjerke, S. Popov, Y. Jamin, A. Jury, M. Valenti, H. Brandon Ade, V. Martins, V. Romanet, S. Jeay, F.I. Raynaud, F. Hofmann, S.P. Robinson, S.A. Eccles, C. Jones, Dependence of Wilms tumor cells on signaling through insulin-like growth factor 1 in an orthotopic xenograft model targetable by specific receptor inhibition, *Proc. Natl. Acad. Sci. U. S. A.* 109 (2012) E1267–E1276.
- [19] N. Eckstein, K. Servan, B. Hildebrandt, A. Politz, G. von Jonquieres, S. Wolf-Kummeth, I. Napierski, A. Hamacher, M.U. Kassack, J. Budczies, M. Beier, M. Diel, B. Royer-Pokora, C. Denkert, H.D. Royer, Hyperactivation of the insulin-like growth factor receptor I signaling pathway is an essential event for cisplatin resistance of ovarian cancer cells, *Cancer Res.* 69 (2009) 2996–3003.
- [20] T. Murañan, L.M. Selfors, D.T. Worster, M.P. Iwanicki, L. Song, F.C. Morales, S. Gao, G.B. Mills, J.S. Brugge, Inhibition of PI3K/mTOR leads to adaptive resistance in matrix-attached cancer cells, *Cancer Cell* 21 (2012) 227–239.
- [21] J. Zorea, M. Prasad, L. Cohen, N. Li, R. Schefzik, S. Ghosh, B. Rotblat, B. Brors, M. Elkabets, IGF1R upregulation confers resistance to isoform-specific inhibitors of PI3K in PIK3CA-driven ovarian cancer, *Cell Death Dis.* 9 (2018) 944.
- [22] C. Crudden, A. Girmita, L. Girmita, Targeting the IGF-1R: the tale of the tortoise and the hare, *Front. Endocrinol.* 6 (2015) 64.
- [23] B. Thakur, P. Ray, p53 loses grip on PIK3CA expression leading to enhanced cell survival during platinum resistance, *Mol. Oncol.* 10 (2016) 1283–1295.
- [24] S.M. Gaikwad, B. Thakur, A. Sakpal, R.K. Singh, P. Ray, Differential activation of NF-kappaB signaling is associated with platinum and taxane resistance in MyD88 deficient epithelial ovarian cancer cells, *Int. J. Biochem. Cell Biol.* 61 (2015) 90–102.
- [25] M. Furlan-Magaril, H. Rincon-Arango, F. Recillas-Targa, Sequential chromatin immunoprecipitation protocol: ChIP-reChIP, *Methods Mol. Biol.* 543 (2009) 253–266.
- [26] J.N. Davis, D. Rogers, L. Adams, T. Yong, J.S. Jung, B. Cheng, K. Fennell, E. Borazanci, Y.W. Moustafa, A. Sun, R. Shi, J. Glass, J.M. Mathis, B.J. Williams, S. Meyers, Association of core-binding factor beta with the malignant phenotype of prostate and ovarian cancer cells, *J. Cell. Physiol.* 225 (2010) 875–887.
- [27] N. Fedchenko, J. Reifenrath, Different approaches for interpretation and reporting of immunohistochemistry analysis results in the bone tissue - a review, *Diagn. Pathol.* 9 (2014) 221.
- [28] T. Kogai, J.J. Schultz, L.S. Johnson, M. Huang, G.A. Brent, Retinoic acid induces sodium/iodide symporter gene expression and radioiodide uptake in the MCF-7 breast cancer cell line, *Proc. Natl. Acad. Sci. U. S. A.* 97 (2000) 8519–8524.
- [29] M.G. Kelkar, K. Senthilkumar, S. Jadhav, S. Gupta, B.-C. Ahn, A. De, Enhancement of human sodium iodide symporter gene therapy for breast cancer by HDAC inhibitor mediated transcriptional modulation, *Sci. Rep.* 6 (2016) 19341.
- [30] T. Kogai, Y. Kanamoto, L.H. Che, K. Taki, F. Moatemed, J.J. Schultz, G.A. Brent, Systemic retinoic acid treatment induces sodium/iodide symporter expression and radioiodide uptake in mouse breast cancer models, *Cancer Res.* 64 (2004) 415–422.
- [31] L. Cunningham, S. Finckbeiner, R.K. Hyde, N. Southall, J. Marugan, V.R. Yedavalli, S.J. Dehdashti, W.C. Reinhold, L. Alemu, L. Zhao, J.R. Yeh, R. Sood, Y. Pommier, C.P. Austin, K.T. Jeang, W. Zheng, P. Liu, Identification of benzodiazepine Ro5-3335 as an inhibitor of CBF leukemia through quantitative high throughput screen against RUNX1-CBFbeta interaction, *Proc. Natl. Acad. Sci. U. S. A.* 109 (2012) 14592–14597.
- [32] N. Pencovich, R. Jaschek, A. Tanay, Y. Groner, Dynamic combinatorial interactions of RUNX1 and cooperating partners regulates megakaryocytic differentiation in cell line models, *Blood* 117 (2011) e1–14.
- [33] W. Ma, A. Trusina, H. El-Samad, W.A. Lim, C. Tang, Defining network topologies that can achieve biochemical adaptation, *Cell* 138 (2009) 760–773.
- [34] D. Muzzezy, C.A. Gomez-Urbe, J.T. Mettetal, A. van Oudenaarden, A systems-level analysis of perfect adaptation in yeast osmoregulation, *Cell* 138 (2009) 160–171.
- [35] K. Yamagata, H. Daitoku, Y. Takahashi, K. Namiki, K. Hisatake, K. Kako, H. Mukai, Y. Kasuya, A. Fukamizu, Arginine methylation of FOXO transcription factors inhibits their phosphorylation by Akt, *Mol. Cell* 32 (2008) 221–231.
- [36] A. Schefold, B.M.C. Jebaraj, E. Tausch, J. Bloehdorn, P. Ghia, A. Yahiaoui, A. Dolnik, T.J. Blatte, L. Bullinger, R.P. Dheendayalan, L. Li, C. Schneider, S.S. Chen, N. Chiorazzi, S. Dietrich, M. Seiffert, S. Tannheimer, H. Dohner, D. Mertens, S. Stilgenbauer, IGF1R as druggable target mediating PI3K-delta inhibitor resistance in a murine model of chronic lymphocytic leukemia, *Blood* 134 (2019) 534–547.
- [37] J.S. Yuen, E. Akkaya, Y. Wang, M. Takiguchi, S. Peak, M. Sullivan, A.S. Protheroe, V.M. Macaulay, Validation of the type 1 insulin-like growth factor receptor as a therapeutic target in renal cancer, *Mol. Cancer Ther.* 8 (2009) 1448–1459.
- [38] R. Sood, Y. Kamikubo, P. Liu, Role of RUNX1 in hematological malignancies, *Blood* 129 (2017) 2070–2082.
- [39] A.I. Riggio, K. Blyth, The enigmatic role of RUNX1 in female-related cancers - current knowledge & future perspectives, *FEBS J.* 284 (2017) 2345–2362.
- [40] C.J.F. Scheitz, T.S. Lee, D.J. McDermitt, T. Tumber, Defining a tissue stem cell-driven Runx1/Stat3 signalling axis in epithelial cancer, *EMBO J.* 31 (2012) 4124–4139.
- [41] T. Ge, M. Yin, M. Yang, T. Liu, G. Lou, MicroRNA-302b suppresses human epithelial ovarian cancer cell growth by targeting RUNX1, *Cell. Physiol. Biochem.* 34 (2014) 2209–2220.
- [42] Q. Li, Q. Lai, C. He, Y. Fang, Q. Yan, Y. Zhang, X. Wang, C. Gu, Y. Wang, L. Ye, L. Han, X. Lin, J. Chen, J. Cai, A. Li, S. Liu, RUNX1 promotes tumour metastasis by activating the Wnt/beta-catenin signalling pathway and EMT in colorectal cancer, *J.*

- Exp. Clin. Cancer Res. 38 (2019) 334.
- [43] L. Wang, J.S. Brugge, K.A. Janes, Intersection of FOXO- and RUNX1-mediated gene expression programs in single breast epithelial cells during morphogenesis and tumor progression, *Proc. Natl. Acad. Sci. U. S. A.* 108 (2011) E803–E812.
- [44] L. Debaize, H. Jakobczyk, S. Avner, J. Gaudichon, A.G. Rio, A.A. Serandour, L. Dorsheimer, F. Chalmel, J.S. Carroll, M. Zornig, M.A. Rieger, O. Delalande, G. Salbert, M.D. Galibert, V. Gandemer, M.B. Troadec, Interplay between transcription regulators RUNX1 and FUBP1 activates an enhancer of the oncogene c-KIT and amplifies cell proliferation, *Nucleic Acids Res.* 46 (2018) 11214–11228.
- [45] J. Gilmour, S.A. Assi, L. Noailles, M. Lichtinger, N. Obier, C. Bonifer, The co-operation of RUNX1 with LDB1, CDK9 and BRD4 drives transcription factor complex relocation during haematopoietic specification, *Sci. Rep.* 8 (2018) 10410.
- [46] G.M. Wildey, P.H. Howe, Runx1 is a co-activator with FOXO3 to mediate transforming growth factor beta (TGFbeta)-induced Bim transcription in hepatic cells, *J. Biol. Chem.* 284 (2009) 20227–20239.
- [47] M.C. Luo, S.Y. Zhou, D.Y. Feng, J. Xiao, W.Y. Li, C.D. Xu, H.Y. Wang, T. Zhou, Runt-related transcription factor 1 (RUNX1) binds to p50 in macrophages and enhances TLR4-triggered inflammation and septic shock, *J. Biol. Chem.* 291 (2016) 22011–22020.

# SCIENTIFIC REPORTS



OPEN

## An active IGF-1R-AKT signaling imparts functional heterogeneity in ovarian CSC population

Ram K. Singh<sup>1</sup>, Ajit Dhadve<sup>1</sup>, Asmita Sakpal<sup>1</sup>, Abhijit De<sup>2</sup> & Pritha Ray<sup>1</sup>

Received: 14 July 2016

Accepted: 17 October 2016

Published: 07 November 2016

Deregulated IGF-1R-AKT signaling influences multiple nodes of cancer cell physiology and assists in migration, metastasis and acquirement of radio/chemoresistance. Enrichment of cancer stem cells (CSC) positively correlates with radio/chemoresistance development in various malignancies. It is unclear though, how IGF-1R-AKT signalling shapes CSC functionality especially in ovarian cancer. Previously we showed that upregulated IGF-1R expression is essential to initiate platinum-taxol resistance at early stage which declines with elevated levels of activated AKT at late resistant stage in ovarian cancer cells. Here, we investigated the effect of this oscillatory IGF-1R-AKT signalling upon CSC functionality during generation of chemoresistance. While gradual increase in CSC properties from early (ER) to late (LR) resistant stages was observed in three different (cisplatin/paclitaxel/cisplatin-paclitaxel) cellular models created in two ovarian cancer cell lines, the stemness gene expressions (*oct4/sox2/nanog*) reached a plateau at early resistant stages. Inhibition of IGF-1R only at ER and AKT inhibition only at LR stages significantly abrogated the CSC phenotype. Interestingly, real time bioluminescence imaging showed CSCs of ER stages possessed faster tumorigenic potential than CSCs belonging to LR stages. Together, our data suggest that IGF-1R-AKT signalling imparts functional heterogeneity in CSCs during acquirement of chemoresistance in ovarian carcinoma.

Insulin like Growth Factor-1 Receptor (IGF-1R) is a transmembrane receptor tyrosine kinase which transmits signal via PI3K-AKT or MAPK-ERK pathways<sup>1-3</sup>. In addition to its essential functions for normal growth and development, deregulated IGF-1R signaling plays a major role in tumor growth and chemoresistance<sup>4-6</sup>. Generation of radio/chemoresistance is a major hurdle in successful treatment of cancers which may arise due to presence of inherently resistant tumor cells or due to acquirement of resistance by these cells<sup>5,7,8</sup>. While molecular alteration in various pathways assist in resistance development<sup>9</sup>, a small subset of inherently resistant cells within tumor bulk known as Cancer Stem Cells (CSC) also aid in acquirement of chemoresistance and relapse<sup>10-12</sup>. Currently considerable effort is undergoing to develop strategies to target these deadly populations for ultimate cure of cancer. Historically CSCs from different malignancies are isolated using a set of biomarkers. However, overlapping presence of these biomarkers in normal cell types poses a real challenge for targeting CSCs. In congruence with intratumoral heterogeneity, recent evidences suggest that CSCs are also not uniform but rather heterogeneous population and highly plastic in nature<sup>13-15</sup>. Existence of such heterogeneity within CSCs adds another layer of complexity for efficient targeting. Till date, CSC heterogeneity has been recognized by presence of biomarkers along with certain functional assays. CD44<sup>+</sup>/CD24<sup>-</sup> and ALDH<sup>+</sup> breast CSCs are reported to be more tumorigenic with poor clinical outcome than CSCs expressing CD44<sup>+</sup>/CD24<sup>-</sup> alone<sup>16</sup>. Additionally, both CD133<sup>+</sup> and CD133<sup>-</sup> CSC population from glioblastoma tumors found to possess self-renewing and tumor-initiating properties thereby casting doubt on biomarker based CSC isolation and characterization<sup>17</sup>. Still biomarker based therapeutic strategy to eradicate CSCs was attempted and patient derived CD44<sup>+</sup> ovarian CSCs possessing high claudin-4 expression were shown to be effectively targeted by *Clostridium perfringens* enterotoxin<sup>18</sup>. Intriguingly, whether and how a signaling pathway bestows heterogeneity in CSC population has so far not been investigated.

Using indigenously developed resistant models against cisplatin, paclitaxel and dual drugs in ovarian cancer cells, we showed that upregulated IGF-1R expression is crucial to initiate resistance and an activated AKT later

<sup>1</sup>Imaging Cell Signaling and Therapeutics Lab, Advanced Centre for Treatment, Research and Education in Cancer (ACTREC), Tata Memorial Centre, Navi Mumbai, Maharashtra, India. <sup>2</sup>Molecular Functional Imaging Laboratory, Advanced Centre for Treatment, Research and Education in Cancer (ACTREC), Tata Memorial Centre, Navi Mumbai, Maharashtra, India. Correspondence and requests for materials should be addressed to P.R. (email: pray@actrec.gov.in)

assists in maintenance of resistance<sup>19,20</sup>. Irrespective of nature of drugs, early resistant (ER) cells of all these models show higher IGF-1R expression, while late resistant (LR) cells possess low IGF-1R but elevated phosphorylated AKT<sup>19</sup>. Role of IGF-1R in developing cisplatin or paclitaxel resistance in ovarian cancer cells were reported by others<sup>5,6</sup>.

Herein we investigated the consequence of this oscillatory IGF-1R-AKT signaling upon CSC properties during acquisition of platinum-taxol resistance. While gradual increase in CSC features were found to be positively correlated with resistance development (from ER to LR stages), the stemness gene expressions reached a plateau early on. Inhibition of IGF-1R at ER and AKT inhibition at LR stages significantly abrogated CSC and chemoresistant phenotype. Interestingly, real time imaging showed CSCs of ER stages possessed higher and faster tumorigenic potential than CSCs belong to LR stages. Inhibition of AKT relieved IGF-1R suppression and sensitized the late resistant cells to combinatorial treatments. This is the first report on an intricate and interdependent relation between IGF-1R and AKT with functional heterogeneity of ovarian cancer stem cells which might emerge as a therapeutic target for the resistant disease.

## Results

### Enrichment of Stem cell like features with acquisition of drug resistance in ovarian cancer cells.

We have previously developed dynamic models of drug resistance against cisplatin, paclitaxel and both drugs by treating A2780 and OAW42 ovarian cancer cell lines with successive and gradually increasing drug concentration and categorized them into early (ER) (Cis<sup>ER</sup>, Pac<sup>ER</sup> and Dual<sup>ER</sup>) and late (LR) (Cis<sup>LR</sup>, Pac<sup>LR</sup> and Dual<sup>LR</sup>) resistant stages depending on their resistant indices<sup>20</sup>. Intriguingly, irrespective of the nature of drugs, elevated levels of IGF-1R and high phosphorylated AKT were found to be associated with early and late stages of resistance which seem to be essential for initiation (at early stage) and maintenance (late stage) of drug resistance<sup>19</sup>.

To understand the association of Cancer Stem Cell dynamics with acquisition of resistance, functional assays and biomarker association were studied in these cellular resistant models. Side population assay (SP) which purifies CSCs based on their innate drug efflux property was used for CSC isolation from different stages of resistance. A gradual and significant enrichment in SP cells ( $3.9 \pm 0.05\%$  in Cis<sup>ER</sup> &  $7.2 \pm 0.42\%$  in Cis<sup>LR</sup> cells) compared to the chemosensitive A2780 cells ( $1.5 \pm 0.05\%$  SP) was observed in cisplatin resistant model ( $p < 0.05$ ). Similar enhancement in SP cells was observed with both Paclitaxel and dual resistant models. The dual resistant model showed maximal enrichment in SP population at late resistant stage ( $19.1 \pm 1.0\%$  (13.2 fold) (Fig. 1A). The OAW42 resistant models also exhibited enhanced SP population across cisplatin, paclitaxel and dual resistant cells compared to OAW42 sensitive cells (Supplementary Table 2). However, the absolute level of SP cells was 2-fold higher in A2780-Dual<sup>LR</sup> than OAW42-Dual<sup>LR</sup> cells ( $19.1\%$  vs.  $9.8\%$ ). Cancer stem cells possess higher self-renewal ability which is assessed through spheroid formation assay. In both A2780 and OAW42 cellular resistant models, significant enhancement in spheroid formation was observed with increasing resistance. When compared between the models, both Pac<sup>ER</sup> and Pac<sup>LR</sup> cells exhibited enhanced spheroid forming ability than Cis<sup>ER</sup> and Cis<sup>LR</sup> cells. However, this trend only met significance for Pac<sup>LR</sup> cells (Fig. 1B,C). It was also observed that both sensitive cells (A2780 and OAW42) cells could form spheroids up to two passage only, while resistant cells were capable of forming spheroids till seven passages. Higher spheroid formation in A2780 resistant models suggests superior self-renewal ability of these cells compared to OAW42 cells.

The level of known ovarian CSC biomarkers (CD44 and CD133) expression was monitored in both A2780 and OAW42 resistant models (Fig. 1D, Supplementary Figure 1). A2780 cells did not show detectable CD44 expression (data not shown) however the level of CD133 showed marked increase with increasing resistance (A2780 = 22%; Cis<sup>ER</sup> = 44.7%; Cis<sup>LR</sup> = 97.1%; Pac<sup>ER</sup> = 66.9%; Pac<sup>LR</sup> = 98.7%; Dual<sup>ER</sup> = 71.3%; Dual<sup>LR</sup> = 95.5%). We also tested the expression of these markers in OAW42 cellular resistant models where CD44 expression showed marked increase with increasing resistance (OAW42 = 12.7%; Cis<sup>ER</sup> = 15.7%; Cis<sup>LR</sup> = 19.9%; Pac<sup>ER</sup> = 24.7%; Pac<sup>LR</sup> = 25.9%; Dual<sup>ER</sup> = 15%; Dual<sup>LR</sup> = 23.9%). Very low expression of CD133 was observed in OAW42 cisplatin and paclitaxel resistant models compared to A2780 resistant models which showed the similar trend of enhanced expression with increasing resistance. The dual resistant model in OAW42 cells showed maximum enhancement in CD133 level (OAW42 = 0.62%; Cis<sup>ER</sup> = 1.48%; Cis<sup>LR</sup> = 1.53%; Pac<sup>ER</sup> = 2.16%; Pac<sup>LR</sup> = 3.84%; Dual<sup>ER</sup> = 5.57%; Dual<sup>LR</sup> = 9.01%) (Fig. 1D, Supplementary Figure 1). Interestingly, real time quantification of *oct4*, *sox2* and *nanog* (Pluripotent genes) expression showed marked increase at early resistance stages compared to the sensitive stages which remained unaltered even at late resistant stages uniformly in all the resistant models (Fig. 1E,F).

### Side population fraction is enriched with cancer stem cell features.

Side population (SP) assay is considered a routine method for CSC characterization. However, the discriminating power of this assay to identify stem cells over non-stem cell population is sometimes criticized<sup>21</sup>. To test the true stemness phenotype of the SP population of all the resistant models (A2780 & OAW42), both self-renewal and differentiation properties were assayed. SP cells sorted from sensitive and early and late resistant stages of all three drug resistant models of A2780 showed significantly higher spheroid formation ( $p < 0.05$ ) than their non-SP counterparts (Fig. 2A). Interestingly, not much difference in spheroid forming ability was found between the early and late resistant cells of each drug resistant models (Fig. 1A,B). When compared across the models, an apparent enhanced spheroid formation was observed for Paclitaxel resistant cells than Cisplatin resistant cells. However, only Pac<sup>LR</sup> cells formed significantly higher number of spheroids compared to Cis<sup>LR</sup> cells ( $p < 0.05$ ). The spheroid forming ability between Cis<sup>ER</sup> and Pac<sup>ER</sup> cells did not show any significant difference.

Transcript levels of *oct4*, *sox2* and *nanog* were significantly higher in SP cells than their NSP counterparts (Fig. 2B,C). *In vitro* differentiation is one of the important characteristic features to assess CSC phenotype. We performed serial sorting of SP and NSP cells from chemosensitive and late cisplatin-resistant A2780 cells for three cycles. Intriguingly, we did not observe an absolute persistence of 100% SP cells from 1<sup>st</sup> to 3<sup>rd</sup> sort, rather

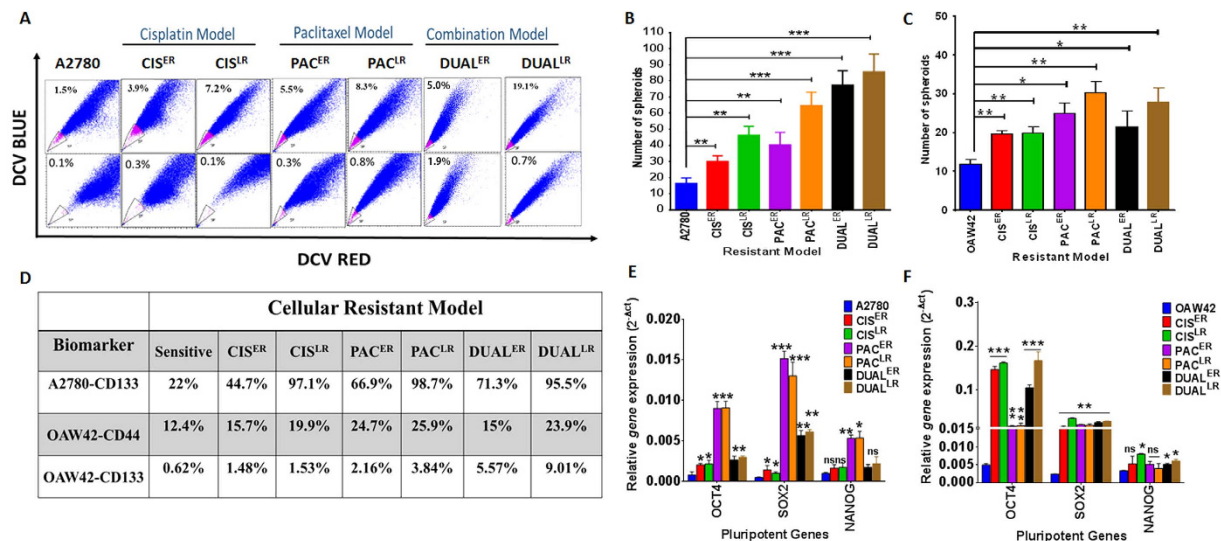


**Figure 1. Characterization of stem cell like features across the cellular resistant models.** (A) Increased Side Population in three different A2780 resistant models (cisplatin, paclitaxel and dual). FACS dot plot showing the distribution of SP cells with or without verapamil treatment which increases with increasing resistance. (B,C) Graphical representation of enhanced spheroid formation observed across all the resistant models. Resistant models in OAW42 cells exhibited slightly lesser spheroids (Cis-Res = 1.63–1.66 fold; Pac-Res = 2.08–2.5 fold; Dual-Res = 1.8–2.3 fold) but resistant models of A2780 cells showed considerably elevated spheroid formation (Cis-Resistant model = 1.8–2.8 fold; Pac-Resistant model = 2.4–3.9 fold; Dual-Resistant model = 3.8–5.3 fold) than the respective sensitive cells. (D) Increased expression of biomarkers (CD133 and CD44) with enhanced resistance observed across the resistant models. Control A2780 cells showed 22% positivity for CD133 expression which increased in each of the drug resistance models; (CD133 expression: A2780 = 22%; Cis<sup>ER</sup> = 44.7%; Cis<sup>LR</sup> = 97.1%; Pac<sup>ER</sup> = 66.9%; Pac<sup>LR</sup> = 98.7%; Dual<sup>ER</sup> = 71.3%; Dual<sup>LR</sup> = 95.5%). A2780 cells did not show detectable CD44. CD44 expression in OAW42 cellular models also showed increments with increasing resistance (OAW42 = 12.7%; Cis<sup>ER</sup> = 15.7%; Cis<sup>LR</sup> = 19.9%; Pac<sup>ER</sup> = 24.7%; Pac<sup>LR</sup> = 25.9%; Dual<sup>ER</sup> = 15%; Dual<sup>LR</sup> = 23.9%). Low but increasing CD133 expression was associated with OAW42 resistant models (OAW42 = 0.62%; Cis<sup>ER</sup> = 1.48%; Cis<sup>LR</sup> = 1.53%; Pac<sup>ER</sup> = 2.16%; Pac<sup>LR</sup> = 3.84%; Dual<sup>ER</sup> = 5.57%; Dual<sup>LR</sup> = 9.01%) (E,F) Real time quantification of *oct4*, *sox2* and *nanog* expression across A2780 resistant models showed maximal expression at early resistant stages which remained constant till late resistant stages. Similar trend was observed in OAW42 resistant models.

a gradual enrichment (A2780~1.4% to 27.1%; A2780 Cis<sup>LR</sup>~7.3% to 49.3%) was found and simultaneously the NSP population decreased. The NSP cells, in contrary did not form any SP cells till third passage (Fig. 2D). In addition to stemness phenotype we also measured the resistant phenotype where SP cells of late resistant models of A2780 showed higher viability at respective IC<sub>50</sub> concentrations (CIS<sup>LR</sup> = 5 µg/ml; PAC<sup>LR</sup> = 125 ng/ml and DUAL<sup>LR</sup> = 500 ng/ml cisplatin + 80 ng/ml paclitaxel) compared to their NSP or main population. The slight difference in survival rate between MP and NSP population suggests that NSP cells can maintain their chemoresistance phenotype but are devoid of stem cell pool (Fig. 2E). We also measured cellular viability of SP, NSP and MP fractions for every cycle during enrichment of SP cells and found that SP cells showed significantly higher viability compared to its respective counterparts (MP and NSP cells) (Supplementary Figure 3).

### Real time monitoring of tumor growth kinetics of SP population by bioluminescence imaging.

The most crucial characteristics that differentiate a cancer stem cell from a normal stem cell lies in its inherent tumorigenic ability. After assessing the self-renewal and differentiation properties, we sought to evaluate the tumorigenic potential of the SP population through *in vitro* clonogenic assay and *in vivo* tumor forming ability in immune compromised mice. As expected the NSP cells from both early and late resistant stages of all the three models of A2780 cells formed significantly lower clones than their SP counterparts. Number of clones formed by the NSP cells was also found to be lower than the number of clones formed by total population across all the resistant models (Fig. 3A). Interestingly SP cells from each of the early resistant stages (Cis<sup>ER</sup>, Pac<sup>ER</sup> and Dual<sup>ER</sup>) showed significantly higher number of colonies than SP cells from late resistant stages (Cis<sup>LR</sup>, Pac<sup>LR</sup> and Dual<sup>LR</sup>) (Fig. 3A). This intriguing differential clonogenic property exhibited by early and late resistant SP cells was further tested in living subjects in real time.

Fifty thousand SP and NSP cells from Pac<sup>ER</sup> and Dual<sup>ER</sup> A2780 cells were sub-cutaneously implanted in both flanks of NOD/SCID mice (n = 5) and longitudinally monitored by bioluminescence imaging. To directly compare the tumorigenic ability of CSC (SP cells) and non-CSC (NSP cells) population of different resistant stages, we purposely implanted higher number of cells to measure the actual tumorigenic potential (even with lower efficiency) of the NSP populations in the same mouse. Though luciferase signal was observed at both SP and NSP sites in all 10 mice at day 0, tumor development was observed in 60% and 80% of mice for Pac and

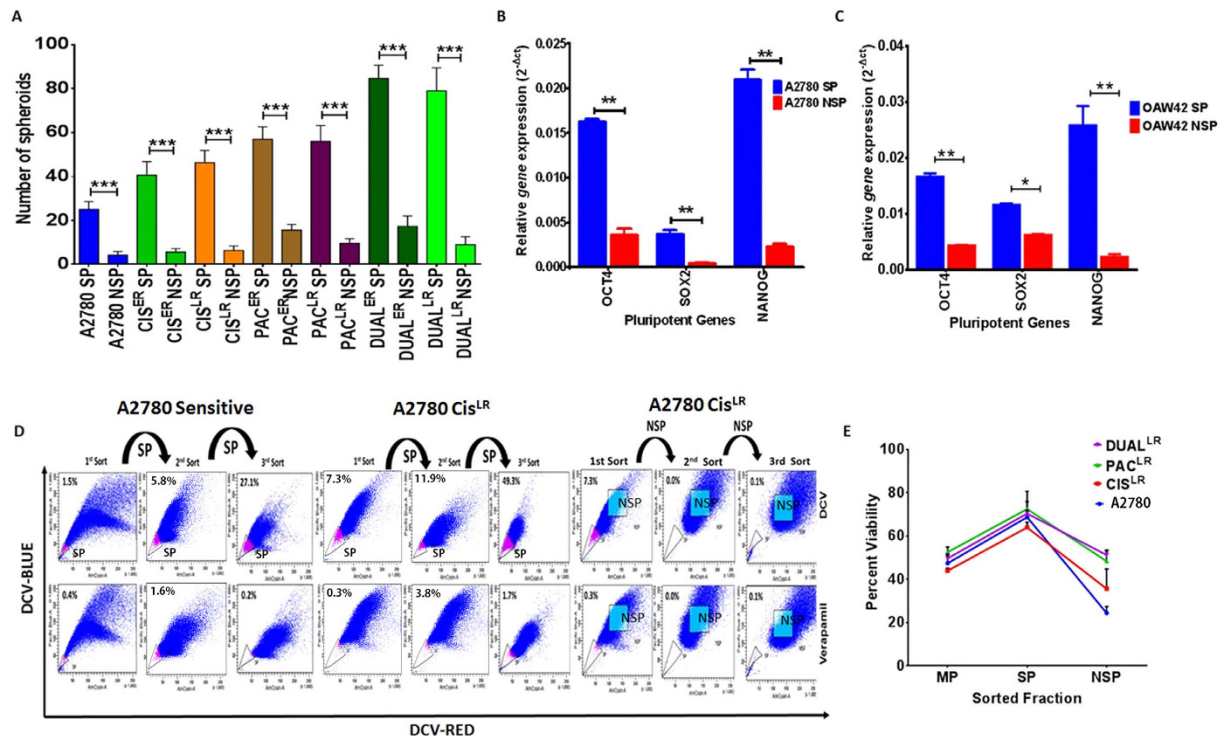


**Figure 2. Characterization of side population cells for their stem cell like features.** (A) Graphical representation of higher spheroid forming ability of SP cells of A2780 sensitive, early and late resistant cells from all the three resistant models than corresponding NSP cells. (B,C) Real time quantification of *oct4*, *sox2* and *nanog* expression in SP and NSP fractions of A2780 and OAW42 sensitive cells showing significantly increased expression of these pluripotent genes in SP cells than NSP cells. (D) FACS analysis of differentiating ability of SP and NSP cells monitored over three subsequent passages by DCV staining. (E) MTT assay showing marked increase in viability of SP cells (A2780 SP = 68.75%, Cis<sup>LR</sup> SP = 63.99%, Pac<sup>LR</sup> SP = 72.4% and Dual<sup>LR</sup> SP = 70.45%) compared to main population (MP) and NSP cells at IC<sub>50</sub> of respective drug concentration. (Data represented as ± SEM; \*p < 0.05; \*\*p < 0.005; \*\*\*p < 0.0005).

dual resistant cells respectively and only at SP cell implantation sites. Enhanced luciferase signal at SP-Pac<sup>ER</sup> tumor site (n = 3) was observed from day 0 to day 25 ( $2.21 \times 10^5 \pm 9.24 \times 10^4$  to  $8.67 \times 10^6 \pm 5.80 \times 10^6$  p/sec/cm<sup>2</sup>/sr) indicating tumor initiation which increased ( $3.54 \times 10^8 \pm 2.05 \times 10^8$  p/sec/cm<sup>2</sup>/sr) and palpable tumors ( $0.98 \pm 0.80$  cm<sup>3</sup>) were observed by day40 (Fig. 3B). In contrary, the NSP-Pac<sup>ER</sup> tumors lost the bioluminescence signal over time and did not show any palpable tumor till 50 days. Similar trends were observed for SP-dual<sup>ER</sup> and NSP-dual<sup>ER</sup> tumors, where bioluminescence signal at SP implantation sites increased from day 0 to day 25 to day 40 ( $1.04 \times 10^6 \pm 5.06 \times 10^5$  to  $9.84 \times 10^6 \pm 2.1 \times 10^5$  to  $5.06 \times 10^7 \pm 1.76 \times 10^7$  p/sec/cm<sup>2</sup>/sr) with palpable tumors ( $0.57 \pm 0.25$  cm<sup>3</sup>) at day 40 were found only for SP cells (Fig. 3C).

Quite distinct and unexpected tumor growth kinetics was observed when SP-Cis<sup>LR</sup> and SP-Pac<sup>LR</sup> A2780 tumors (n = 5 each) were monitored in real time. To characterize late resistant SP population independent of nature of drug used, the cisplatin resistant cells were used along with paclitaxel resistant cells. For both SP and NSP tumor sites, no increase in bioluminescence signal was found from day 0 to day 50 (data not shown). Unlike SP-Pac<sup>ER</sup> cells where tumor initiation noticed from day 25, first detectable luminescence signal from SP-Pac<sup>LR</sup> tumors was found on day 80 ( $2.65 \times 10^5 \pm 6.37 \times 10^4$  to  $1.65 \times 10^6 \pm 1.49 \times 10^6$  p/sec/cm<sup>2</sup>/sr) and a sharp increase in bioluminescence was observed within 10 days ( $2.73 \times 10^7 \pm 1.43 \times 10^7$  p/sec/cm<sup>2</sup>/sr) (Fig. 3D). No tumors or bioluminescence was observed at the site of NSP cells implantation. Compared to SP-Pac<sup>ER</sup> cells, SP-Pac<sup>LR</sup> cells produced significantly smaller tumors (SP PAC<sup>ER</sup> =  $1.52 \pm 0.76$  cm<sup>3</sup>; SP PAC<sup>LR</sup> =  $0.28 \pm 1.9$  cm<sup>3</sup>). For SP-Cis<sup>LR</sup> tumors, detectable signal was found on day 80 ( $7.60 \times 10^4 \pm 2.26 \times 10^4$  p/sec/cm<sup>2</sup>/sr) followed by gradual increase in signal ( $1.27 \times 10^7 \pm 6.7 \times 10^6$  p/sec/cm<sup>2</sup>/sr) and tumor volume ( $0.76 \pm 0.058$  cm<sup>3</sup>) till day 100 (Fig. 3E). Again loss of bioluminescence signal and no tumor formation were observed at NSP cells implantation sites. Only 60% mice for both these group of late resistant cells developed tumors.

The higher tumorigenic potential found in SP cells of early resistant stages is quite unexpected and might be driven by an active signalling cascade involved in cellular proliferation. We have previously reported that irrespective of the nature of the drugs, the early resistant cells possess enhanced expression of IGF-1R which decreases at late stages of resistance<sup>19</sup>. Thus this crucial cell proliferating signalling cascade governed by IGF-1R might have influence on the enhanced tumorigenic potential of SP cells of early resistant stages.

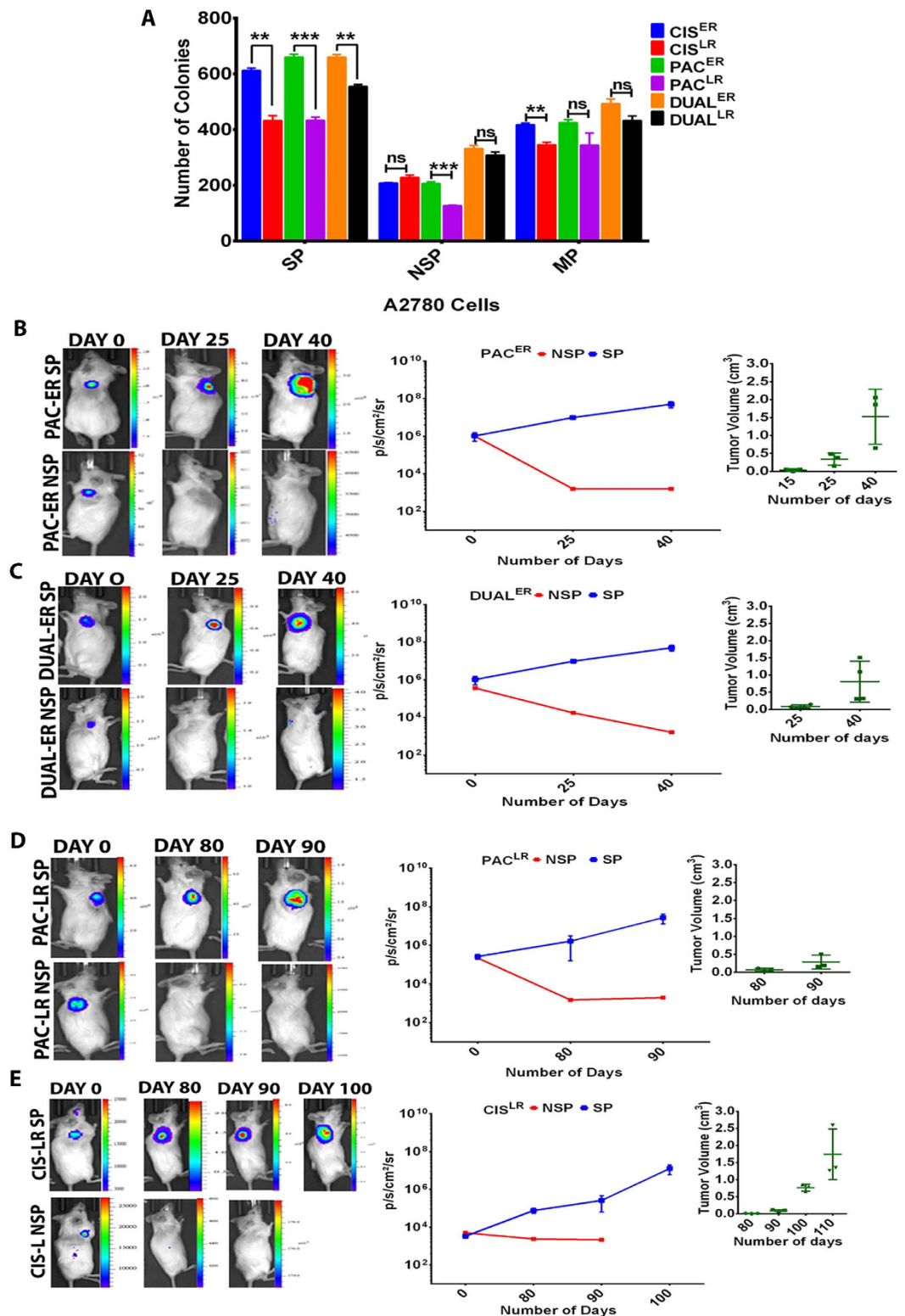


**Figure 3. Monitoring tumorigenic properties of SP/NSP cells from early and late resistant stages of A2780 resistant models in real time.** (A) Bar graph showing significant increase in the clonogenic potential of ER-SP cells than LR-SP cells. (B,C) Representative bioluminescence images of early resistant cells (Pac<sup>ER</sup> and Dual<sup>ER</sup>) from day 0 to day 40 and graphical representation showing increased bioluminescence signal and tumor volume by SP cells. NSP cells showed significant decrease in bioluminescence and absence of tumor formation ( $p < 0.05$ ), [Data represented as  $\pm$  SEM for  $n = 3$ ]. (D,E) Representative bioluminescence images of late resistant cells (Pac<sup>LR</sup> and Cis<sup>LR</sup>) from day 0 to day 90 and graphical representation showing increased bioluminescence signal and tumor volume by SP cells. NSP cells showed significant decrease in bioluminescence signal and absence of tumor formation ( $p < 0.05$ ) [Data represented as  $\pm$  SEM for  $n = 3$ ].

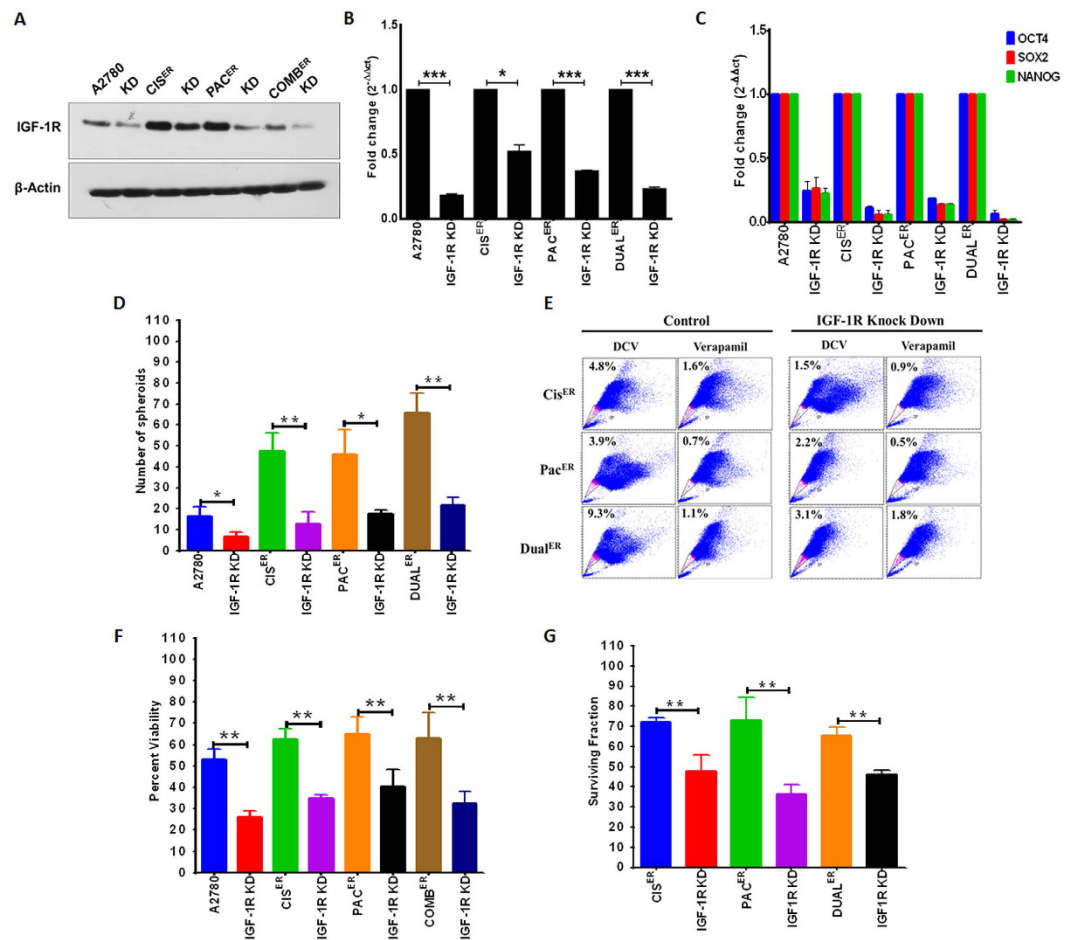


**Figure 4. Effect of IGF-1R inhibition upon CSC and resistance phenotypes at early stages of all cellular resistant models.** (A,B) Western blot analysis and RT PCR showing marked decrease in the levels of IGF-1R in A2780-Cis<sup>ER</sup>, A2780-Pac<sup>ER</sup> and A2780-Dual<sup>ER</sup> IGF-1R knockdown cells compared to the respective controls. (C) Bar Graph showing fold decrease in expression of pluripotent genes (*oct4*, *sox2* and *nanog*) in A2780-IGF-1R knockdown cells compared to their parental cells where dual<sup>ER</sup> knockdown cells showed maximum down regulation. (D) Graphical representation of spheroid forming ability of A2780, Cis<sup>ER</sup>, Pac<sup>ER</sup> and Dual<sup>ER</sup> control cells and their respective IGF-1R knockdown cells. (E) MTT assay showing marked decrease in the cell viability post drug treatment (IC<sub>50</sub>) in the A2780-IGF-1R KD cells. (F) Bar Graph showing decreased surviving cells in A2780-IGF-1R KD cells post drug treatment (IC<sub>50</sub>) compared to their parental cells. (G) FACS dot plot showing decreased SP cells after knockdown of IGF-1R cells compared to their respective control cells.

**Effect of IGF-1R inhibition upon cancer stem cells and chemoresistant phenotype.** Till date, association of IGF-1R signaling with CSC phenotype is reported for colon and breast cancers<sup>22,23</sup>. Whether and how IGF-1R signaling influences the stemness phenotype in chemoresistant ovarian cancer cells is never investigated. We next attempted to investigate the association of upregulated IGF-1R with CSC features by inhibiting IGF-1R with different strategies and testing the various properties of CSCs. Treatment with Picropodophyllin (PPP), a small molecule inhibitor of IGF-1R decreased spheroid forming ability and pluripotent gene expression in sensitive, ER and LR cells from different resistant models of A2780 cells (Supplementary Figure 2). Maximal inhibition in spheroid formation and stemness gene expression was observed in early resistant stages compared to sensitive and late resistant stages except for the dual resistant model where reduction in levels of spheroid formation did not differ between early and late resistant stages. Decreased stemness properties by PPP in late resistant cells were unexpected and could have caused by overall inhibition of IGF-1R signaling. Additionally, PPP, though specifically inhibits IGF-1R over insulin receptor can exert some toxicity through microtubules inhibition<sup>24</sup> which prompted us to adapt shRNA mediated stable knockdown strategy for early resistant stages of A2780 cellular models. Western blot analysis and RT PCR showed significant decrease in IGF-1R level in knockdown cells (Fig. 4A,B). Silencing of IGF-1R resulted in drastic decrease in the levels of pluripotent gene expression (*oct4*, *sox2* and *nanog*) compared to their parental cells and this decrease was maximally observed in Dual<sup>ER</sup> cells (Fig. 4C). The effect of IGF-1R knockdown was even more prominent on self-renewal ability, showing significant decrease in their spheroid forming capacity (A2780 sensitive cells~2.5 fold, Cis<sup>ER</sup>~3.66 fold, Pac<sup>ER</sup>~2.6 fold and dual<sup>ER</sup>~3.04 fold) and SP phenotype (Cis<sup>ER</sup>~3.2 fold, Pac<sup>ER</sup>~1.7 fold and dual<sup>ER</sup>~3 fold) (Fig. 4D,E). IGF-1R silencing in early resistant cells also affected their chemoresistant phenotype as observed by decrease in percent

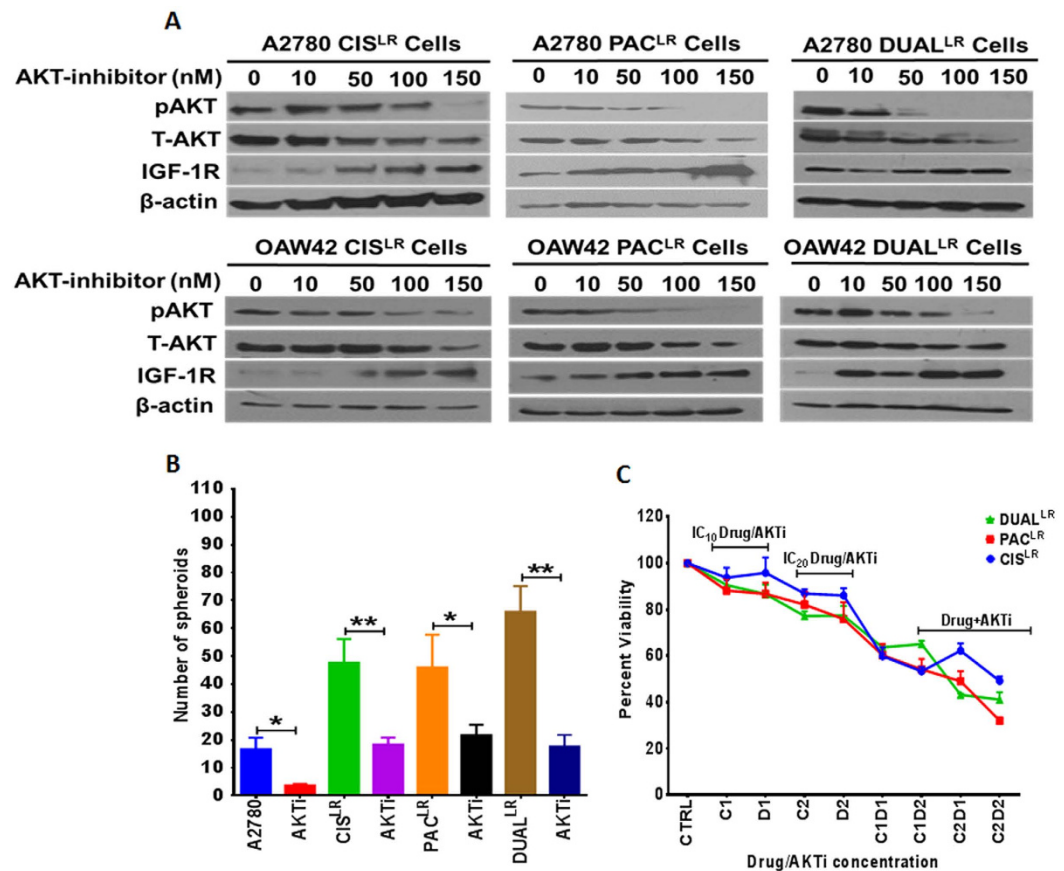


**Figure 5. Effect of AKT inhibition upon CSC and resistance phenotypes at late stages of all cellular resistant models.** (A) Western blot analysis showing AKT inhibitor treatment led to decreased levels of pAKT with increasing IGF-1R levels in a dose dependent manner across all the late resistant cells (A2780 & OAW42).  $\beta$  actin was used as a loading control. (B) Decreased spheroid forming ability of late resistant cells across all the resistant models (cisplatin, paclitaxel and dual) after treatment with AKT inhibitor (150 nM). (C) MTT assay showing least percent viability for all the late resistant A2780 cells after combinatorial treatment of AKT inhibitor and respective drugs (at  $IC_{20}$  concentrations) in comparison to treatments of inhibitor and drug alone (at respective  $IC_{10}$ ,  $IC_{20}$  concentrations) or combinatorial treatment at  $IC_{10}$  concentrations. (Data represented as  $\pm$  SEM, \* $p < 0.05$ ; \*\* $p < 0.005$ ).

viability and clonogenic potential (Fig. 4E,G). Since late resistant stages possessed very little IGF-1R expression (Singh *et al.*)<sup>19</sup> our attempt to silencing did not result in further decrease (data not shown).

**A feedback loop in IGF-1R-AKT axis influence resistance maintenance and CSC features.** In spite of low IGF-1R expression, late resistant cells of all the different drug resistant models have high levels of phosphorylated AKT<sup>19</sup> indicating that AKT could be a critical player in the maintenance of both chemoresistance and CSC phenotype. Indeed treatment with an AKT inhibitor decreased p-AKT levels in a dose dependent manner and also spheroid formation in Cis<sup>LR</sup>, PAC<sup>LR</sup> and Dual<sup>LR</sup> A2780 cells (Cis<sup>LR</sup>~2.6 fold, Pac<sup>LR</sup>~2.12 fold and dual<sup>LR</sup>~3.8 fold) (Fig. 5A,B). Levels of total AKT also slightly decreased after treating the cells with high concentration of the inhibitor (150 nm). Intriguingly AKT inhibition resulted in marked increase in IGF-1R levels (Fig. 5A), suggesting of a possible feedback loop in the IGF-1R-AKT axis during development of chemoresistance in ovarian cancer cells. Similar trend was also seen in other drug resistant models (cisplatin, paclitaxel and Dual) of OAW42 cells. Since we observed a feedback loop in IGF-1R-AKT axis, an AKT inhibitor alone and in combinations of drugs (cisplatin, paclitaxel and cisplatin + paclitaxel) at lowest possible doses ( $IC_{10}$  and  $IC_{20}$  concentrations) was used to treat the cellular models. Maximum cell kill (Cis<sup>LR</sup> = 50.79%; Pac<sup>LR</sup> = 68% and Dual<sup>LR</sup> = 59%) was observed in combinatorial treatment of the inhibitor and  $IC_{20}$  concentrations (Cis<sup>LR</sup> = 2  $\mu$ g/ml, PAC<sup>LR</sup> = 50 ng/ml and Dual<sup>LR</sup> = 7 ng/ml cisplatin + 40 ng/ml paclitaxel) of drug/s in comparison to  $IC_{10}$  combinatorial treatments as well as drugs and inhibitor alone (Fig. 5C). Exertion of a negative feedback loop upon an upstream molecule (IGF-1R) by a downstream member (Akt) of the same signalling cascade prompted us to analyse the efficacy of combinatorial treatment of IGF-1R and AKT inhibitors in late resistant cells. Significantly higher cell death (~2 fold) and reduced IGF-1R and pAkt levels were observed in combinatorial treatments ( $IC_{20}$  doses of PPP and AKT inhibitor) than single treatments as measured through MTT assay and western blotting (Supplementary Figure 4A,B).

## Discussion

Presence of stem cell like population in various malignancies and their enrichment as the disease turns radio/chemoresistant is a challenging affair for successful treatment. The quiescent and resistant nature of the cancer stem cells act as double edged sword to battle the therapeutic effects of cytotoxic drugs especially for those which target replication machinery of the cells. Understanding and identifying signalling pathways critical for CSC functionality is therefore an active area of current biomedical research. Though acquirement of chemoresistance is a common problem for majority of the cancers, it is particularly devastating for epithelial ovarian cancer patients. Several recent studies suggest the presence and deleterious effect of CSCs in this chemoresistant patient population<sup>9,10</sup>. Acquirement of resistance towards drug is a dynamic and multifactorial process and dominated by enrichment of CSC population. To understand this intricate relation between CSCs and enhanced drug resistance, we have used dynamic cellular models of resistance developed indigenously against Cisplatin, Paclitaxel and Dual drugs in A2780 and OAW42 ovarian cancer cells<sup>20</sup>. Based on the resistance indices, these cellular models are categorized into early and late resistant stages and shown to possess preferential up regulation of IGF-1R and activated AKT at early and late resistant stages respectively<sup>19</sup>. We hypothesized that not only the number but the properties of CSCs might enhance with increasing chemoresistance and targeting these population at right stages could be therapeutically beneficial. Thus in this study, we assessed two crucial functional properties (self-renewal and differentiation) of cancer stem cells through side population and spheroid formation assays and compared their *in vivo* tumorigenicity at early and late resistant stages of A2780 chemoresistant models. As expected significant enrichment of SP population was observed across all the resistant models (cisplatin, paclitaxel and Cisplatin + Paclitaxel) in both cell lines. Self-renewal is a central character of both normal and cancer stem cells to maintain their own pool which is assessed by spheroid forming capabilities. Increased spheroid forming ability from early to late resistant cells indicated that self-renewal properties of cancer cells dynamically enhance with increased drug resistance. Co-ordinated protein-protein interaction of Oct4 and Sox2 transcription factors initiates Nanog transcription and these three proteins in coordination are thought to be central regulatory factors of several other genes that balance self-renewal and differentiation. Intriguingly, expression of *oct4* and *sox2* significantly increased from sensitive to early resistant stages and then remained plateau till late stages of resistance suggesting that an early up regulation of pluripotent gene expression is essential for maintenance of both self-renewal and differentiating ability of CSCs. An apparent trend of enhanced spheroid formation in paclitaxel resistant cells compared to cisplatin resistant cells might result from increased pluripotent gene expression at early stage. However, a detail investigation is required to understand the drug specific effects of pluripotent gene expression and self-renewal ability.

Intriguingly, despite of similar levels of IGF-1R expression, the CIS<sup>ER</sup> cells possess lower expression of all the three pluripotent genes than PAC<sup>ER</sup> cells. Several signaling pathways (LIF/Stat3, Wnt/GSK3 $\beta$  and TGF $\beta$ /Smad3) that regulate pluripotent gene expression in a context dependent manner exhibit cross talk with IGF-1R signaling<sup>25</sup>. It is still not known how and to what extent upregulated IGF-1R influences these pathways in cisplatin and paclitaxel resistance. However, it is well known that response of ovarian cancer cells to platinum and taxol drugs are variable through differential gene signatures<sup>26</sup>. Earlier publication from our lab showed that induction of NF- $\kappa$ B is essential for maintenance of only cisplatin resistance but not for paclitaxel resistance at late stages<sup>20</sup>. Thus, it is possible that a co-operative effect of IGF-1R along with other regulatory molecules exert differential levels of activation of the pluripotent genes during diverse drug resistance.

Higher spheroid formation and successive differentiation of SP cells to chemosensitive NSP lineages indicated that the SP fractions are enriched with CSC population. Ovarian Cancer Stem Cell biomarkers (CD133 and CD44) also showed increased expression with increasing resistance. However heterogeneity lies within these two cellular resistant models where A2780 and OAW42 showed differential biomarker expression. A2780 resistant model showed increased CD133 expression without a detectable expression of CD44. On the other hand, OAW42 cellular resistant models showed incremental CD44 expression and minimal levels of CD133. When tumorigenic ability of SP population from early and late resistant stages of A2780 cells was assessed in real time by optical imaging, faster tumor formation was observed in early resistant groups. Since these early resistant cells possess elevated IGF-1R expression, inhibition of IGF-1R by a small molecule inhibitor or specific shRNA significantly diminished SP population, spheroid formation as well as pluripotent gene expression. Intriguingly, when the late resistant cells were challenged with an AKT inhibitor, stemness features were declined and IGF-1R expression was elevated. Thus our data suggests that dynamic changes in chemoresistance development in ovarian cancer cells influence functionality of CSC pool which is tightly regulated by IGF-1R-AKT signalling cascade.

Insulin like growth factor 1 receptor signals through PI3K-AKT or MAPK-Erk pathway to directly control the cellular proliferation via activation of a series of protein kinases during the course of developmental process<sup>1,27</sup>. This upregulated IGF-1R signaling has also been shown to have a critical role in acquirement of chemoresistance<sup>5,6,19</sup> and CSC phenotype primarily in human breast cancer and hepatocellular carcinoma<sup>23,28</sup>.

Herein we for the first time elucidated the role of IGF-1R signaling in enrichment of CSC phenotype during acquirement of chemoresistance in ovarian cancer cells. Though acquirement of drug resistance involves many molecular and biochemical changes in cellular machineries, a class of transporter proteins known as multi drug resistance proteins plays key role in diminishing chemotherapeutic effects. Side population assay, a classical method to measure drug efflux properties of cells, has been adapted to assess CSC enrichment in various studies<sup>29-33</sup>. The SP cells showed higher cisplatin/paclitaxel/dual drug resistance than the main and NSP cells and higher spheroid formation and pluripotent gene expression in our models. Intriguingly, occurrence of more than 50% of NSP cells in repeatedly sorted and successively cultured SP cells indicated differentiation abilities of these CSCs. Till date, neuronal, haematopoietic and cancer stem cells were characterised for lineage specific differentiation<sup>34</sup>. A recent study by Touil *et al.*<sup>35</sup> using Rhodamine 123 (Rh123) exclusion assay (similar to SP assay) showed that a small subset of (Rh123)low cells from metastatic human melanomas and melanoma cell lines is enriched for stem cell like features and can produce non-stem (Rh123(high)) progeny and melanosphere<sup>35</sup>. Our study thus

provides a similar evidence of differentiation ability of ovarian cancer stem cells into non-stem and relatively drug sensitive progeny. In addition reduction in IGF-1R expression through small molecule inhibitor or shRNA predominantly decreased the stemness features in early resistant cells, while inhibition of AKT diminished spheroid formation in late resistant cells indicating an intricate influence of IGF-1R-AKT signalling on cancer stem cell functionalities.

In accordance with cancer cell heterogeneity residing in single tumor, diversity in cancer stem cell population in the same tumor or cell line has been identified<sup>13,34</sup>. This heterogeneity is majorly identified through presence or absence of biomarkers in conjugation with ALDH assay<sup>17</sup>. The biggest disadvantage of biomarker based segregation is the inability of utilizing them for targeting due to their presence in normal cells. Active attempts are being made to understand and utilize the targetable molecules in the diverse population of CSCs. High claudin 4 expression in patient derived CD44<sup>+</sup> ovarian CSCs was shown to be a potential target for *Clostridium perfringens* enterotoxin<sup>18</sup>. The intrigue observation of faster tumorigenicity by SP fraction of early resistant cells (A2780 Pac<sup>ER</sup> and dual<sup>ER</sup>) cells compared to their late resistant counterparts as well as other late resistant SP cells (A2780 Cis<sup>LR</sup> and Pac<sup>LR</sup>) in NOD/SCID mice demonstrates existence of functional heterogeneity in CSC population of the same cellular model. This heterogeneity does not depend on the nature of drug since early resistant cells from both Paclitaxel and dual resistant model showed similar rate of tumor formation. Real time monitoring of tumor growth by optical imaging conclusively demonstrated the non-tumorigenic nature of the NSP cells isolated from early as well as late resistant cells of A2780 chemoresistant models. While an upregulated IGF-1R expression could be a plausible factor for faster tumorigenic nature of the early resistant cells, the molecular factors behind the slower tumorigenic potential of late resistant cells are yet to be identified. Predominant presence of activated AKT contrasts this relatively dormant nature of late resistant cells, however, higher spheroid forming ability indicate greater degree of cellular quiescence and slower proliferation in these highly resistant population. This slow proliferative nature of the late resistant A2780 cells was reported earlier by us<sup>20</sup>. Recently, a rare subpopulation melanoma Rh123<sup>low</sup> stem like cells existing in quiescent and slow cycling stage showed to possess higher proportion of activated AKT compared to their Rh123<sup>high</sup> counterpart cells<sup>35</sup>. Phosphorylated AKT is known to control cellular quiescence through HIF1 $\alpha$  and c-Myc inactivation and repression of oxidative phosphorylation<sup>36–38</sup>. It could be possible that the late resistant cells in our models are more quiescent and slow cycling in nature and thus exhibit slower tumor proliferation. Further study to identifying the exact mechanism is in progress. Re-appearance of IGF-1R post AKT inhibition signifies presence of a feedback loop in these resistant models which is independent of nature of drug or cell lines. Previous report of such feedback loop in breast cancer cells showed that AKT inhibition resulted in up regulation of HER2, HER3, IGF-1R and INSR expression and downstream signaling<sup>39</sup>. As expected, treatments with IGF-1R and Akt inhibitors led to reduced cell growth and IGF-1R expression possibly due to interruption in the feedback loop in IGF-1R-Akt signalling. We speculate that such dual inhibition for members of same signalling cascade exhibiting feedback loop could be a more effective therapeutic strategy. Interestingly, combinatorial treatments of AKT inhibitor and chemotherapeutic drugs at low concentration (IC<sub>10</sub> & IC<sub>20</sub>) also showed significant decrease in viability in late resistant cells possibly due to an overall inhibition of IGF-1R-AKT signaling.

Recent evidences supporting the link between CSC and therapy resistance open the possibility of targeting resistant population as an approach to CSC eradication. Our study demonstrates existence of IGF-1R-AKT signaling mediated functional heterogeneity in the ovarian CSC population which causes differential tumorigenic ability in living subjects. Irrespective of the nature of drugs, this IGF-1R-AKT axis bestows a feedback loop during generation of chemoresistance. Our report thus specifies IGF-1R-AKT signaling as a prime determinant of cancer stem cell functionality and chemoresistance and a potential therapeutic target axis in ovarian carcinoma.

## Materials and Methods

**Cell Culture.** A2780, IGF-1R knockdown A2780 and OAW42 cells were cultured in DMEM and MEM medium respectively supplemented with 10% foetal bovine serum and 1% penicillin-streptomycin.

**Spheroid formation.** Spheroids were generated in low adherent 24-well dishes using 2000 cells/well in special medium (serum devoid DMEM or MEM complemented with FGF (20 ng/ml), EGF (10 ng/ml), Insulin (20 ng/ml), LIF (10 ng/ml) and 0.1% pen-strep) and cultured till 3<sup>rd</sup> passage. Quantitative assessment of spheroids was blindly performed by counting them under microscope. For the successive sphere-forming assay, cells from primary spheres were collected by centrifugation, dissociated with trypsin-EDTA and mechanically disrupted with a pipette. Two thousand single cells were proceeded for sphere-forming assay.

**Western blotting.** Western blotting was performed as described earlier<sup>19</sup>. Antibodies against IGF-1R  $\beta$ -subunit, AKT, pAKT and beta actin were from Cell Signaling Technology.

**Quantitative real-time PCR.** Two micrograms of total RNA was reverse transcribed with cDNA synthesis kit (Invitrogen). RT PCR was performed using SYBR Green method (Invitrogen) and appropriate gene specific primers and GAPDH as normalization control.

**FACS.** Side and Non Side population cells were sorted using Dye Cycle Violet (DCV) dye (Invitrogen)<sup>40</sup> and BD FACS Aria tagged with violet laser. Membrane drug transporter blocker Verapamil (50  $\mu$ M; Sigma) was used as negative control and gating. Data analysis was performed through DIVA software. Cell surface biomarker (CD44 and CD133) analysis was performed with FlowJo version 10 software. Anti CD44 and Anti CD133 antibodies were procured from Cell Signaling Technologies and Abcam respectively.

**Lentivirus production.** Lentiviruses carrying IGF-1R target sequence (5'AGACCTGAAAGGAAGCGGAGA-3')<sup>41</sup> were produced in 293FT cells by transfection with lentivector plasmid, P-delta packaging plasmid,

VSVG envelope protein plasmid (4:2:1 ratio) and lipofectamine (Invitrogen). Viruses were collected post 60 hours of transfection. Early cisplatin, paclitaxel and dual drug resistant cells were transduced with lentiviruses and stable cells expressing shIGF-1R constructs were sorted using GFP.

**MTT cell cytotoxicity assay.** To evaluate cytotoxicity of various chemotherapeutic drugs (cisplatin, paclitaxel and combination),  $2 \times 10^3$  cells were seeded in 96 well plates (Corning, USA). Cells were exposed to different concentrations of drugs for 48 hours. Cell viability was assessed using the MTT (3-[4,5-dimethylthiazol-2-yl] c-2,5-diphenyltetrazolium bromide) (Sigma, USA).

**Bioluminescence imaging.** All of the experiments were approved by the Institutional animal ethics committee of ACTREC and were performed in accordance with the approved guidelines. Fifty thousand SP & NSP cells were injected subcutaneously on two shoulders of 6–8 weeks old NOD/SCID mice. Bioluminescence imaging was performed by injecting D-Luciferin substrate (30 mg/ml) on the day 0 and subsequently to monitor tumor initiation and progression using IVIS Spectrum (Perkin Elmer). The mice were maintained under isoflurane (Foreknew<sup>®</sup>, ChoongWae Co., Korea) anaesthesia during the entire process. Data analysis was performed using Living Image 4.4 software. Tumor volume was measured using Vernier calliper and the calculated by the formula (Tumor volume =  $\frac{1}{2} \times \text{Length} \times (\text{Width})^2$ ).

**Statistical Analysis.** Data represent the mean  $\pm$  SEM of at least three independent experiments and were analysed as a biological replicates for significance using unpaired Student's t test. P value  $\leq 0.05$  was considered as significant.

## References

- Chapuis, N. *et al.* Autocrine IGF-1/IGF-1R signaling is responsible for constitutive PI3K/Akt activation in acute myeloid leukemia: therapeutic value of neutralizing anti-IGF-1R antibody. *Haematologica* **95**, 415–423, doi: 10.3324/haematol.2009.010785 (2010).
- Chen, J. *et al.* Functional significance of type 1 insulin-like growth factor-mediated nuclear translocation of the insulin receptor substrate-1 and beta-catenin. *The Journal of biological chemistry* **280**, 29912–29920, doi: 10.1074/jbc.M504516200 (2005).
- Chitnis, M. M., Yuen, J. S., Protheroe, A. S., Pollak, M. & Macaulay, V. M. The type 1 insulin-like growth factor receptor pathway. *Clinical cancer research: an official journal of the American Association for Cancer Research* **14**, 6364–6370, doi: 10.1158/1078-0432.CCR-07-4879 (2008).
- Baserga, R. The IGF-I receptor in cancer research. *Experimental cell research* **253**, 1–6, doi: 10.1006/excr.1999.4667 (1999).
- Eckstein, N. *et al.* Hyperactivation of the insulin-like growth factor receptor 1 signaling pathway is an essential event for cisplatin resistance of ovarian cancer cells. *Cancer research* **69**, 2996–3003, doi: 10.1158/0008-5472.CAN-08-3153 (2009).
- Huang, G. S. *et al.* Insulin-like growth factor 2 expression modulates Taxol resistance and is a candidate biomarker for reduced disease-free survival in ovarian cancer. *Clinical cancer research: an official journal of the American Association for Cancer Research* **16**, 2999–3010, doi: 10.1158/1078-0432.CCR-09-3233 (2010).
- Eliasz, S. *et al.* Notch-1 stimulates survival of lung adenocarcinoma cells during hypoxia by activating the IGF-1R pathway. *Oncogene* **29**, 2488–2498, doi: 10.1038/ncr.2010.7 (2010).
- Medyouf, H. *et al.* High-level IGF1R expression is required for leukemia-initiating cell activity in T-ALL and is supported by Notch signaling. *The Journal of experimental medicine* **208**, 1809–1822, doi: 10.1084/jem.20110121 (2011).
- Chau, W. K., Ip, C. K., Mak, A. S., Lai, H. C. & Wong, A. S. c-Kit mediates chemoresistance and tumor-initiating capacity of ovarian cancer cells through activation of Wnt/beta-catenin-ATP-binding cassette G2 signaling. *Oncogene* **32**, 2767–2781, doi: 10.1038/ncr.2012.290 (2013).
- Alvero, A. B. *et al.* Molecular phenotyping of human ovarian cancer stem cells unravels the mechanisms for repair and chemoresistance. *Cell cycle* **8**, 158–166, doi: 10.4161/cc.8.1.7533 (2009).
- Abdullah, L. N. & Chow, E. K.-H. Mechanisms of chemoresistance in cancer stem cells. *Clin Transl Med* **2**, 3, doi: 10.1186/2001-1326-2-3 (2013).
- Dean, M., Fojo, T. & Bates, S. Tumour stem cells and drug resistance. *Nature reviews. Cancer* **5**, 275–284, doi: 10.1038/nrc1590 (2005).
- Wang, A., Chen, L., Li, C. & Zhu, Y. Heterogeneity in cancer stem cells. *Cancer letters* **357**, 63–68, doi: 10.1016/j.canlet.2014.11.040 (2015).
- Meacham, C. E. & Morrison, S. J. Tumour heterogeneity and cancer cell plasticity. *Nature* **501**, 328–337, doi: 10.1038/nature12624 (2013).
- Tang, D. G. Understanding cancer stem cell heterogeneity and plasticity. *Cell research* **22**, 457–472, doi: 10.1038/cr.2012.13 (2012).
- Ginestier, C. *et al.* ALDH1 is a marker of normal and malignant human mammary stem cells and a predictor of poor clinical outcome. *Cell stem cell* **1**, 555–567, doi: 10.1016/j.stem.2007.08.014 (2007).
- Beier, D. *et al.* CD133(+) and CD133(−) glioblastoma-derived cancer stem cells show differential growth characteristics and molecular profiles. *Cancer research* **67**, 4010–4015, doi: 10.1158/0008-5472.CAN-06-4180 (2007).
- Casagrande, F. *et al.* Eradication of chemotherapy-resistant CD44+ human ovarian cancer stem cells in mice by intraperitoneal administration of Clostridium perfringens enterotoxin. *Cancer* **117**, 5519–5528, doi: 10.1002/cncr.26215 (2011).
- Singh, R. K. *et al.* IGF-1R inhibition potentiates cytotoxic effects of chemotherapeutic agents in early stages of chemoresistant ovarian cancer cells. *Cancer letters* **354**, 254–262, doi: 10.1016/j.canlet.2014.08.023 (2014).
- Gaikwad, S. M., Thakur, B., Sakpal, A., Singh, R. K. & Ray, P. Differential activation of NF-kappaB signaling is associated with platinum and taxane resistance in MyD88 deficient epithelial ovarian cancer cells. *The international journal of biochemistry & cell biology* **61**, 90–102, doi: 10.1016/j.biocel.2015.02.001 (2015).
- Broadley, K. W. *et al.* Side population is not necessary or sufficient for a cancer stem cell phenotype in glioblastoma multiforme. *Stem cells* **29**, 452–461, doi: 10.1002/stem.582 (2011).
- Hart, L. S. *et al.* Human colon cancer stem cells are enriched by insulin-like growth factor-1 and are sensitive to figitumumab. *Cell Cycle* **10**, 2331–2338, doi: 10.4161/cc.10.14.16418 (2014).
- Chang, W. W. *et al.* The expression and significance of insulin-like growth factor-1 receptor and its pathway on breast cancer stem/progenitors. *Breast cancer research: BCR* **15**, R39, doi: 10.1186/bcr3423 (2013).
- Wu, X. *et al.* Alternative cytotoxic effects of the postulated IGF-IR inhibitor picropodophyllin *in vitro*. *Molecular cancer therapeutics* **12**, 1526–1536, doi: 10.1158/1535-7163.MCT-13-0091 (2013).
- Li, Y. & Geng, Y.-J. A potential role for insulin-like growth factor signaling in induction of pluripotent stem cell formation. *Growth Hormone & IGF Research* **20**, 391–398, doi: 10.1016/j.ghir.2010.09.005 (2010).
- Koussounadis, A., Langdon, S., Harrison, D. & Smith, V. A. Chemotherapy-induced dynamic gene expression changes *in vivo* are prognostic in ovarian cancer. *British journal of cancer*, doi: 10.1038/bjc.2014.258 (2014).

27. Zhang, W. & Liu, H. T. MAPK signal pathways in the regulation of cell proliferation in mammalian cells. *Cell research* **12**, 9–18, doi: 10.1038/sj.cr.7290105 (2002).
28. Shan, J. *et al.* Nanog regulates self-renewal of cancer stem cells through the insulin-like growth factor pathway in human hepatocellular carcinoma. *Hepatology* **56**, 1004–1014, doi: 10.1002/hep.25745 (2012).
29. Bleau, A.-M. *et al.* PTEN/PI3K/Akt pathway regulates the side population phenotype and ABCG2 activity in glioma tumor stem-like cells. *Cell stem cell* **4**, 226–235, doi: 10.1038/sj.cr.7290105 (2009).
30. Geng, S. *et al.* Isolation and identification of a distinct side population cancer cells in the human epidermal squamous cancer cell line A431. *Archives of dermatological research* **303**, 181–189, doi: 10.1007/s00403-010-1100-1 (2011).
31. Goodell, M. A., McKinney-Freeman, S. & Camargo, F. D. in *Basic Cell Culture Protocols* 343–352 (Springer, 2005).
32. Haraguchi, N. *et al.* Characterization of a side population of cancer cells from human gastrointestinal system. *Stem cells* **24**, 506–513, doi: 10.1634/stemcells.2005-0282 (2006).
33. Hirschmann-Jax, C. *et al.* A distinct “side population” of cells with high drug efflux capacity in human tumor cells. *Proceedings of the National Academy of Sciences of the United States of America* **101**, 14228–14233, doi: 10.1073/pnas.0400067101 (2004).
34. Huang, Z., Wu, T., Liu, A. Y. & Ouyang, G. Differentiation and transdifferentiation potentials of cancer stem cells. *Oncotarget* **6**, 39550, doi: 10.18632/oncotarget.6098 (2015).
35. Toutil, Y. *et al.* The PI3K/AKT Signaling Pathway Controls the Quiescence of the Low-Rhodamine123-Retention Cell Compartment Enriched for Melanoma Stem Cell Activity. *Stem cells* **31**, 641–651, doi: 10.1002/stem.1333 (2013).
36. Kang, J., Shakya, A. & Tantin, D. Stem cells, stress, metabolism and cancer: a drama in two Acts. *Trends in biochemical sciences* **34**, 491–499, doi: 10.1016/j.tibs.2009.06.003 (2009).
37. Suda, T., Takubo, K. & Semenza, G. L. Metabolic regulation of hematopoietic stem cells in the hypoxic niche. *Cell stem cell* **9**, 298–310, doi: 10.1016/j.stem.2011.09.010 (2011).
38. Koshiji, M. *et al.* HIF-1 $\alpha$  induces cell cycle arrest by functionally counteracting Myc. *The EMBO journal* **23**, 1949–1956, doi: 10.1038/sj.emboj.7600196 (2004).
39. Chandarlapaty, S. *et al.* AKT inhibition relieves feedback suppression of receptor tyrosine kinase expression and activity. *Cancer cell* **19**, 58–71, doi: 10.1016/j.ccr.2010.10.031 (2011).
40. Telford, W. G., Bradford, J., Godfrey, W., Robey, R. W. & Bates, S. E. Side population analysis using a violet-excited cell-permeable DNA binding dye. *Stem cells* **25**, 1029–1036, doi: 10.1634/stemcells.2006-0567 (2007).
41. Chen, Y., Zhu, C., Peng, Z., Dai, Y. & Gu, Y. Lentivirus-mediated short-hairpin RNA targeting IGF-1R inhibits growth and lymphangiogenesis in breast cancer. *Oncol Rep* **28**, 1778–1784, doi: 10.3892/or.2012.1964 (2012).

## Acknowledgements

R.K.S. and A.D. acknowledge UGC and ACTREC for fellowship. P.R. acknowledges TMC-IRG and ACTREC for funding.

## Author Contributions

P.R. and A. De supervised the study; P.R. and R.K.S. designed the experiments; R.K.S., A.D. and A.S. performed the experiments; R.K.S. and P.R. analysed the data; P.R. and R.K.S. wrote the manuscript. All authors reviewed, edited, and approved the manuscript.

## Additional Information

**Supplementary information** accompanies this paper at <http://www.nature.com/srep>

**Competing financial interests:** The authors declare no competing interests.

**How to cite this article:** Singh, R. K. *et al.* An active IGF-1R-AKT signaling imparts functional heterogeneity in ovarian CSC population. *Sci. Rep.* **6**, 36612; doi: 10.1038/srep36612 (2016).

**Publisher's note:** Springer Nature remains neutral with regard to jurisdictional claims in published maps and institutional affiliations.



This work is licensed under a Creative Commons Attribution 4.0 International License. The images or other third party material in this article are included in the article's Creative Commons license, unless indicated otherwise in the credit line; if the material is not included under the Creative Commons license, users will need to obtain permission from the license holder to reproduce the material. To view a copy of this license, visit <http://creativecommons.org/licenses/by/4.0/>

© The Author(s) 2016

## Thesis Highlight

**Name of the Student:** Ajit Chandrakant Dhadve

**Name of the CI/OCC:** Tata Memorial Centre, Advanced Centre for Treatment, Research and Education in Cancer

**Enrolment No.:** LIFE09201404011

**Thesis Title:** Investigating the Role of IGF-1R Signalling in Development and Maintenance of Chemoresistance in Ovarian Carcinoma

**Discipline:** Life Sciences      **Sub-Area of Discipline:** Gene regulation and cell signalling

**Date of viva voce:** 4<sup>th</sup> January, 2021

Hyperactive Insulin like growth factor-1-receptor (IGF1R) signalling has been linked to resistance against not only to wide range of chemotherapeutic agents but also against radiotherapy, and targeted therapies. Intrinsic and acquired chemoresistance, an inevitable fate of chemotherapeutic agents, continues to be a persistent hurdle in treatment of human malignancies including epithelial ovarian cancer (EOC). Using isogenic EOC Cisplatin-Paclitaxel chemoresistance models we reported augmented levels of IGF1R imparted resistance against Cisplatin-Paclitaxel at early stages of chemoresistance development, moreover therapy induced IGF1R expression was also observed in tumors of a small cohort of high grade serous EOC patients. Deciphering the underlying mechanisms behind this undulating IGF1R expression during progression of resistance is important to identify a therapeutic window for devising successful anti-IGF1R therapies.

Here, for the first time we report RUNX1 as a unique regulator of IGF1R promoter which exerts a cooperative interaction with FOXO3a and dynamically modulate IGF1R expression during acquirement of chemoresistance in EOC cells. Genetic and pharmacological inhibition followed CHIP and CHIP-re-CHIP assay revealed that RUNX1 strengthened FOXO3a occupancy on IGF1R promoter, leading to a transcriptional surge during initiation of resistance which is lost at the late stages. Further an active AKT-FOXO3a negative feedback loop was shown to maintain the pulsatile behavior of IGF1R and FOXO3a. We also showed that upregulated IGF1R at onset of resistance confers resistance to Cisplatin-Paclitaxel though modulation of CSC phenotype and inhibition apoptosis by downstream IGF1R/MAPK/ERK signalling. IGF1R expression has been shown to be primarily regulated at transcriptional level by plethora of transcription factors in different cancer types, however none of these studies have investigated potential of targeting IGF1R by inhibiting its transcription. Perturbation of RUNX1 activity severely compromised IGF1R promoter activity *in vivo* and sensitized the tumors of early resistant cells to platinum-taxol treatment, as monitored by non-invasive imaging. Altogether our findings delineate a dynamic interplay between several molecular regulators (RUNX1/FOXO3a/AKT) driving pulsatile IGF1R expression and identifies a new avenue for targeting EOC through RUNX1-IGF1R axis during acquirement of chemoresistance.

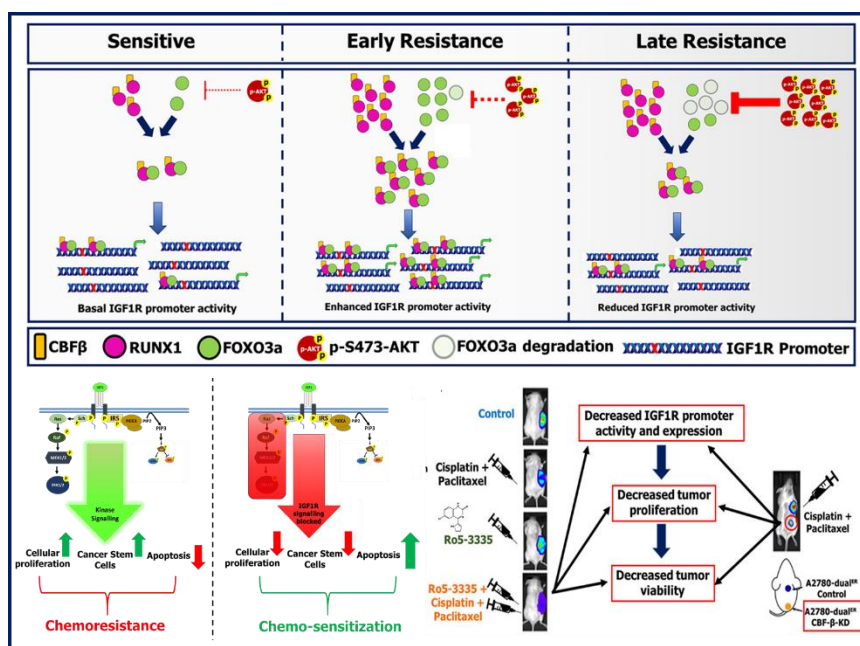


*Figure 1: Dynamic model of IGF1R promoter modulation by RUNX1/FOXO3a/AKT and IGF1R/MAPK/ERK signalling mediated chemoresistance during acquirement of chemoresistance development in EOC cells.*

Perturbation of RUNX1 activity severely compromised IGF1R promoter activity *in vivo* and sensitized the tumors of early resistant cells to platinum-taxol treatment, as monitored by non-invasive imaging. Altogether our findings delineate a dynamic interplay between several molecular regulators (RUNX1/FOXO3a/AKT) driving pulsatile IGF1R expression and identifies a new avenue for targeting EOC through RUNX1-IGF1R axis during acquirement of chemoresistance.

## Thesis Abstract

Name: Mr. Ajit Chandrakant Dhadve

Enrollment Number: LIFE09201404011

Thesis Title: Investigating the Role of IGF-1R Signalling in Development and Maintenance of Chemoresistance in Ovarian Carcinoma

Hyperactive Insulin like growth factor-1-receptor (IGF1R) signalling is associated with development of therapy resistance in many human malignancies including epithelial ovarian cancer (EOC). We recently reported a pulsatile nature of IGF1R expression during acquirement of platinum-taxol resistance in EOC cells and a similar therapy induced IGF1R expression was also observed in tumors of a small cohort of high grade serous EOC patients. In this study, we identify Runt-related transcription factor 1 (RUNX1) as a novel regulator of IGF1R promoter which exerts a cooperative interaction with Forkhead Box O3 (FOXO3a) and dynamically modulate IGF1R expression during platinum-taxol resistance development in EOC cells. Genetic and pharmacological inhibition of RUNX1 transcriptional activity followed ChIP and ChIP-re-ChIP assay revealed that RUNX1 strengthened FOXO3a occupancy on IGF1R promoter leading to a transcriptional surge during onset of resistance. Intriguingly such co-operativity falls apart when cells attain maximal resistance due to an active AKT-FOXO3a negative feedback loop exclusively present in the highly resistant cells eliciting the pulsatile behavior of IGF1R and FOXO3a. This augmented IGF1R levels at onset of resistance were shown to confer resistance against platinum-taxol through maintenance of cancer stem cell phenotype and inhibition apoptosis by downstream IGF1R/MAPK/ERK signalling. Perturbation of RUNX1 activity severely compromised IGF1R promoter activity *in vivo*, decreased tumorigenicity and sensitized the tumors of early resistant cells to platinum-taxol treatment, as monitored by non-invasive imaging. Altogether our findings delineate a dynamic interplay between several molecular regulators (RUNX1/FOXO3a/AKT) driving pulsatile IGF1R expression. Such molecular knowledge of regulation of IGF1R expression during chemoresistance development enabled indirect therapeutic targeting of IGF1R by inhibiting its transcription, thus identifying a new therapeutic window for devising successful anti-IGF1R therapies.

Signature: .....  
Ajit Chandrakant Dhadve

Forwarded through:

Signature: .....  
Dr. Pritha Ray

S. N. Dalal  
Dr. Sorab N Dalal, 24/2/2021  
Chairperson, Academic &  
Training Programme, ACTREC  
(Dr. Sorab N. Dalal)  
Chairperson, Academic & Training Programme  
Tata Memorial Center, ACTREC,  
Kharghar, Navi Mumbai - 410210

Dr. S. D. Banavali,  
Dean (Academics)  
T.M.C.

PROF. S. D. BANAVALI, MD  
DEAN (ACADEMICS)  
TATA MEMORIAL CENTRE  
MUMBAI - 400 012.